DNA INCORPORATED ONE-DIMENSIONAL TERNARY PHOTONIC CRYSTAL STRUCTURES: A PATHWAY TO MULTIFUNCTIONAL OPTICAL PLATFORMS

Thesis submitted to the
University of Calicut for the partial fulfilment of
the requirements for the award of the degree of

DOCTOR OF PHILOSOPHY IN PHYSICS

By
BHAGYASREE G S

Under the Guidance of

Dr. NITHYAJA B
Associate Professor of Physics

Research and Post Graduate Department of Physics
Government College Madappally, Vadakara
2025

DEPARTMENT OF PHYSICS
GOVT. COLLEGE MADAPPALLY, VADAKARA

Dr. Nithyaja B
Associate Professor
Department of Physics

13 August 2025

CERTIFICATE

This is to certify that the thesis entitled **"DNA INCORPORATED ONE-DIMENSIONAL TERNARY PHOTONIC CRYSTAL STRUCTURES: A PATHWAY TO MULTIFUNCTIONAL OPTICAL PLATFORMS"** is a report of original work carried out by **Mrs. Bhagyasree G S**, under my supervision and guidance in the Department of Physics, Govt. College Madappally, Vadakara, Calicut, Kerala and that no part thereof has been presented for the award of any other degree.

The thesis is revised as per the modifications and recommendations reported by the adjudicators. Soft copy attached is the same as that of the revised copy.

Dr. Nithyaja B
Research Supervisor

Dr. NITHYAJA. B
PEN: 674969
Associate Professor of Physics
Govt. College Madappally
Vatakara - 673 102

P.O. Madappally College, Vadakara, Kerala-673102
Ph: 0496 2512587, Email: physicsdeptgcm@gmail.com

GOVERNMENT COLLEGE MADAPPALLY

DECLARATION

I hereby declare that the work presented in the thesis entitled "**DNA INCORPORATED ONE-DIMENSIONAL TERNARY PHOTONIC CRYSTAL STRUCTURES: A PATHWAY TO MULTIFUNCTIONAL OPTICAL PLATFORMS**", is based on the original work done by me under the guidance of Dr. Nithyaja B, Associate Professor, Department of Physics, Govt. College Madappally, Vadakara, Kerala, and has not been included in any other thesis submitted previously for the award of any degree. The contents of the thesis are under grown plajirism check using iThenticate software at C.H.M.K Library, University of Calicut, and the similarity index found within the permissible limit. I also declare that the thesis is free from AI generated contents.

Bhagyasree G S
Research Scholar
Photonics Materials Research Lab
Department of Physics
Govt. College Madappally,
Vadakara Kozhikode, Kerala

Madappally

August 13, 2025

Signature of the Supervising Teacher:

Name : Dr. NITHYAJA. B
PEN: 674969
Associate Professor of Physics
Govt.College Madappally
Vatakara - 673 102

GOVERNMENT COLLEGE MADAPPALLY

UNIVERSITY OF CALICUT

CERTIFICATE ON PLAGIARISM CHECK

1.	Name of the Research Scholar	BHAGYASREE G S	
2.	Title of thesis / dissertation	DNA incorporated one-dimensional ternary photonic crystal structures: A pathway to multifunctional optical platforms	
3.	Name of the Supervisor	Dr. NITHYAJA B	
4.	Department/Institution	Research Scholar,Department of Physics, Govt. College Madappally Vadakara,Calicut University	
5.	Similar content (%) identified	Non Core	Core
		Introduction/ Theoretical overview/Review of literature/ Materials & Methods/ Methodology	**Analysis/Result/Discussion /Summary/Conclusion/ Recommendations**
		4	3
	Acceptable maximum limit (%)	10	10
6.	Software used	iThenticate	
7.	Date of verification	Thu May 08 2025 00:00:00 GMT+0530 (India Standard Time)	

**Report on plagiarism check, specifying included/excluded items with % of similarity to be attached.*

Checked by (with name, designation & signature) Dr. Nasirudheen. T Assistant Librarian University of Calicut, Kerala.

Name and signature of the Researcher Bhagyasree G.S.

Name and signature of the Supervisor. Dr. Nithyaja. B

The Doctoral Committee* has verified the report on plagiarism check with the contents of the thesis, as summarized above and appropriate measures have been taken to ensure originality of the Research accomplished herein.

Name & Signature of the HoD/HoI (Chairperson of the Doctoral Committee) Shimi Pakkshara Malammal

Principal
Government College Madappally
Madappally College (P.O)
PIN 673 102

**In case of languages like Malayalam, Tamil etc..on which no software is available for plagiarism check, a manual check shall be made by the Doctoral Committee, for which an additional certificate has to be attached.*

ACKNOWLEDGEMENTS

I know the years I spent at Govt. College Madapplly are recognized as one of the most valuable phases of my life where I was literally reborn with the new dawn of perception of different levels of life, that paved my destiny.

As we know that a research outcome cannot be entitled to the hard work of a single person, as it is the result of collective support and encouragement of many known and unknown individuals. It is my honour to remember and share my gratitude to those people who stood by my side throughout my research journey.

On the auspicious moment of completing my PhD thesis, I recollect to those people who encouraged me to overcome the heavy moments came during accomplishing my research goals. I feel this is the great moment to acknowledge the support and love of each and every person who directly or indirectly involved to accomplish my research work.

I feel overwhelming to express my deep love and gratitude to my research guide, Dr. Nithyaja B, (Associate professor, Department of Physics, Govt. College Madappally, Vadakara), whose guidance, and mentorship have been invaluable throughout my research journey. I sincerely grateful to the time and expertise she has generously shared with me, enriching my understanding and molding me into a more diligent scholar. I fondly recollect her unbounded patience to listening to me, unwavering support throughout my years of research, forgiving

my lapses, her timely involvements to strengthen me when I felt low, and providing immense freedom to work.

I express my thanks to Shinu P M, Principal, as well as all the previous principals during my research period at Govt. College Madappally, Vadakara, Kozhikode for providing all the facilities in the department to accomplish my research work.

I extend my heartfelt gratitude to Dr. Suneera T.P, head of the department of Physics, for her guidance to fix the errors associated with my theoretical research work.

I express my gratitude to Hameed (Associate Professor), Dr. Harikrishnan G (Associate Professor), Sri. Mubash MCV (Assistant Professsor) and Dr. Santhi Krishna U (Assistant Professor) of the Physics Department, Govt. College Madappally for their constant support and understanding.

I express my sincere thanks to all the non-teaching staff of the department for their help in arranging lab requirements.

I am grateful to Sajitha N. M, Assistant Professor, Department of Physics, for her boundless help, warm friendship and I appreciate her patience to fix he errors of my theoretical programmes of the research work in her busy academic research work.

I am grateful to Pro. Chandrasekhar, Department of Physics, NIT Calicut, for his candid mind and boundless help to configure my research problem. I recall that when I chose my research field I went to meet him to seek his suggestions in this field. He introduced his

research student to me and told me to approach his lab whenever I need. As he said, whenever I approached for experimental and theoretical support from his side, he happily received my request and allowed me to do my experimental investigations in his laboratory.

I am grateful to Prof. Sandhyarani, Professor, NIT Calicut, my former MSc project guide, for her guidance and broaden heart shown towards me to do my research experiments in her laboratory. I recall that whenever I had approached her to do my research experiments in her lab, she relentlessly gave permission and she tried to set a warm ambience to me in her laboratories with her research scholars.

I felt overwhelming to say gratitude to Dr. Natesan Yogesh, Assistant Professor, Department of Physics, NIT Calicut for his invaluable advice and help to install softwares which I used to find solutions of my entire theoretical problems.

I am obliged to Dr. Nikhil Puthan Purayil, Post doctoral fellow, IIT Kanpur, for his immense advice and suggestions to solve my research problem during his academic constarints. Besides, I recall that he relentlessly answered to my queries about research problem even if he was busy with his research work.

I am grateful to Dr. Athulya K S for her valuable help to conduct experiments to analyse my research samples during her busy academic constraints. Besides, she always shows willingness to answer my each and every query regarding my research work.

I am grateful to Athira Research Scholar, NIT Calicut for her valuable help to do my experimental analysis and I appreciate her effort to conduct my research experiments even in her holidays too.

I am grateful to Sandeep K V, Assistant Professor, Mahathma Gandhi Govt. Arts College, Mahe, for his valuable suggestions and support to fix theoretical codes and software installation.

I extend my gratitude to Dr. Shanasree M for her boundless help and valuable presence as a good scholar, mentor and friend throughout my research period. Dear Shanasree M, your presence in my research period was a good source of relief.

I am grateful to Bivitha T K, Assistant Professor, Department of Physics, SN College Kannur for her warm talks, advice and helping to research work. She was the only research colleague literally present with me in the COVID time. So, her warm friendship and presence helped me to do research work even in the COVID time.

I would like to express my sincere gratitude to the Head of Zoology, Chemistry and Botany departments for providing different research facilities for the advancement of my work.

I express my sincere gratitude to Anju. K Research scholar, Department of Zoology for her valuable helping to use her research facilities to do my experiments and I appreciate her timely response to my every query regarding research program.

I express my sincere gratitude to Athira T R, Research scholar, Department of Zoology for her valuable advice in the final lap of

documentation of thesis and I appreciate her timely response to my every query regarding thesis documentation.

I am glad to express my gratitude to Anjana T M, Research scholar, department of Chemistry for her valuable and timely actions and suggestions about the chemicals which I used to do my experiments. I would like to share with great gratitude that she explained about the peculiar features of the polyoxometalate one of the class materials in the research areas. One of her most important roles in my research work is that she relentlessly shared her expensive chemicals to me to do my research work in my crucial time. It is rare to encounter individuals who help without seeking personal gain. I would like to add that she made a beautiful cordial presence throughout my research work.

I am glad to express my gratitude to Vaidehi E K, Research Scholar, Department of Chemistry, for her warm friendship and support in my research life.

Thanks to Dr. Binitha M P, Head of the department of Physics, Govt. Arts and Science College Calicut for giving enough consideration and support to do my research work. I am grateful to you for giving me permission to use your department lab to do my drafting of thesis.

Thanks to Dr. Priya P, Principal of Govt. Arts and science College Calicut for giving permission to access college research lab to do my research work.

Thanks to Dr. Shaji C V, Principal of SARBTM Gov. College for granting permission to access college physics department research lab facilities to do my research experiments during COVID-19 period.

Thanks to Dr. Muraleedharan, Assistant Professor (former assistant professor of Physics, SARBTM Govt. College Koyilandy) for granting me the permission to access department research lab facilities during COVID-19 pandemic.

Dr. Rajasekharan K, former Professor and Head of the Department of Physics, Malabar Christian College, Kozhikode, my former tutor who gave the first inspiration to aspire my research passion.

Dr. Sabri Girisun, Assistant Professor, Department of Physics, Bharathidasan Universiy Thrichy, Tamil Nadu. I extended my warm gratitude to his collaboration for the nonlinear optical characterization of my research samples.

Thanks to the Technicians, CSIF-Calicut University, NIT Calicut for various characterizations and analysis for the research work.

Amma, ***Gitanjali*** *who built a strong base of my academic journey through her boundless love, sacrifice and determination. It was her passion to provide a quality-based education to me, for that she herself dedicated to achieve my goals. I couldn't find any ornamental words to narrate her role to shape my entire life. I am always indebted to her love, determination and perseverance as a strong woman.*

I am always indebted to my father Sreedharan Chathoth who always stood by my side to pursue my academic journey with love, and care.

I am so grateful to my sister Mrs. Anjana to hold my life during my difficult times to accomplish my journey and, also a place comfort. I would like to add that she is my first teacher in my life before I was entering into my academic journey. During my childhood, she was there to hold my hand to direct me in my studies and she is the only reason for me to choose Physics as my main subject to pursue my higher education. Her deep knowledge in Mathematics helped me to shape my scientific concepts.

I am always grateful to my brother Prasobh, apart from my teachers, he is the first person in my family to force to dream about Ph.D. Once it was his effort to pave the seeds of research ambitions in my thought. He gave the strength and support to attend UGC-JRF entrance exams. I am always obliged to his vision about my education, love and care. I added that after I achieved my MSc. Graduation he filled my Email with mails that containing Ph.D related instructions and links. From that point, I was wondered about how deeply he dreamt about my career in research.

I express my gratitude to my sister Mrs. Lintu Prasobh for her great support and presence during my toughest time of research.

I am always grateful to my sister Sangeetha Parnasseri to provide all the support and love to full fill my goals. She was there when I felt low and her mentoring during the last lap of thesis was so powerful and great.

I am very obliged to my mother-in law and Father-in law for their whole support and love to accomplish my dream.

Big thanks to Dr. Reena V.N, Assistant Professor, Department of Physics, Govt. Arts and Science College Kozhikode, for her sincere assistance during the entire period of my research. Apart from a research collegue, she is there always as mentor, friend and my financial supporter at the earlier time of my research. I began my experiments by using her chemicals in my lab during the COVID-19 pandemic. She always shattered good support in my difficult times and share her warm friendship as a source of relief until she left the research lab. Dear Reena ma'am I am sharing my heartfelt gratitude for your warm presence.

I express my heartfelt love and gratitude to Preetha U, Assistant Professor, Department of Physics, Govt. College Madappally for her warm presence as a mentor and friend in my heavy research period.

Sandeep Parnasseri my "partner in crime", I purely dedicated my thesis to him, because he is the only backbone of everything. I couldn't find words to explain how deeply he put effort to accomplish my dream journey. Apart from my guide, he is the only person who keeps fueling me in my crucial days of research. I know, he has been dreaming with me about accomplishing my goals since we met. Dear Sandeep, your presence has been a source of comfort, alleviating my stress during the research period.

Thanks to all other friends for their support on this endeavor.

Thanks to my Almighty God

Bhagyasree G S

Dedicated to

SANDEEP PARNASSERY

&

Almighty God

ABSTRACT

Photonic crystals are an integral part of photonics, where light is manipulated through carefully engineered structural features. These crystals consist of periodic microstructures formed by dielectric or metallo-dielectric materials. When light interacts with such periodic structures, only specific frequencies are allowed to propagate, while others are blocked. The frequency range at which light cannot pass is known as the photonic bandgap (PBG). Depending on the direction of periodic refractive index contrast between adjacent dielectric materials, photonic crystals are classified as one-dimensional (1D), two-dimensional (2D), or three-dimensional (3D). In 1D photonic crystals, light propagation is confined to a single direction. In contrast, 2D and 3D structures allow light confinement in two and three directions, respectively, making them versatile in numerous optical applications, including filters, sensors, and laser devices.

Among these, 1D photonic crystals stand out due to their fabrication simplicity, making them attractive candidates in both scientific and technological fields. This research presents a comprehensive theoretical and experimental analysis of 1D ternary dielectric photonic crystals for diverse potential applications. Theoretical simulations were carried out using the Transfer Matrix Method (TMM) and COMSOL Multiphysics software to explore the photonic band structure characteristics. The analysis reveals that ternary 1D structures offer significant advantages over traditional bilayer systems, such as wider photonic bandgaps, the emergence of multiple bandgaps, and the formation of defect modes with large Full Width at Half Maximum (FWHM).

This work further investigates DNA-incorporated 1D ternary photonic crystals and DNA-templated nanoparticles, emphasizing the dual role of DNA as both a functional polymer layer and a templating agent for nanoparticle synthesis. DNA significantly influences surface morphology, nonlinear optical behavior, and the bandgap features of these photonic crystals. Several combinations, such as Silica/DNA/ZnO and Silica/DNA/PVA, were designed and studied. Dip-coating techniques were employed to fabricate Silica/DNA/ZnO multilayer thin films experimentally. Theoretical models were

developed for systems involving other dielectric materials like alumina and graphite oxide, including configurations such as Silica/DNA/Alumina, Silica/DNA/Graphite Oxide, and Graphite Oxide/DNA/ZnO.

Dielectric/DNA/Dielectric structures display remarkable features like broad photonic bandgaps, multiple gap regions, and high oscillation densities. Increasing the number of periods leads to enhanced oscillation density, bandgap broadening, and spectral shifts. Notably, the Silica/DNA/PVA system demonstrates promising potential for low-temperature fabrication using inkjet printing technology, paving the way for scalable three-dimensional photonic structures.

Experimental studies on Silica/DNA/ZnO ternary structures were carried out to explore their biosensing capabilities for bovine serum albumin (BSA) and their nonlinear optical properties. Theoretical predictions for BSA detection showed a strong correlation with experimental observations, validating the biosensing efficiency of these structures. Nonlinear optical characterization using open-aperture Z-scan revealed tunable responses in both pristine and defective photonic crystals. The defect layer, consisting of DNA-capped silicotungstate, significantly enhances the nonlinear behavior, suggesting broad applicability in advanced photonic devices.

In conclusion, the investigation of 1D ternary photonic crystal systems underscores their significant potential across a range of photonic applications, offering new avenues in sensing, light manipulation, and nonlinear optics.

ഡി.എൻ. എ. സംയോജിത ഏകമാന-ത്രിതീയ പാളി ഫോട്ടോണിക് പരലുകൾ: പ്രകാശത്തിന്റെ ബഹുമുഖോപയോഗ സാധ്യതകളിലേക്കൊരു പാത

സംഗ്രഹം

ഇന്നത്തെ ശാസ്ത്ര രംഗത്ത് വളരെ നൂതനമായതും ഫോട്ടോണിക്സ് ശാസ്ത്ര വിഭാഗത്തിൽ ഒരു അവിഭാജ്യ ഘടകവുമാണ് ഫോട്ടോണിക് ക്രിസ്റ്റലുകൾ. പേരു സൂചിപ്പിക്കുന്നതുപോലെ പ്രകാശത്തിനു സഞ്ചരിക്കുവാൻ സാധിക്കുന്ന സവിശേഷമായ സുതാര്യമായ പരലുകളാണ് ഫോട്ടോണിക് ക്രിസ്റ്റലുകൾ.

വൈവിധ്യമാർന്ന സാധ്യതയുള്ള ഉപയോഗങ്ങൾക്കായി ഏകമാനക ദിശാ വിഭാഗത്തിൽ പെടുന്ന ത്രിതീയ പാളികളുടെ ആവർത്തന യൂണിറ്റ് വരുന്ന ഫോട്ടോണിക് പരലുകളുടെ സമഗ്രമായ സൈദ്ധാന്തികവും പരീക്ഷണാത്മക വുമായ വിശകലനം ഈ ഗവേഷണം അവതരിപ്പിക്കുന്നു. പ്രകാശ തരാംഗാ ന്തരത്തിലെ സവിശേഷതകൾ പര്യവേക്ഷണം ചെയ്യുന്നതിനായി ട്രാൻസ്ഫർ മാട്രിക്സ് രീതി (TMM), കൊംസോൾ (COMSOL) മൾട്ടിഫിസിക്സ് സോഫ്റ്റ്വെയർ എന്നിവയുടെ സഹായത്തിൽ ഗണിത സൂത്രവാക്യങ്ങൾ പരിഹരിച്ച് പ്രകാശത്തിന്റെ പ്രസരണത്തിലെ സവിശേഷതകൾ വിശകലനം ചെയ്തു. പ്രകാശം കടന്നു പോകുമ്പോൾ വീതി കൂടിയതും ഒന്നിലധികവും പ്രകാശ തരാംഗാന്തരങ്ങൾ ഉണ്ടാവുന്നത് ഇത്തരം ഏകമാനക ത്രിതീയഫോട്ടോണിക് പരലുകളുടെ സവിശേഷതകളാണ്. കൂടാതെ, അർദ്ധ തരംഗോന്നതിയുടെ തരംഗ വ്യത്യാസം (Full Width at Half Maximum), ഫോട്ടോണിക് പരലുകളിൽ ഉണ്ടാവുന്ന ഘടനാവ്യത്യാസം കാരണം രൂപപ്പെടുന്ന അനുരണാനാവൃത്തി യുടെ രൂപീകരണം എന്നിവ പോലുള്ള പരമ്പരാഗത ദ്വിതീയ ഫോട്ടോണിക് പരലുകളെ സിസ്റ്റങ്ങളെ അപേക്ഷിച്ച് ടെർണറി 1D ഘടനകൾ ഗണ്യമായ നേട്ടങ്ങൾ വാഗ്ദാനം നൽകുന്നതായി പഠനം വെളിപ്പെടുത്തുന്നു. ഈ പഠനം ഡിഎൻഎ-സംയോജിത 1D ത്രിതീയ ഫോട്ടോണിക് പരലുകളെ കുറിച്ചും ഡിഎൻഎയുടെ സാന്നിധ്യത്തിൽ നിർമ്മിച്ച നാനോപാർട്ടിക്കിളുകളെയും കുറിച്ചുള്ള ഒരു സംയോജിത അന്വേഷണമാണ്. ഈ പഠനത്തിൽ ഡി. എൻ എ എന്ന ജൈവിക പോളിമറിനെ സുതാര്യ പാളിയായും നാനോ കണികകളുടെ നിർമ്മാണത്തിനായുള്ള ഒരു മാധ്യമം എന്ന നിലയിലുമുള്ള പങ്കിനെ കുറിച്ചും വിശദമായി അന്വേഷിക്കുന്നു. ഡി.എൻ.എ യുടെ സാന്നിധ്യം അവയുടെ സാന്നിധ്യത്തിൽ നിർമ്മിച്ച കണികകളുടെ രൂപഘടന, തീവ്ര ലേസർ പ്രകാശവുമായി സംവദിക്കുമ്പോൾ പദാർത്ഥത്തിന്റെ സ്വഭാവം എങ്ങനെ വ്യത്യാസപ്പെടുന്നു, ഏകമാനക ത്രിതീയ ഫോട്ടോണിക് പരലുകളിലെ പ്രകാശ തരാംഗന്തരത്തിന്റെ സ്വഭാവം എന്നിവയെല്ലാം എങ്ങനെ ഗണ്യമായി സ്വാധീനിക്കുന്നു എന്നതെല്ലാം ഈ പഠനത്തിന്റെ വിഷയമാകുന്നു. സിലിക്ക/ഡിഎൻഎ/സിങ്ക് ഓക്സൈഡ്, സിലിക്ക/ ഡിഎൻഎ/പിവിഎ തുടങ്ങിയ നിരവധി സംയോജനങ്ങൾ രൂപകൽപ്പന ചെയ്യുകയും പരീക്ഷണാടിസ്ഥാനത്തിൽ നിർമ്മിക്കുകയും ചെയ്തു.

സിലിക്ക/ഡിഎൻഎ/ സിങ്ക് ഓക്സൈഡ് ബഹുപാളികളായുള്ള മൈക്രോ വല്യപ്പത്തിലുള്ള പരലുകൾ പരീക്ഷണാത്മകമായി നിർമ്മിക്കുന്നതിന് ഡിപ്-കോട്ടിംഗ് സാങ്കേതിക വിദ്യ ഉപയോഗിച്ചു. അലുമിന, ഗ്രാഫൈറ്റ് ഓക്സൈഡ് പോലുള്ള മറ്റ് സുതാര്യമായതും അചാലകങ്ങളുമായ പദാർത്ഥങ്ങൾ ഉൾപ്പെടുന്ന സിലിക്ക/ഡിഎൻഎ/അലുമിന, സിലിക്ക/ഡിഎൻഎ/ഗ്രാഫൈറ്റ് ഓക്സൈഡ്, ഗ്രാഫൈറ്റ് ഓക്സൈഡ്/ഡിഎൻഎ/സിങ്ക് ഓക്സൈഡ് തുടങ്ങിയ 1D ത്രിതീയ ഫോട്ടോണിക് പരലുകളുടെ രൂപകൽപ്പനകൾക്ക് ഗണിത സൂത്രവാക്യങ്ങൾ ഉപയോഗിച്ച് അവയിലൂടെ പ്രകാശം കടന്നു പോകുന്ന പ്രതിഭാസങ്ങളുടെ

മാതൃകകൾ വികസിപ്പിച്ചെടുത്തു. ഈ പഠനത്തിലൂടെ വിശകലനം ചെയ്ത ഏകമാനക ത്രിതീയ ഫോട്ടോണിക് പരലുകൾ വീതി കൂടിയതും ഒന്നിലധികം എണ്ണത്തിൽ കൂടുതലുമായ പ്രകാശ തരംഗാന്തരം ഉയർന്ന ആന്ദോളന സാന്ദ്രത എന്നിവ പോലുള്ള ശ്രദ്ധേയമായ സവിശേഷതകൾ പ്രദർശിപ്പിക്കുന്നു. ഫോട്ടോണിക് പരലിന്റെ ആവർത്തനത്തിന്റെ എണ്ണം വർദ്ധിപ്പിക്കുന്നത് അവയിലെ പ്രകാശത്തിന്റെ സാന്ദ്രത, വീതി കൂടിയ പ്രകാശ തരംഗാന്തരം, പ്രകാശ തരംഗാന്തര സ്ഥാനമാറ്റം എന്നിവയിലേക്ക് നയിക്കുന്നു. ഈ പഠനത്തിൽ ശ്രദ്ധേയമായ മറ്റൊരു വസ്തുത, സിലിക്ക/ഡിഎൻഎ/പിവിഎ ഘടന പ്രതിനിധാനം ചെയ്യുന്ന പോളിമർ പോലുള്ള ഘടനകൾ ഇങ്ക്ജെറ്റ് പ്രിന്റിംഗ് എന്ന സാങ്കേതികവിദ്യ ഉപയോഗിച്ച് കുറഞ്ഞ താപനിലയിൽ നിർമ്മിക്കുന്നതിനുള്ള സാധ്യതകൾ പ്രകടമാക്കുന്നു. ഇത് ത്രിമാന ഫോട്ടോണിക് ഘടനകളുടെ നിർമ്മാണത്തിന് വഴിയൊരുക്കുന്നു.

1D സിലിക്ക/ഡിഎൻഎ/സിങ്ക് ഓക്സൈഡ് ത്രിതീയ ഫോട്ടോണിക് പരൽ ഘടനകളെക്കുറിച്ചുള്ള പരീക്ഷണാത്മക പഠനങ്ങൾ, ബോവിൻ സെറം ആൽബുമിൻ (BSA) എന്ന ജൈവികമാംസ്യ തന്മാത്രകളുടെ തിരിച്ചറിയുന്ന തിനായ് സഹായിക്കുന്ന ഉപകരണത്തിന്റെ ക്ഷമത പരിശോധിക്കുവാനുള്ള പര്യവേക്ഷണം നടത്തി. ജൈവിക തന്മാത്രയായ BSA-യുടെ ഗാഢത ജലത്തിൽ തിരിച്ചറിയുന്നതിനുള്ള പരിശോധന ഗണിത സൂത്രവാക്യങ്ങൾ ഉപയോഗിച്ച് പരീക്ഷിക്കുകയും നിരീക്ഷണ പഠനങ്ങൾ ശക്തമായ കാര്യക്ഷമത പ്രദർശിപ്പിക്കുകയും ചെയ്തു. ഓപ്പൺ-അപ്പേർച്ചർ Z-സ്കാൻ എന്ന സാങ്കേതികത ഉപയോഗിച്ച 1D സിലിക്ക/ഡി.എൻ.എ /സിങ്ക് ഓക്സൈഡ് ത്രിതീയ ഫോട്ടോണിക് പരലുകൾക്ക് തീവ്ര ലേസർ പ്രകാശത്തിനോടുള്ള പ്രതികരണം പഠിച്ചു. ഈ പഠനം തീവ്രലേസർ പ്രകാശത്തിന്റെ സാന്നിധ്യത്തിൽ ഘടനയുടെ മൗലിക സ്വഭാവങ്ങളായ പ്രകാശ തരംഗാന്തരം, അനുരണനാവൃത്തി എന്നിവ ആവശ്യാനുസരണം മാറ്റുവാൻ സാധിക്കും എന്നു മനസ്സിലായി. ഡിഎൻഎയുടെ സാന്നിധ്യത്തിൽ നിർമ്മിച്ച സിലിക്കോടംഗ്സ്റ്റേറ്റ് എന്ന പോളിഓക്സോ മെറ്റലേറ്റ് വിഭാഗത്തില്പ്പെടുന്ന പദാർത്ഥത്തെ പാളി രൂപത്തിലാക്കി പ്രസ്തുത ഫോട്ടോണിക് പരലിന്റെ ഘടനയിൽ വ്യതിയാനം സൃഷ്ടിച്ചതിനു ശേഷം അതിന്റെ സ്വഭാവം തീവ്ര ലേസർ പ്രകാശത്തിൽ എങ്ങനെ മാറുന്നു എന്നും പരീക്ഷണാടിസ്ഥാനത്തിൽ പരിശോധിച്ചു.

1D ത്രിതീയ ഫോട്ടോണിക് പരലുകളുടെ ഘടനകളുടെ അന്വേഷണം ഫോട്ടോണിക് ശാസ്ത്രരംഗത്തെ നിരവധി ഉപയോഗങ്ങൾക്ക് അവയുടെ ഗണ്യമായ സാധ്യതയെ അടിവരയിടുന്നു, സെൻസിംഗ്, പ്രകാശ പ്രസരണ നിയന്ത്രണം, തീവ്ര ലേസർ പ്രകാശവുമായി ബന്ധപ്പെട്ട പ്രകാശപഠന രംഗം എന്നിവയിൽ പ്രസ്തുത ഫോട്ടോണിക് ഘടന പുതിയ വഴികൾ വാഗ്ദാനം ചെയ്യുന്നു.

ABBREVIATIONS USED

PC	Photonic crystal
PBG	Photonic bandgap
DNA	Deoxyribo nucleic acid
DMSO	Dimethyl sulfoxide
HCl	Hydrochloric acid
Al_2O_3	Aluminium oxide (Alumina)
GO	Graphite oxide
ZnO	Zinc oxide
UV	Ultraviolet
XRD	X-ray Diffraction
SEM	Scanning Electron Microscope
LED	Light Emitting Diode
LCD	Liquid Crystal Display
H_2SO_4	Sulphuric acid
CTAB	Cetyl trimethyl ammonium bromide
CTAC	Cetyl trimethyl ammonium chloride
TMM	Transfer matrix method
PWE	Plane wave expansion
FDTD	Finite time domain time difference
FEM	Finite elemental method
N	Number of period (Number of unit cell, commonly known as number of order)

L	Layer
BSA	Bovine serum albumin
Q	Quality factor
F	Figure of merit
S	Sensitivity
FWHM	Full width at half maximum
D	Dimension
1D	One-dimensional
2D	Two-dimensional
3D	Three-dimensional
PVA	Polyvinyl alcohol
CD Complex	CTAB – DNA Complex
DI	Deionized
POM	Polyoxometalate
D-POM	DNA-capped Polyoxometalate
NLO	Non-linear optical
NLA	Nonlinear absorption
RSA	Reverse saturable absorption
TPA	Two photon absorption
SA	Saturable absorption

PREFACE

Photonic crystals bring together a wide range of interdisciplinary fields within integrated photonics and modern technology**.** Advances in engineering and materials science have significantly expanded the scope of photonic crystals in both fundamental research and technological applications. These structures provide a novel platform in photonics, where the interaction of light with matter can be precisely enhanced and tailored. This tunability opens up numerous opportunities in contemporary science and technology, including applications in sensing, solar energy harvesting, optical communication, quantum computing, bioimaging, light-emitting devices, and nonlinear optical systems.

The thesis is an investigation of the realm of one-dimensional ternary photonic crystals, their basic theory, and scope in contemporary science and technological demands. The use of repeated ternary unit structures composed of isotropic materials enhances light confinement efficiency and simplifies the fabrication process. This approach offers significant advantages for the integrated photonics industry, enabling the development of various photonic devices that rely on light confinement mechanisms. The role of DNA is prominently exploited with the periodic microstructures. The optical properties of DNA such that its role as template element for the nanoparticle synthesis and thin film properties are suitably examined for the entire work of the research work.

The thesis is divided into nine chapters. **Chapter 1** discusses the general features of photonic crystals, the role of one-dimensional ternary photonic crystals, and the characteristics of DNA-incorporated microarrays of unit cells. **Chapter 2** presents the general theoretical framework used for designing one-dimensional ternary photonic crystals. **Chapter 3** illustrates the optical features of six examples of one-dimensional photonic crystal structures. The systems studied include Silica/DNA/ZnO, Silica/DNA/Alumina, Silica/DNA/Graphite Oxide, Graphite Oxide/DNA/ZnO, Alumina/DNA/Graphite Oxide, and Alumina/DNA/ZnO. The study examines the optical properties, including transmission and defect modes, of these structures when illuminated with light in the wavelength range of 350 to 750 nm. This investigation is intended to explore the potential applications of one-dimensional DNA-incorporated ternary photonic crystals.

Chapter 4 explores the scope of one- dimensional ternary Silica/DNA/ZnO photonic crystal for the detection of bovine serum albumin detection for various concentrations. **Chapter 5** is an insight of the synthesis of DNA templated silica nanoparticles and DNA templated silicotungstate for obtaining nonlinear optical nanoparticles to incorporate with the fabrication of one- dimensional ternary photonic crystals. The nonlinear optical properties of the obtained DNA-templated silica nanoparticles and DNA-templated silicotungstate were investigated using the open-aperture Z-scan method.

Chapter 6 explores the fabrication and characterizations of one-dimensional Silica/DNA/ZnO photonic crystal for tuning the nonlinear

optical properties of the structure where the defective photonic crystal structure is realized by incorporating DNA templated silicotungstate.

Chapter 7 discusses the features of one-dimensional ternary photonic crystal of Silica/DNA/Polyvinyl Alcohol composition for 3D inkjet printing applications, where the study focused to design a polymer-based microstructures that use low temperature fabrication conditions. **Chapter 8** unfolds the summary of the conclusions of the entire works and the recommendation of the research outcomes. Thus, this study contributes to advancing an emerging platform for interdisciplinary science and integrated photonic research.

List of Publications

1. Bhagyasree G S and Nithyaja B. (2022) Theoretical Studies of One-Dimensional DNA Templated Silica/Metal Oxides, Graphite Oxide Photonic Crystals, *ECS Trans*. 107 12161, DOI: 10.1149/10701.12161ecst (Publisher: ECS)

2. Bhagyasree G S, Reena V N, Abith M, Sabari Girisun T C, Nithyaja,B (2023) Enhanced adsorption and non-linear optical properties of DNA-CTAB functionalized mesoporous silica nanoparticles and their influence on enhancement of photoluminescence of Rhodamine 6G dye. AIP Advances, 13(5), 055017. (Publisher: AIP)

3. Bhagyasree G S, Nithyaja B, Reena V N, Anusha T, Sabari Girisun T. C. (2025). Tunable nonlinear optical responses in defective DNA-capped polyoxometalate ([α-SiW12O40] 4-) one-dimensional silica/DNA/ZnO ternary photonic crystal systems. *Applied Optics*, *64*(9), 2125-2138. (Publisher: Optica)

4. Bhagyasree G S, Sreenilayam S, Brabazon D, Reena V N, Nithyaja B (2022) Transmission characteristics of DNA templated 1D photonic crystal system for 3D printing Simulation. Results in Engineering, 16, 100750. (Publisher: Elsevier)

Coauthored publications

1. Reena V N, Bhagyasree G S, Shilpa T, Aswati Nair R, & Nithyaja B (2024). Multifaceted Applications of DNA-Capped Silver Nanoparticles in Photonics, Photocatalysis, Antibacterial Activity, Cytotoxicity, and Bioimaging. Journal of Fluorescence, 1-15. (Publisher: Springer Nature)

2. Reena V N, Bhagyasree G S, Shilpa T, Aswati Nair R, Misha H, & Nithyaja, B. (2024). Photocatalytic, Antibacterial, Cytotoxic and Bioimaging Applications of Fluorescent CdS Nanoparticles Prepared in DNA Biotemplate. Journal of Fluorescence, 34(1), 437-448. (Publisher: Springer Nature)

3. Reena V N, Kumar K S, Shilpa T, Aswati Nair R, Bhagyasree, G. S., & Nithyaja, B. (2023). Photocatalytic and enhanced biological activities of schiff base capped fluorescent CdS nanoparticles. Journal of Fluorescence, 33(5), 1927-1940. (Publisher: Springer Nature)

4. Reena V N, Misha H, Bhagyasree G S, Nithyaja B. (2022). Enhanced photoluminescence and colour tuning from Rhodamine 6G-doped sol–gel glass matrix via DNA templated CdS nanoparticles. AIP Advances, 12(10), 105217. (Publisher: AIP)

5. Reena V N, Kumar K S, Bhagyasree G S, Nithyaja, B (2022) One- pot synthesis, characterization, optical studies and biological activities of a novel ultrasonically synthesized Schiff

base ligand and its Ni (II) complex. Results in Chemistry, 4, 100576. (Publisher: Elsevier)

6. Reena V N, Shanasree M, Kumar S, Bhagyasree G S, Nithyaja B (2022) Mosquito Larvicidal Activity of DNA Capped Colloidal Silver Nanoparticles. IOP Conference Series: Materials Science and Engineering, 1221, 012051. (Publisher: IOP Publishing)

Conference Papers

International Conference

1. Characterization of Silica/Metal Oxides and Silica/Graphite Oxide Photonic crystals for Enhancing Efficiency Of Solar Cells, Bhagyasree G. S, Nithyaja B. International conference on "Materials and processes for production of solar hydrogen", Online platform,5-7 May, 2021

2. Theoretical Studies of DNA Templated Silica/Metal Oxides One Dimensional Photonic Crystals, Bhagyasree G. S, Nithyaja B, First international conference on Technologies of smart green connected society, online platform, 2021

3. Synthesis and characterization of one dimensional bio-inorganic photonic crystal, Bhagyasree G. S, Akshay Sukumaran, Reena V.N, Nithyaja B, 9 th International Conference on Perspectives in Vibrational Spectroscopy (ICOPVS-22), Indore, 2022

4. Influence Of DNA Template on Nonlinear Optical Properties Polyoxometalate, Bhagyasree G. S and Nithyaja B, Internatinal Conefrence On Advanced Functional Materials -2025, Manipal University, Manipal.

National

1. DNA templated Photonic Crystal system for 3D printing: Simulation, Bhagyasree G. S, Reena V.N. Nithyaja B, National symposium on Women in optics in India 2022 at RRI Bangalore.

2. Effect of DNA-CTAB Capped Silica Nanoparticles on Enhancement of Photoluminescence of Rhodamine 6G Dye Bhagyasree G. S, Nithyaja B, Proceedings of National Photonics Symposium 2023 at Photonics department, Cochin University.

CONTENTS

LIST OF FIGURES

List of tables

Chapter 1

Tailored Microstructures for Manipulating Light: A New Era in Photonics

This chapter explores the domain of photonic crystals, including their general features, theories, classifications, and their relevance to various scientific and technological aspects. The discussion switches to the features and applications of one-dimensional (1D) ternary photonic crystal (PC) systems. The chapter highlights the significant advantages of 1D ternary PCs over 1D bilayer PCs. In addition, it briefly discusses the methods used for fabricating one-dimensional ternary PCs. This chapter is followed by an overview of the various fields that exploit the benefits of 1D ternary PCs. The chapter also addresses the current challenges and prospects associated with these systems.

1.1 Introduction

The growth of science and technology is meticulously linked to the availability and advancement of materials. Specific applications demand materials with tailored properties to meet precise and efficient technical requirements. Hence, materials are the key elements that can be applied for different purposes by adjusting their physical, chemical, electronic and optical properties to meet specific application requirements. In the mid-1960s, a statement by the renowned scientist Richard Feynman about the size of particles illuminated the potential of nanotechnology, paving the way for the emergence of nanoparticles. Evolution of nanomaterials marked a turning point that sparked a long-lasting impact on the field of materials science and technology. Microscopic structures are known to play crucial roles across various scientific fields. Gradually, nanoparticle synthesis has led to widespread exploration and application of methods to tailor particle features. Thereafter, materials at microscopic to nanoscopic scales have been developed, and their tailored features can be used to manipulate various forms of energy arising from the fundamental configurations of material properties, such as mechanical, electrical, and optical characteristics. The scope of tailored materials is being vastly exploited to manipulate light for various applications, which have an inevitable influence in vital scientific sectors such as electronics and semiconductor devices, information technology, telecommunication, and medical diagnosis. Thus, different kinds of materials can be assigned to specific functions. Hence, tailored material properties enable efficient manipulation of different energy

forms, advancing technology in a structured and streamlined manner [1-18].

Eventually, the research focus has mainly shifted toward developing technologies that can control the optical properties of materials. For the past few decades, numerous scientific methods have been developed to engineer these properties in order to tune the desired frequencies of the optical band through reflection and transmission processes. As a result, such materials can be effectively used to confine, reflect, and transmit light waves at specific frequencies. The present telecommunication industry owes much to optical fibre cables, which have brought about transformative and long-lasting benefits to humanity. Alongside laser technology, high-speed computing and spectroscopy are also significant advances arising from the engineered optical properties of materials. [1-23].

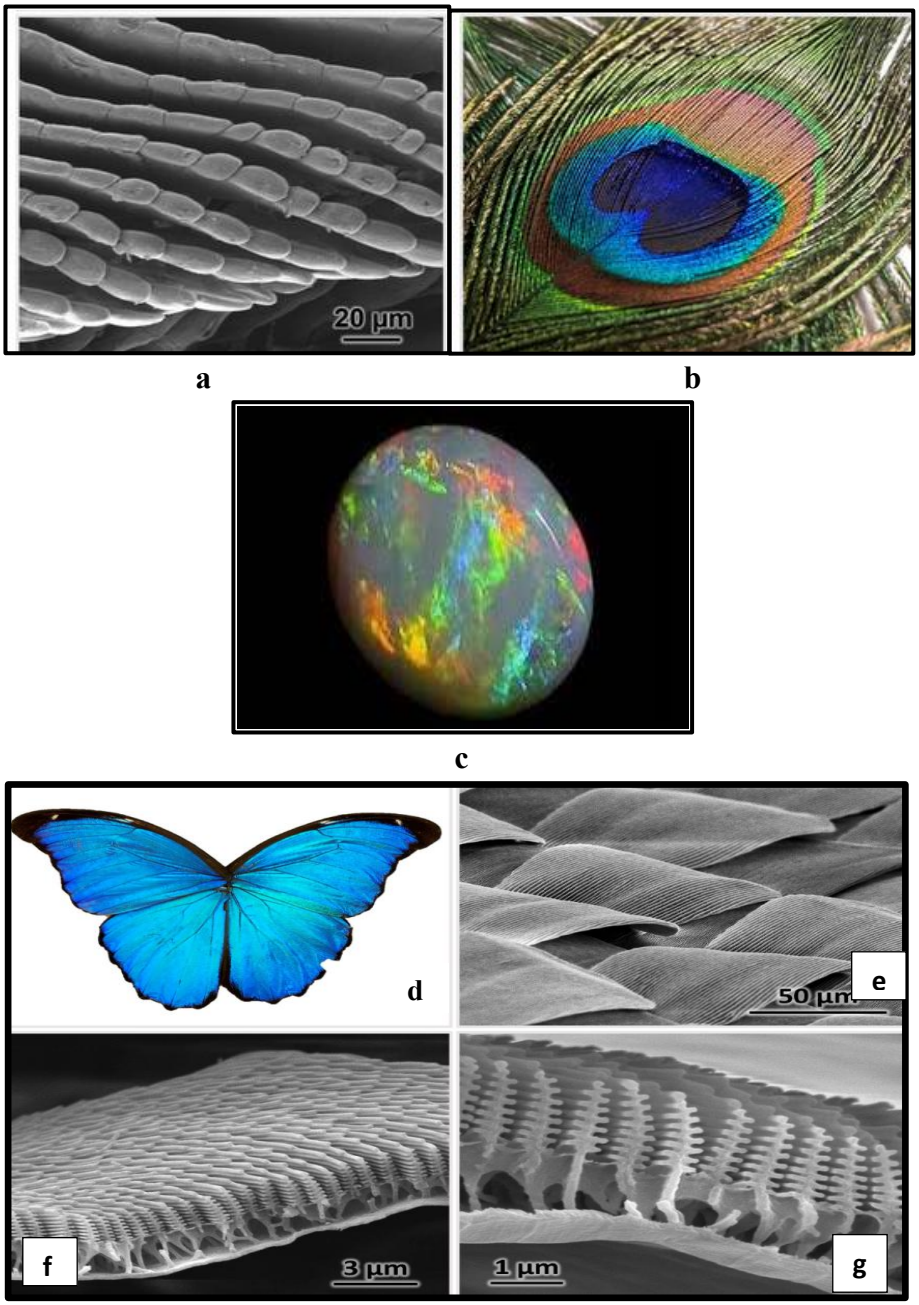

Figure 1.1: Naturally occurring PCs a) feathers of peacock b) SEM of peacock feather c) a gemstone, d) feather of butterfly, e), f) and g) SEM images of f butterfly feather [44-46].

The concept of optically engineered materials dates back to the early 17th century, with Lord Rayleigh's work on periodic dielectric stacks, which introduced the idea of a 1D photonic bandgap (PBG) where specific frequencies of light propagate unidirectionally. This early foundation established the key developments of PCs from 1960s to 1980s, including the discovery of Bragg diffraction and groundbreaking studies by Eli Yablonovitch and Sajeev John, who independently proposed the theoretical basis of PCs in 1987. They demonstrated that periodic dielectric structures could manipulate light propagation in a manner similar to how semiconductors control electron flow via electronic bandgaps [1, 18-60].

The era 1990 faced a drastic revolution of PC structures widely. Theoretical advancements led to gradual experimental realizations of PCs. In the year 1991, E. Yablonovitch et al experimentally fabricated a 3D PC structure [56]. Subsequently, in 1995, 2D PCs were fabricated using etched dielectric materials [57]. The 2000s witnessed rapid progress in 2D and 3D PCs, including the development of PC fibres. In 2003, a complete 3D PBG (PBG) was experimentally verified [60]. Recent research brought topological PCs, expanding applications in communications, sensing, and nanophotonics [1-60].

Though typically PCs are structurally analogous to atomic crystals, they differ in scale and propagation principles. Instead of affecting electrons via periodic atomic potentials, PCs modulate light through periodic variations in the refractive index, forming PBG where a range of frequency of light propagation is forbidden [1-40].

In principle, the PCs are engineered microstructures that control light via constructive and destructive interference caused by periodic dielectric contrasts. The PBG is central to their functionality and depends on parameters such as the periodic length scale (comparable to the wavelength of light), refractive index contrast between the adjacent materials, number of periods, and structural geometry [1-60].

Theoretically, the PBG effect arises from multiple scattering at the interfaces within a periodic medium, leading to constructive and destructive interferences and forbidden frequencies for light, analogous to electronic bandgaps in semiconductors. The bandgap's width and position can be tuned by altering refractive index contrast, lattice symmetry (e.g., square, hexagonal, cubic), configuration (1D, 2D, and 3D), and lattice geometry, enabling diverse and tunable optical properties for advanced applications [1–60]. Figure 1.1 displays examples of naturally occurring PCs [44-46]. The Figure 1.1a shows a peacock feather, and its SEM image, revealing the periodic protein structures, is presented in the Figure 1.1b [44]. Figure 1.1c [45] represents the surface of a gemstone, while, Figure 1.1d shows a butterfly wing, Figure 1.1e, f, and g show the SEM images of feather of butterfly [46]. It is well clear that the examples of naturally occurring PCs shown in Figure 1.1 come in the range of microscopic scale. The multi colors seen on the body of such creatures are arisen when the periodical arrangement of microscopic particles presents in their body interact with light and create PBG for specific light resulting reflection of those light waves.

1.2 Configuration of photonic crystals

In describing all the properties of PCs, it is unavoidable to discuss their classification. The general properties, such as unit cell, period, PBG, and dispersion relation, differ in different types of dimensional PCs. Basically, PCs are classified by the number of spatial dimensions in which their periodicity exists. The features of PCs are vast in their variety. Based on the light confinement in PCs, they are classified into three categories. As previously mentioned, PCs are made up of a periodic alignment of alternatively placed micro-sized thicknesses of dielectric thin films in space. Due to these alternatively placed dielectric constants, a fixed refractive index contrast is achieved between the adjacent layers or interfaces of the unit cell of the PC. The refractive index contrast repeats throughout the entire PC after a particular period length (repetition of the unit cell). The direction of repetition of the refractive index contrast defines the direction of the propagation of light and the dimension of the PC. Therefore, PCs are divided into three categories based on the direction of confinement of light within the structure [1-24].

1.2.1 One-dimensional photonic crystals

Among the various kinds of configurations, 1D PCs are the most widely recognized and simplest structures of the PC family. They offer highly tunable PBGs, birefringence, and homogeneous structures. They avoid fabrication complexities compared to other higher-dimensional PC structures. Their simple configuration makes them easily fabricable for integrated photonic devices. According to the properties of 1D PCs,

light confinement takes place along a single direction only. Generally, a 1D PC is a planar structure where the refractive index varies along a single spatial direction by arranging different layers of materials with different dielectric constants in an alternating periodic order, which leads to the restriction of propagation of light to a single direction. The stratified periodic structures cause destructive and constructive interferences, resulting in a pass band where a certain range of frequencies can pass through, and a forbidden gap that prevents the passage of certain wavelengths falling within the PBG frequency range [1, 23-40].

The unit cell of a 1D PC consists of two or more alternating layers of different dielectric or metal/dielectric thin film microstructures. The period of the structure is defined as the sum of the thicknesses of the adjacent layers in the unit cell. The PBG increases as the refractive index contrast between the adjacent dielectric layers increases. Figure 1.2 represents the schematic illustration of a 1D bilayer PC, where the unit cell consists of two elemental layers having refractive indices n_1 and n_2 and thicknesses d_1 and d_2 with a period N = 4 (N is taken as an arbitrary value) and lattice parameter d, which accounts for the sum of d_1 and d_2, respectively.

In summary, the 1D PCs are mainly applicable to silicon-based photonic devices and integrated photonic systems, where photons replace electrons. Examples of 1D PCs include multilayer dielectric mirrors or Bragg reflectors, in which alternating dielectric/metal-dielectric layers are arranged in a stacked structure along a single direction. Their roles in biochemical, physical, and solar cell sensing,

as well as in nonlinear optical studies, have attracted extensive research attention [24-40].

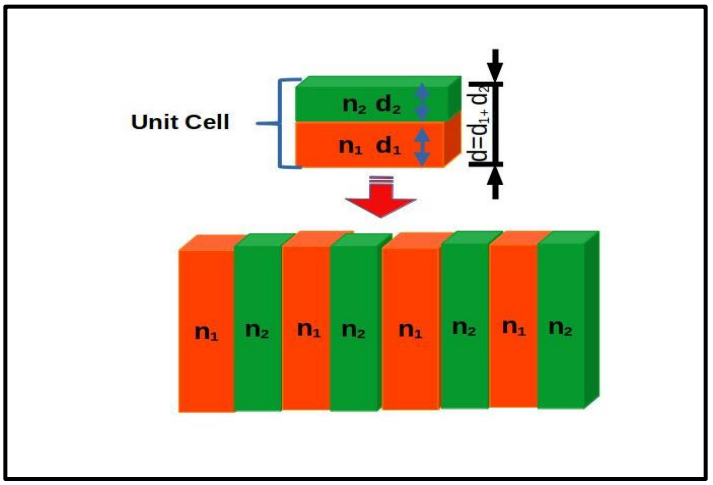

Figure 1.2: Schematic representation of a of 1D PC where N=4

1.2.2 Two- dimensional photonic crystal

In the context of 2D PC, it contains regularly arranged rods or holes in a plane surface of a dielectric matrix, which gives rise to a perforated surface appearance. In such a case, the refractive index varies along two independent spatial directions. Thus, light is confined to two dimensions only. The 2D PC offers versatile topological symmetries. Generally, the unit cell structures of 2D PC include square, hexagonal, and triangular lattices. The symmetry of the unit cell plays a crucial role in determining the PBG effect. The symmetry can be classified into various groups based on the arrangement of holes and rods in the lattice. For instance, a square lattice has 4-fold symmetry, while a hexagonal lattice has 6-fold symmetry. The higher the symmetry, the more directional control over the light's propagation the system can provide, and it can result in more robust and wider PBGs. Additionally,

symmetry can also influence the dispersion relations of the system specifically, how the wavevector relates to the frequency of light, which is key to understanding how light behaves in a PC [41-47].

When considering the PBG formation in a 2D PC, it arises due to the periodic arrangement of the materials, which causes constructive interference between waves at different points in the lattice. It can be tailored to operate in specific frequency ranges in the optical band (visible, IR, and microwave bands), depending on the material and design. However, based on the periodic array of crystal lattices, they are classified into three types. They are square lattices, hexagonal lattices, and honeycomb lattices.

a. Square lattice of circular holes: They are the simplest and most studied designs, in which a periodic array of air holes is drilled into a dielectric matrix (eg, silicon) in a square lattice. Figure 1.3a represents a schematic view of a square lattice of 2D PC and Figure 1.3b represents its first Brilliouin zone.

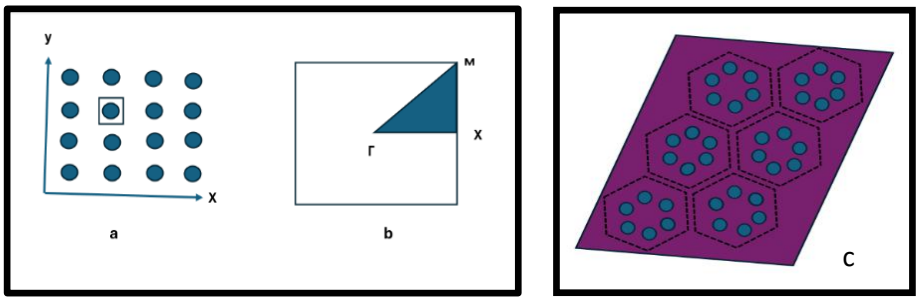

Figure 1.3: Square lattice, b) its first Brillouin zone of square lattice, [54], and c) Hexagonal lattice of rods or holes [50]

b. Hexagonal lattice of rods or holes: This structure is composed of a regular repetitive arrangement of dielectric rods/cylinders (or other

shapes) in a hexagonal structure. It is a more complex arrangement that can support a broader and more versatile bandgap compared to the square lattice. This structure often provides better light confinement, a tunable PBG, and the features of the PBG remain uniform in all directions. Figure 1.3c displays the schematic image of the hexagonal lattice structure of 2D PC [46-48].

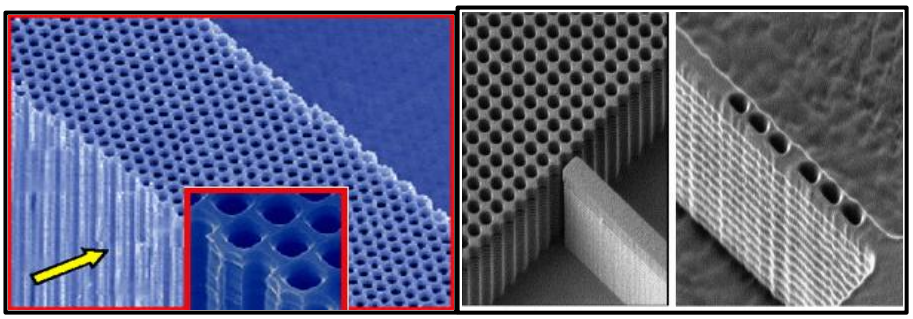

a **b**

Figure 1.4: a) and b) SEM images of honeycomb structure of 2D PC [50-51, 53-54]. Inset shows an enlarged portion of honeycomb structure.

c. Honeycomb (triangular) lattice:

Figures 1.4a and 1.4b show an SEM image of the honeycomb structure of a 2D PC, a commonly used configuration for specialized applications [52]. Figure 1.5 a displays the triangular lattice and Figure 1.5 b represents its first Brillouin zone. Due to their structural features and unique light confinement capabilities, 2D PCs play a vital role in advanced optical and electronic technologies. They are used to guide light in photonic circuits, act as optical filters, trap light in resonators, and enhance laser performance by precisely controlling emission properties. Their ability to respond to environmental changes makes

them suitable for biosensing and chemical detection. Additionally, certain 2D PCs can be engineered to slow down light, improving light–matter interactions in nonlinear optical applications. These features highlight the potential of 2D PCs in enabling the development of next-generation optical devices. [41-55, 55].

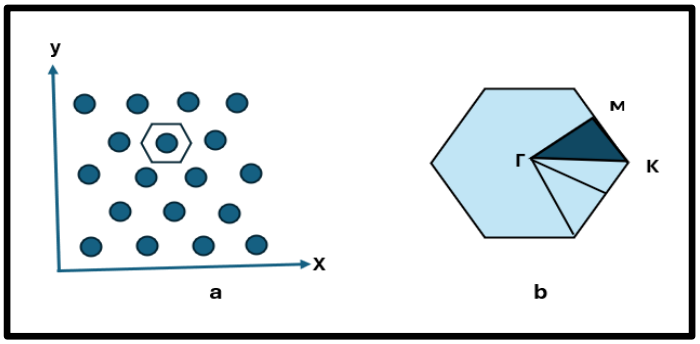

Figure 1.5: a) Trigonal lattice and b) it's first Brillouin zone [54]

1.2.3 Three -dimensional photonic crystal

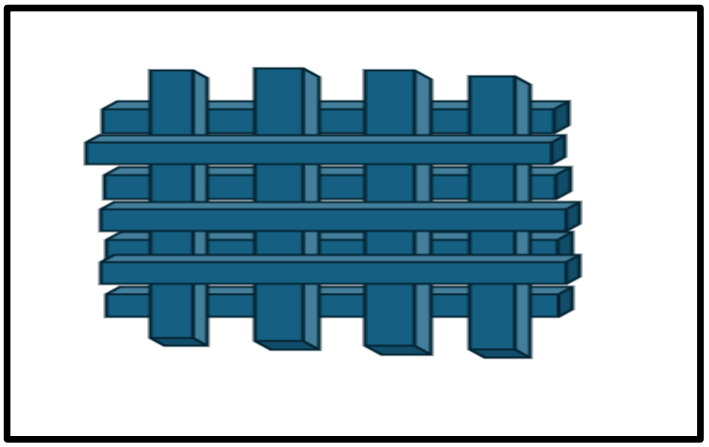

Figure 1.6: Schematic representation of 3D woodpile PC [57]

The periodic microstructures of dielectric materials in which the refractive index variation occurs in all three spatial directions are called three-dimensional (3D) PCs. They extended the concepts of 1D and 2D PCs into three dimensions. Therefore, they can confine and control the propagation of light more effectively than other dimensional PCs. A 3D PC consists of a periodic arrangement of materials with different refractive indices defined in 3D space. This periodicity influences the light propagation through the microstructures. The structure size can be about various length scales, typically ranging from hundreds of nanometers to a few micrometers, aligning with the order of the optical band. Similar to 1D and 2D PC structures, they can be made up of materials including dielectric, semiconductors, and metallic materials. The periodic structures can take any lattice form, such as simple cubic, body-centered cubic (BCC), and face-centered cubic (FCC) lattices, which all depend on the design as well [1,23,55, 57-63].

The symmetries of a 3D PC refer to the inherent geometric and translational properties of its periodic structure that determine whether the modes are allowed to propagate through the structure. The 3D PC lattice exhibits translational, rotational, mirror, inversion, screw and glide, and point group symmetry [55, 57-62]. Figure 1.6 shows a schematic representation of 3D woodpile PC [57].

According to the light manipulation of 3D PCs, they exhibit high efficiency in guiding light along specific directions. The localization of light is highly enhanced in 3D PC, causing light to become trapped in certain regions, similar to electron localization in defective

semiconductors. In some designs, they can slow down light, which can be suitably used for increasing interaction between light and matter. These features make 3D PCs a promise of laser devices [56, 58-62].

The fabrication of 3D PCs can be realized through various methods such as self-assembly, lithography, and additive manufacturing. These methods are generally classified as either top-down or bottom-up approaches. The top-down methods include techniques like photolithography, where the structure is etched or patterned onto a substrate. These methods can provide high-quality PCs but may face limitations in scaling to 3D structures. The bottom-up methods involve a self-assembly process where materials spontaneously organize into the desired periodic structures. Techniques like colloidal crystal assembly or molecular beam epitaxy (MBE) can be used to create 3D PCs. Hybrid methods are also approached for fabricating 3D structures, where both top-down and bottom-up techniques are combined to fabricate [55, 57-58].

Due to their versatile structural features and ability to control light in all directions, 3D PCs have spanned their roles in modern photonics and optoelectronics. They are used in optical communication and switching systems to enhance data transmission efficiency and reduce signal loss. Their wavelength sensitivity makes them ideal for sensing applications such as biosensing, chemical detection, and environmental monitoring. In photonic devices like filters, beam splitters, and lasers, 3D PCs offer precise light manipulation, enabling the development of compact and efficient photonic circuits. In 2023 R. K. Gangwar et al reported a review on PC structures where they described that 3D PC

structures also enhance light trapping in solar cells, improving energy conversion efficiency, and are essential in microcavity design for stronger light–matter interactions in miniaturized lasers. In the realm of quantum technologies, 3D PCs facilitate control over photon states and entangled photon generation, aiding advancements in quantum computing and photonics [62-63].

Additionally, their integration into photonic circuits allows for sophisticated on-chip optical processing. At the same time, their structural configurations contribute to metamaterials with unique optical properties, beneficial for innovations like invisibility cloaks and superlenses. The most significant advantage of 3D PCs is their ability to exhibit a complete PBG in all directions, owing to their high symmetry and periodicity [1, 23-24, 55-63].

1.3 Structural parameters of photonic crystal

A comprehensive understanding of PBG effects requires consideration of key structural parameters that define the nature of PCs. The formation of PBG and its properties are influenced by several factors including dielectric property of the elemental layers, thickness of the elemental layers, periodicity, symmetry, and unit cell. These factors collectively determine the formation and characteristics of the PBG, offering a complete structural description of a PC [1-69].

1.3.1 Elemental layers of photonic crystal

The selection of elemental layers is a crucial aspect in designing a PC, as they serve as the fundamental building blocks of a PC. The choice

of materials typically focuses on parameters such as refractive index, bandgap range, isotropy, optical properties, fabrication feasibility, and long-term performance.

Interestingly, the unique property of PCs lies in their ability to be selectively opaque to specific frequency ranges. It is achieved by constructing a structure in which transparent thin films are alternately stacked. This arrangement allows the PC to exhibit reflective properties, depending on the specific configuration and orientation of the dielectric layers.

One of the main factors contributing to the formation of a PBG is the refractive index contrast between adjacent dielectric layers. The refractive index contrast plays a critical role in determining the size (width) and effectiveness of the photonic band gap. When materials are arranged in a lattice, the initial layer upon which light is incident should be a low refractive index material, followed by a high refractive index material. This configuration helps to confine light more effectively.

Another factor regarding the material criteria of PCs is the bandgap range, which is to be manipulated. Certain materials possess a wide range of bandgap within the optical band, such as silicon and gallium arsenide. This will be essential for tuning desired band structures of the PC for operating at infrared and telecommunication bands, where PCs become a focus of wide research interest.

Among all the criteria for material selection, the most important consideration is to fulfill all these requirements together in a practical,

durable, and economical manner during the fabrication of the PC. The main challenges faced during the fabrication process include the feasibility of making the dielectric thin films, compatibility with the fabrication process, and high reproducibility. Alongside, the physical properties of the material always influence precise fabrication. Materials with isotropic properties are highly recommended for the fabrication of PC structures due to their uniform mechanical, electrical, thermal, and optical properties, as well as their symmetry. These properties do not depend on the direction in which they are measured. More precisely, the response of isotropic materials is uniform in structure and behavior when stress, strain, heat, or electrical current is applied. It can help to avoid situations such as optical energy absorption and a decrease in thermal resistance. These characteristics enhance the stability and durability of the PC. This symmetry and these properties make PCs more durable and stable structures [1-69].

1.3.2 Symmetry of photonic crystal

The symmetry defines the entire structural properties of the PC, which refers to the invariance of its structure under various transformations, such as translations, rotations, and reflections [1,5]. It reveals the nature of the structure, such as whether they are anisotropic or isotropic. These symmetries help to shape the band structure, dispersion relation, and PBG of the material. In PCs, symmetry plays a crucial role in determining the behaviour of light within the material, especially in terms of how light interacts with the periodic structure. PCs are defined by their periodicity of arranging microstructures that decides the formation of the PBG effect. John D. Joannopoulos et al

[1] explores different symmetries of PC structures. Vaidya S et al [63] reported the topological phases of symmetris of PC structures. Thus, different symmetry defines the nature of the formation of PBGs [1-23]. Generally, a 1D PC follows a simple symmetry of arrangement of lattice space [1-23]. However, 2D PC generally exhibits a square lattice, hexagonal or triangular lattice structure, and 3D PC follows comparatively complex symmetries [1-23]. As symmetries go higher and complex, the PBG goes wider. Various symmetries are typically associated with different lattice structures and dimensionalities of the PC (1D, 2D, and 3D) [1-63]. They are as follows;

a. **Translational symmetry** is one of the symmetries associated with the lattice structure of the PC. When the lattice parameter of the unit cell is shifted, the properties of the entire structure remain the same as before. It is the fundamental symmetry that creates a PBG. It determines the periodicity of the crystal and affects the allowed and forbidden energy bands of light. In most cases, 1D PC exhibits translational symmetry.

b. Rotational symmetry refers to the invariance of the PC structure under rotation by a certain angle around an axis. Rotational symmetry can create the degeneracy of the photonic bands along specific directions in the Brillouin zone. Rotational symmetry can create the degeneracy of the photonic bands along specific directions in the Brillouin zone. 1D PC often exhibits simple rotational symmetries (e.g., 180^0 or 360^0), whereas 2D PC exhibits complex rotational symmetries and follows 60^0, 90^0, and 120^0 rotations for hexagonal and square lattices. As 3D PCs have

possessed cubic, tetrahedral, and octahedral lattices, they can have high rotational symmetries, including 4-fold, 3-fold, or 6-fold symmetries, respectively.

c. **Mirror symmetry (Reflection symmetry)** defines that the properties of PCs remain unchanged under mirror plane. This symmetry can often influence the polarization, propagation direction of light and lead to degeneracy of photonic band gaps where PBGs will be symmetric with respect to a mirror plane. Thus, a symmetric dispersion relations would be assigned for light travelling in opposite directions.

d. **Inversion symmetry** can lead to the degeneracy of modes.

e. **Bravais lattice symmetry (Symmetry of the Lattice)** describes how different geometrical structures define different symmetries based on their periodicity. The geometrical arrangement describes a group of symmetries derived from the Bravais lattice system. Higher-dimensional PC structures, such as 2D and 3D PCs, possess the Bravais lattice symmetries. For 2D photonic lattice structures, including square, rectangular, and triangular lattices, and 3D crystals, the most common Bravais lattices are cubic, body-centered cubic (BCC), and face-centered cubic (FCC) lattices. The symmetry of the Bravais lattice conforms to the allowed symmetry operations, such as translational, rotational, and reflection. It has impacts on polarization of light, dispersion relation, PBG formation, and the localized modes within the structures as well.

Moreover, symmetry of a PC directly influences its optical properties, such as the formation of the PBG, the propagation of light, and the polarization states of electromagnetic waves. By carefully choosing the symmetry and structure of the PC, designers can tailor the crystal for specific applications, such as light guiding, sensing, or filtering. Understanding the symmetries in PCs is thus essential for predicting and controlling their behaviours in various optical devices [1].

1.3.3 Unit cell

The smallest repetitive structure that defines the periodicity of the optical properties of a PC is referred to as the unit cell of the system. A unit cell is constituted of elemental layers designed to manipulate electromagnetic waves in the optical band through periodic structures. These repetitive units are responsible for creating PBG to reflect a certain range that comes in the optical band of electromagnetic waves.

The unit cell consists of two or more elemental layers with differing refractive indices. The lattice space where all the elemental layers are arranged in a unit cell is called the lattice parameter, analogous to the lattice in a crystal structure, where atoms/electrons are arranged periodically in a unit cell. Based on the geometry of elemental layers, the geometry of the unit cell is also varied. For example, a stratified unit cell is used in the design of planar PCs, also known as 1D (1D) PCs. Structures such as dielectric rods or air holes within a dielectric matrix are characteristic of two-dimensional (2D) and three-dimensional (3D) PCs. Depending on the design, the unit cell arrangement can follow simple cubic, hexagonal, or face-centered cubic lattice structures [1-63].

Additionally, the unit cell possesses certain fundamental features that are essential for the configuration and characterization of a PC [1-63]. They are;

a. Symmetry: Based on the Bravais lattice of the unit cell, the properties of the entire structure remain the same in all directions or along a specific direction, depending on the crystal type.

b. Size: The size of the unit cell typically comes in the order of the wavelength of light over which the crystal is designed to manipulate.

c. Materials: In principle, the unit cell consists of a high refractive index material and a low refractive index material.

d. Dimensions: The unit cell exhibits three different dimensions that depend on the direction in which the refractive index variation occurs. Based on this fact, a unit cell of a PC can be seen in 1D, 2D, and 3D structures. Thus, the entire structure of the PC follows the dimensions of its unit cell.

1.3.4 Period

The period of a PC refers to the special repetition unit of the periodic structure that defines the crystal. The tailored microstructures, PCs, are the materials that have a periodic arrangement of dielectric or metallic microstructures on the scale of the wavelength of light. These periodic structures are responsible for the complete control of the propagation of the wavelength range of interest in a way that semiconductors control electron flow.

The period is measured as the distance over which the properties of elemental structures repeat, and it is denoted as '**a'.** The period is a

function of the dielectric constant, as the spatial repetition of the unit cell is based on the dielectric contrast between the dielectric layers. Generally, the scaling of the period is comparable to the wavelength of light in the material. However, the exact size depends on the PC's design and the wavelength range of interest. However, in a dimensional PC, the period is the sum of the thickness of each layer of a unit cell. In other words, the distance between the adjacent unit cells of a PC or lattice parameter. In a 2D and 3D PC, the period is the spacing between the repeating unit cells in the respective directions [1-64].

1.4 Defects

The structural imperfections, called defects highly influence the optical properties of PCs, analogous to the structural imperfections seen in semiconductors. Defects play a crucial role in manipulating the optical properties for desired applications of PCs. Their presence enhances the scope of PC- based applications, including sensing, nonlinear optical devices, waveguides, and optical filters. Generally, the defects affect significant variation over the properties of PCs; however, they can improve the scope of tailored functions of PCs for vivid applications. Usually, the presence of defects introduces a perturbation in the PBG. A defect can trap specific frequencies of light within the PBG, causing the light to become localized around the defect. Despite the periodic structure of a PC, which provides the PBG to control the propagation of light, defects can modify the bandgap and influence the way light behaves, especially in terms of how it propagates, interacts with the crystal, or becomes confined. Defects can be intentionally introduced

into PCs to modify their optical properties. Alternatively, imperfections may occur unintentionally during fabrication. Intentionally created defects are designed to serve various purposes, such as [1-60]:

1.4.1. Creation of defect modes (Localized states)

A defect mode or localized state is created when a defect is introduced into the unit cell structure using an additional new layer in between the constituent layers, or by removing an existing layer from the unit cell. The missing layer or the additionally included layer for creating defect mode is known as the defective layer of the PC. The defect mode is a state where light is trapped within the PBG. The advantage of creating defect modes is that they can interact with the material, which can be utilized to enhance light-matter interactions. It is commonly applied in areas such as nonlinear optics and quantum effects. The defective PCs are highly useful for applications including microcavities, lasers, and resonators where defective modes are confined in a defective region, which enhances interactions with materials [1-60].

Regardless of the dimensionality of PCs, defect modes can be introduced in 1D, two-dimensional, and three-dimensional PCs. In a 1D PC, the missing layer or addition of a new layer creates a localized state (defective mode) within the PBG. It can be utilized for sensing applications where the defective layer acts as the analyte that is to be analysed. Besides, nonlinear material can also be introduced as the defective layer, and the defect mode generated in this manner can be utilized in lasing applications. A similar way can be used to create

defect modes in 2D and 3D PCs to be subject to applications like microlasers, sensors, and optical resonators [1-60].

The light confinement effect of defect mode can be exploited for applications like waveguides which to be used for guiding the path of light to a confined route or direction without significant loss. It can be achieved by creating either linear defects in 1D PCs or curved defects in complex structures like 2D and 3D PCs. It will be useful for integrated photonic devices and on-chip optical devices.

Additionally, defects can tune the PBG and photon transmission. The presence of defects can alter the size and shape of the PBG which resulting in a shift of both the frequencies at which light propagates and the forbidden. It is how PCs can be selectively tuned for desired (specific) frequencies for transmission while blocking others. Thus, they are placed to apply highly effective optical filters. The formation of microcavities is another prominent feature possessed by the defective PCs, which is important to enhance the interaction between light and matter. When creating defects like small holes or variations in the periodicity of the dielectric function in the microstructure, the microcavities are formed, the small regions where light is trapped and allowed to resonate. This feature is engineered in devices like optical sensors, microlasers, and quantum light sources with the intention to confine light with low loss. For high-efficiency lasers, modes with low decay rates are important, such that a defective PC micro cavity can be designed to support studying quantum effects in light-matter interactions [1-60].

In some PCs, defects can lead to the formation of flat bands, where the photonic density of states remains uniform at specific frequencies. The flat band modes feature highly localized light modes and a high density of states can provide intense light–matter coupling will make them highly useful for generating entangled photons in quantum optics applications and nonlinear optical devices. Moreover, defects in PCs are not merely imperfections but an effective tool that can be purposefully exploited to manipulate and control light in desired ways. Thus, the engineering ability and precision to break the structural periodicity of PCs opens up a wide range of opportunities for the development of advanced photonic technologies [1-64]

1.5 Characterization of photonic band gap effect

The features of the PBG effect can be explored through several ways, including experimental and numerical methods. The spectral characterization of the entire crystal structure needs specific numerical methods to solve the electromagnetic wave propagation [1-69].

1.5.1 Dispersion relation and photonic band structure

The dispersion relation in PCs describes the relationship between the frequency (or wavelength) of light and its wavevector as it propagates through the structure. Fundamentally, it is important for understanding the photonic band structure, which determines which frequencies of light can or cannot propagate through the PC. Thus, the dispersion relation for PCs shows how the frequency of light varies with its wavevector (spatial frequency) in different directions of the crystal. This relationship is central to the behavior of electromagnetic waves in

periodic media, and it ultimately determines the presence of the PBG. The unique feature PBG is the result of destructive interference, which prevents specific wavelengths from propagating along certain directions. Hence unit cell is enough to describe the dispersion relation of a PC, as it is essential to know the symmetry and dimensions of the unit cell.

However, the dispersion relation can be represented by the plot of the band structure of the system. The photonic band structure is a plot of the relation between the photonic frequency (wavelength) and the wave vector (spatial frequency). Therefore, a photonic band structure displays the optical transfer properties of a PC. The band structure, which describes the entire allowed modes and forbidden modes of a PC characterized by the dispersion relation of a PC in the ω-k space. The band structure analysis provides detailed information about the regions where allowed solutions exist, meaning light can propagate, the presence of continuous dispersion curves, and the PBG, which refers to a range of frequencies where no solution for light propagation exists and light cannot pass through the PC. In the photonic band structure plots, the bandgap is typically observed along specific directions in the Brillouin zone of the crystal, which is the reciprocal space corresponding to the periodic lattice [1-69].

1.5.2 Dispersion Relation in 1D, 2D, and 3D photonic crystals

a) 1D PCs: A 1D PC typically consists of alternating layers of two materials with different refractive indices. The dispersion relation in this case is relatively simple, and the PBG arises due to the periodic dielectric structure along one dimension.

b) 2D PCs: In a 2D PC (e.g., a square or hexagonal lattice of holes in a dielectric material), the dispersion relation is more complex, and the bandgap can appear for light traveling in specific directions in the plane of the crystal.

c) 3D PCs: A 3D PC has periodicity in all three directions, resulting in a more intricate dispersion relation and potentially a full 3D PBG that blocks all propagation directions for specific frequencies.

Thus, based on the classification of PCs the nature of dispersion relations also varies. Besides, the dispersion relation briefly illustrates the allowed mode and prohibited mode of propagation of light.

1.5.3 Methods for finding the dispersion relation

There are several methods to calculate the dispersion relation in PCs. These methods are based on solving Maxwell's equations in the context of the crystal's periodic structure. For a 1D PC, the first Brillouin zone is defined as the locus of wave vectors. The dispersion relation of the unit cell gives the complete information about the allowed modes and prohibited modes of the entire PC system. Such that the wave vector change in the first Brillouin zone can obtain the solutions of the fundamental equations (eigenvalues) of PCs. Electromagnetic modes with discrete resonant frequencies can arise from the boundaries of the Brillouin zone, which represent the loci of wave vectors where Bragg reflection occurs, acting as reflecting planes. Below are some of the main techniques used to solve the eigenvalue problem of the master equations in PCs to determine the dispersion relation [1-69]:

1. Plane Wave Expansion (PWE) method

The plane wave expansion method is one of the extensively used powerful computational techniques in electromagnetics to solve Maxwell's equations by creating an eigenvalue problem apart from the equations over an inhomogeneous or periodic structure. This method is widely recognized and popular for solving the photonic band structure (dispersion relation) in PCs. It assumes a linear combination of plane waves as a solution of Maxwell's equation in a defined lattice. It expresses the electric field as a sum of plane waves. It can be applied in the Fourier domain using the periodicity of the dielectric function for the dielectric structures to find the eigenfrequencies and wave vectors that satisfy the boundary conditions of the system. J. Vasseur [64] reported the features of PWE method in detail for aquastic metamaterials. In 2024, A.F. Fernanda et [65] all studied the PBG of 2D PC structures. It is very easy to obtain the band structure once the direction is specified. This method provides all the propagating modes along the specified direction [64-66].

The method can be applied well for periodic PCs for arbitrary shapes and complexities. It provides accurate results for both the band structure and dispersion relations. On the contrary, the PWE method faces computationally expensive, especially for 3D crystals with complex structures. So that this method is linked to the memory storage that depends on the number of plane waves used for the expansion of the field, and this number escalates when the PC diverges from a periodic structure. Besides, the calculation of defects is not possible by this method [1-66].

2. Finite Difference Time Domain (FDTD) Method

The finite difference time domain method is one of the renowned numerical computational methods to solve electromagnetic wave propagation that uses the fundamental Maxwell's equations of electromagnetic waves for a given structure [1]. This method is widely recognized as one of the simulation tools for solving the master equation of a PC to obtain band structures. The FDTD method adopts a simulation over the time evolution of the electromagnetic fields [1, 5, 26, 30, 67-68]. It extracts the band structure by analysing the time response of the system rather than solving the dispersion relation directly. For this, the crystal structure is discretized into a grid to solve Maxwell's equations for the time evolution of the electric and magnetic fields. The FDTD method is simulated by performing a Fourier transform for the time domain solutions to the frequency wave vector space domain to obtain the dispersion relation. The FDTD method is suitable for handling materials including periodic, non-periodic, arbitrary, and complex geometry structures. Along with this, it is highly flexible and able to model the effects of defects or nonlinearities in PCs. Despite its efficiency in modelling higher-dimensional and defect-oriented PC structures, it is more computationally expensive than the plane wave expansion (PWE) for extensive or highly detailed structures. Additionally, it requires large amounts of computational power for accurate results [1, 69].

3. Finite Elemental Method (FEM)

The finite elemental method is another numerical simulation technique used for solving the photonic band structure [1, 5, 26-27, 30, 69]. In this method, the structure is divided into a mesh of small elements, and

Maxwell's equations are solved for each element. The eigenvalues and eigen vectors corresponding to the allowed frequencies and wave vectors are then computed to display the dispersion relation of the specific PC structure. This method is often used for solving complex geometrical structures of materials with homogeneous properties. The method is beneficial for complex geometries and heterogenous structures such as 3D PCs and is adaptable to different materials and boundary conditions. Despite these merits, the FEM method requires a good understanding of mesh generation and boundary conditions; otherwise, it could be computationally intensive [1, 26-27, 69].

4. Transfer Matrix Method (TMM)

The transfer matrix method (TMM) is known as the simplest and frequently used numerical computational method in various fields of science and engineering. The method is applicable to analyse layered structures such as wave propagation through different media or vibrations of multi-layered beams. It is widely applied in fields such as optics, acoustics, and structural dynamics. The transfer matrix method uses a matrix to explain how the properties of a structure (periodic structure) change as electromagnetic waves or signals propagate through different components of the structure. The system is divided into smaller sections as layers so that the transfer matrix method performs on a layer-by-layer structure to solve Maxwell's equations. The TMM provides the dispersion relation, reflectivity, and transmission coefficients [1, 5, 26-27,30].

The dispersion relation of PCs of 1D, 2D, and 3D structures can be figured out using TMM in the wave vector space and rewriting them

on a mesh. The defective structures are considered as a supercell to perform calculations. Despite its demerits linked with memory storage, due to accuracy, and simplicity in the performance of analysis, TMM is widely used among researchers [1-69].

a. Transmittance spectrum

The characterization of a PC can be observed by obtaining the transmittance spectrum. It displays the allowed band and forbidden band width when an incident light is propagating through a PC. The transmittance of the band width at which the PBG is ideally zero in a transmittance spectrum, whereas at the pass band it would be 100%. In a transmittance spectrum, the dip formed along the spectrum represents the frequency range of the PBG. Despite the material intrinsic absorption, the transmittance spectrum gives the complete information of the PBG, such as the position and frequency range as well [1-38]. It can be experimentally tracked by using spectroscopes such as UV-VIS spectrometers and reflectometers. The theoretical study of transmittance spectra can be studied using the support of numerical methods, including TMM, FEM, PEM, and FDTD, and several software also available, such as Lumerica and Comsol [1-69].

b. Reflectance spectrum

The reflectance spectrum of a PC gives rise to the frequency range of both the photonic band gap and the pass band. The dip along the reflectance spectrum represents the frequency range of propagated waves, so that the reflectance of the pass band is ideally zero. The peak shown in a reflectance spectrum represents the PBG of the system, and

the reflectance of the corresponding frequency range would be shown as 100%. Despite the intrinsic absorption of the material, the reflectance peak gives the exact frequency range and the position of the PBG [1-69].

1.6 Quality factor

Quality factor (Q) of a PC plays a crucial roles in the functioning of a PC. It refers to how efficient a PC in order to respond against the change in the defect mode shift formed as a result of the change in the periodicity (defect) of the structure. It is the ratio of the resonant frequency to the full width at half maximum (FWHM) of the resonant peak. More specifically Q factor describes how efficient a PC is against an infinitesimally small change in the periodicity of the structure. It indicates that the narrower the defect mode, the more efficient the PC to trapping the defect mode. Applications such as sensors, nonlinear PCs for lasing, and optical filters are based on the Q factor of the PC. If a PC with a high Q value, it means that the PC is highly capable of showing a change in the defect mode [1,5,42].

1.7 1D Ternary photonic crystals: a review

Generally, 1D all-dielectric or metallo-dielectric PCs are designed using two or more dielectric materials arranged alternately in a periodic structure. Depending on the demand of outcomes, the designing of the PBG can be controlled by the structural parameters and the refractive index contrast between the adjacent materials. So far, due to the simplicity in designing and fabrication, 1D bilayer PCs are widely considered for research interest. Though the 1D PCs that have more than two distinct dielectric layers are also found to be significant

for their efficiency in tuning the PBG at the desired wavelength range. Moreover, they are also efficient for confining localized modes with a high Q value. They can be applicable to design tunable omnidirectional reflectors, infrared reflectors, optical filters, sensors, and lasers. They can also be designed with metallo-dielectric layers and metamaterials similar to the designing of 1D bilayer PC structures [1, 43,58-83].

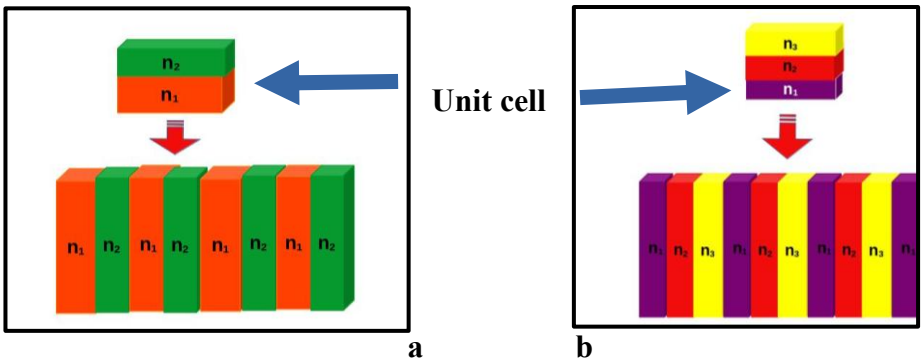

Figure 1.7: Schematic representation of a) 1D bilayer PC and b) 1D ternary PC

Figure 1.7 a represents a schematic representation of 1D binary (bilayer) PC and Figure 1.7b represents the schematic representation of 1D ternary PC structure.

Among various configurations of 1D PCs, 1D ternary PCs have garnered the attention of recent photonic research. 1D ternary PC is constituted with unit cells of three different dielectric materials. Apart from dielectric materials, the choice of materials can be extended to different combinations that are used generally or in the fabrication, such as metals and metamaterials. This configuration provides tunable PBG effects that are more beneficial than those of the bilayer configuration. The differences between 1D ternary and bilayer

structures arise from the nature of the PBG. The 1D bilayer PC forms a single PBG in the optical band, whereas 1D ternary structures form more than one PBG within the optical band. Besides, the PBG exhibits a large width. The defect mode shows high intensity, and the full width at half maximum (FWHM) has a significant value when compared with its counter bilayer structure. Their response to shifting the resonant mode with respect to a change in the refractive index is also higher. These features are found beneficial for them to be used in applications like sensing, nonlinear optical devices, and optical filters. Moreover, their features are yet to be covered; recent research studies have exploited the properties of 1D ternary PC for different applications.

In 2008, Awasthi et al. [70] observed the optical behaviour of a band-pass filter in a way that uses ternary PC. The theoretical analogy of PC was examined with Kroning penny model, theory of solids. Their studies suggested that 1D ternary periodic structures provided better control in dispersion relation as compared to a binary structure, as it has two more controlling parameters relative to those binary one. They observed that three layers involved in a periodic structure achieved a much broader range of dispersion control. Moreover, their ternary periodic structure is capable of tuning the system at the desired frequency range by altering the structural and refractive index parameters [70].

In the following year, 2015, Laxmi Shiveshwari et al. [71] discovered an omnidirectional PBG formed 1D PC composed of metamaterials as one of the components. The proposed system was studied with the

transfer matrix method. The report claimed that the proposed system can trap light in three-dimensional space due to the elimination of Brewster's angle transmission resonance, allowing the existence of a complete PBG. The results are obtained as the PBG as a function of incident angle, layer thickness, dielectric constant of the dielectric material, and number of unit cells for both transverse electric (TE) and transverse magnetic (TM) polarizations. They suggested that a structure can be used for a multichannel transmission filter without introducing a defect along the structure [71].

A drastic increase in research on PCs is observed after 2017, where numerous theoretical approaches with a variety of applications, theoretical, novel combinations of designs involving unique material compositions were reported. Apart from dielectric composition, the studies on PBG extended to metallo-dielectric structures. One of the significant studies on metallo- dielectric composition was conducted theoretically by G.N. Pandey [72] in 2017. He investigated the enlargement of the PBG width as on increasing the thickness of the metallic film increases at normal incidence of the light. He approached the transfer matrix method incorporated with the Drude model to investigate the optical properties of the proposed metallo-dielectric structure [72]. In 2018, Hussein A Elsayed [73] conducted a unique theoretical investigation of a 1D ternary PC composed of metallic nanoparticles of Ag in a transparent matrix of a dielectric layer. The characteristic matrix method and Maxwell-Garnett model were used to obtain the numerical results for the proposed work. The studies included to examine the effect of volume fraction on the permittivity of

the nanoparticles and how the system responds to the transmission of light corresponding to the parameters such as the thickness of the nanocomposite layer, the permittivity of the host dielectric material, and the spherical radius of the nanoparticles. The proposed structure is found to be applicable in THz optical filters, reflectors, and optical switches [73]. In 2019, Hala J. El-Khozondar et. al. [74] proposed a numerical study on a 1D ternary PC-based refractive index sensor. They designed a cavity mode defective PC where blood samples are infiltrated and surrounded by graphene layers in the middle region of the PC. The transmittance spectrum of the whole structure is observed to form over the type of infrared region 800nm-1200nm. They have tested the system for the resonant wave shift for a concentration of the blood plasma values on an increment of 10g/l. Another theoretical study of a 1D ternary PC-based biosensor was carried out for sensing fat concentration in milk was reported by Zaky A Zaky et al. in the year 2021 [75]. They used the transfer matrix method to observe the optical and sensing properties of the proposed work. Both symmetric and asymmetric defective PCs were subject to study of the optical behaviour of the proposed structure [75].

The research team, K.M. Abohassan et al. [76] proposed a theoretical approach for a 1D ternary PC, which is composed of a ZnSe/ZnS/BK7 unit cell system. The system is proposed to obtain wide-angle infrared reflectors. The features of the PBG are determined by TMM, and the well-known Floquet-Bosh theory is used to find the spectral locations of the photonic band edge. The dependence of PBG width on the

number of unit cells, layer thickness, angle of incidence, and temperature is examined [76].

In 2021, Bhuvaneshwer Suthar et al. [77] reported an investigation of the optical properties of 1D ternary metamaterial PC structures. For this, they approached a harmful permittivity material (ENG)/ dielectric material/negative permeability material (MNG) system to study. They used to transfer matrix method to exploit the optical behaviour of the system. Their studies support applying ternary metamaterial PCs to be applicable for tunable optical filters [77]. The investigation of metallo dielectric-metamaterial composition in the ternary planar PC was also conducted by G. N Pandey et.al [78] in their report by 2022. In which the research team examined the tunable optical behaviour of 1D ternary metallo/dielectric/metamaterial periodic structure for opto-electronic and photonic applications, such as multichannel filters, broadband reflectors, and switches. They used the transfer matrix method to observe the PBG structures of the periodic structure. The study involved with type of configuration (based on symmetry), as a function of the number of unit cells, the thickness of the layers, and the angle of incidence of the electromagnetic wave [78].

Additionally, in the same year, G. N. Pandey et al. [79] also investigated the tunable dispersion characteristics of TE and TM modes along a polymer-based 1D ternary PC system composed of graphene, silicon, and polymer, respectively. The studies are based on the tunability with the thickness variation of the polymer and the angle of incidence. The results show an enlargement of the photonic band width as on increasing the polymer thickness. Such a system is

suggested for designing optical devices in the visible region, such as broadband reflectors, narrowband 1D reflectors, and low-loss perfect reflectors for solar cells [79].

A significant research work on 1D ternary periodic structures was reported by Matter et al. [80] in the year 2022. They investigated a theoretical analysis on a 1D ternary PC, composed of polycarbonate and non-glassy materials (polycarbonate/Al_2O_3, polycarbonate /MgF_2, Polycarbonate /BaF_2, and polycarbonate /TiO_2) for a scan range from far UV to near IR of the optical band region. The transfer matrix method employed theoretical analysis, which showed that the structure exhibits zero transmission in the UV and near IR regions. Hence, they suggested that the proposed structure can be exploited for the fabrication of advanced solar cell designs consisting of 1D photonic mirror-based luminescence and reflection concentrators. Alongside, the system can be helpful in fixing satellite-related cryogenic technical issues [80]. In the same year, Malek G. Daher et al. [81] proposed a novel biosensor for sensing creatinine concentration in blood serum samples based on a 1D ternary PC composed of silicon, tin, and SiO_2 as elemental layers. The numerical verification of the ternary planar PC is achieved by the transfer matrix method. For that, they provided a cavity layer in between the ternary structure in a way that the right-side part and left side portion of the system are set into two equal structures. The blood sample can be infiltrated into the cavity layer with different concentrations. The research work reported that the 1D ternary PC structure realized a sensitivity of 938.02 nm/RIU, which is comparable to most recent work published in this area. Besides, the researchers

claimed that the proposed system has additional features such as low fabrication cost, real-time detection, and simplicity in design, making it a good candidate for the realization of the fabrication of such a system at an industrial level.

Since 2022, the research interest in biosensing devices has accelerated in both material science and industry. The demand for novel real-time detectors has been found to be increasing. It also reflects on PC-based research interest. In 2024, Fereshtech Firouzi et.al. [82] proposed their investigation on a 1D ternary PC-based biosensor for quick and easy sensing of bacterial presence, where they designed the structure with quantum dots of aluminium gallium nitride, gallium arsenide, silica, and polyaniline polymer. The study shows that the presence of quantum dots increased the sensitivity of the biosensor. The proposed design provided two PBGs with multiple suitable detection modes in the infrared and visible regions, with linear behaviour. The study was done with a standard blood sample, and bacterial blood samples were determined using the optimal parameters [82].

Hence, the technological recognition of 1D ternary PC is not limited, and research interest in 1D ternary PC is an ongoing process. The literature survey reveals that the scope of 1D ternary PC has been distributed through all the technological needs in integrated photonic devices, including multichannel propagation filters, sensors, and lasers. The discussed research works pointed out that the 1Dternary PC structures got attention and started growing since the research focused on PCs. The research work shows that a wide variety of materials compositions, including all-dielectric materials, metallo-dielectric

compositions, metallo-dielectric–metamaterial compositions, polymers, and polycarbonate materials, are examined for designing the 1D ternary PC structures. However, the experimental realization of 1D ternary PCs remains a complex question. Due to the proper technical facilities for the fabrication of multithin film structures, the industrial-level production of 1D ternary PCs is slowed down, like other PCs. However, the theoretical analysis on 1D ternary PCs and different material compositions included designs would be a significant help for the realization of cost-effective and highly efficient tunable structures [70-82].

1.8 Role of DNA as photonic material in photonic crystals

Biomaterials are now the talk of photonic material science due to their versatile properties. Recently, functionalized organic polymers have been extensively exploited for photonic device applications such as optoelectronic devices (LEDs, which currently replace small LCDs in electronic devices, and nonlinear optoelectronic devices). Moreover, they exhibit unusual properties that cannot be obtained from conventional organic-inorganic materials. Besides, they offer various advantages over other chemical materials, such as cost-effective mass production, naturally abundant and renewable resources, and biodegradable [84-94].

Among various biomaterials, DNA is the most fascinating candidate that humanity has ever known. The polymer material that carries genetic information of all living organisms extends vivid scopes in both science and technology. It has a double helical structure formed

by two interwound sugar-phosphate chains linked through hydrogen-bonded nitrogen base pairs. DNA is known as the longest polymer, as its double helix width is about two nanometers, and the length of the DNA molecule depends on the number of base pairs (≈1/3 of a nanometer per base pair). The length of a DNA molecule in a human cell is about 2m long, and it contains 3 billion base pairs! The versatile nature of DNA structure allows for making its different modified structures up to the nanoscale. The promising applications of DNA mainly involve the material synthesis, photonic and molecular electronic devices, nanoscale robotics, and DNA-based computation. The resources of double-stranded DNA polymer are mainly from salmon sperm and the thymus gland of calves [84-94].

DNA domain-based photonics is categorized into two types: wet devices and solid-state devices. Wet devices involve optofluidic systems where DNA molecules are used in their aqueous or organic solution forms, primarily as catalysts. They are mainly exploited as catalysts in the chemical synthesis of nanoparticles. Studies show that aqueous or organic solutions of DNA can modify the optical and geometrical properties of nanoparticles. On the other hand, solid-state devices mainly involve thin films of DNA, where DNA is processed into thin films using a surfactant counter polymer (either cetyltrimethylammonium bromide (CTAB) or cetyltrimethyl-ammonium (CTMA)). The linkage between DNA and the surfactant polymer forms thin films that offer potential features, including high-temperature stability (200°C–250°C) [91] under thermogravimetric conditions, and high transparency in the 350 nm–1600 nm region of

the electromagnetic spectrum. The UV-visible absorption spectrum shows a peak at 260 nm. The refractive index values are reported to be in the range of 1.535 to 1.48 for the 350 nm–1600 nm region of the electromagnetic spectrum [94].

Studies reveal that DNA can perform as a perfect dielectric thin film, showing a dielectric constant value of 7.8 and a high electrical resistivity of 10^{15} Ω·cm. These features make DNA a perfect candidate for photonic applications [84-94].

1.9 Nonlinear photonic crystals

The response of every material in the presence of a high-intensity Gaussian pulse (applied electric field) gives a nonlinear relation with the polarization of the system. Every material in nature exhibits its nonlinear property with respect to the applied field strength. This phenomenon is characteristic of both the applied electric field and the material properties (dielectric nature). The term nonlinear PC combines nonlinear optical properties with the periodic properties of PCs. In general, the realm of PCs explores the interaction of light and matter. The significant engineering ability for the localization and guiding of light with external field support makes PCs prominent in the nonlinear optical domain. PCs can enhance the interaction between light and matter with the support of an external intense electromagnetic field. Thus, this can be well applied to the nonlinear optical utilization of PCs. The nonlinear optical response of the material depends on the response of the refractive index in relation to the intensity of the light

passing through it. Thus, the nonlinear optical properties of PCs can achieve various goals in laser optics and ultrafast photonics [95-97].

The core factor of PCs that plays a key role in defining periodicity responsible for the propagation control over transmitted light is the dielectric function of the system. Moreover, unlike other multi-thin-film structures, PCs have an enhanced ability to confine light within the structure. The light confinement of PCs can be enhanced by introducing defects, which can generate localized modes in the structure. These factors contribute to the nonlinear optical properties of PCs. Nonlinear optical properties can give rise to a variety of fascinating phenomena, including self-focusing, solitons, second harmonic generation, slow light effects, and third harmonic generation. These properties can be exploited in all-optical signal processing, laser sources, quantum information, and light control [95-97].

In 1998, V. Berger et al. [96] reported their study on second-order nonlinear susceptibility in 2D PCs for the application of multiple-beam second harmonic generation and multiple-wavelength frequency conversion. After two decades, in 2018, Fernando et al. [97] conducted a simulation for optical switching and limiting in 2D PCs with square lattice structures having Kerr nonlinearity. In 2021, Y. Zhang et al. [98] reported a review on second harmonic frequency generation in 2D PC structures, where they explored the generation and control of coherent light at new frequencies and the scope of 3D periodic structures of PCs for quadratic nonlinearities. The reviews pointed out that the studies on nonlinear optical properties of PCs need to be explored in the case of 1D ternary periodic microstructures.

One of the key advantages of 1D ternary PCs in nonlinear optical applications is their enhanced ability to confine light, thereby strengthening light-matter interactions compared to other configurations of PC systems. The characteristics of their defect modes largely influence this capability. The defect mode of 1D ternary PC possessed a larger full width at half maximum (FWHM) than its counter bilayer structure and exhibits a high Q value for the resolution. Moreover, the presence of a periodic array of DNA along with the system would add a nonlinear optical property to the 1D ternary PC systems. Hence, 1D ternary PC would be a novel platform for enhanced nonlinear optical applications [95-98].

1.10 Objectives of the thesis

- To investigate the properties of 1D ternary PCs and their role in biosensing applications and integrated photonic devices.
- To generate theoretical results using numerical methods, including the TMM, and simulation tools such as COMSOL, for studying electromagnetic wave propagation through the proposed 1D ternary PCs
- To design theoretical models and develop different cost-effective methods for fabricating 1D ternary PCs incorporated with biopolymers (DNA) and metal oxides such as Alumina, Zinc oxide, Graphite oxide and polyvinyl alcohol (PVA).
- To fabricate 1D ternary PCs incorporated with biopolymer, DNA, using cost-effective methods

- To synthesise nonlinear optical nanoparticles (silica and polyoxometalate) to fabricate 1D ternary nonlinear PCs
- To study the structural properties of the 1D ternary PCs using SEM, XRD, and UV
- To study the linear optical behaviour of the proposed 1D ternary PC with a reflectometer
- To study the non-linear behaviour of the proposed 1D ternary PCs using open open-aperture Z scan method.

1.11 Relevance of this study

This research work extends the scope of study into various fields, including the theoretical simulation of electromagnetic waves through multilayered periodic structures, the experimental realization of 1D ternary PCs using cost effective fabrication methods, the synthesis and characterization of nonlinear nanoparticles such as silica and polyoxometalates using DNA biopolymer as a biotemplate, and the fabrication and characterization of 1D ternary PCs incorporating biopolymers and nonlinear materials.

The materials selected for designing the proposed structure—silica, ZnO, polyoxometalate, and cellulose acetate—are generally easy to handle, cost effective, and nontoxic. As the experimental realization of PCs is often difficult and time consuming due to technical constraints, this research successfully demonstrated a laboratory level structure of 1D ternary PCs.

Furthermore, the study focuses on fabricating a PC integrated with nonlinear features for various applications, such as biosensing, laser and integrated photonic devices. Therefore, this research is considered relevant and valuable for the advancement of PC studies.

1.12 Conclusions

This chapter presents a summary of the thesis. It outlines the fundamentals of PCs, their properties, classifications, and related branches, including their applications. In addition, the chapter highlights the relevance of 1D ternary PCs, which are simple yet highly effective structures capable of efficiently manipulating the flow of light compared to other PC configurations.

References

[1] John D. Joannopoulos, Steven G. Johnson, Joshua N. Winn and Robert D. Meade, Photonic Crystals Molding the Flow of Light, Princeton University Press.

[2] Amsalu, K., & Palani, S. (2020). A review on photonics and its applications. Materials Today: Proceedings, 33, 3372-3377.

[3] Thylén, L., & Wosinski, L. (2014). Integrated photonics in the 21st century. Photonics Research, 2(2), 75-81.

[4] Mahmoud, M. G., Hares, A. S., Hameed, M. F. O., El-Azab, M. S., & Obayya, S. S. (2024). AI-driven photonics: Unleashing the power of AI to disrupt the future of photonics. APL Photonics, 9(8).

[5] Gong, Q., & Hu, X. (Eds.). (2014). PCs: principles and applications. CRC press.

[6] Aly, A. H., Ameen, A. A., Mahmoud, M. A., Matar, Z. S., Al-Dossari, M., & Elsayed, H. A. (2021, September). Photonic crystal enhanced by metamaterial for measuring electric permittivity in GHz range. In Photonics (Vol. 8, No. 10, p. 416). MDPI.

[7] Aly, A. H., Mohamed, D., & Mohaseb, M. A. (2020). Metamaterial control of hybrid multifunctional High-Tc superconducting PCs for 1D Quasi-periodic structure potential applications. Materials Research, 23.

[8] Jasim, K. A., & Alwan, T. J. (2009). Journal of superconductivity and novel magnetism.

[9] Aly, A. H., Sabra, W., & Elsayed, H. A. (2017). Cutoff frequency in metamaterials photonic crystals within Terahertz frequencies. International Journal of Modern Physics B, 31(15), 1750123.

[10] Al-Dossari, M., Awasthi, S. K., Mohamed, A. M., Abd El-Gawaad, N. S., Sabra, W., & Aly, A. H. (2022). Bio-Alcohol Sensor Based on One-Dimensional PCs for Detection of Organic Materials in Wastewater. Materials, 15(11), 4012.

[11] Zhang, X., Jiao, Y. C., Weng, Z. B., Zhang, Y. X., & Feng, S. (2019). Wideband magneto-electric dipole antenna with a claw shaped reflector for 5G communication systems. Microwave and Optical Technology Letters, 61(9), 2098-2104.

[12] Natesan, A., Govindasamy, K. P., Gopal, T. R., Dhasarathan, V., & Aly, A. H. (2019). Tricore photonic crystal fibre based refractive index sensor for glucose detection. IET Optoelectronics, 13(3), 118-123.

[13] Aly, A. H., Ghany, S. S. A., Kamal, B. M., & Vigneswaran, D. (2020). Theoretical studies of hybrid multifunctional YaBa2Cu3O7 PCs within visible and infra-red regions. Ceramics International, 46(1), 365-369.

[14] Hossain, M., & Sen, S. (2021). Design and performance improvement of optical chemical sensor based photonic crystal fiber (PCF) in the terahertz (THz) wave propagation. Silicon, 13(11), 3879-3887.

[15] Aly, A. H., & Mohamed, D. (2015). BSCCO/SrTiO3 one dimensional superconducting photonic crystal for many applications. Journal of Superconductivity and Novel Magnetism, 28(6), 1699-1703.

[16] Zaky, Z. A., Alamri, S., Zhaketov, V. D., & Aly, A. H. (2022). Refractive index sensor with magnified resonant signal. Scientific Reports, 12(1), 1-16.

[17] Aly, A. H., Awasthi, S. K., Mohamed, A. M., Al-Dossari, M., Matar, Z. S., Mohaseb, M. A., ... & Amin, A. F. (2021). 1D reconfigurable bistable photonic device composed of phase change material for detection of reproductive female hormones. Physica Scripta, 96(12), 125533.

[18] Liao, J., Ye, C., Guo, J., Garciamendez-Mijares, C. E., Agrawal, P., Kuang, X., ... & Zhang, Y. S. (2022). 3D-printable colloidal PCs. Materials Today, 56, 29-41.

[19] Busch, K., Lölkes, S., Wehrspohn, R. B., & Föll, H. (Eds.). (2006). PCs: advances in design, fabrication, and characterization. John Wiley & Sons.

[20] ar, M., Doll, T., kovi, J., & Scherer, A. (2000). Design and fabrication of silicon photonic crystal optical waveguides. Journal of lightwave technology, 18(10), 1402.

[21] Inoue, K., & Ohtaka, K. (Eds.). (2004). PCs: physics, fabrication and applications (Vol. 94). Springer Science & Business Media.

[22] Soukoulis, C. M. (2002). The history and a review of the modelling and fabrication of PCs. Nanotechnology, 13(3), 420.

[23] Cheng, C. C., & Scherer, A. (1995). Fabrication of photonic band-gap crystals. Journal of Vacuum Science & Technology B: Microelectronics and Nanometer Structures Processing, Measurement, and Phenomena, 13(6), 2696-2700.

[24] Wu, K., Gu, W. X., Wu, C., Ma, J. L., & Ma, X. Y. (2014). Study on the Optical Transmission Properties of One-dimensional Photonic Crystal of MoS2. Advanced Materials Research, 1056, 42-46.

[25] Hudak, Y. I. (2017). On the mathematics problem of multilayered dielectric systems in the classical electrodynamic. Russian Technological Journal, 5(3), 160-188.

[26] J. Pandey, (2017), Transfer Matrix Method for One Dimensional PCs, Journal of Ramanujan Society of Mathematics and Mathematical Science, 6,(1), 121-130.

[27] Villa-Villa, F., & Gaspar-Armenta, J. A. (2006). Brewster angle and optical tunneling in one-dimensional PCs composed of left-and right-handed materials. JOSA B, 23(2), 375-380.

[28] Lekner, J. (2013). Theory of reflection of electromagnetic and particle waves (Vol. 3). Springer Science & Business Media. [61] Pedrotti, F. L., Pedrotti, L. M., & Pedrotti, L. S. (2018). Introduction to optics. Cambridge University Press.

[29] Abbas, S., Salman, S. R., & Abbas, A. S. (2021). Studying of the polarization modes TE and TM for oblique incidence of light on thin films. Digest Journal of Nanomaterials and Biostructures, 16(2), 647-657. [63] Pendry, J. B. (1994). Photonic band structures. Journal of modern optics, 41(2), 209-229.

[30] Akbar, F., Syahriar, A., & Lubis, A. H. (2014, November). Dispersion relation of 1D photonic crystal. In 2014 International Conference on Electrical Engineering and Computer Science (ICEECS) (pp. 69-73). IEEE.

[31] Deng, WM., Chen, ZM., Li, MY. et al. Ideal nodal rings of one-dimensional PCs in the visible region. Light Sci Appl **11**, 134 (2022).

[32] Yashaswini, P. R., Gayathri, H. N., Bahaddur, I., & Srikanth, P. C. (2023). Design and simulation of a highly sensitive one-dimensional

photonic crystal for different chemical sensing applications. Results in Optics, 11, 100376.

[33] Shen, H., Wang, Z., Wu, Y., & Yang, B. (2016). One-dimensional PCs: fabrication, responsiveness and emerging applications in 3D construction. RSC advances, 6(6), 4505-4520.

[34] Emeliantsev, P. S., Pyshkov, N. I., & Svyakhovskiy, S. E. (2023). Designing the structure of a one-dimensional photonic crystal with a given spectrum of the reflection coefficient. JETP Letters, 117(11), 821-826.

[35] Elsayed, H.A., Medhat, M., Hajjiah, A. et al. A promising high-sensitive 1D photonic crystal magnetic field sensor based on the coupling of Fano\Tamm resonance in far IR region. Sci Rep **15**, 1977 (2025).

[36] Bahramipour, S. S., & Askarpour, A. N. (2024). One-dimensional photonic crystal with tilted termination and its angular filtering properties for radiative cooling. Optics Express, 32(4), 5191-5205.

[37] Däntl, M., Jiménez-Solano, A., & Lotsch, B. V. (2022). Stimuli-responsive one-dimensional PCs: design, fabrication and sensing. Materials Advances, 3(20), 7406-7424.

[38] Ben Abdelaziz, K., Soltani, O. & Kanzari, M. Theoretical Study of Symmetrical 1D Photonic Crystal as a Blood Cancer Sensor. Phys. Solid State **66**, 149–156 (2024).

[39] Elshahat, S., Abood, I., Esmail, M. S. M., Ouyang, Z., & Lu, C. (2021). One-dimensional topological photonic crystal mirror heterostructure for sensing. Nanomaterials, 11(8), 1940.

[40] Yu, S. P., Muniz, J. A., Hung, C. L., & Kimble, H. J. (2019). Two-dimensional PCs for engineering atom–light interactions. Proceedings of the National Academy of Sciences, 116(26), 12743-12751.

[41] Divya, J., Selvendran, S., & Raja, A. S. (2018). Photonic crystal-based optical biosensor: a brief investigation. Laser Physics, 28(6), 066206.

[42] Inoue, K. (2004). Two-Dimensional PCs. In: Inoue, K., Ohtaka, K. (eds) PCs. Springer Series in OPTICAL SCIENCES, vol 94. Springer, Berlin, Heidelberg. https://doi.org/10.1007/978-3-540-40032-5_5

[43] Chen, H., Li, N., Gu, Z., Gu, H., & Wang, J. (2023). Magnetic photonic crystals for biomedical applications. Smart medicine, 2(2), e20220039.

[44] Sun, L., Xie, Z., Xu, H., Xu, M., Han, G., Wang, C., & Gu, Z. (2012). A thermally tunable inverse opal photonic crystal for monitoring glass transition. Journal of Nanoscience and Nanotechnology, 12(3), 1984-1987.

[45] Bhushan, B. (2018). Structural coloration. In Biomimetics: Bioinspired Hierarchical-Structured Surfaces for Green Science and Technology (pp. 879-910). Cham: Springer International Publishing.

[46] Wen, F., David, S., Checoury, X., El Kurdi, M., & Boucaud, P. (2008). Two-dimensional PCs with large complete photonic band gaps in both TE and TM polarizations. Optics express, 16(16), 12278-12289.

[47] Patil, H.J., Indumathi, T.S., Sharan, P., Nandi, S. (2020). Interpretation of Photonic Crystals with Hexagonal Symmetry. In: Barolli, L., Xhafa, F., Hussain, O. (eds) Innovative Mobile and Internet Services in Ubiquitous Computing . IMIS 2019. Advances in Intelligent Systems and Computing, vol 994. Springer, Cham. https://doi.org/10.1007/978-3-030-22263-5_86

[48] Baker, J. E., Sriram, R., & Miller, B. L. (2015). Two-dimensional PCs for sensitive microscale chemical and biochemical sensing. Lab on a Chip, 15(4), 971-990.

[49] Song, Z., Liu, H., Huang, N., & Wang, Z. (2018). Electrically tunable robust edge states in graphene-based topological photonic crystal slabs. Journal of Physics D: Applied Physics, 51(9), 095108.

[50] Yang, Y., Jiang, H. & Hang, Z.H. (2018) Topological Valley Transport in Two-dimensional Honeycomb Photonic Crystals. Sci Rep **8**, 1588. https://doi.org/10.1038/s41598-018-20001-3

[51] Heidari, F., Parandin, F., Boochani, A. et al. Design of a two-dimensional photonic crystal biosensor to identify blood cholesterol in humans. Discov Electron **1**, 4 (2024). https://doi.org/10.1007/s44291-024-00003-4

[52] Wang, Ken & Yu, Zongfu & Liu, Victor & Raman, Aaswath & Cui, Yi & Fan, Shanhui. (2014). Light trapping in PCs. Energy Environ. Sci. 7. 10.1039/C4EE00839A

[53] Yu, S. P., Muniz, J. A., Hung, C. L., & Kimble, H. J. (2019). Two-dimensional photonic crystals for engineering atom–light interactions. Proceedings of the National Academy of Sciences, 116(26), 12743-12751.

[54] Popescu, D. G. (2013). Two dimensional photonic crystals with different symmetries for waveguides and resonant cavities applications. Applied Mathematics and Physics, 75.

[55] Yablonovitch, E., Gmitter, T. J., & Leung, K. M. (1991). Photonic band structure: The face-centered-cubic case employing nonspherical atoms. Physical review letters, 67(17), 2295.

[56] Krauss, T. F., Rue, R. M. D. L., & Brand, S. (1996). Two-dimensional photonic-bandgap structures operating at near-infrared wavelengths. Nature, 383(6602), 699-702.

[57] Cersonsky, R. K., Antonaglia, J., Dice, B. D., & Glotzer, S. C. (2021). The diversity of three-dimensional PCs. Nature communications, 12(1), 2543.

[58] Suzuki, K., Kitano, K., Ishizaki, K., & Noda, S. (2014). Three-dimensional PCs created by single-step multi-directional plasma etching. Optics Express, 22(14), 17099-17106.

[59] Noda, S., Kawashima, T., Kawakami, S. (2004). Three-Dimensional PCs. In: Inoue, K., Ohtaka, K. (eds) PCs. Springer Series in OPTICAL SCIENCES, vol 94. Springer, Berlin, Heidelberg. https://doi.org/10.1007/978-3-540-40032-5_7

[60] Chen, CW., Hou, CT., Li, CC. et al. Large three-dimensional PCs based on monocrystalline liquid crystal blue phases. Nat Commun **8**, 727 (2017). https://doi.org/10.1038/s41467-017-00822-y

[61] Gangwar, R. K., Pathak, A. K., & Kumar, S. (2023, October). Recent progress in photonic crystal devices and their applications: a review. In Photonics (Vol. 10, No. 11, p. 1199). MDPI.

[62] Vaidya, S., Ghorashi, A., Christensen, T., Rechtsman, M. C., & Benalcazar, W. A. (2023). Topological phases of photonic crystals under crystalline symmetries. *Physical Review B*, *108*(8), 085116.

[63] Noda, S. (1999, August). Three-dimensional photonic crystals and their applications. In Technical Digest. CLEO/Pacific Rim'99. Pacific Rim Conference on Lasers and Electro-Optics (Cat. No. 99TH8464) (Vol. 2, pp. 187-188). IEEE.

[64] Vasseur, J. (2019). The plane wave expansion method. Fundamentals and Applications of Acoustic Metamaterials: From Seismic to Radio Frequency, 1, 107-141.

[65] Fernanda, A. F., Rezeki, Y. A., Jamaluddin, A., Budiawanti, S., & Rahmasari, L. (2024, June). Calculation of two dimensional photonic bandgap using the Plane Wave Expansion (PWE) method. In AIP Conference Proceedings (Vol. 3074, No. 1, p. 020010). AIP Publishing LLC.

[66] Shi, S., Chen, C., & Prather, D. W. (2004). Plane-wave expansion method for calculating band structure of photonic crystal slabs with perfectly matched layers. Journal of the optical society of America A, 21(9), 1769-1775.

[67] Chen, J. B., Shen, Y., Zhou, W. X., Zheng, Y. X., Zhao, H. B., & Chen, L. Y. (2011). Comparison study of the band-gap structure of a 1D-photonic crystal by using TMM and FDTD analyses. Journal of the Korean Physical Society, 58(4), 1014-1020.

[68] Qiu, M. (2000). Computational methods for the analysis and design of photonic bandgap structures (Doctoral dissertation, KTH).

[69] Degirmenci, E., & Landais, P. (2013). Finite element method analysis of band gap and transmission of two-dimensional metallic photonic crystals at terahertz frequencies. Applied optics, 52(30), 7367-7375.

[70] Awasthi, S., & Ojha, S. (2008). Design of a tunable optical filter by using a one-dimensional ternary photonic band gap material. Progress In Electromagnetics Research M, 4, 117-132.

[71] Shiveshwari, L., & Awasthi, S. K. (2015). Transmission properties of one-dimensional ternary plasma PCs. Physics of Plasmas, 22(9).

[72] Pandey G. N. (2017), Photonic Band Gap in One-Dimensional Ternary Metal-Dielectric Photonic Crystal, Int. Journal of Engineering Research and Applications, ISSN : 2248-9622, 7(7)87-91

[73] Elsayed, H. A. (2018). Transmittance properties of one dimensional ternary nanocomposite PCs. Materials Research Express, 5(3), 036209.

[74] El-Khozondar, H. J., Mahalakshmi, P., El-Khozondar, R. J., Ramanujam, N. R., Amiri, I. S., & Yupapin, P. (2019). Design of one

dimensional refractive index sensor using ternary photonic crystal waveguide for plasma blood samples applications. Physica E: Low-dimensional Systems and Nanostructures, 111, 29-36.

[75] Zaky A. Zaky 1 & Arvind Sharma 2 & Sagr Alamri 3 & Nahla Saleh 4 & Arafa H. Aly, Detection of Fat Concentration in Milk Using Ternary Photonic Crystal, Silicon, 2021, https://doi.org/10.1007/s12633-021-01379-8

[76] Abohassan, K. M., Ashour, H. S., & Abadla, M. M. (2021). One-dimensional ZnSe/ZnS/BK7 ternary planar PCs as wide angle infrared reflectors. Results in Physics, 22, 103882.

[77] Suthar, B., & Pandey, G. N. (2021, June). Optical properties of one-dimensional ternary metamaterial photonic crystal. In Macromolecular Symposia (Vol. 397, No. 1, p. 2000340).

[78] Pandey, G. N., Kumar, N., Singh, P., Thapa, K. B., & Pandey, J. P. (2022). Transmission properties of one-dimensional symmetric ternary structures of metamaterials and dielectric materials with two different configurations. In Journal of Physics: Conference Series (Vol. 2357, No. 1, p. 012009). IOP Publishing.

[79] Pandey, G. N., Kumar, N., Singh, P., & Thapa, K. B. (2022). Analysis of photonic band structure tunability for te and tm modes in a silicon and polymer based ternary photonic crystal for visible range devices. Silicon, 14(17), 11659-11666.

[80] Matar, Z. S., Al-Dossari, M., Awasthi, S. K., Abd El-Gawaad, N. S., Hanafy, H., Amin, R. M., ... & Aly, A. H. (2022). Theoretical study on polycarbonate-based one-dimensional ternary photonic structures from far-ultraviolet to near-infrared regions of electromagnetic spectrum. Crystals, 12(5), 642.

[81] Wu, F., Cheng, Z., She, Y., Li, Y., & Panda, A. (2023). Large omnidirectional mid-infrared photonic bandgap in a one-dimensional ternary photonic crystal consisting of isotropic dielectric, elliptical metamaterial and plasma. Physica Scripta, 98(7), 075507.

[82] Firouzi, F., Vahedi, A., & Hagipour, S. (2025). Ternary one-dimensional photonic crystal biosensors for efficient bacteria detection: Role of quantum dots and material combinations. Physica B: Condensed Matter, 698, 416766.

[83] Armenise, M. N., Campanella, C. E., Ciminelli, C., Dell'Olio, F., & Passaro, V. M. (2010). Phononic and photonic band gap structures: modelling and applications. Physics Procedia, 3(1), 357-364.

[84] Joyce, D. M. (2013). The development of DNA-based bio-polymer hybrid thin films for capacitor applications (Doctoral dissertation, University of Dayton).

[85] Kokkiligadda, S., Dugasani, S. R., Komarala, E. P., Jeon, S., Jeong, J. H., & Park, S. H. (2021). Controlling physical characteristics of DNA and DNA-CTMA thin films by embedding with graphene oxide and riboflavin. Journal of Physics D: Applied Physics, 54(37), 375401.

[86] Vaclav Prajzler, Woohyun Jung, Kyunghwan Oh, Jakub Cajzal and Pavla Nekvindova, Optical Properties of Deoxyribonucleic Acid Thin Layers Deposited on an Elastomer Substrate, Optical Materials Express 421, Vol. 10, No2/1 February 2020, doi.org/10.1364/OME.1000421

[87] Hebda, E., Jancia, M., Kajzar, F., Niziol, J., Pielichowski, J., Rau, I., & Tane, A. (2012). Optical properties of thin films of DNA-CTMA and DNA-CTMA doped with Nile blue. Molecular Crystals and Liquid Crystals, 556(1), 309-316.

[88] Nithyaja, B., Misha, H., & Nampoori, V. P. N. (2012). Synthesis of silver nanoparticles in DNA template and its influence on nonlinear optical properties. Nanosci Nanotechnol, 2(4), 99-103.

[89] Inagaki, T., Hamm, R. N., Arakawa, E. T., & Painter, L. R. (1974). Optical and dielectric properties of DNA in the extreme ultraviolet. The journal of chemical physics, 61(10), 4246-4250.

[90] Cuervo, A., Dans, P. D., Carrascosa, J. L., Orozco, M., Gomila, G., & Fumagalli, L. (2014). Direct measurement of the dielectric polarization properties of DNA. Proceedings of the National Academy of Sciences, 111(35), E3624-E3630.

[91] Steckl, A. DNA – a new material for photonics?. Nature Photon **1**, 3–5 (2007). https://doi.org/10.1038/nphoton.2006.56

[92] Kalinowski, J. (2018). Organic Light-Emitting Diodes: Principles, Characteristics & Processes. CRC press.

[93] Gheorghe, P., Petris, A., & Anton, A. M. (2023). Optical limiting properties of DNA biopolymer doped with natural dyes. Polymers, 16(1), 96.

[94] Khazaeinezhad, R., Hosseinzadeh Kassani, S., Paulson, B., Jeong, H., Gwak, J., Rotermund, F., ... & Oh, K. (2017). Ultrafast nonlinear optical properties of thin-solid DNA film and their application as a saturable absorber in femtosecond mode-locked fiber laser. Scientific reports, 7(1), 41480.

[95] Bowden, C. M., & Zheltikov, A. M. (2002). Nonlinear optics of PCs. Journal of the Optical Society of America B Optical Physics, 19(9), 2046-2048.

[96] Berger, V. (1998). Nonlinear PCs. Physical review letters, 81(19), 4136.

[97] Fernando, M. G., & Wijewardena Gamalath, K. A. I. L. (2018). Nonlinear optical properties of PCs. World Scientific News, 97, 1-27.

[98] Zhang, Y., Sheng, Y., Zhu, S., Xiao, M., & Krolikowski, W. (2021). Nonlinear PCs: from 2D to 3D. Optica, 8(3), 372-381.

Chapter 2

Theoretical and Experimental Design of One-Dimensional Ternary Photonic Crystal

This chapter presents an in-depth analysis of one-dimensional ternary photonic crystal, focusing on its fundamental theoretical framework and optical properties. Starting from Maxwell's differential equations, the master equations governing electromagnetic wave propagation through dielectric media are derived. Using the transfer matrix method implemented on the Python platform, the dispersion relations for one-dimensional ternary photonic crystals are analyzed. The photonic bandgap structures of these one-dimensional ternary photonic crystals are investigated in detail, highlighting their frequency filtering capabilities. Additionally, the impact of introducing defect layers within the one-dimensional ternary photonic crystal is examined, demonstrating how defect modes alter the photonic bandgap characteristics. This study provides essential insights into the design and simulation of advanced photonic crystal structures for controlled light manipulation.

2.1 Introduction

In the previous chapter, the nature of PCs, their interaction with light, and their various classifications were discussed. This chapter focuses on the fundamental theory and numerical methods used to describe the propagation of light in one-dimensional PCs. Maxwell's equations govern the propagation of electromagnetic waves through any medium; however, obtaining analytical solutions for wave transmission through multilayer stack structures is often complex. When exploring the theory and properties of PCs, it is important to draw an analogy with semiconductors. In general, a PC is a periodic multilayer structure composed of alternating dielectric materials, where the propagation of photons can be controlled by the creation of a PBG, the frequency range in which the density of photon states becomes zero. This phenomenon is analogous to the formation of electronic band gaps in semiconductor crystals, where the periodic potential of the atomic lattice restricts the motion of electrons. Due to this close resemblance, the behaviour of photons in PCs can be effectively described by the confluence of Maxwell's electromagnetic wave equations and Bloch functions, much like the approach used to understand electron dynamics in periodic semiconductor lattices [1–25].

The property that makes PCs distinct from other photonic materials is the presence of the PBG effect, which is a unique characteristic of such structures. Therefore, they are often referred to as PBG materials. The primary function of the effect is to control the propagation of light within a specific spectral frequency range. Although incident light contains a broad range of frequencies, only selected frequencies can

pass through PCs. It enables a fundamental method to manipulate the origin of the PBG and control the frequency of light at will. PCs are composed of repeated elementary cells, consisting of periodically arranged dielectric layers. The elementary or unit cell serves as the basic structural element of a PC, and its repetition over a certain length ensures a well-defined photon density oscillation within the desired passband range. The refractive index contrast between the interfaces of the elemental layers is maintained uniformly across all unit cells in the structure. In essence, PCs represent a periodic distribution of the dielectric function, with the periodicity being on the same order as the wavelength of the incident electromagnetic wave. The physical origin of the PBG arises from strong multiple scattering of the incident electromagnetic wave at the interfaces between different dielectric materials, followed by destructive interference. Despite being microscale structures, the propagation of electromagnetic waves through PCs can be explained on a macroscopic level using the four fundamental Maxwell's electromagnetic wave equations [1–5]. In the SI unit system,

$$\boldsymbol{\nabla}.\boldsymbol{E} = \rho/\varepsilon \tag{2.1}$$

$$\boldsymbol{\nabla} \cdot \boldsymbol{B} = \mathbf{0} \tag{2.2}$$

$$\boldsymbol{\nabla} \times \boldsymbol{E} + \frac{\boldsymbol{\partial B}}{\boldsymbol{\partial t}} = \mathbf{0} \tag{2.3}$$

$$\boldsymbol{\nabla} \times \boldsymbol{H} - \frac{\boldsymbol{\partial D}}{\boldsymbol{\partial t}} = \mathbf{J} \tag{2.4}$$

Where **E** and **H** represent the macroscopic electric and magnetic fields, **B** and **D** are the magnetic induction and electric displacement fields,

and ρ and **J** are the free charge and current densities, respectively[1-2]. Although the PC regime is typically defined by a periodic arrangement of different dielectric materials that are isotropic, homogeneous, and transparent materials. In such case, the parameters ρ and J are considered to be zero. As a result, equations 2.1 and 2.2 reduce to zero. Therefore, equations 2.1 to 2.4 can be expressed in the following form:

$$\boldsymbol{\nabla}.\boldsymbol{E} = \mathbf{0} \tag{2.5}$$

$$\boldsymbol{\nabla} \cdot \boldsymbol{B} = \mathbf{0} \tag{2.6}$$

$$\boldsymbol{\nabla} \times \boldsymbol{E} + \frac{\boldsymbol{\partial B}}{\boldsymbol{\partial t}} = \mathbf{0} \tag{2.7}$$

$$\boldsymbol{\nabla} \times \boldsymbol{H} - \frac{\boldsymbol{\partial D}}{\boldsymbol{\partial t}} = \mathbf{0} \tag{2.8}$$

The above electromagnetic field equations can be used to describe the information about electromagnetic wave propagation through the PC system. However, specific material properties must be discussed to conform the behavior of the PC to craft the ideal figure of the propagation of light through them. The material property has been used to show the linear relation between them with the electromagnetic field equations in terms of the electric field is given as [1-2];

$$\boldsymbol{D}(\boldsymbol{r}) = \varepsilon_0 \varepsilon(\boldsymbol{r}) \boldsymbol{E}(\boldsymbol{r}) \tag{2.9}$$

Where ε_0 is the permittivity of free space and its value is 8.854×10^{-12} [1-2]. The materials chosen for the PCs are macroscopic and isotropic, which contribute a scalar dielectric function $\varepsilon(r)$, known as the dielectric constant or relative permittivity of the material, to be multiplied by the permittivity of free space ε_0. Another factor lies in the field strength, which is considered to be low. Consequently, the

relation that connects the electric field with the nonlinear absorption process from equation 2.9 can be neglected. In consequence, the materials have only linear dependency on the electric field. This material is considered non-dispersive, meaning its dielectric constant remains constant over the operating frequency range of light. Additionally, the refractive index is assumed to be honest and positive, as the chosen material is transparent to light. Similarly, the relation between the magnetic field and the material property is stated as [1-2];

$$\boldsymbol{B}(\boldsymbol{r}) = \mu_0 \mu(\boldsymbol{r}) \boldsymbol{H}(\boldsymbol{r}) \qquad 2.10$$

Where u_0 is the permeability of free space, and it is quantified as $4\pi x10^7$ Henry/m [1-2]. The term μ (r) mentioned in equation 2.10 is the relative permeability of the material, which is found to be unity in most of the dielectric materials. As a consequence, the equation 2.10 can be simplified as [1-2];

$$\boldsymbol{B}(\boldsymbol{r}) = \mu_0 \boldsymbol{H}(\boldsymbol{r}) \qquad 2.11$$

Then the four Maxwell's equations 2.5 to 2.8 are rewritten by including the changSes formed in **D(r)** and **B(r)** shown in equations 2.10 and 2.11, as follows [1-2];

$$\boldsymbol{\nabla}.\boldsymbol{E}(\boldsymbol{r},t) = \mathbf{0} \qquad 2.12$$

$$\boldsymbol{\nabla} \cdot \boldsymbol{H}(\boldsymbol{r},t) = \mathbf{0} \qquad 2.13$$

$$\boldsymbol{\nabla} \times \boldsymbol{E}(\boldsymbol{r},t) + \frac{\boldsymbol{\mu_0 \partial H(r,t)}}{\boldsymbol{\partial t}} = \mathbf{0} \qquad 2.14$$

$$\boldsymbol{\nabla} \times \boldsymbol{H}(\boldsymbol{r},t) - \frac{\boldsymbol{\varepsilon_0 \varepsilon(r) \partial E(r,t)}}{\boldsymbol{\partial t}} = \mathbf{0} \qquad 2.15$$

In principle, Maxwell's equations are linear and complex functions of both time and space. From this scenario, the equations can be separated in terms of explicit functions of time and space independently. Then Maxwell's field equations can be transformed into a set of harmonic modes. Thus, this gives a clear picture of Maxwell's equations, which are solutions of sinusoidal functions of time. The solutions of Maxwell's equations can be represented as a state or a mode of a wave system. Therefore, the harmonic mode of electromagnetic fields can be represented explicitly as spatial fields in terms of the exponential complex power of frequency, ω, as [1-2];

$$\boldsymbol{H}(\boldsymbol{r},t) = \boldsymbol{H}(\boldsymbol{r})\boldsymbol{e}^{-\boldsymbol{i}\boldsymbol{\omega}\boldsymbol{t}} \tag{2.16}$$

$$\boldsymbol{E}(\boldsymbol{r},t) = \boldsymbol{E}(\boldsymbol{r})\boldsymbol{e}^{-\boldsymbol{i}\boldsymbol{\omega}\boldsymbol{t}} \tag{2.17}$$

The equations 2.16 and 2.17 represent the frequency mode profile of the wave propagation system. In consequence divergence of these equations 2.16 and 2.17 has the form of [1-2];

$$\boldsymbol{\nabla}\cdot\boldsymbol{H}(\boldsymbol{r}) = \boldsymbol{0}, \boldsymbol{\nabla}.\varepsilon\boldsymbol{E}(\boldsymbol{r}) = \boldsymbol{0} \tag{2.18}$$

Equation 2.18 again confirms that there is no point source or sink of displacement of the field along the medium of propagation. In addition to this, the electromagnetic waves are in a transverse mode of propagation.

Thus, the rest of equations 2.12-2.15, the divergence can be applicable to the two curl equations 2.14 and 2.15. The curl equations will be in the expanded form as [1-2];

$$\boldsymbol{\nabla} \times \boldsymbol{E}(\boldsymbol{r}) - i\omega\mu_0 \boldsymbol{H}(\boldsymbol{r}) = \boldsymbol{0} \quad 2.19$$

$$\boldsymbol{\nabla} \times \boldsymbol{H}(\boldsymbol{r}) + i\omega\varepsilon_0 \varepsilon(\boldsymbol{r}) \boldsymbol{E}(\boldsymbol{r}) = \boldsymbol{0} \quad 2.20$$

Again, taking curl to the form in equations 2.19 and 2.20 after decouple the equations as

$$\boldsymbol{\nabla} \times \boldsymbol{\nabla} \times \boldsymbol{E}(\boldsymbol{r}) = i\omega\mu_0 \big(\boldsymbol{\nabla} \times \boldsymbol{H}(\boldsymbol{r})\big) \quad 2.21$$

Which results in;

$$\boldsymbol{\nabla} \times \boldsymbol{\nabla} \times \boldsymbol{E}(\boldsymbol{r}) = (\mu\omega^2)\epsilon(\boldsymbol{r}) \boldsymbol{E}(\boldsymbol{r}) \quad 2.22$$

It is the **Master equation** of the PC in terms of the electric field.

Similarly, in terms of the magnetic field, it is given as;

$$\boldsymbol{\nabla} \times \left(\frac{\mathbf{1}}{\epsilon(\boldsymbol{r})} \boldsymbol{\nabla} \times \boldsymbol{H}(\boldsymbol{r}) \right) = (\mu\omega^2) \boldsymbol{H}(\boldsymbol{r}) \quad 2.23$$

On that account, the master equation 2.22 carries all the information about the propagation of electromagnetic waves along the medium ε(**r**). By using an appropriate numerical approach, the master equation can be solved to find the harmonic modes of propagation and corresponding frequencies along with PBG structures. The equation 2.19, the magnetic field can be expressed as [1-2];

$$\boldsymbol{H}(\boldsymbol{r}) = \frac{-i}{\omega\mu_0} \boldsymbol{\nabla} \times \boldsymbol{E}(\boldsymbol{r}) \quad 2.24$$

As well as the solution of E(r) can be deduced from equation 2.20

$$\boldsymbol{E}(\boldsymbol{r}) = \frac{i}{\omega \varepsilon_0 \varepsilon(r)} \boldsymbol{\nabla} \times \boldsymbol{H}(\boldsymbol{r}) \qquad 2.25$$

The provided master equations 2.22 and 2.23 are exploited to find out the allowed modes of propagation. These equations are an eigenvalue problem; as a consequence, the solutions of these equations would provide the frequency modes where the electromagnetic waves are propagated and forbidden [1-2].

2.2 Photonic bandgap structure of the 1D ternary photonic crystal

The equation characterized by the light as they travel through a homogenous, non-lossy, nonmagnetic, isotropic, and dielectric material is represented as [1-2];

$$\omega = \frac{\boldsymbol{ck}}{n} \qquad 2.26$$

Where ω is the photon angular frequency, c is the speed of light, k is the photon wave vector, and n is the refractive index of the dielectric material. It is the well-known dispersion relation. Although light propagation, especially concerning confinement and refractive index alignment, depends on the direction within the dielectric medium, equation 2.26 shows that the angular frequency is directly proportional to the wave vector and inversely proportional to the refractive index of the material. For more convenience, the dispersion relation will be different along the direction in which the refractive index varies.

When the dispersion relation comes in the domain of PCs, where the dielectric function becomes a periodic function. Such that, the

dielectric constants are arranged along the three different methods, namely one, two, or three dimensions, where light travels along the direction of refractive index variation, more precisely, a PC is configured in space such that it is a periodic arrangement of dielectric materials where a fixed refractive index contrast is set in a fixed step length called lattice parameter **l,** formed a periodic microstructure as shown in Figure 2.1.

a **b** **c**

Figure 2. 1: Schematic representation of a) 1D PC, b) 2D PC, and c) 3D PC

As seen in Figure 2.1 a., the 1D PC consists of a stack of unit cells, and each layer in a unit cell has different dielectric constants in a periodic modulation. In consequence, the 1D PC has a form of a multilayer thin film. This concept was initially presented by Lord Raleigh in 1887 as he published the optical properties of multilayer thin films. As a multilayer stack of thin films, the propagation of the photons through the layers generates multiple reflections and refractions at the interfaces. The term photonic band structures can illustrate it. Before entering into the band structures, the symmetry of the PC should come into play. Being an infinite layer-by-layer structure, the confinement of photons is possible only along the Z direction, so that the periodicity is designed along the Z direction. In consequence, the modes of

propagation of light (photons) through the periodic structure can be figured out by using the Bloch form [1-31, 33];

$$\boldsymbol{H(r)} = e^{i\boldsymbol{k}_{II}\cdot\boldsymbol{\rho}} e^{i\boldsymbol{k}_z} \boldsymbol{u}_{l,\boldsymbol{k}_z,\boldsymbol{k}_{II}}(\boldsymbol{z}) \qquad 2.27$$

Where **H(r)** is the Bloch function, and k_{II}, k_z, and l are the wave vector in the plane, wave vector along the z direction, and the band number. The function **u (z)** is the periodic envelope function which satisfies the condition; **u(z)= u (z+D)**, only when **D** is an integral multiple of the spatial period a. In the Bloch theory, the dispersion relation for the propagation of photons depends on the first Brillouin zone in the reciprocal lattice space [1-2].

Since the 1D PC has a continuous translational symmetry in the xy plane, k_{II} can have any value; however, the translational symmetry along the z direction is discrete, so that the value of k_z is restricted to the Brillouin zone: $\frac{-\pi}{l} < \boldsymbol{k_z} \leq \frac{\pi}{l}$, when a$\hat{z}$ becomes the primitive lattice vector in the reciprocal space. For normal incidence at the dielectric interface, k_{II} is zero; in that case, k_z is only considered to be important so that the propagation mode is possible only along the z- direction [1-12].

The master equations provided in equations (2.22) and (2.23) in section 2.1 are the primary sources for finding the harmonic modes of propagation and corresponding frequency of electromagnetic waves through the 1D PC. Besides, the PBG structures are also determined from solving the master equations. Since the master equations are treated as an eigenvalue problem, the solutions of the master equations are the eigenvalues, which corresponding frequencies of the propagation modes. At the forbidden band, the eigenvalues will not

exist. By incorporating Maxwell's equations with the Bloch theory of electrons, the solutions of the Master equations can be found [1-2].

There are finite numerical methods available to solve Maxwell's equations so as to discuss the band structures of the PC. The prominent numerical methods are the TMM, plane wave expansion method (PWE), and finite difference time domain method (FDTD). These methods are generally used for analyzing optical properties of one-dimensional PCs, and they have been discussed in section 2.2.1 onwards [1-31].

2.2.1 Designing of 1D ternary PC structure using TMM

The TMM is the simplest and compact method widely used for the description of the optical transfer features of stratified layered structures. Among other numerical methods such as finite difference time domain method and, plane wave expansion method, the TMM provides less complexity and robust method. Generally, this is carried out using a suitable analytical matrix approach, involving layer-by-layer calculations to evaluate the optical characteristics of one, two, and three-dimensional PCs. The method, TMM is typically applied to systems with cubic symmetry and requires the structure to be composed of microscale multilayers. In this method, each layer is represented by its transfer matrix, and the overall optical response of the system is determined by multiplying these individual matrices, resulting in a final 2×2 transfer matrix for the entire multilayer structure. This method can accurately determine the optical features such as band structures, transmission coefficients, and reflectivity, finitely and simply. Since the electromagnetic waves inside the PC are spanned in terms of a basis set of plane waves, the information of the

coupled modes (TE and TM) is represented by equations of a 2x2 matrix solution based on Maxwell's equations in the frequency domain, known as k-space, with appropriate boundary conditions. The matrix operations have been performed by utilizing the boundary conditions that connect the amplitudes of the electromagnetic fields at the interfaces of the different regions of the elemental structure. The results of the TMM provided the complete band analysis of the PC structure by showing the allowed and forbidden frequency ranges within the crystal. That is the fundamental information about the photonic band gap of the PC structure. In summary, the transverse matrix method is a mathematical approach used to analyze the dispersion properties and PBGs in PCs by solving the wave equation and applying appropriate boundary conditions [1-31, 34].

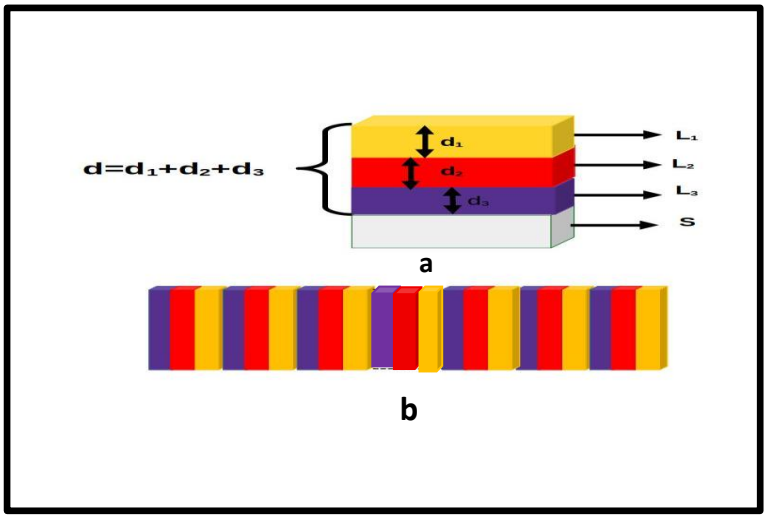

Figure 2.2: Schematic diagram of a 1D ternary PC, where a) unit cell and b) 1D ternary PC of infinite period length

When an electromagnetic wave with a wavelength λ is incident on the PCs, it undergoes a propagation that will be changed due to the periodicity of the structures. The propagation phenomena, such as

reflections and transmissions take place at the interfaces of the PC can be explained using the TMM. The propagation of electromagnetic waves through thin films involves several theories that unite to form the TMM. As the system constitutes a multilayer structure, the parameters such as refractive index, thickness of the dielectric layer, number of elemental layers, and period (number of unit cells). When light is incident on an isotropic thin film material stack, it gets partially reflected and transmitted at each interface. To explain the reflection and transmission, the Fresnel equations for a thin film are exploited.

Regarding this, the surface of the interface is exactly smooth enough to produce linear polarizations (plane polarization) to the incident electromagnetic wave, such that TE polarized and TM polarized waves are produced. In consequence, Fresnel coefficients are dependent on these two polarization conditions. However, at normal incidence, the Fresnel coefficients are treated as the same for both TM and TE polarizations.

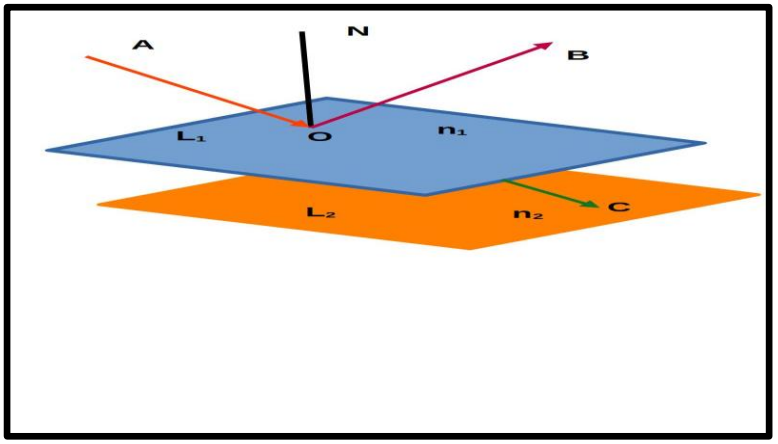

Figure 2.3: A schematic diagram of the interaction of light and a dielectric multilayer thin film structure, where L_1 and L_2 are the dielectric thin films

When the electromagnetic wave is passing through a periodic structure of a unit cell of the ternary PC, where the unit cell consists of isotropic thin films with thicknesses d_1, d_2, and d_3, and corresponding refractive indices are n_1, n_2, and n_3, respectively. Whenever the light hits each interface of the dielectric thin film, transmission and reflection take place. It can be explained well by using the TMM. For an electric field, the amplitude of the incident beam is E_I, the corresponding reflected beam is E_R, and the transmitted electric field can be represented as E_t. In consequence, the relation between them can be shown only if the fields and their derivatives are continuous at the interface. Since they are continuous, the amplitudes of the plane waves can be expressed using the boundary condition. By combining the boundary conditions, the amplitudes of the electromagnetic wave (linear polarized plane waves) at the interface can be represented as;

For the first interface (between layer 1 and layer 2), the electric field becomes

$$\boldsymbol{E_1 e^{k_1 x - i\omega t} = E_{T1} e^{k_1 l_1 - i\omega t} + E_{R1} e^{-(k_1 l_1 - i\omega t)}} \qquad 2.28$$

For the second interface (between layer 2 and layer 3), the field becomes;

$$\boldsymbol{E_2 e^{k_2 x - i\omega t} = E_{T2} e^{k_2 l_2 - i\omega t} + E_{R2} e^{-(k_2 l_2 - i\omega t)}} \qquad 2.29$$

For the third interface (between layer 3 and layer 1)

$$\boldsymbol{E_3 e^{k_3 x - i\omega t} = E_{T3} e^{k_3 l_3 - i\omega t} + E_{R3} e^{-(k_3 l_3 - i\omega t)}} \qquad 2.30$$

Where E_{T1}, E_{R1}, E_{T2}, E_{R2}, E_{T3}, and E_{R3} are the amplitudes of the corresponding transmitted and reflected electric fields, and k_1, k_2, and k_3 are wave numbers defined as [1-2, 23];

$$\mathbf{k_1}=\frac{\omega n_1 cos\theta_1}{c} \quad 2.31$$

$$\mathbf{k_2}=\frac{\omega n_2 cos\theta_2}{c} \quad 2.32$$

$$\mathbf{k_3}=\frac{\omega n_3 cos\theta_3}{c} \quad 2.33$$

where θ_1, θ_2 and θ_3 are the incidence angles with respect to the three mediums D_1, D_2 and D_3 respectively. Since the system consists of a stack of multilayer thin films, the equations describing the incident and transmitted fields can generally be coupled in matrix form. Using the TMM, the propagation of light through each interface can be expressed as follows [1-2]:

$$\begin{bmatrix} E_{T2} \\ E_{R2} \end{bmatrix} = M_{12} \begin{bmatrix} E_{I1} \\ E_{R1} \end{bmatrix} \quad 2.34$$

$$\begin{bmatrix} E_{T3} \\ E_{R3} \end{bmatrix} = = M_{23} \begin{bmatrix} E_{T2} \\ E_{R2} \end{bmatrix} = M_{23} M_{12} \begin{bmatrix} E_{I1} \\ E_{R1} \end{bmatrix} \quad 2.35$$

Similarly,

$$\begin{bmatrix} E_{T4} \\ E_{R4} \end{bmatrix} = = M_{31} \begin{bmatrix} E_{T3} \\ E_{R3} \end{bmatrix} = M_{31} M_{23} M_{12} \begin{bmatrix} E_{I1} \\ E_{R1} \end{bmatrix} \quad 2.36$$

Generalising the field equations as

$$\begin{bmatrix} E_{T4} \\ E_{R4} \end{bmatrix} = M_{ij} \begin{bmatrix} E_{I1} \\ E_{R1} \end{bmatrix} \quad 2.37$$

Where $M_{ij}= M_{31}M_{23}M_{12}$ 2.38

In general, M_{ij} is known as the transfer matrix and has the form;

$$M_i=\begin{bmatrix} cos\delta_i & i\eta_i{}^{-1}sin\delta_1 \\ i\eta_i sin\delta_i & cos\delta_i \end{bmatrix} \quad 2.39$$

$$\text{Where } \delta_i = \frac{2\pi n_i d_i cos\theta_i}{\lambda} \quad 2.40$$

$$\eta = \begin{Bmatrix} \frac{n_i}{cos\theta_i}, & P\ polariesd \\ n_i cos\theta_i, & S\ polarised \end{Bmatrix} \quad 2.41$$

Where n_i is the refractive index and d_i is the thickness of the dielectric material, θ_i is the angle between light and the interface normal. η_i is the modified admittance which is approximately equal to the refractive index of the dielectric material when the electromagnetic wave is in the optical band [1-31].

For the dielectric layer L_1 transfer matrix is defined as;

$$M_1=\begin{bmatrix} cos\delta_1 & i\eta^{-1}sin\delta_1 \\ i\eta sin\delta_1 & cos\delta_1 \end{bmatrix} \quad 2.42$$

Transfer matrix for the layer L_2;

$$M_2=\begin{bmatrix} cos\delta_2 & i\eta^{-1}sin\delta_2 \\ i\eta sin\delta_2 & cos\delta_2 \end{bmatrix} \quad 2.43$$

Similarly,

$$M_3=\begin{bmatrix} cos\delta_3 & i\eta^{-1}sin\delta_3 \\ i\eta sin\delta_3 & cos\delta_3 \end{bmatrix} \quad 2.44$$

Therefore, three transfer matrices M_1, M_2, and M_3 are involved for describing the transmission properties of the three-layered unit system, and the solutions of the master equation 1 (Electric field) for the entire PC system become;

$M_T=M_1M_2M_3$

$$=\begin{pmatrix} cosk_1n_1d_1 & \frac{i}{n_1}sink_1n_1d_1 \\ i\eta sink_1n_1d_1 & cosk_1n_1d_1 \end{pmatrix}\begin{pmatrix} cosk_2n_2d_2 & \frac{i}{n_2}sink_2n_2d_2 \\ in_2sink_2n_2d_2 & cosk_2n_2d_2 \end{pmatrix} \quad 2.45$$

$$= M_{ij} = \begin{bmatrix} m_{11} & m_{22} \\ m_{21} & m_{22} \end{bmatrix} \quad 2.46$$

For the PC system, where the number of periods is N and the transfer matrix of the whole system

$$M_T= (M_{ij})^N \quad 2.47$$

To find the elements of the final transfer matrix M_T, the relation between the powers of matrix and Chebyshev polynomial of the second kind can be expressed in terms of matrix exponentiation, especially for symmetric matrices [1,21,36-37].

The n^{-th} power of the Chebyshev polynomial of the second kind can be expressed as

$$U_n(x) = \frac{sin\left((n+1)\theta\right)}{sin\theta} \quad 2.48$$

$$\text{Where } x= \cos(\theta) \quad 2.49$$

In this context. The total transfer matrix can be related to the Chebyshev polynomial of the second kind. Specifically, the eigenvalues of the matrix can be expressed in terms of Chebyshev polynomials.

If λ_1 and λ_1 are the eigenvalues of the transfer matrix, the transfer matrix becomes

$$M_T = \begin{pmatrix} U_N(\lambda_1) & \frac{U_{N-1}(\lambda_1)}{d} \\ dU_{N-1}(\lambda_1) & U_N(\lambda_1) \end{pmatrix} \quad 2.50$$

Where d is the factor for the layer properties, such as refractive index and thickness.

Using the recursion relation of the Chebyshev polynomial, the elements of the final transfer matrix

M_T for the N periods can be obtained [1,21,36-40]; such that

$$U_N(x) = 2xU_{N-1}(x) - U_{N-2}(x) \quad 2.51$$

This relationship allows for computing higher-order matrices from lower-order matrices iteratively.

a. Transmission coefficient (T) of the transfer matrix

Equation 2.24 gives a 2x2 characteristic matrix M_{ij} for the proposed three-layered one-dimensional dielectric PC system. It can be modified accordingly to tune the PCs for the desired frequency range. In other words, the future behaviour of PCs can be engineered using the characteristic matrix. The transmittance (t) and reflectance (r) can be

obtained from the characteristic matrix [1-40]; If the refractive index of the front and back layer of the PCs is air, then the equation for transmission coefficient T is obtained as [1-40];

$$T = |t|^2 \tag{2.52}$$

$$\text{where } t = \frac{2}{m_{11}+m_{12}+m_{21}+m_{22}} \; ; \tag{2.53}$$

Moreover, t is known as the transmittance. Using equation 2.51, the entire optical properties including, PBG effect, and allowed transmission modes of the 1D ternary PC can be elucidated.

2.3 Dispersion relations in 1D ternary photonic crystals

According to the Bloch theorem, the propagation of electromagnetic waves in a periodic medium is not altered, and modulated plane waves can simulate their behaviour because the Bloch state is a plane wave multiplied by a periodic function $u_k(x)$. All the scattering events are again formed into coherent waves, which results periodic $u_k(x)$ in consequence, k is reserved. The periodicity condition can be expressed as [1-31];

$$u_k(x) = u_k(x+d) \tag{2.54}$$

$$\frac{-\Pi}{l} \leq k < \frac{\Pi}{l} \tag{2. 55}$$

where l is the lattice parameter.

This periodic condition restricts the Hermitian eigenvalue problem in equations 2.1 and 2.2 and leads to a discrete spectrum of eigenvalues. So being a periodic medium, the electromagnetic modes of 1D PCs can

be explained by the Maxwell equations. By considering equations 2.1 and 2.2, which are the eigen problems of both magnetic and electric fields, the obtained eigenvalues $(\omega/c)^2$ give the possible magnetic and electric modes with respect to the change in the wave vector k in the first Brillouin zone. The bands between the discrete resonant frequencies (pass bands) of the PCs are called photonic band gaps, where no eigenvalues exist for the master equations 2.1 and 2.2 [1-31]. For an infinite lattice extending on the whole x-axis, the solution of the master equation can be written in terms of Bloch waves [1];

$$\mathbf{E}(x, k) = \mathbf{U}_k(x)e^{ik(\omega)x} \tag{2.56}$$

Where the parameter k(ω) is called the Bloch wave number or dispersion relation for a periodic lattice with indices n_1, n_2, and n_3. The dispersion relation can be deduced using the Kronig-Penney model of the electron theory of solids.

It can be explicitly represented as follows;

$$k(\omega) = \frac{1}{d}\cos^{-1}\left(\frac{1}{2}Tr\left(M_{ij}\right)\right) \tag{2.57}$$

$$= \frac{1}{d}cos^{-1}\left(\frac{1}{2}\left((2cosk_1d_1n_1cosk_2d_2n_2cosk_3d_3n_3) - \left(\frac{n_1}{n_2} + \frac{n_2}{n_1}\right)sink_1d_1n_1cosk_2d_2n_2cosk_3d_3n_3\right)\right)$$

$$\left(\left(+\left(\frac{n_3}{n_2} + \frac{n_2}{n_3}\right)sink_2d_2n_2sink_3d_3n_3cosk_1d_1n_1 + \left(\frac{n_1}{n_3} + \frac{n_3}{n_1}\right)sink_1d_1n_1sink_3d_3n_3cosk_2d_2n_2\right)\right) \tag{2.58}$$

Equation 2.58 gives rise to the dispersion relation for a ternary 1D PC.

2.4 Formulation of the thickness of the elemental layers of the 1D ternary photonic crystal

The design of the thickness of the dielectric materials of the 1D ternary PC is strictly crucial. The thickness of the constituent dielectric layer is measured based on the constructive interference formula of a multilayer film stack. There are two methods followed to design the thickness of the layers; they are constructive interference and Bragg's quarter-wave condition.

2.4.1 Condition for constructive interference of multilayer thin films

In PCs, the PBG is formed due to the constructive interference that occurs at the interfaces of the dielectric layers. As the light encounters the surface of the PC, it undergoes constructive and destructive interference. According to constructive interference, the condition for constructive interference for a multilayer stack of films depends on the wavelength λ, refractive index (n), and thickness (l) of the thin film. In 2013, Gong, Q et al [2] described the Bragg's law for finding the thickness of the constituent layers of a PC. The relation between the wavelength and the optical thickness of the film is represented as [1-25, 32-35];

$$m\lambda = 2n_i l_i \qquad 2.59$$

Where $2n_il_i$ is the optical thickness of the thin film, and i is an integer representing the order of the layer. For a multi-layered stack of film, the condition for constructive interference becomes;

$$m\lambda = 2(n_1l_1 + n_2l_2 + n_3l_3 + n_4l_4 + \ldots . n_il_i) \quad 2.60$$

Where m is the order of the constructive interference and i is an integer. In the case of a 1D ternary PC, the reflections occur from higher index materials to the lower index materials. In consequence, the constructive interference does not depend on the phase shift of the propagation. Thus, the equation becomes;

$$m\lambda = 2(n_1l_1 + n_2l_2 + n_3l_3) \quad 2.61$$

From this equation, the thickness of each layer can be deduced by applying two conditions;

Case 1: For $l_1=l_2=l_3=l$, for a particular symmetry, photonic band gap of wavelength λ, and m; the thickness will be assigned as

$$l = \frac{m\lambda}{2(n_1+n_2+n_3)} \quad 2.62$$

Case II: When the optical thickness would be the same for all three layers, such that;

$$2n_1l_1 = 2n_2l_2 = 2n_3l_3 \quad 2.63$$

Then the total optical thickness of the unit cell becomes

$$= 2n_1l_1 + 2n_2l_2 + 2n_3l_3 = 2(n_1l_1 + n_2l_2 + n_3l_3) \quad 2.64$$

Then the condition for constructive interference

$$m\lambda = 6n_1l_1 = 6n_2l_2 = 6n_3l_3 \quad 2.65$$

$$l_1 = \frac{m\lambda}{6n_1} \quad 2.66$$

$$l_2 = \frac{m\lambda}{6n_2} \quad 2.67$$

$$l_3 = \frac{m\lambda}{6n_3} \quad 2.68$$

In summary the thickness for an elemental layer of a1D ternary PC can be found by

$$\sum_i n_i l_i = \frac{m\lambda}{2} \quad \text{where i is integer} \quad 2.69$$

2.4.2 Bragg's quarter-wave condition

Generally, Bragg's quarter-wave condition is used to determine the thickness of elemental layer in 1D binary PC. It is found to be decisive for designing multilayer thin films for antireflective coatings and mirror applications. This condition is achieved only when the optical thickness of the layer is equal to one-fourth of the wavelength [32-35]. According to Bragg reflection condition, for a constructive interference

$$2n_i l_i cos\theta = \text{m}\lambda \qquad \text{where i=1,2,3……} \quad 2.69$$

Where n is the refractive index, l is the thickness of the layer, and θ is the angle of incidence, m is the order of the interference pattern, usually it is 1, and λ is the wavelength in vacuum.

For normal incidence, θ=0, thus cos θ =1

The equation 2.69 can be rewritten as

$$2n_i l_i = \text{m}\lambda \quad 2.70$$

$$n_i l_i = \frac{\lambda}{2} \quad 2.71$$

For a quarter wave layer

$$n_i l_i = \frac{\lambda}{4} \quad 2.72$$

Though, this is suitable for binary 1D binary PC structures, the equation 2.72 is slightly changed when the 1D ternary PC structure is considered. Such that, the

$$\sum_i n_i l_i = \frac{m\lambda}{2} \quad 2.73$$

These methods are generally considered for designing the thickness of the 1D ternary PCs.

2.5 Defects in 1D ternary photonic crystals

The periodicity of PCs gives rise to their unique feature: the photonic band gap, within which the density of photons at specific frequencies drops to zero. Any alteration of this periodicity can create defects in the PC, leading to the formation of defect modes within the PBG region. Apart from the filters and antireflecting coating, the diverse features of PCs can be brought about by creating defect modes. The defect mode can be achieved by altering the periodicity by means of several ways, such as introducing a significantly different material to any of the unit cells by replacing the existing dielectric layer, increasing the thickness of the constituent dielectric layers, or repeating the same constituent layer instead of placing by adjacent different layer. This kind of defect is generally referred to as a point

defect, which means the defect occurs in a unit cell. Thus, point defect can cause localized modes which can trap photons within the micro cavity. It facilitates the interaction of light and matter within the cavity, like what a resonator will do. This ability will be utilized for many applications, including nonlinear optical applications, sensing, and optical devices. There are another two more types of defect are known; they are line defects and surface defects. Line defects are achieved by altering the line of unit cells. This kind of defect is utilized for wave guiding purposes for guiding light. Another possible defect is a surface defect that results from imperfections on the surface of the PCs.

2.5.1 Symmetric and asymmetric defective photonic crystals

When a defect is introduced in PC, usually a narrow defect mode (resonant mode) will be present in the PBG. In such situation the symmetry of the defect with respect to the centre of the structure matters in producing defect mode.

When considering the symmetry of the PC after introducing a defect, generally two types of defective PCs are known. If the structure is not mirror-symmetrical about the defect, such a configuration is called an asymmetric defective PC. It provides a single defect mode within the PBG and has a remarkably high-quality factor (Q). In contrast, when the structure is symmetric about the defective layer, such a defective PC is called symmetric defective PC. In symmetric defective PC the defect divides the PC into two subparts of PCs. The symmetric defective PC will experience two defect modes in a PBG, and the light confinement duration is comparatively lower than as that of

asymmetric defective structures. Therefore, asymmetric defective PC stretches potential applications of PCs, including sensors and laser devices. Asymmetric configurations can be achieved in a 1D dimensional PC. Figure 2.4 shows differences in the both alignment of PC about the defective layer in asymmetric and symmetric defective PCs. In a symmetric defective structure, both sides of the defective layer are symmetric with respect to the defective layer [1-30].

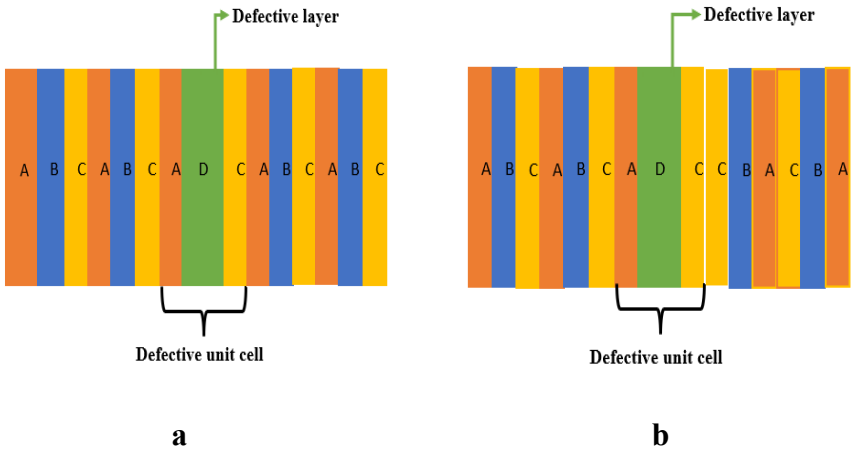

Figure 2.4: Schematic diagram of a) defective symmetric on 1D ternary PC and b) defective asymmetric 1D ternary PC

Figure 2.4a represents symmetric defective PC where both side of the PC structure about the defective layer are symmetric. The alignment of a symmetric PC looks like as $(ABC)^{N}ADC(CBA)^{N}$. Figure 2.4b represents an asymmetric 1D ternary defective PC where D is the defective layer. About the defective unit cell, the structure is asymmetric in nature. Thus, for a 1D ternary PC the asymmetric can be shown as $(ABC)^{N}$ $ADC((ABC)^{N})$.

The defect modes in the symmetric and asymmetric 1D PCs can be tuned by the general parameters such that thickness and dielectric properties of the constituent elements and angle of incidence of light. These can effectively influence the properties of a defect mode such as number, position, intensity, bandwidth and confinement duration of light.

2.5.2 The effect of the defect layer in 1D ternary photonic crystals

The presence of a defect in a ternary PC structure results in the formation of a defect mode with a narrow peak. This narrow transmission mode can have a significant impact on light-matter interaction. The narrow peak has high intensity that can enhance light-matter interaction. Thereupon, the narrow width can suitable applicable for sensing purposes.

The optical properties (dispersion relations) of a defective PC can be exploited by using TMM in the same way as for a standard PC. The transfer matrix of the defective layer would be;

$$M_D=\begin{bmatrix} cos\theta & \frac{-i}{\eta}sin\theta \\ isin\theta & cos\theta \end{bmatrix} \quad 2.74$$

Where, M_D represents the transfer matrix for the defective layer,

The characteristic matrix of the entire configuration of the one-dimensional asymmetric ternary PC would be;

$$M_D= (M_1M_2M_3)^{N-x}(M_1M_dM_3)(M_1M_2M_3)^x \quad 2.\ 75$$

Where M_D represents the characteristic matrix for the whole structure, having N number of unit cells, M_1, M_2, and M_3 are corresponding transfer matrices of layer L_1, L_2, and L_3, and x represents the number of orders left due to the defective unit cell. The Figure shows the differences between the PBG of a standard PC structure and a defective PC structure. Figure 2.5a represents the optical response of a standard 1D ternary PC. Figure 2.5 b shows the optical response of a 1D defective ternary PC. A narrow defective mode within the PBG can be seen in Figure 2.5.b. The presence of a defect mode also influences the position and width of the PBG. This defect mode can be manipulated by altering properties of the defective layer, such as its refractive index, thickness, and material concentration. These changes will result in the position and FWHM of the defect mode. These properties can be monitored for the applications of sensing, optical filters, and laser devices.

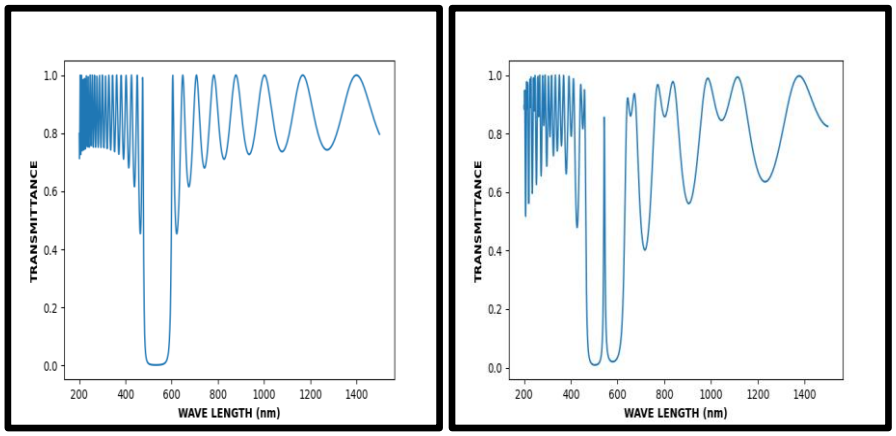

a b

Figure 2.5: Optical responses of a) 1D ternary PC and b)1D defective asymmetric ternary PC obtained by TMM.

2.6 Conclusion

This chapter describes the formation of master equations for 1D PC structures using Maxwell's electromagnetic theory. Additionally, the features of one-dimensional PCs, such as the PBG, transmission, reflection, and dispersion relation, are described in detail using the master equations along with the Bloch equation of electron motion in solids. From the perspective of the general theory of one-dimensional PCs, this chapter presents the derivation of equations for transmittance, reflectance, and dispersion theory for ternary structures based on the fundamental principles of multilayer dielectric films and PCs. In addition, the condition for thickness of the 1D ternary PC is also derived. Apart from the transmission modes, the chapter also discussed the defect mode obtained in the 1D ternary PC structure, which results from the presence of a defective layer.

References

[1] John D. Joannopoulos, Steven G. Johnson, Joshua N. Winn, and Robert D. Meade, Photonic Crystals: Molding the Flow of Light, Princeton University Press.

[2] Gong, Q., & Hu, X. (2013). PCs. In Principles and Applications. Pan stanford publishing.

[3] Shalaby, A. S., Alamri, S., Mohamed, D., Aly, A. H., Awasthi, S. K., Matar, Z. S., & Tamam, M. T. (2021). Theoretical study of a one-dimensional defect PC as a high-performance sensor for water-borne bacteria. Optical and Quantum Electronics, 53, 1-14.

[4] Emeliantsev, P. S., Pyshkov, N. I., & Svyakhovskiy, S. E. (2023). Designing the structure of a one-dimensional photonic crystal with a given spectrum of the reflection coefficient. JETP Letters, 117(11), 821-826.

[5] Aly, A. H., Ameen, A. A., Mahmoud, M. A., Matar, Z. S., Al-Dossari, M., & Elsayed, H. A. (2021, September). Photonic crystal enhanced by metamaterial for measuring electric permittivity in the GHz range. In Photonics (Vol. 8, No. 10, p. 416). MDPI.

[6] Aly, A. H., Mohamed, D., & Mohaseb, M. A. (2020). Metamaterial control of hybrid multifunctional High-Tc superconducting photonic crystals for 1D Quasi-periodic structure potential applications: Materials Research, 23.

[7] Jasim, K. A., & Alwan, T. J. (2009). Journal of superconductivity and novel magnetism.

[8] Aly, A. H., Sabra, W., & Elsayed, H. A. (2017). Cutoff frequency in metamaterials photonic crystals within the Terahertz frequencies. International Journal of Modern Physics B, 31(15), 1750123.

[9] Al-Dossari, M., Awasthi, S. K., Mohamed, A. M., Abd El-Gawaad, N. S., Sabra, W., & Aly, A. H. (2022). Bio-Alcohol Sensor Based on One-Dimensional Photonic Crystals for Detection of Organic Materials in Wastewater. Materials, 15(11), 4012.

[10] Zhang, X., Jiao, Y. C., Weng, Z. B., Zhang, Y. X., & Feng, S. (2019). Wideband magneto-electric dipole antenna with a claw-shaped reflector for 5G communication systems. Microwave and Optical Technology Letters, 61(9), 2098-2104.

[11] Natesan, A., Govindasamy, K. P., Gopal, T. R., Dhasarathan, V., & Aly, A. H. (2019). Tricore photonic crystal fibre-based refractive index sensor for glucose detection. IET Optoelectronics, 13(3), 118-123.

[12] Aly, A. H., Ghany, S. S. A., Kamal, B. M., & Vigneswaran, D. (2020). Theoretical studies of hybrid multifunctional YaBa2Cu3O7 photonic crystals within visible and infrared regions. Ceramics International, 46(1), 365-369.

[13] Hossain, M., & Sen, S. (2021). Design and performance improvement of an optical chemical sensor based photonic crystal fiber (PCF) in the terahertz (THz) wave propagation. Silicon, 13(11), 3879-3887.

[14] Aly, A. H., & Mohamed, D. (2015). BSCCO/SrTiO3 one-dimensional superconducting photonic crystal for many applications. Journal of Superconductivity and Novel Magnetism, 28(6), 1699-1703.

[15] Zaky, Z. A., Alamri, S., Zhaketov, V. D., & Aly, A. H. (2022). Refractive index sensor with magnified resonant signal. Scientific Reports, 12(1), 1-16.

[16] Aly, A. H., Awasthi, S. K., Mohamed, A. M., Al-Dossari, M., Matar, Z. S., Mohaseb, M. A., .& Amin, A. F. (2021). 1D reconfigurable bistable photonic device composed of phase change material for the detection of reproductive female hormones. Physica Scripta, 96(12), 125533.

[17] Liao, J., Ye, C., Guo, J., Garciamendez-Mijares, C. E., Agrawal, P., Kuang, X.,& Zhang, Y. S. (2022). 3D-printable colloidal photonic crystals. Materials Today, 56, 29-41.

[18] Liu, Y., Wang, H., Ho, J., Ng, R. C., Ng, R. J., Hall-Chen, V. H., ... & Yang, J. K. (2019). Structural color three-dimensional printing by shrinking photonic crystals. Nature communications, 10(1), 4340.

[19] Wang, J., Wang, L., Song, Y., & Jiang, L. (2013). Patterned photonic crystals fabricated by inkjet printing. Journal of Materials Chemistry C, 1(38), 6048-6058.

[20] Nam, H., Song, K., Ha, D., & Kim, T. (2016). Inkjet printing-based mono-layered photonic crystal patterning for anti-counterfeiting structural colors. Scientific reports, 6(1), 30885.

[21] Awasthi, S., & Ojha, S. (2008). Design of a tunable optical filter by using a one-dimensional ternary photonic band gap material. Progress In Electromagnetics Research M, 4, 117-132.

[22] Shiveshwari, L., & Awasthi, S. K. (2015). Transmission properties of one-dimensional ternary plasma photonic crystals. Physics of Plasmas, 22(9).

[23] Pandey G. N. (2017), Photonic Band Gap in One-Dimensional Ternary Metal-Dielectric Photonic Crystal, Int. Journal of Engineering Research and Applications, ISSN: 2248-9622, 7(7)87-91

[24] Elsayed, H. A. (2018). Transmittance properties of one-dimensional ternary nanocomposite photonic crystals. Materials Research Express, 5(3), 036209.

[25] El-Khozondar, H. J., Mahalakshmi, P., El-Khozondar, R. J., Ramanujam, N. R., Amiri, I. S., & Yupapin, P. (2019). Design of a one-dimensional refractive index sensor using a ternary photonic crystal waveguide for plasma and blood sample applications. Physica E: Low-dimensional Systems and Nanostructures, 111, 29-36.

[26] Zaky A. Zaky 1 & Arvind Sharma 2 & Sagr Alamri 3 & Nahla Saleh 4 & Arafa H. Aly, Detection of Fat Concentration in Milk Using Ternary Photonic Crystal, Silicon, 2021, https://doi.org/10.1007/s12633-021-01379-8

[27] Abohassan, K. M., Ashour, H. S., & Abadla, M. M. (2021). One-dimensional ZnSe/ZnS/BK7 ternary planar photonic crystals as wide-angle infrared reflectors. Results in Physics, 22, 103882.

[28] Suthar, B., & Pandey, G. N. (2021, June). Optical properties of one-dimensional ternary metamaterial photonic crystal. In Macromolecular Symposia (Vol. 397, No. 1, p. 2000340).

[29] Pandey, G. N., Kumar, N., Singh, P., Thapa, K. B., & Pandey, J. P. (2022, October). Transmission properties of one-dimensional symmetric ternary structures of metamaterials and dielectric materials with two different configurations. In Journal of Physics: Conference Series (Vol. 2357, No. 1, p. 012009). IOP Publishing.

[30] Pandey, G. N., Kumar, N., Singh, P., & Thapa, K. B. (2022). Analysis of photonic band structure tunability for te and tm modes in a silicon and polymer based ternary photonic crystal for visible range devices. Silicon, 14(17), 11659-11666.

[31] Matar, Z. S., Al-Dossari, M., Awasthi, S. K., Abd El-Gawaad, N. S., Hanafy, H., Amin, R. M., ... & Aly, A. H. (2022). Theoretical study on polycarbonate-based one-dimensional ternary photonic structures from far-ultraviolet to near-infrared regions of the electromagnetic spectrum. Crystals, 12(5), 642.

[32] Zaky, Z. A., Sharma, A., Alamri, S., Saleh, N., & Aly, A. H. (2021). Detection of fat concentration in milk using a ternary photonic crystal. Silicon, 1-11.

[33] Aly, A. H., Mohamed, B. A., Al-Dossari, M., Awasthi, S. K., Fouad, E., & Amin, A. F. (2023). Ultra-high sensitive cancerous cells detection and sensing capabilities of a photonic biosensor. Scientific Reports, 13(1), 19524.

[34] Wu, F., Cheng, Z., She, Y., Li, Y., & Panday, A. (2023). Large omnidirectional mid-infrared PBG in a one-dimensional ternary photonic crystal consisting of an isotropic dielectric, an elliptical metamaterial, and plasma. Physica Scripta, 98(7), 075507.

[35] Firouzi, F., Vahedi, A., & Hagipour, S. (2025). Ternary one-dimensional photonic crystal biosensors for efficient bacteria detection: Role of quantum dots and material combinations. Physica B: Condensed Matter, 698, 416766.

[36] Knittel, Z. (1976). Optics of thin films. (An optical multilayer theory). Wiley series in pure and applied optics (New York, NY (USA): John Wiley & Sons), 548 p.

[37] Armenise, M. N., Campanella, C. E., Ciminelli, C., Dell'Olio, F., & Passaro, V. M. (2010). Phononic and photonic band gap structures: modelling and applications. Physics Procedia, 3(1), 357-364.

[38] Eby, G.N., 2004, Principles of Environmental Geochemistry. Brooks/Cole-Thomson Learning, pp. 212-214.

[39] Alamrani, F., & Alsharaeh, E. (2022). Controlling the band gaps of one-dimensional TiO2/SiO2, TiO2/SnO2, and SiO2/SnO2 photonic crystals using the transfer matrix method. Optics and Photonics Journal, 12(7), 171-189.

[40] Bananej, A., Hamidi, S. M., Li, W., Li, C., & Tehranchi, M. M. (2008). A flexible design for one-dimensional photonic crystals with controllable PBG width. Optical Materials, 30(12), 1822-1827.

[41] Saeidi, F. S., & Moradi, M. (2023). Designing a multi-periodic photonic crystal with adjustable transmission peak for optical filter applications. Journal of Nanostructures, 13(1), 66-75.

[42] Mahmoodi, S., Moradi, M., & Saeidi, F. S. (2021). The nearly perfect optical filter composed of [SiO2/ZrO2] Stacks using one-dimensional photonic crystals. Journal of Nanostructures, 11(3), 618-627.

[43] Alamrani, F., & Alsharaeh, E. (2022). Controlling the bandgaps of one-dimensional TiO2/SiO2, TiO2/SnO2, and SiO2/SnO2 photonic crystals using the transfer matrix method. Optics and Photonics Journal, 12(7), 171-189.

Chapter 3

Theoretical Study of One-Dimensional DNA Templated Silica/ Metal Oxides, Graphite Oxide Photonic Crystals for Multifaceted Applications

This chapter explores the novel features of DNA-templated one-dimensional (1D) photonic crystals and their potential for diverse applications. It begins with a theoretical analysis of 1D photonic crystals composed of silica/metal oxides and graphite oxide structured on a DNA template. The investigation involves studying the optical responses in the region of 200-1200 nm of the electromagnetic spectrum using the transfer matrix method (TMM). The study further compares the performance of ternary photonic crystal (PC) systems with their corresponding bilayer counterparts, focusing on transmittance and the emergence of defect modes. The chapter highlights the promising applications of DNA-templated ternary 1D PCs in areas such as biosensing, optical filtering, and nonlinear optical devices.

The results of this chapter are published as
Theoretical Studies of One- Dimensional DNA Templated Silica/Metal Oxides, Graphite Oxide
Photonic Crystals, Bhagyasree G S and Nithyaja B, 2022 ECS Trans. 107 12161, DOI:
10.1149/10701.12161ecst, ISSN: 1938-6737, Journal link: https://iopscience.iop.org/journal/1938- 5862

3.1 Introduction

The fundamental concepts of photonic crystals (PCs), including the photonic bandgap (PBG) and its dependence on structural parameters such as thickness, refractive index, and periodicity, were detailed in chapters 1 and 2. This chapter focuses on the mechanism and transmission characteristics of one-dimensional ternary photonic crystals composed of metal oxides, graphite oxides, and a bio-templated dielectric layer. The organic polymer deoxyribonucleic acid (DNA) can be used as a template for various film-based applications. DNA, a fundamental organic molecule, is essential for storing and transmitting genetic information. DNA is increasingly recognized for its role in photonic and bio-templated applications. In material science, its significance is growing rapidly, both as a biotemplate and as a functional material, making it a promising component for advanced technological applications. The attractive feature of DNA includes its lengthy double helical nucleotide structure and ligand-like properties. Due to the structural and functional groups present in DNA, it exhibits excellent mechanical, electrical, and optical properties [1-8,36-39]. DNA is optically transparent in the visible region of light. This feature of DNA can be effectively used for making DNA-based thin films. The film-forming properties of DNA are enhanced by complexing it with surfactant molecules such as cetyltrimethylammonium bromide (CTAB) and cetyltrimethylammonium chloride (CTAC), enabling its transformation into a stable film. DNA has been used as a stabilizing agent for the synthesis of nanoparticles due to its ability to control

particle size and modify the refractive index of the resulting nanostructures [1-31].

The work presented in this chapter investigates the optical behaviour of 1D ternary PCs composed of various combinations of silica, zinc oxide (ZnO), alumina (Al_2O_3), graphite oxide, along with DNA. The structures are designed to be multi-stack of Silica/DNA/ZnO, Silica/DNA/Alumina, Silica/DNA/Graphite oxide, ZnO/DNA/Alumina, ZnO/DNA/Graphite Oxide, and Alumina/DNA/Graphite oxide. The transmission properties of these six different configurations were studied, and their optical responses were analyzed using the TMM. The design aims to achieve an optical response within the visible region of the spectrum. When using a DNA template, the microperiodic structures offer relatively low refractive index contrast between adjacent layers, and an increased number of interfaces within each unit cell as well. This study focuses on how such a ternary biotemplate layered structural configuration enhances light confinement in the visible region and strengthens the photonic band gap effect for improving the efficiency of the structures for visible light applications [24-31, 32-44].

Additionally, the presence of defects is essential for expanding the applicability of PCs in areas such as sensing, laser devices, optical filters, and solar cells. Studies have shown that defects in PCs enhance light-matter interactions. A defect functions like a cavity within the dielectric microstructure, allowing light to be firmly confined and promoting increased interaction between light and the surrounding medium [1-23, 32-44].

This work further investigates the role of DNA-templated one-dimensional PCs by analysing the changes in optical responses such as transmittance, reflectance, and PBG as the number of periods and interfaces within the unit cell varies, using theoretical modelling based on the TMM. The influence of defects within ternary unit structures is also explored. To create a defect mode, a material with a refractive index equivalent to that of water (n_w=1.33) is introduced. All the theoretical analyses are conducted within the visible region of the electromagnetic spectrum [24-31, 45-51].

3.2 Theoretical formulation of TMM for 1D DNA-templated photonic crystal

The propagation of electromagnetic waves through the PCs can be exploited by the fundamental Maxwell's differential equations of electromagnetic waves in dielectric media.

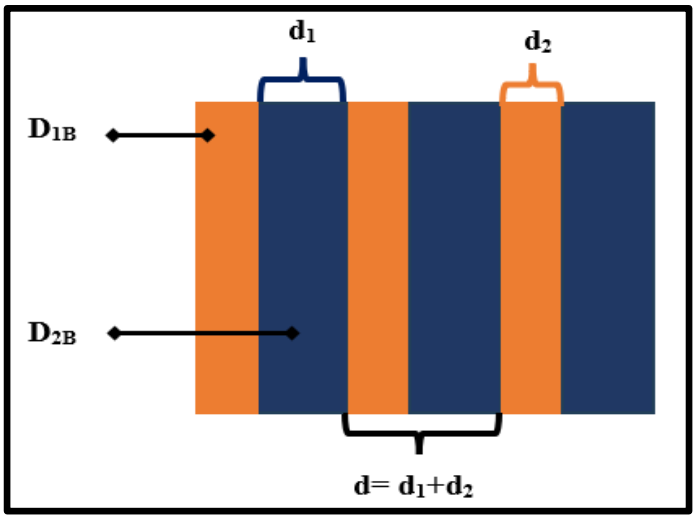

Figure 3.1. Schematic representation of a 1D binary PC

The propagation of electromagnetic waves through the 1D ternary PC is studied by using the fundamental Maxwell's equations. The numerical method used to study the behaviour of electromagnetic waves through the microstructures is the TMM. The derivation of the solution for the propagation of electromagnetic waves in the 1D ternary PC is well explained in chapter 2[1-23, 32-43].

In this chapter a comparative theoretical study on 1D ternary PC systems with their counter 1D bilayer structures are also discussed. It would help to understand the physical significance of the 1D ternary PC structures over 1D bilayer PC structures. The numerical studies were conducted using TMM separately for both 1D ternary microstructures and 1D bilayer PC systems.

In general, a bilayer 1D PC consists of a stalk of alternatively arranged two distinct dielectric or isotropic materials in a unit cell. In consequence of that, each layer requires a propagation matrix to describe the propagation of electromagnetic waves through the periodic microstructures. The TMM for 1D bilayer microstructure is configured for the two constituent layers of the unit cell.

Figure 3.1 illustrates a schematic diagram of a 1D bilayer PC system where the dielectric layers are shown, namely D_{1B} and D_{2B}, corresponding to layer one and layer 2. The thickness of the layers is d_1 and d_2. Hence, the period (lattice constant) of the PC is $d= d_1+d_2$ [1-10]. As an electromagnetic wave with a wavelength λ is incident on the PCs, its propagation is altered due to the periodicity of the structures. The reflections and transmissions that occur at the interfaces

of the PC can be explained using the TMM. The transfer matrices for each layer are represented using the equations illustrated in chapter 2.

For dielectric layer $D_{1B,}$ the transfer matrix is defined as;

$$M_{1B}=\begin{bmatrix} cos\delta_{B1} & i\eta^{-1}sin\delta_{B1} \\ i\eta sin\delta_{B1} & cos\delta_{B1} \end{bmatrix} \quad 3.1$$

Transfer matrix for the layer $D_{2B;}$

$$M_{2B}=\begin{bmatrix} cos\delta_{B2} & i\eta^{-1}sin\delta_{2B} \\ i\eta sin\delta_{B2} & cos\delta_{B2} \end{bmatrix} \quad 3.2$$

The equations 3.1 and 3.2 represent the transfer matrices for the corresponding layers D_{B1} and D_{B2}. Using equations 3.1 and 3.2, the characteristic matrix M_B for the entire unit cell of the 1D bilayer PC system is shown as

$$M_{B=}\ M_{1B}\ M_{2B=}\begin{bmatrix} cos\delta_{B1} & i\eta^{-1}sin\delta_{B1} \\ i\eta sin\delta_{B1} & cos\delta_{B1} \end{bmatrix}\begin{bmatrix} cos\delta_{B2} & i\eta^{-1}sin\delta_{2B} \\ i\eta sin\delta_{B2} & cos\delta_{B2} \end{bmatrix} \quad 3.3$$

$$= \begin{bmatrix} m_{B11} & m_{B12} \\ m_{B21} & m_{B22} \end{bmatrix} \quad 3.4$$

$$\text{Where } \delta_{Bi} = \frac{2\pi n_{Bi} d_{Bi} cos\theta_{Bi}}{\lambda} \quad 3.5$$

It is the phase shift experienced by the electromagnetic waves when they encounter the interfaces of the 1D bilayer PC system, and the i represents the order of the layer. Equation 3.5 is obtained from the equations 2.28-2.46 provided in chapter 2. Besides, n_{Bi} is the refractive index and d_{Bi} is the thickness of the dielectric material, and $\Theta_B i$ is the angle between light and the interface normal.

From equation 3.5, the quantities m_{B11}, m_{B12}, m_{B21}, and m_{B22} are the elements of the matrix M_B. Equation 3.4 is the characteristic matrix for the propagation of an electromagnetic wave through a unit cell only. In this work, the propagation of electromagnetic waves through both 1D bilayer and 1D ternary systems is extended to different numbers of periods (N). Consequently, the characteristic matrix for a particular number of periods (N) can be found using the equation provided in chapter 2 [equations 2.28-2.46].

Moreover, the characteristic matrix provides the transmission coefficient, which is essential to study the transmission properties of the propagated waves. Consequently, the transmission coefficient for the 1D bilayer PC system can be expressed as T_B, and its magnitude can be obtained from the characteristic matrix provided in equation 3.4. Generally, the quantification of T_B depends on the number of periods, N. Based on N, the optical density of transmission has been changed. It will reflect on the value of the transmission coefficient. Thus, the equation of the transmission coefficient is referenced from chapter 2 (equation 2.52). The transmission coefficient for the 1D bilayer PC can be rewritten as

$$T_B = |t_B|^2 \tag{3.6}$$

Where,

$$t_B = \left| \frac{2}{m_{B11} + m_{B12} + m_{B21} + m_{B22}} \right| \tag{3.7}$$

the elements m_{B11}, m_{B12}, m_{B21}, and m_{B22} are obtained from the equation 3.4.

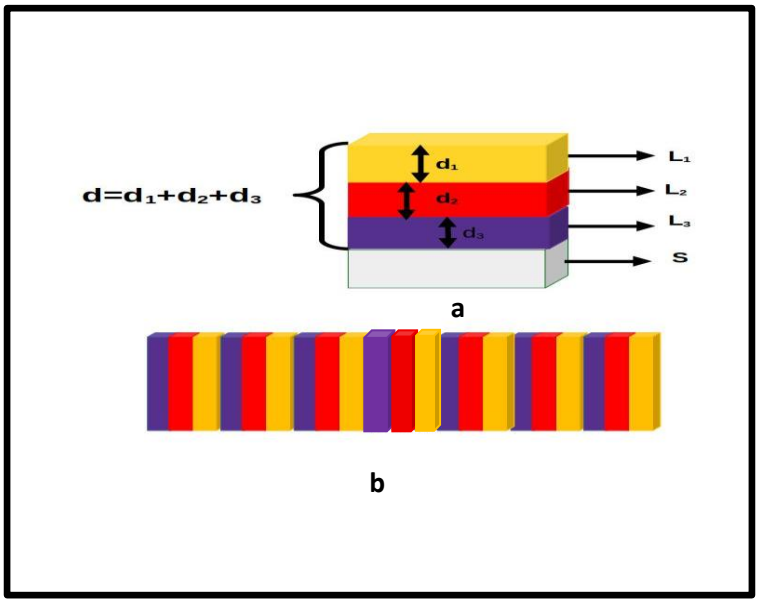

Figure 3.2. Schematic representation of 1D DNA-templated PC (1D ternary PC) where a) unit cell and b) 1D ternary PC of period N=7

According to the DNA-templated PC, the unit cell contains three dielectric layers with refractive indices n_1, n_2, and n_3 and thicknesses d_1, d_2, and d_3. Therefore, we have three transfer matrices for describing the transmission properties of the system, and they are M_{T1}, M_{T2}, and M_{T3}, respectively. Figure 3.2 shows a schematic diagram of a 1D ternary PC system where the isotropic layers that constitute the unit cell are named as L_1, L_2, and L_3. The characteristic matrix of the 1D ternary PC system includes the product of three propagation matrices corresponding to three distinct periodically arranged isotropic materials. Their corresponding transfer matrices are given as

For layer L_1,

$$M_{T1}=\begin{bmatrix} cos\delta_{T1} & i\eta^{-1}sin\delta_{T1} \\ i\eta sin\delta_{T1} & cos\delta_{T1} \end{bmatrix} \quad 3.8$$

For layer L_2,

$$M_{T2}=\begin{bmatrix} cos\delta_{T2} & i\eta^{-1}sin\delta_{T2} \\ i\eta sin\delta_{T2} & cos\delta_{T2} \end{bmatrix} \quad 3.9$$

For layer L_3, the transfer matrix becomes;

$$M_{T3}=\begin{bmatrix} cos\delta_{T3} & i\eta^{-1}sin\delta_{T3} \\ i\eta sin\delta_{T3} & cos\delta_{T3} \end{bmatrix} \quad 3.10$$

$$\text{Where, } \delta_{Ti} = \frac{2\pi n_{Ti} d_{Ti} cos\theta_{Ti}}{\lambda} \quad 3.11$$

It is the phase shift experienced by the electromagnetic wave at each interface in the structure, and i represents the number of layers 1, 2, and 3. Similarly, n_{Ti} is the refractive index and d_{Ti} is the thickness of the dielectric material, θ_{Ti} is the angle between light and the interface normal of the 1D ternary PC system.

In the case of a 1D bilayer PC system, the characteristic matrix of the unit cell of a 1D ternary PC system can be expressed as the product of the transfer matrix of each three layers L_1, L_2, and L_3. The characteristic matrix, M_T, is obtained as;

$$M_T = M_{T1}M_{T2}M_{T3} = \begin{bmatrix} cos\delta_{T1} & i\eta^{-1}sin\delta_{T1} \\ i\eta sin\delta_{T1} & cos\delta_{T1} \end{bmatrix}\begin{bmatrix} cos\delta_{T2} & i\eta^{-1}sin\delta_{T2} \\ i\eta sin\delta_{T2} & cos\delta_{T2} \end{bmatrix}\begin{bmatrix} cos\delta_{T3} & i\eta^{-1}sin\delta_{T3} \\ i\eta sin\delta_{T3} & cos\delta_{T3} \end{bmatrix} \quad 3.13$$

$$= \begin{bmatrix} m_{T11} & m_{T12} \\ m_{T21} & m_{T22} \end{bmatrix} \quad 3.14$$

Where, m_{T11}, m_{T12}, m_{T21}, and m_{T22} are the elements of the 2x2 matrix M_T.

The transmission coefficient for the 1D ternary PC system can be expressed as

$$\boldsymbol{T_T} = |t_T|^2 \qquad 3.15$$

$$\text{Where, } t_T = \left|\frac{2}{m_{T11}+m_{T12}+m_{T21}+m_{T22}}\right| \qquad 3.16$$

The elements, m_{T11}, m_{T12}, m_{T21}, and m_{T22} are obtained from equation 3.14.

Equations 3.6 and 3.15 provide the complete information regarding the optical transfer properties of the 1D bilayer PC and 1D ternary PC systems.

3.3 Theoretical observation and analysis

The properties of PCs can be altered by changing the refractive index, thickness, and number of layers of the PCs. This study focuses on the effects of a template in the PBG by changing the periodicity of the microstructures. When introducing a layer with a refractive index n as a template for every layer of the unit cell, the thickness of the entire unit cell has been changed. It will alter the periodicity of the PC, so the bandgap. The changes can be analysed using the TMM. This work has introduced DNA as the template because of its unique optical property in the visible region of light. The materials selected for the theoretical simulation are silica, zinc oxide (ZnO), alumina, and graphite oxide (GO). By using these materials, six PC systems such as Silica/ZnO, Silica/Alumina, Silica/ Graphite oxide (GO), Alumina/GO, Alumina/ZnO, and GO/ZnO are designed. The refractive index of

silica, zinc oxide, alumina, graphite oxide, and DNA are 1.4585, 2.0034, 1.7682, 1.96, and 1.5826, respectively. The thickness, d, of layers (lattice constant) of all the PC systems is taken from 50nm - 600nm. The number of period (N) of the PCs are taken from 1-100[24-31, 45-51].

3.3.1 Transmission properties of the unit cell of the photonic crystals with and without the presence of DNA template

A unit cell is described as the fundamental microstructure of a PC, as the unit cell in a crystal system. The number and thickness of the dielectric layers in a unit cell of the PC are repeated periodically for the entire system to form a PC. The transmission behaviour of the PC of the unit cell in the absence and presence of a DNA-template is observed. The transmission behaviour of the PCs has been observed in 200-1200 nm region of electromagnetic wave spectra. The thickness of the layers of the unit cell is taken as d_1 50 nm and d_2 =100 nm, and the thickness taken for the DNA layer, $d_{DNA,}$ is 90 nm.

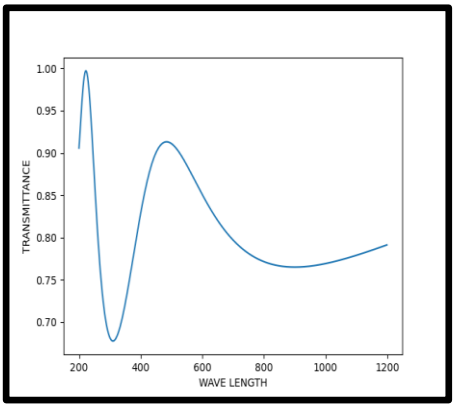

Figure 3.3: Transmission properties of 1D Silica/ZnO PC in the absence of DNA template
N=1; d_1=50 nm, d_2=100 nm

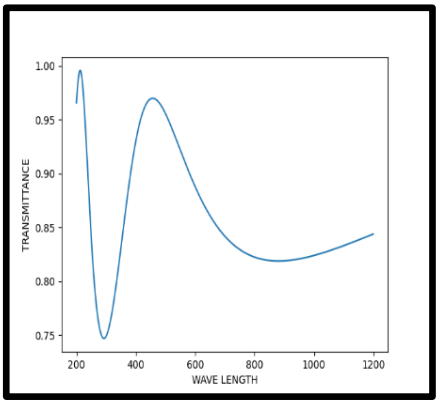

Figure 3.4: Transmission properties of 1D Silica/Alumina PC in the absence of DNA template
N=1; d_1=50 nm, d_2= 100 nm

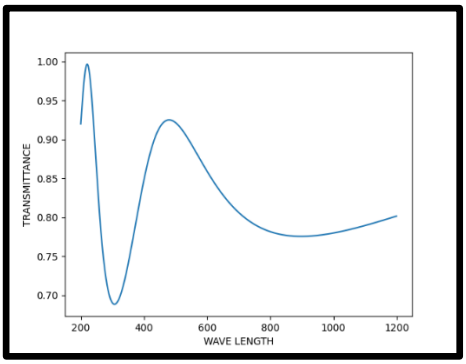

Figure 3.6: Transmission properties of 1D GO/ZnO PC in the absence of DNA template
N=1;d_1=50 nm, d_2=100 nm

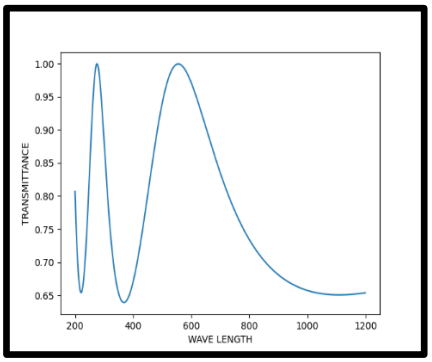

Figure 3.5: Transmission properties of 1D Silica/GO PC in the absence of DNA template
N=1;d_1=50 nm, d_2=100 nm

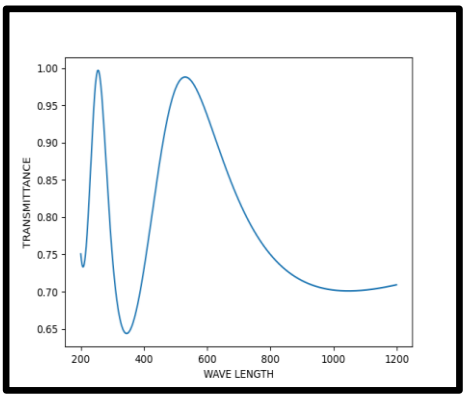

Figure 3.7 : Transmission properties of 1D Alumina/GO PC in the absence of DNA template
N=1;d_1=50 nm, d_2=100 nm

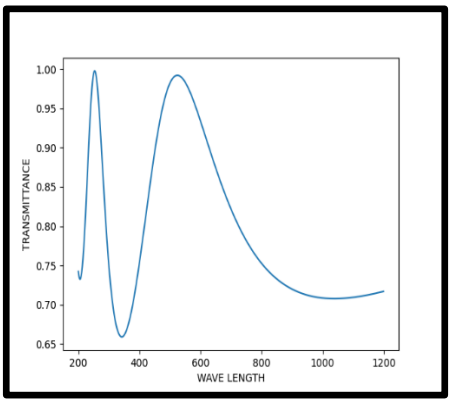

Figure 3.8 : Transmission properties of 1D Alumina/ZnO PC in the absence of DNA template
N=1;d_1= 50 nm, d_2=100nm

Figure 3.3-3.8 shows the transmission properties of 1D PCs in the absence of DNA template for a unit cell within the electromagnetic spectrum range of 200–1200 nm. In the absence of the DNA template, a PBG is observed in the 300–400 nm range, corresponding to the visible region of light. All six proposed 1D PC unit systems in the absence of DNA-template exhibit maximum transmittance at around 600 nm.

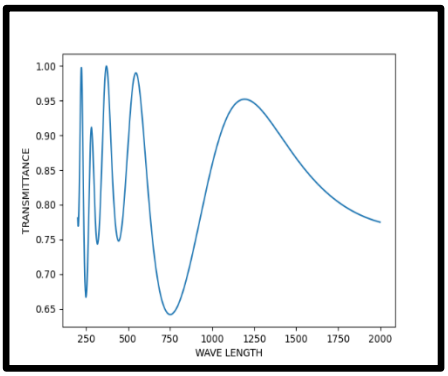

Figure 3.9 : Transmission properties of DNA templated 1D Silica/Alumina PC N=1; d_1=50 nm, d_2=100nm , d_{DNA}= 90 nm

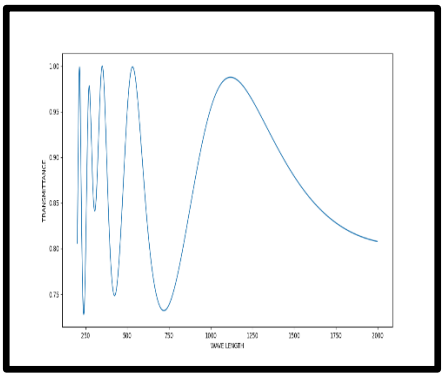

Figure 3.10 : Transmission properties of 1D DNA templated Silica/ZnO PC N=1; d1= 50 nm, d2=100 nm, d_{DNA}=90 nm

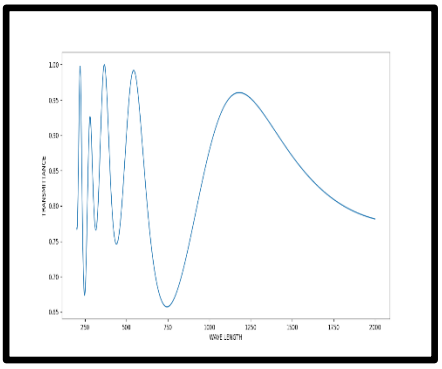

Figure 3.11 : Transmission properties of 1D DNA templated Silica/GO PC N=1; d_1=50 nm, d_2= 100 nm, d_{DNA}=90 nm

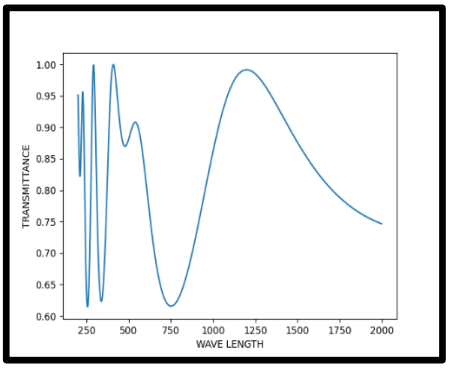

Figure 3.12 : Transmission properties of 1D DNA templated GO/ZnO PC N=1;d_1=50 nm, d_2= 100 nm, d_{DNA}=90 nm

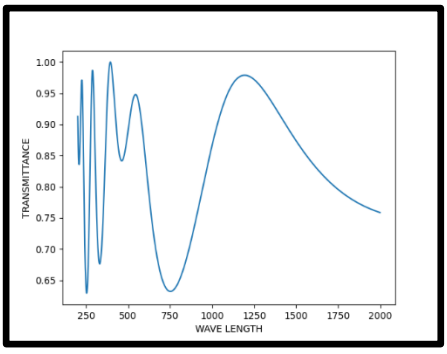

Figure 3. 13: Transmission properties of 1D DNA templated Alumina/GO PC N=1;d_1= 50 nm, d_2= 100 nm, d_{DNA}=90 nm

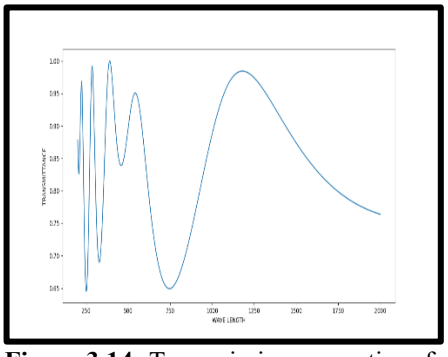

Figure 3.14: Transmission properties of 1D DNA templated Alumina/ZnO PC N=1;d_1= 50 nm, d_2= 100 nm, d_{DNA}=90 nm

The transmission properties of the unit cell of the proposed 1D DNA templated PCs are shown in Figures 3.9-14. In the presence of a DNA template, photonic band gaps are present in the visible region at 400 nm-600 nm. In the case of DNA templated PCs, the transmittance peak shifts into the longer region of the light. The maximum transmittance is shown at 700 – 1200 nm of the electromagnetic spectrum. The changes are the result of the DNA template in the PC system. Due to the presence of the template, the periodicity, thickness, and refractive index contrast between the adjacent layers of the microstructures have been changed. This affects the increase in the formation of band gaps in the system.

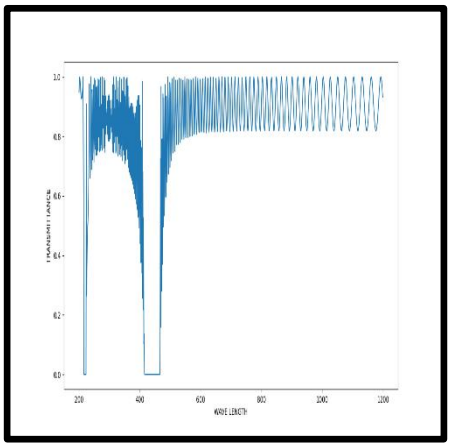

Figure 3.15: Transmission properties of 1D Silica /ZnO photonic crystals in the absence of DNA template
N=100;d_1=50 nm, d_2= 100 nm

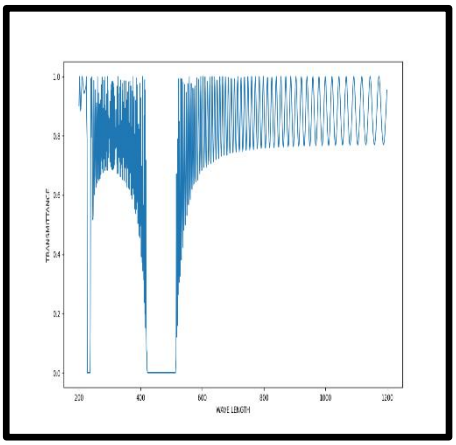

Figure 3.16: Transmission properties of 1D Silica /Alumina PC in the absence of DNA template
N=100;d_1= 50 nm, d_2= 100 nm

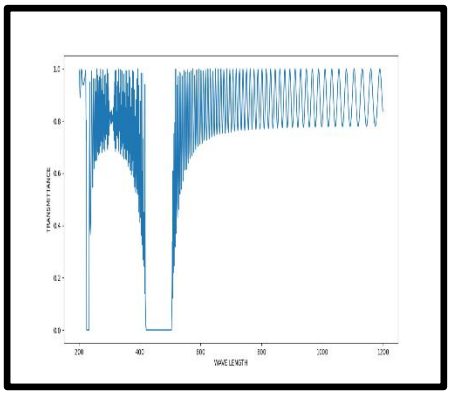

Figure 3.17: Transmission properties of 1D Silica/GO PC in the absence of DNA template,
N=100;d_1= 50 nm, d_2= 100 nm

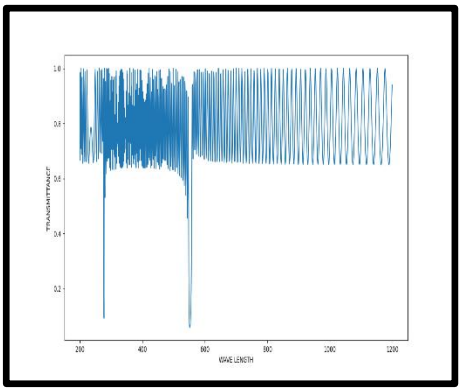

Figure 3.18: Transmission properties of 1D GO/ZnO PC in the absence of DNA template,
N=100;d_1= 50 nm, d_2= 100 nm

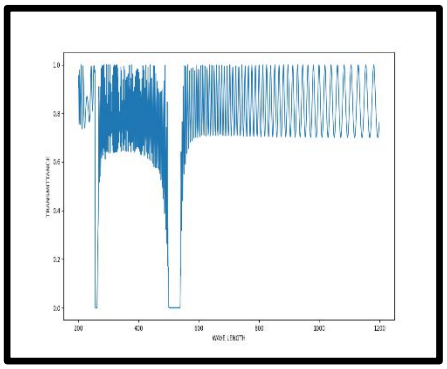

Figure 3.19 : Transmission properties of 1D Alumina/GO PC in the absence of DNA template
N=100;d_1= 50 nm, d_2= 100 nm

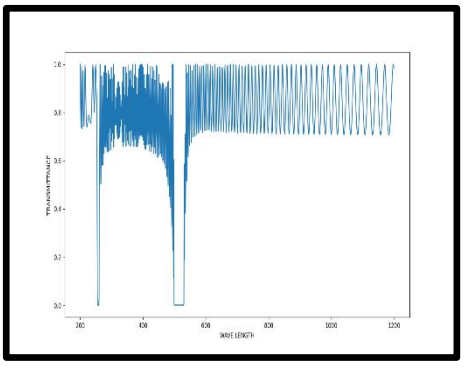

Figure 3.20 ; Transmission properties of 1D Alumina/ZnO PC in the absence of DNA template
N=100;d_1= 50 nm, d_2= 100 nm

3.3.2 Transmission properties of 1D photonic crystal for N=100 with and without the presence of DNA template

The transmission properties of a single unit cell are insufficient to fully understand the effect of the DNA template in PCs, as the transmittance peaks obtained for the unit cell are not clearly distinguishable. To

obtain well-resolved transmission spectra, it is necessary to increase the number of layers in the PC structure. Therefore, the number of periodicities is increased up to 100 and the changes are observed. As the number of layers (N) increases, the band gap effects are significantly changed. Figures 3.15- 3.20 show the bandgap effects of the PCs in the absence of a DNA template. From these results, a PBG is seen at 400 nm-500nm regions of light. Among these results, the width of the bandgap of the 1D GO/ZnO PCs is reduced significantly as compared to other combinations of the PCs. The refractive index contrast of the ZnO layer and the GO layer is very small compared to other dielectric layers of the PCs. The PBG increases with a larger refractive index contrast, whereas for structures with smaller layer widths, a lower refractive index contrast is preferred [1–23].

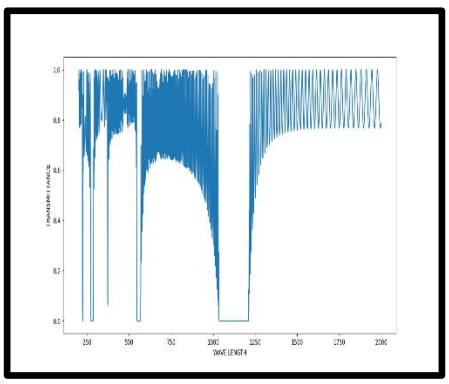

Figure 3.21 : Transmission properties of 1D DNA templated Silica /ZnO photonic crystals, N=100; d_1= 50 nm, d_2= 100 nm, d_{DNA}= 90 nm

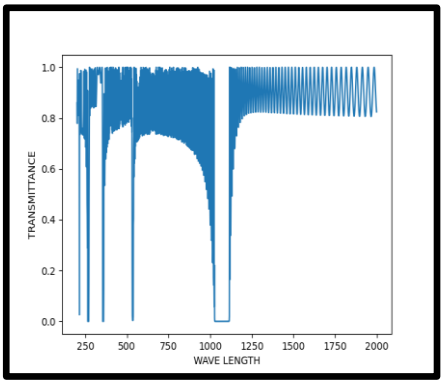

Figure 3.22 : Transmission properties of 1D DNA templated Silica /Alumina photonic crystals, N=100; d_1= 50 nm, d_2= 100 nm, d_{DNA}= 90 nm

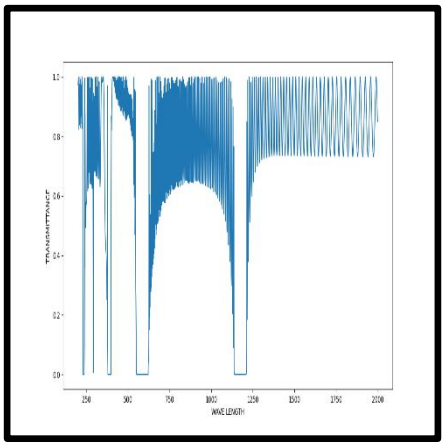

Figure 3.23 : Transmission properties of 1D DNA templated Silica/GO photonic crystals N=100;d_1= 50 nm, d_2= 100 nm, d_{DNA}= 90 nm

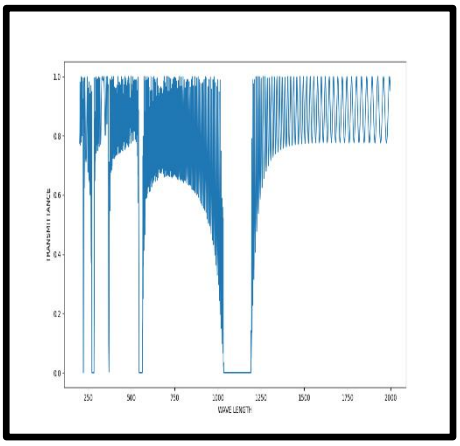

Figure 3.24 : Transmission properties of 1D DNA templated GO/ZnO photonic crystals N=100;d_1= 50 nm, d_2= 100 nm, d_{DNA}= 90 nm

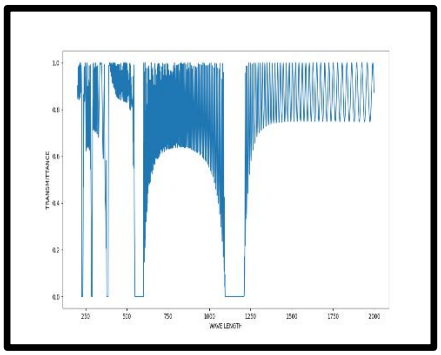

Figure 3.25. Transmission properties of 1D Alumina/GO photonic crystals in the absence of DNA template N=100; d_1= 50 nm, d_2= 100 nm,

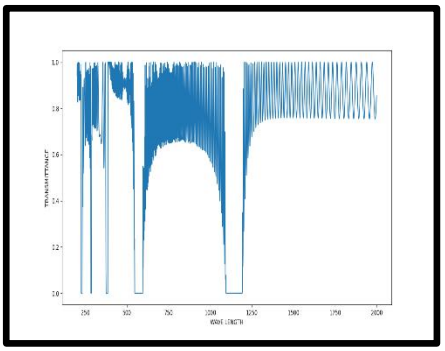

Figure 3.26. Transmission properties of 1D DNA templated Alumina/ZnO photonic crystals N=100;d_1= 50 nm, d_2= 100 nm, d_{DNA}=

Figures 3.21-3.26 show the transmission properties of the PCs in the presence of a DNA template. As compared to the figures 15-20, these results show that the width, the position, and the number of PBG are changed. From Figure 21-26, two band gaps are seen, and one of the band gaps is seen at the 530nm-550 nm region of the electromagnetic

spectrum, and the second band gap is located at the 1000 nm- 1200 nm region of the electromagnetic spectrum. One of the important changes seen in the presence of the DNA template is that the width of the bandgap formed in the visible region is significantly reduced as compared to the band gap formed in the absence of the DNA template. Apart from, the width of the PBG of 1D DNA templated Silica/ Alumina, Silica/ GO and Silica/ ZnO PCs seen at the visible region is very narrow as compared to the width of the bandgap seen for the 1D DNA templated GO/ZnO, Alumina/GO, Alumina/ ZnO, 1D non-DNA templated Silica/ Alumina, Silica/ GO and Silica/ ZnO PCs. According to PCs, the optical parameters such as thickness, refractive index, and number of layers of the microstructures affect the PBG of the PC system. When DNA is introduced as a template between two different microstructures, the refractive index contrast is reduced, while the thickness, number of layers, and number of interfaces within the unit cell increase. These modifications impart unique properties to the 1D ternary PCs, distinguishing them from their corresponding bilayer structures.

From the theoretical results, it is observed that more than one band gap is seen in the transmission spectrum. The formation of multiple band gaps is due to the increased number of interfaces within the unit cell. The diffraction forms the PBG that occurs at the interfaces of the unit cell as light encounters them. In the case of a bilayer PC, the interference after the diffracted waves occurs due to the two interfaces. However, in the case of a ternary unit cell, three interfaces are formed. Hence, the diffraction at the interfaces becomes complex to get more

than one PBG.The narrow width of the PBG is due to the low refractive index contrast between the adjacent layers.

Among the six combinations of DNA templated structures, Silica/DNA/ZnO provides a large PBG width in the range of 1000 nm-1250 nm. By selecting an appropriate central wavelength, this gap can be tuned into the visible region. Moreover, this configuration also shows a higher oscillation density compared to the others.

The refractive index of the DNA at the optical band is comparatively near to the refractive index of the silica, which results in a reduced bandgap width in the visible region. On the other hand, if the refractive index contrast and thickness are increased, the PBG width is increased and its position is shifted to the longer wavelength region of the optical band. It is evident from Figures 3.21 to 3.26.

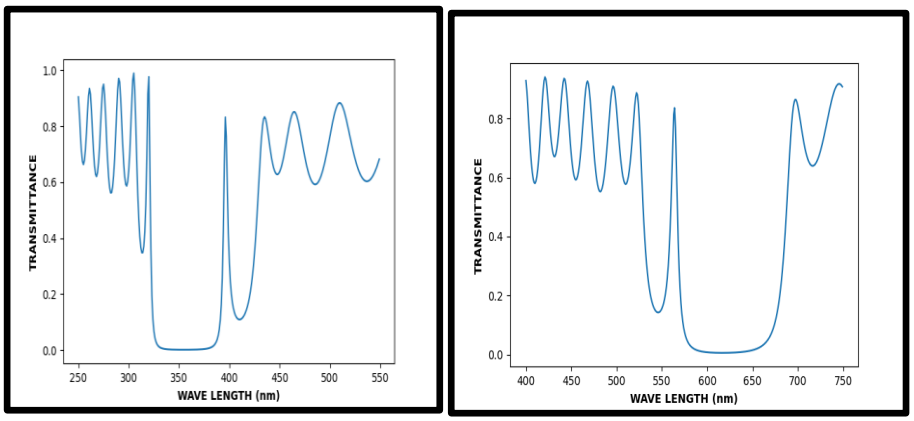

a **b**

Figure 3.27: Defective modes of a) 1D defective bilayer Silica/ZnO PC and b) 1D defective ternary Silica/DNA/ZnO PC

3.3.3 The Optical response of 1D ternary defective Silica/DNA/ZnO photonic crystal

It is very crucial to study the optical behaviour of the PC within the optical band 350nm-750nm, where most of the applications, including optical filters, nonlinear optical devices of the photonic crystal, deal with. Keeping this view, the PBG effect of the proposed structures is to be designed in the optical band. Hence, the DNA-templated Silica/ZnO structures were selected from among the six studied systems due to their enhanced PBG characteristics.

Figure 3.27 exemplifies how defective modes of 1D bilayer and ternary structures of PC differ from each other. We have fixed the defective layer thickness as 120 nm, and the refractive index of the defective layer is taken as 1.33, equivalent to the refractive index of water. Figure 3.27a represents the defective modes of a 1D binary defective Silica/ZnO PC, where the PBG is obtained around 330 nm-425 nm. The thickness of the silica and ZnO for obtaining the PBG at this range is taken as 69 nm and 40 nm, respectively. The defect mode is obtained around 390 nm-420 nm. The full width at half maximum (FWHM) of the defect mode is obtained as 5.6 nm, and the defect mode intensity is found to be 83.3%. Whereas in the case 1D ternary Silica/DNA/ZnO, the thickness of the elemental layers is taken as 68 nm, 66 nm, and 50 nm for silica, DNA, and ZnO, respectively. The PBG is obtained around 530 nm-680 nm. The defect mode is formed at 564.2 nm with an intensity 84%. The FWHM of the defect mode is measured as 8.7 nm. From these results, it is more convenient that the features of 1D ternary PCs are more significant than their counter

bilayer structure. These data highlight that the proposed 1D ternary Silica/DNA/ZnO can be a promise for multifaceted purposes, including biosensors, optical filters, and nonlinear optical applications. Table 3.1 summarises the performance of the defective mode of 1D Silica/DNA/ZnO ternary PC over its counter 1D bilayer Silica/ZnO PC for the same number of periods, N=13.

Table 3.1 Comparison between the defect modes in 1D ternary Silica/DNA/ZnO PC and 1D bilayer Silica/ZnO PC

Sl No	PC system	PBG width (nm)	Defect Mode (nm)	FWHM (nm)	Intensity (%)
1	Silica/DNA/ZnO	135	564.2	8.7	84
2	Silica/ZnO	95	396.1	5.6	83.3

3.4 Conclusions

In this chapter, the transmission properties of DNA-templated 1D ternary silica/DNA/metal oxides and silica/DNA/graphite oxide PC (PC) systems in the wavelength range of 200–1200 nm of the electromagnetic spectrum were investigated using the TMM. The thickness and number of layers for each PC were kept constant across all samples to enable a comparison of the changes in transmission properties under the same experimental conditions. It was found that, in the absence of the DNA template, the bandgap formed in the visible region is located around 400 nm, and its width varies significantly depending on the refractive index contrast of the layers. However, in the presence of a DNA template, two band gaps are observed—one in

the visible region and the other in the infrared (IR) region. The bandgap in the visible region is located at the longer wavelength range (530–650 nm) and is relatively narrow, while the second bandgap in the IR region is comparatively wider. The inclusion of the DNA template alters the refractive index contrast and the adequate thickness of the microstructures. This change in periodicity influences the position, number, and width of the photonic band gaps. Due to the optical transparency of DNA polymer in the visible region, it can be effectively used to tune the bandgap of PCs. Among the six DNA-templated configurations, the 1D ternary Silica/DNA/ZnO PC exhibits notable PBG effects. Additionally, we examined the defect mode of the 1D ternary defective Silica/DNA/ZnO PC. A comparative study was conducted with its counterpart, the 1D bilayer defective Silica/ZnO PC. The results show that the 1D ternary PC offers a defect mode with higher intensity and a larger full width at half maximum (FWHM) compared to its bilayer counterpart. Hence, the confinement effect in DNA-templated 1D PCs within the visible region can be utilized for label-free biosensing, nonlinear optical studies, and optical filtering in solar cell applications. Therefore, it can be concluded that selecting an appropriate template can significantly enhance the performance of PCs for various applications.

References

[1] Joannopoulos, J. D., Johnson, S. G., Winn, J. N., & Meade, R. D. (2008). Molding the flow of light. Princet. Univ. Press. Princeton, NJ [ua], 12.

[2] Swaby, B. (2002). Simple computations involving two-component symmetric trilayers. Applied optics, 41(28), 5984-5988.

[3] Wu, K., Gu, W. X., Wu, C., Ma, J. L., & Ma, X. Y. (2014). Study on the Optical Transmission Properties of One-dimensional PC of MoS2. Advanced Materials Research, 1056, 42-46.

[4] Gong, Q., & Hu, X. (2013). PCs. In Principles and Applications. Pan Stanford Publishing.

[5] Inan, H., Poyraz, M., Inci, F., Lifson, M. A., Baday, M., Cunningham, B. T., & Demirci, U. (2017). PCs: emerging biosensors and their promise for point-of-care applications. Chemical society reviews, 46(2), 366-388.

[6] Divya, J., Selvendran, S., & Raja, A. S. (2018). PC-based optical biosensor: a brief investigation. Laser Physics, 28(6), 066206.

[7] Arunkumar, R., Suaganya, T., & Robinson, S. (2019). Design and analysis of 2D PC based biosensor to detect different blood components. Photonic Sensors, 9, 69-77.

[8] Armenise, M. N., Campanella, C. E., Ciminelli, C., Dell'Olio, F., & Passaro, V. M. (2010). Phononic and photonic band gap structures: modelling and applications. Physics Procedia, 3(1), 357-364.

[9] Cunningham, B. T., Zhang, M., Zhuo, Y., Kwon, L., & Race, C. (2015). Recent advances in biosensing with PC surfaces: a review. IEEE Sensors Journal, 16(10), 3349-3366.

[10] Akbar, F., Syahriar, A., & Lubis, A. H. (2014, November). Dispersion relation of 1D PC. In 2014 International Conference on Electrical Engineering and Computer Science (ICEECS) (pp. 69-73). IEEE.

[11] Armenise, M. N., Campanella, C. E., Ciminelli, C., Dell'Olio, F., & Passaro, V. M. (2010). Phononic and photonic band gap structures: modelling and applications. Physics Procedia, 3(1), 357-364.

[12] Aly, A. H., Ameen, A. A., Mahmoud, M. A., Matar, Z. S., Al-Dossari, M., & Elsayed, H. A. (2021, September). Photonic crystal

enhanced by metamaterial for measuring electric permittivity in GHz range. In Photonics (Vol. 8, No. 10, p. 416). MDPI.

[13] Aly, A. H., Mohamed, D., & Mohaseb, M. A. (2020). Metamaterial control of hybrid multifunctional High-Tc superconducting photonic crystals for 1D Quasi-periodic structure potential applications. Materials Research, 23(3), e20190695.

[14] Watan, A. W., Mohammed, I. A., Hameed, H. K., Jasim, K. A., & Shaba, A. H. (2022). Thermal and Mechanical Behaviour of Heat-resistant Clay-silica Composites. NeuroQuantology, 20(3), 43.

[15] Aly, A. H., Sabra, W., & Elsayed, H. A. (2017). Cutoff frequency in metamaterials photonic crystals within Terahertz frequencies. International Journal of Modern Physics B, 31(15), 1750123.

[16] Al-Dossari, M., Awasthi, S. K., Mohamed, A. M., Abd El-Gawaad, N. S., Sabra, W., & Aly, A. H. (2022). Bio-alcohol sensor based on one-dimensional photonic crystals for detection of organic materials in wastewater. Materials, 15(11), 4012.

[17] Zhang, X., Jiao, Y. C., Weng, Z. B., Zhang, Y. X., & Feng, S. (2019). Wideband magneto-electric dipole antenna with a claw shaped reflector for 5G communication systems. Microwave and Optical Technology Letters, 61(9), 2098-2104.

[18] Natesan, A., Govindasamy, K. P., Gopal, T. R., Dhasarathan, V., & Aly, A. H. (2019). Tricore photonic crystal fibre based refractive index sensor for glucose detection. IET Optoelectronics, 13(3), 118-123.

[19] A.H. Aly, S.S.A. Ghany, B.M. Kamal, D. Vigneswaran, Theoretical studies of hybrid multifunctional YaBa2Cu3O7 photonic crystals within visible and infra-red regions. Ceramics International, 46(1), 365-369.2020.

[20] Hossain, M. S., & Sen, S. (2021). Design and performance improvement of optical chemical sensor based photonic crystal fiber (PCF) in the terahertz (THz) wave propagation. Silicon, 13(11), 3879-3887.

[21] Aly, A. H., & Mohamed, D. (2015). BSCCO/SrTiO 3 one dimensional superconducting photonic crystal for many applications. Journal of Superconductivity and Novel Magnetism, 28, 1699-1703.

[22] Zaky, Z. A., Alamri, S., Zhaketov, V. D., & Aly, A. H. (2022). Refractive index sensor with magnified resonant signal. Scientific Reports, 12(1), 13777.

[23] Aly, A. H., Awasthi, S. K., Mohamed, A. M., Al-Dossari, M., Matar, Z. S., Mohaseb, M. A., ... & Amin, A. F. (2021). 1D reconfigurable bistable photonic device composed of phase change material for detection of reproductive female hormones. Physica Scripta, 96(12), 125533.

[24] Inagaki, T., Hamm, R. N., Arakawa, E. T., & Painter, L. R. (1974). Optical and dielectric properties of DNA in the extreme ultraviolet. The journal of chemical physics, 61(10), 4246-4250.

[25] Joyce, D. M. (2013). The development of DNA-based bio-polymer hybrid thin films for capacitor applications (Doctoral dissertation, University of Dayton).

[26] Dugasani, S. R., Gnapareddy, B., Kesama, M. R., Jeon, S., Jeong, J. H., & Park, S. H. (2019). Optoelectronic properties of DNA thin films implanted with titania nanoparticle-coated multiwalled carbon nanotubes. AIP Advances, 9(1).

[27] Kokkiligadda, S., Dugasani, S. R., Komarala, E. P., Jeon, S., Jeong, J. H., & Park, S. H. (2021). Controlling physical characteristics of DNA and DNA-CTMA thin films by embedding with graphene oxide and riboflavin. Journal of Physics D: Applied Physics, 54(37), 375401.

[28] Prajzler, V., Jung, W., Oh, K., Cajzl, J., & Nekvindova, P. (2020). Optical properties of deoxyribonucleic acid thin layers deposited on an elastomer substrate. Optical Materials Express, 10(2), 421-433.

[29] Hebda, E., Jancia, M., Kajzar, F., Niziol, J., Pielichowski, J., Rau, I., & Tane, A. (2012). Optical properties of thin films of DNA-CTMA and DNA-CTMA doped with Nile blue. Molecular Crystals and Liquid Crystals, 556(1), 309-316.

[30] Nithyaja, B., Misha, H., & Nampoori, V. P. N. (2012). Synthesis of silver nanoparticles in DNA template and its influence on nonlinear optical properties. Nanosci Nanotechnol, 2(4), 99-103.

[31] Cuervo, A., Dans, P. D., Carrascosa, J. L., Orozco, M., Gomila, G., & Fumagalli, L. (2014). Direct measurement of the dielectric polarization properties of DNA. Proceedings of the National Academy of Sciences, 111(35), E3624-E3630.

[32] Ankita, Suthar, B., & Bhargava, A. (2021). Biosensor application of one-dimensional photonic crystal for malaria diagnosis. Plasmonics, 16(1), 59-63.

[33] Aly, A. H., Zaky, Z. A., Shalaby, A. S., Ahmed, A. M., & Vigneswaran, D. (2020). Theoretical study of hybrid multifunctional one-dimensional photonic crystal as a flexible blood sugar sensor. Physica Scripta, 95(3), 035510.

[34] ar, M., Doll, T., kovi, J., & Scherer, A. (2000). Design and fabrication of silicon photonic crystal optical waveguides. Journal of lightwave technology, 18(10), 1402.

[35] Inoue, K., & Ohtaka, K. (Eds.). (2004). Photonic crystals: physics, fabrication and applications (Vol. 94). Springer Science & Business Media.

[36] Soukoulis, C. M. (2002). The history and a review of the modelling and fabrication of photonic crystals. Nanotechnology, 13(3), 420.

[37] Cheng, C. C., & Scherer, A. (1995). Fabrication of photonic band-gap crystals. Journal of Vacuum Science & Technology B: Microelectronics and Nanometer Structures Processing, Measurement, and Phenomena, 13(6), 2696-2700.

[38] Busch, K., Lölkes, S., Wehrspohn, R. B., & Föll, H. (Eds.). (2006). Photonic crystals: advances in design, fabrication, and characterization. John Wiley & Sons.

[39] Hudak, Y. I. (2017). On the mathematics problem of multilayered dielectric systems in the classical electrodynamic. Russian Technological Journal, 5(3), 160-188.

[40] Pandey, J. P. (2017). Transfer matrix method for one-dimensional photonic crystals. J. Ramanujan Soc. Math Math Sc, 6(1), 121-130.

[41] Villa-Villa, F., & Gaspar-Armenta, J. A. (2006). Brewster angle and optical tunneling in one-dimensional photonic crystals composed of left-and right-handed materials. JOSA B, 23(2), 375-380.

[42] Lekner, J. (2013). Theory of reflection of electromagnetic and particle waves (Vol. 3). Springer Science & Business Media. [67] Pedrotti, F. L., Pedrotti, L. M., & Pedrotti, L. S. (2018). Introduction to optics. Cambridge University Press.

[43] Abbas, S., Salman, S. R., & Abbas, A. S. (2021). Studying of the polarization modes TE and TM for oblique incidence of light on thin

films. Digest Journal of Nanomaterials and Biostructures, 16(2), 647-657.

[44] Pendry, J. B. (1994). Photonic band structures. Journal of modern optics, 41(2), 209-229.

[45] Satvekar, R. K., Phadatare, M. R., Karande, V. A., Patil, R. N., Tiwale, B. M., & Pawar, S. H. (2012). Influence of silane content on the optical properties of sol gel derived spin coated silica thin films. Int. J. Basic Appl. Sci, 1(9).

[46] Bond, W. L. (1965). Measurement of the refractive indices of several crystals. Journal of Applied Physics, 36(5), 1674-1677.

[47] Martin, J. E., Anderson, M. T., Odinek, J., & Newcomer, P. (1997). Synthesis of periodic mesoporous silica thin films. Langmuir, 13(15), 4133-4141.

[48] Rahman, I. A., & Padavettan, V. (2012). Synthesis of silica nanoparticles by sol-gel: size-dependent properties, surface modification, and applications in silica-polymer nanocomposites—a review. Journal of nanomaterials, 2012(1), 132424.

[49] Malitson, I. H. (1965). Interspecimen comparison of the refractive index of fused silica. Josa, 55(10), 1205-1209.

[50] Tan, C. Z. (1998). Determination of refractive index of silica glass for infrared wavelengths by IR spectroscopy. Journal of Non-Crystalline Solids, 223(1-2), 158-163.

W.L.Bond, Measurement of the refractive indices of several crystals, J.Appl.Phys.36, 1674-1677(1965)

[51] Malitson, I. H., & Dodge, M. J. (1972). Refractive index and birefringence of synthetic sapphire. J. Opt. Soc. Am, 62(11), 1405. M. J. Dodge, "Refractive Index" in Handbook of Laser Science and Technology, Volume IV, Optical Materials: Part 2, CRC Press, Boca Raton, 1986, p. 30

Chapter 4

Design and Experimental Performance of 1D Silica/DNA/ZnO Photonic Crystal for Bovine Serum Albumin Detection in Blood

This chapter discusses the role of one-dimensional (1D) ternary photonic crystal (PC) as a biosensor. A novel 1D ternary PC has been fabricated, and its sensing performance has been analyzed for the detection of bovine serum albumin (BSA). The fabrication of the proposed system is realized by using the dip coating method at low temperature film treatment. The unit cell consists of silica, deoxyribonucleic acid (DNA) complex (CD), and zinc oxide (ZnO), along with BSA used as the defective layer, respectively. The optical properties have been exploited both theoretically and experimentally. The theoretical study has been done by the transfer matrix method (TMM) and COMSOL software. The experimental studies are carried out by analyzing the reflection spectrum. The PC system provides two photonic band gaps at the range of wavelength 430 nm – 470nm and near IR region of wavelength in the range of 862nm-949nm. The defect mode was observed at 430 nm -470 nm of the electromagnetic spectrum. The experimental value of sensitivity is 858 nm/RIU, which is in good agreement with the theoretical result for the same concentration of BSA. Hence, this system can be a promising element for biosensing applications and environmental monitoring as well.

4.1 Introduction

Biosensors are the key and primary devices for diagnosing diseases. They are exploited to monitor the biological elements such as sugar, various enzymes, hormones, antigens, antibodies, and proteins in the blood. There are diverse biological sensors (biosensors) available for monitoring blood sugar via an in vitro method. The majority of in vitro methods use chemical labelling in which the analyte undergoes a chemical reaction with the chemical reagents set in the sensor and gives rise to a signal in the form of fluorescence. These kinds of biosensors should be highly stable with surrounding physical parameters like temperature, humidity, pressure, and chemical parameters such as pH, and concentration of the analyte and reagents as well. The failure in maintaining the factors affects the basic features such as specificity, resolution, accuracy, time, pH, and simplicity of biosensors. Any failure to maintain the proper condition of any of these parameters fails to provide accurate and precise data for analyte monitoring. To overcome these drawbacks, diverse analytical methods are possible [1-32].

The term PC is now widely recognized as an ideal candidate for biosensing applications due to its tunable property that can facilitate light-matter interactions. In spite of chemical labelling methods, label-free biosensors are also considered better sensing devices. They use optical, electrical, or acoustic signals that result in the biological response of the analyte without using any fluorescent labels or reactants. Since, the PC operates purely based on the optical property of the materials, biosensors which utilize PC come in the label-free

category. As they are known for their ability to control the propagation of light, despite chemical reagents, they use the change in the refractive index of the analyte material. This peculiar condition of a PC based biosensor essentially removes the main drawbacks of labelled or fluorescent-based biosensors. Such that a labelled biosensor typically faces the chemical durability of the active chemical reagent of the sensor. The chemicals may undergo an oxidation process at room temperature. It will affect the pH and chemical reaction between the analyte and chemical reagent, which subsequently affects the credibility of the result [1-32].

Apart from the various prominent label-free optical biosensors, PC-based biosensors are instinct to have good performance and highly sensitive to even small amounts of biomarkers. Their ability to make the interaction between light and matter is inherent. Thus, they would be the emerging key devices that can be proposed for biosensors for detecting various biochemical markers. In principle, PC-based biosensors are referred to as refractive index sensors, since they are made to recognize the refractive index change of the analyte. Their sensitivity depends not only on the refractive index variation, but also on the thickness of the composition and angle of the incident wave in a similar way to how these parameters affect bandgap formation. The formation of the photonic band gap depends on specific parameters such as the refractive index contrast, the thickness of the dielectric layers, the angle of incidence, and the period. Once all these parameters are fixed, a translational symmetry will be formed due to the regular repetition of the unit cell. By creating defects in any of the

parameters within a unit cell, PCs can be effectively used for tuning the bandgap formation for various applications, including sensing. When creating a defect in a PC, a transmission mode will be formed within the bandgap. The defect can be introduced by altering the regular structure or repeating pattern of the unit cell. That can be done by introducing a new material (changing refractive index) and the thickness of any of the constituent layers of the unit cell itself. Thereby, a transmission (defect) mode will be formed within the bandgap range. The physical nature of the transmission mode, such as full width at half maximum (FWHM), and resonant wavelength position can be altered by introducing a change in the material property, such as refractive index and thickness of the defective material [1-32]. That is what is applied in a PC-based biosensor, where the analyte is treated as a defective layer.

The presence of an analyte introduced as a defect in a standard periodic PC system, thereby a defect mode is formed within the PBG. When the analyte concentration is changed, the refractive index of the analyte will be changed, resulting in a shift in the resonance mode. The shift in the resonance mode in response to the change in the refractive index can be monitored and quantified as sensitivity. The resolution of the PC-based biosensor is defined in terms of its sensitivity to minute changes in the refractive index of the analyte [1-32]. Moreover, their optical properties, the highlighting features of PCs that can be suitable for applying them as biosensors, are their dynamic structural properties. However, a PC is a nanoscale thin film of dielectric materials that is fabricated under high-temperature treatment above

room temperature. Thus, the films are processed to be highly stable against any temperature variation that comes below the manufacturing temperature. Another factor that contributes to the durability of PCs is the dielectric nature of their components, as the component films are inert to any chemical reactions, they will not interact chemically with the analyte and air. So, the optical parameter (refractive index) and chemical properties of the analyte will not be changed. It increases the accuracy and precision of working and the result of a PC-based biosensor [1-32].

The previously reported research articles mainly dealt with binary photonic systems, whereas ternary PC systems are less recognised in this area. In 2024, Nasr et al. reported a 1D binary PC based PC for sensing blood infection with a maximum sensitivity of 625 nm/RIU against infected blood plasma component [16]. Numayer A Zaman *et al.* reported a theoretical simulation study on a 1D binary PC of Si/Silica to detect waterborne bacteria. They reported the sensitivity of the proposed binary PC is 2489nm/RIU [17]. A theoretical study on annular 1D binary PC for salinity sensing is reported in 2023 by Sayed et al. [18]. They observed that the system has a sensitivity of 782 nm/RIU. In 2021, S E-S Abd El-Ghany et al. designed and analysed theoretically a 1D binary Si/SiO2 defective PC system for blood haemoglobin sensing. They have observed that the system has an average sensitivity of 1025 nm/RIU [19]. In 2009, A. Banerjee proposed a 1D ternary PC-based biosensor. He reported that one-dimensional ternary PCs are suggested as refractometric sensing elements for sensing minimal refractive index changes of a medium.

Besides, he observed that 1D ternary PC is more sensitive than 1D binary PC-based sensing element [20]. In 2023, Mouncharih et. al reported a 1D ternary PC for sensing glucose concentration in human urine. They have observed that the sensitivity of the proposed ternary PC is 965 nm/RIU, where the period of the system is 6 [21]. These observations revealed that the scope of PCs as biosensors is yet to come, and their tailored conformations should be widely used for biosensing purposes, especially 1D binary and ternary PC, and 2D PC [22-32].

This work proposed a ternary unit cell system to constitute a 1D PC structure that shall be intended to perform as a biosensor. The performance of the PC as a biosensor is investigated theoretically and experimentally. The proposed 1D ternary PC is a Silica/DNA/ZnO PC system for sensing the blood plasma component, namely serum albumin protein. It is considered an essential factor for living body functions. The materials chosen for designing PCs are silica (SiO_2), deoxyribonucleic acid (DNA), and ZnO[33-43]. These materials have nearly adjacent refractive indices, but they can behave as stable films at low temperature and are comparatively highly transparent to visible light. Their absorption in the visible range and near-IR range is found to be negligible. The other features that make them popular are that their making cost is very cheap. Their film structure can be fabricated by either dip coating or spin coating method at a temperature below 150 °C so that the physical or chemical properties of biological analytes of either liquid or solid film samples cannot be altered during biosensing monitoring.

4.2 Working of a biosensor

A biosensor is an inventive device that paves the interconnection between the biological and digital domains. A biosensor is an analytical instrument that converts biological responses from the biological samples (analyte) into an electrical signal to distinguish the chemical composition involved in a biological sample. The structure of a biosensor is designed in four stages: the biological element, the receptor, the transducer, and the reader interface. The biological element may be a chemical substance (biomolecules) or microorganisms such as viruses, bacteria, or fungi. The biological responses are detected and transferred by the transducer, known as sensors, to an analyzer. The signal responses from the biological element are transferred to an electronic system, which displays the signal from the detector in a user-friendly way [11-15].

The biological responses originated from the biological components of the samples and are converted into chemical, optical, thermal, or electrical signals in a readable form. This process takes place soon after the receptor element present in the device reacts with the biological samples. Based on the type of receptors, the nature of the biosensors also changes. In most cases, the receptors in biosensors are chemical labels or reagents that can react with the chemicals in the samples and emit different forms of responses, like electrical, optical (fluorescence), and thermal signals. This type of biosensor is called a label biosensor. Except for chemical label receptors, materials that can be used to detect the changes in the optical parameters of the analyte are referred to label label-free receptors and biosensors, which use such materials and analyse optical signals are called label-free optical

biosensors. As the receptor-analyte meeting results in variation in the signals that can be sent to the sensing unit of the biosensor, the analogue signals, which are captured by the sensing unit, will be converted into a readable form by the user interface unit of the biosensor. The result may be in a visual form, which indicates a colour code, a graphical representation, or a digital form. The summary of a structure and working of a biosensor is provided as a schematic representation in Figure 4.1.

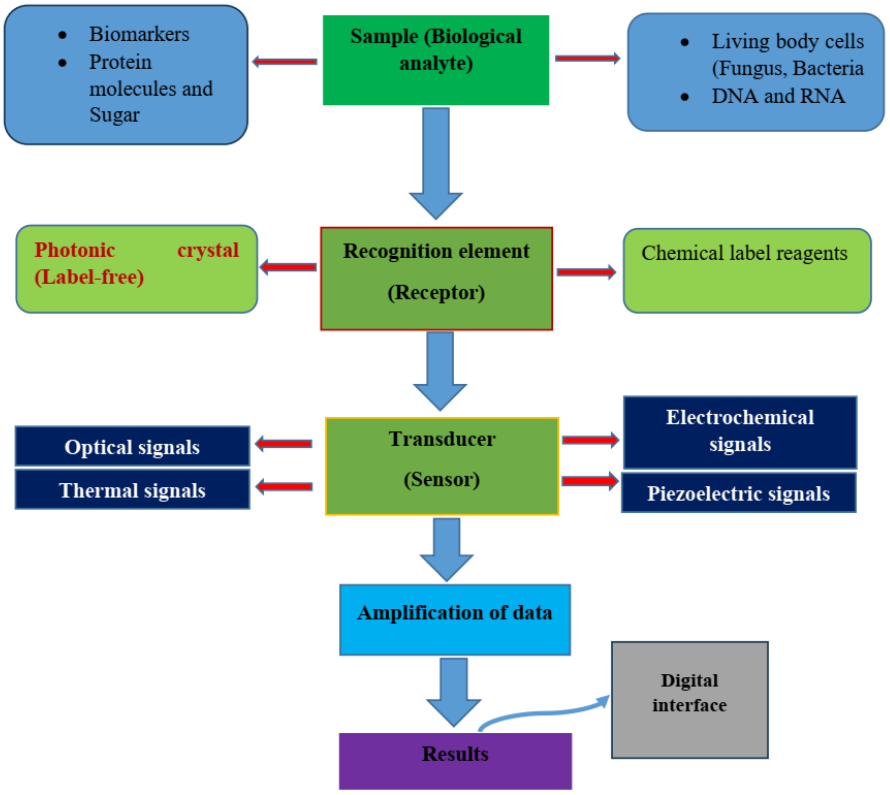

Figure 4.1: Schematic representation of the general structure of a biosensor

As a result, PC-based biosensors belong to label-free optical biosensors in which the device senses the minute changes of the optical parameter, such as the refractive index of the reference material, with respect to the concentration of the analyte. Moreover, the transducing mechanism is based on an optical phenomenon. Such that the process of recognition of the analyte while it interacts with the recognizing element moulds the optical radiation in a user-friendly analytical sensing way. The significant advantages of the optical biosensors are that they are non-corrosive, they do not suffer from electromagnetic interference, and they afford parallel, non-contact readout [11-20]. However, optical biosensors can be divided into fluorescence-based and label-free devices [11-20]. Whereas the fluorescent sensing devices have some demerits on carrying sensing the analyte, though they can be a promising element to detect even single molecules of the analyte [11-20]. One of the significant drawbacks of them is that they can interact with the function of the biomolecules and interrupt the measurements. This scenario demands the need to focus on label-free optical methods. The label-free sensing devices are mainly based on a waveguide mechanism where the light passes through a waveguide and the light interacts with the analyte through an evanescent field as the analyte-surface binding leads to a change in the effective refractive index, which in turn affects the modulation of the resonant structure of the guided mode [11-20]. This change in resonant wavelength can be recorded and analysed for sensing the analyte in a readable form. That is how the major community of optical biosensors is termed as refractive index sensors [11-22].

4.3 Theoretical designing of 1D ternary Silica/DNA/ZnO photonic crystal for biosensing

Generally, the numerical Method TMM is used to design the structure of the proposed 1D ternary PC system incorporated with the fundamental equations of PC [1-20]. It is necessary to study the nature of both photonic bandgap formation and the defect mode for a PC-based biosensor. The information about the photonic bandgap effect provides the details of the photonic bandgap position, width, and photonic bandgap edges. These data will be exploited to locate the defect mode, which is to be obtained by the presence of defective material.

4.3.1 Description of the 1D ternary Silica/DNA/ZnO photonic crystal to evaluate for biosensing of the BSA sample

The 1D ternary PC to be presented in this work is designed with a ternary layered elementary structure that has the form $(ABC)^N$, where A stands for silica, B stands for DNA, and C stands for ZnO. Figure 4.2 shows the schematic representation of a ternary PC. The system is designed with non-dispersive, isotropic, and non-lossy materials so that the relative permeability is treated as unity. The refractive indices of the constituent layers are obtained from the refractive index info database and the refractive index of each layer as n_{silica} 1.4585, n_{CD} =1.506, and n_{ZnO} 2.008, respectively. The optical thicknesses of silica, DNA, and ZnO were designed to be λ/6, which follows as $n_{SILICA}t_1=n_{cd}t_2=n_{silica}t_3$, where t_1, t_2, and t_3 are the thicknesses for silica, DNA, and ZnO, respectively. The thickness of the whole unit cell, t,

which is the period of the PC, can be deduced as the sum of the individual thicknesses of the constitute layers such that t $t_1+t_2+t_3$, and the thicknesses are provided as t_1=68.96 nm, t_2=66.65 nm, and t_3=50 nm respectively. The thickness of the defective layer is t_D, is taken as 120 nm. The dielectric constants of the materials are ε_1=3.5, ε_2=8, and ε_3=8 for silica, DNA, and ZnO, respectively [33-43]. The number of unit cells (N, the number of periods of the PC) assigned to fabricate the stack is 13. The proposed structure was theoretically analysed by the well-known numerical tool TMM. The features of TMM are well discussed in chapters 1 and 2. This fundamental numerical method is used to explain the mechanism of the 1D ternary Silica/DNA/ZnO PC system for biosensing the BSA sample.

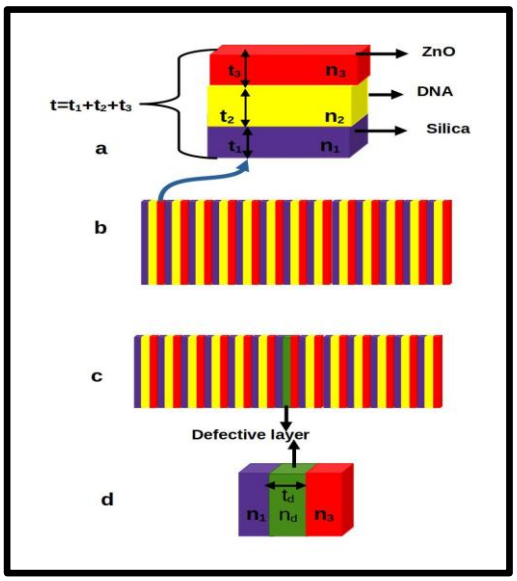

Figure 4.2: Schematic diagram of a) unit cell, b) whole structure of the 1D ternary Silica/DNA/ZnO PC, where N=13, c) defective 1D Silica/DNA/ZnO PC with a defective layer is placed at the 7th unit cell, where DNA is replaced by the defective layer BSA.

4.3.2 Description of the analyte sample (BSA)

Bovine serum albumin (BSA) is a very crucial protein present in the blood serum of cattle. It is commonly used in laboratories as a supplement in biochemical and tissue culture feeders. It has 76% structural resemblance to human serum albumin, so it is widely used as a model for human serum albumin (HSA) protein. Serum albumin is the most abundant protein in blood. It is the responsible transportation substrate for central cell functioning molecules, such as hydrophobic molecules in the blood, such as hormones, long chain fatty acids, bilirubin, drugs, minerals, and metal ions. Together with that, its plays as an anticoagulant and an antioxidant as well [46-47].

This macromolecule is produced in the liver. Its chemical composition is made of a polypeptide chain bio-macromolecule composed of 538 amino acids, containing carboxyl and amino groups, and it is highly soluble in water. The normal concentration of serum albumin present in a healthy adult's blood is 3.4-5.4 grams/decilitre (g/dL). The level of albumin below the normal range can be lowered to a situation called hypoalbuminemia due to infection, and inflammation from sepsis, surgery, or other health conditions. An albumin test can help assess liver and kidney health and overall well-being. Additionally, albumin test is unavoidable for monitoring the health condition of the patients who undergo surgery treatment [50-52].

Apart from the inevitable role of BSA in medical diagnosis, the factors that make BSA as an attractive candidate for the study including its comparatively small size, stable structure, and moderately non-reactive nature (isoelectric point is 4.7 at 25°C) and non-toxicity. It is commonly known for the application of immunohistochemistry, in

which the BSA acts as a blocker at the sites where unwanted linkages of antigen-antibody are formed. In animal blood serum, it acts as a carrier protein to transport hormones, vitamins, salts, and fatty acids. BSA is also used as a nutrient in cell culture and an impediment for polymerase chain reaction (PCR) [50-52]. Despite the laboratory limits, BSA is cheaper than other proteins and widely available for conducting bio-organic compound sensing experiments and industrial applications. Hence, BSA is found as a vital and suitable element for executing the analytical efficiency of the proposed PC based biosensor.

4.3.3 Biosensing evaluation of the BSA sample using photonic crystal systems

The biosensing of a sample can be done based on evaluating the parameters such that sensitivity (S), quality factor (Q), and figure of merit (F). These three measurements mainly define how efficient the proposed system is for sensing a particular analyte. The physical significance of the parameter, sensitivity (S), is to measure the resolution of the biosensor for examining even significantly diluted analyte concentrations. For PC based biosensing, the sensitivity of a biosensor can be mathematically defined as;

$$S=\frac{\Delta\lambda}{\Delta n} \qquad 4.1$$

For calculating the sensitivity, the reference for the resonant wavelength of the normal concentration of BSA in blood is chosen. In equation (14), Δλ is the change in the resonant wavelength of the defective BSA with respect to the reference solvent (here water). Δn is defined as the refractive index contrast between the defective BSA layer to the layer of reference solvent. Such that;

$$\Delta\lambda = \lambda_B - \lambda_R \quad 4.2$$

$$\Delta n = n_B - n_R \quad 4.3$$

Where λ_B, λ_R, n_B, and n_R are the resonant modes obtained for the BSA sample, the reference solvent the refractive indices of BSA and reference solvent, respectively. The selected specific range of optical band lies between 350 THz to 950 THz. Thus, it is assumed that all the materials are non-dispersive, such that the refractive indices of the layers are frequency independent.

4.4 Transfer properties of 1D ternary Silica/DNA/ZnO defective photonic crystal for evaluating its biosensing performance for BSA detection

This work is an investigation to design and observe a biocompatible 1-D ternary PC that can meet the objectives such as high resolution, simplicity in designing, cost-effective, and durability as a biosensor. Using the transfer matrix method (TMM) and COMSOL software, the optical properties of the proposed 1D PC structure have been exploited. The graphical representation of the cross-sectional view of the unit cell of 1D ternary Silica/DNA/ZnO PC is represented in Figure 4.2.a. The selection of the period number is based on achieving a finite PBG, which is obtained by a trial-and-error method by executing a Python program using TMM. In which the program is executed until obtaining a number of periods at which a finite PBG width and transmission band width within the preferred range are obtained. Figure 4.2.b shows the 1D ternary Silica/DNA/ZnO PC where the number of periods is 13. From the theoretical results, it is observed that the changes in the transfer properties of the 1D Silica/DNA/ZnO PC

system are caused by assigning a defective cavity to the system. The cavity is assigned to fill with BSA sample solution with a thickness of 120 nm. Figure 4.2.c shows the defective 1D Silica/DNA/ZnO PC system. To examine the defective system for biosensing performance, the concentration of BSA was changed 6 times. As on increasing the refractive index parameter of the defective layer BSA sample is increased, a red shift is noticed in the resonant mode peak. The refractive index of the BSA solution was measured using an Abbe refractometer for six different concentrations of BSA. The details of measurements of the RI of BSA for different concentrations are tabulated in **Table 4.1**. The six concentrations of BSA samples were taken as 1g, 1.5 g, 2g, 2.5g, 3g, and 3.5g respectively in 100 ml of water.

Table 4.1: Refractive index (RI) measurements of BSA samples for varying concentration

Sl No	Weight of BSA in 100 mL of water	Weight percentage of BSA in 100 ml water (%)	Refractive Index (RI)
1	0	--	1.3324
2	1	0.99	1.3357
3	1.5	1.47	1.3414
4	2	1.96	1.3468
5	2.5	2.43	1.3503
6	3	2.91	1.3631
7	3.5	3.38	1.3724

The RI measurements were carried out at laboratory room temperature, 27°C. These values are for liquid samples of BSA concentrations. The

RI of a film depends on thickness, temperature, pressure, porosity, electric-magnetic fields, wavelength, chemical impurities, and defects of the sample. Apart from these, the RI of the liquid sample is different from the film sample. However, these results are spoiled to find out the theoretical study for determining the biosensing of the BSA samples as changing its concentration changes. The model proposed in this work can be applicable to both liquid and dry samples for biosensing. With the help of lithographic techniques, the PC based liquid sample sensing devices can be fabricated. Hence, these studies can be a footstep for analysing the PC based biosensor. The literature studies show that the RI of the BSA film sample can be varied from 1.45 to 1.55. Hence, for the theoretical study, the measured values of RI were taken for liquid samples of BSA due to the experimental limitations.

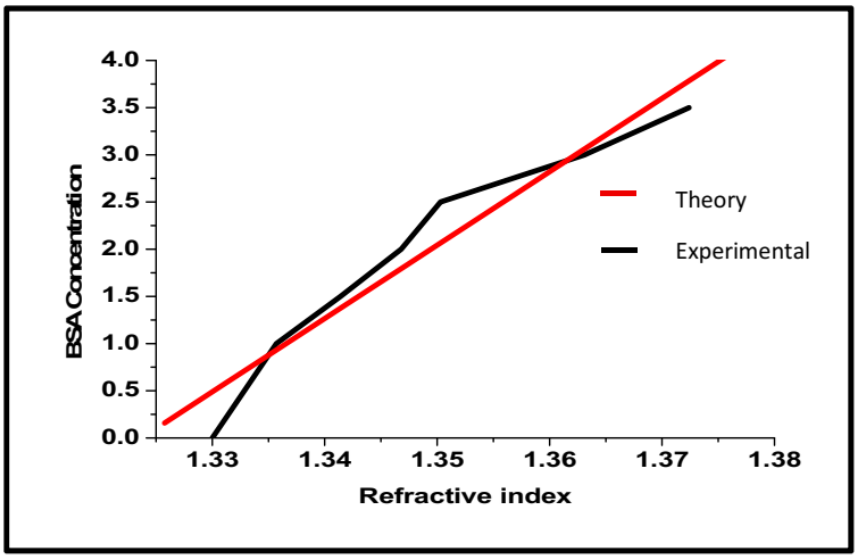

Figure 4. 3: Linear relation of refractive index to the concentration of BSA samples

Figure 4.3 illustrates a linear relation of refractive index variation with increasing concentration of BSA. To prove this linearity, a curve fitting approximation is performed. Based on the curve fitting data, a linear relation that connects the refractive index of the BSA to the concentration of BSA is obtained.

$$C_{BSA}=77.73922*n_R-102.90499 \quad 4.4$$

Where C_{BSA} is the concentration of BSA, and n_R is the refractive index of the reference solvent (water) to which BSA is dissolved. From the curve fitting data, the square of the correlation coefficient (R^2) is obtained as 0.932778. It is used to indicate the accuracy between the simulated and curve curve-fitting data. The higher value of R^2 validates the results. The general relation between the refractive index and the concentration of a sample is that they are directly proportional to each other. As the concentration of a sample is increasing, the refractive index also increases; moreover, the change in concentration results in a change in refractive index. One of the base parameters of the PC system that affects the formation of the PBG is the refractive index contrast between the adjacent layers. As already mentioned, when the refractive index is replaced or varied, it will result in the formation of a resonant transmission mode within the PBG. Moreover, if the concentration of the defective layer is changed, the corresponding refractive index is also varied; hence, a shift occurs in the transmission mode. This shift in the resonant wavelength can be mathematically connected to the change in refractive index by the equation (12) to find the sensitivity of the biosensor. The physical

quantity sensitivity is the measure of the degree of accuracy of a biosensor.

As well, the response in the resonance mode corresponding to each concentration is represented in Fig.4, where the resonance mode shift is increasing towards the IR region as the refractive index of the defective sample increases.

The performance of a biosensor is exploited with sensitivity (S), quality factor (Q), and figure of merit (F). These three parameters of a biosensor are correlated with the resonant wavelength shift.

The quality factor (Q) of a biosensor is defined by using the formula;

$$Q=\frac{\lambda_{res}}{\lambda_{FWHM}} \quad 4.5$$

The figure of merit (F) is defined by using the formula;

$$F=\frac{S}{\lambda_{FWHM}} \quad 4.6$$

Equations 4.5 and 4.6 are crucial for the performance of a biosensor.

4.4.1 Theoretical results for 1D ternary Silica/DNA/ZnO photonic crystal system for BSA sensing

The behaviour of the periodic structures on the basis of the electric field intensity is observed theoretically using COMSOL software. The Figure. 4.4a. illustrates the electric field intensity distribution along 1D ternary Silica/DNA/ZnO PC, where N=13. Figure 4.4b clearly shows that the maximum intensity of the field is concentrated in the defective

layer region. While considering the other periodic layers, the maximum field intensity is concentrated on low refractive index regions such that along the interfaces between air and silica, and ZnO and silica and low intensity field is concentrated along high refractive index region, such that interfaces between DNA and ZnO.

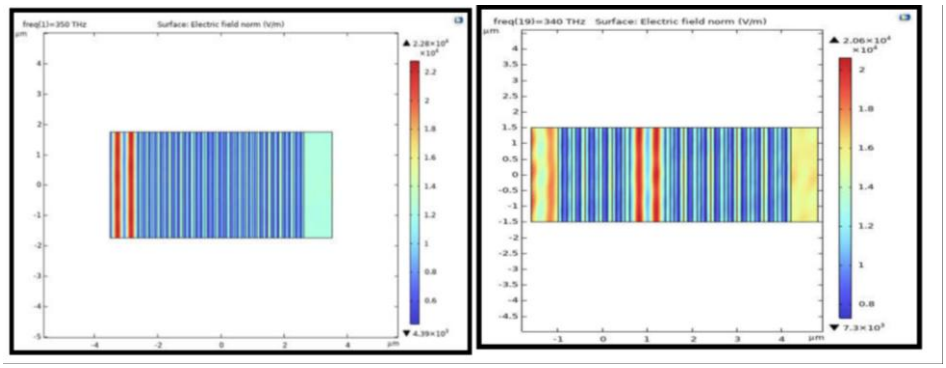

a **b**

Figure 4.4: Electric field intensity distribution along a) 1D ternary Silica/DNA/ZnO PC, where N=13, and b) defective 1D ternary Silica/DNA/ZnO with defective layer BSA is placed at the 7th unit cell by replacing DNA.

The optical transmission properties have been discussed using TMM, and the obtained results are shown in Figure 4.5. The transfer properties have been studied in the range of 350 nm-1200 nm of the electromagnetic spectrum**.** The optical transfer properties of a 1D ternary PC and the response of a defective BSA layer have been exploited using the TMM method. Additionally, a relevant comparison is also conducted between the 1D ternary PC and 1D binary PC to highlight the significance of the 1D ternary PC over the 1D binary PC. Figure 4.5a represents the optical transfer properties of both 1D binary Silica/ZnO PC and ternary Silica/DNA/ZnO PC systems for a period

N=13. The optical properties of the binary Silica/ZnO PC system are characterized by the line binary PC, and the ternary Silica/DNA/ZnO PC is characterized by the line Ternary PC. When the optical properties of the Silica/ZnO PC system are considered, it shows that the PBG is formed in the 320 nm-400 nm region of the optical band. The PBG bandwidth is about 80 nm. The optical density at the pass band region is not seen as intense in the visible region of the optical band.

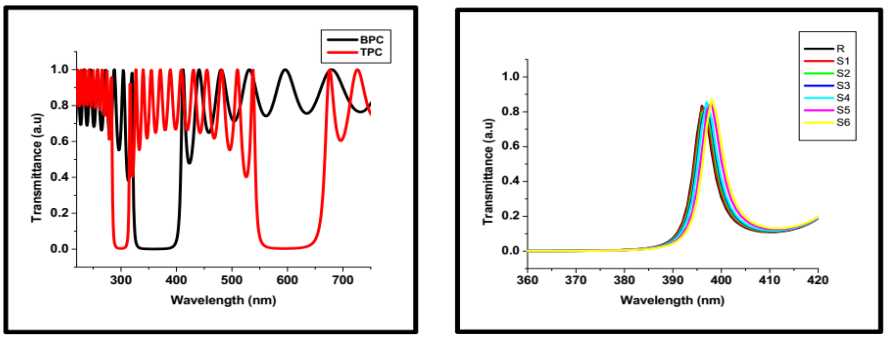

a b

Figure 4.5: Optical transfer responses of a) 1D binary Silica/ZnO PC system characterized by the line binary PC and 1- D ternary Silica/DNA/ZnO system characterized by the line TPC where N=13, b) resonance mode shift in response of the defective layer BSA (analyte) in 1D defective silica/ZnO PC system, where R, S1, S2, S3, S4, S5 and S6 are the resonant shift modes corresponding to the RI, n= 1.3324, 1.3357, 1.3414, 1.3458, 1.3521, 1.3541, and 1.3554 respectively.

However, the transfer properties of the 1D ternary PC are pretty different from the binary Silica/ZnO PC system. The number of PBGs in the optical band formed in the 1D ternary Silica/DNA/ZnO PC system is two. One of the PBG is formed at 290 nm- 315 nm of the optical band. Moreover, the second PBG is formed at 550 nm -650 nm of the optical band regions. Whereas the photon density of the pass

band region between the two PBGs is found to be larger than the photon density at the same region of the 1D Silica/ZnO PC. Moreover, for the sensing purpose, the suitable band region considered belongs to the visible region of the optical band. It preserves the biological sample from damaging the chemical composition by exposing it to high-energy radiation. Most of the bio-organic molecules are chemically and physically stable from the visible radiation exposure. Keeping this point, from the comparison results shown in Figure 4.5.a, is that 1D ternary Silica/DNA/ZnO can be a better choice for bio-sensing purposes of the bio-analyte samples.

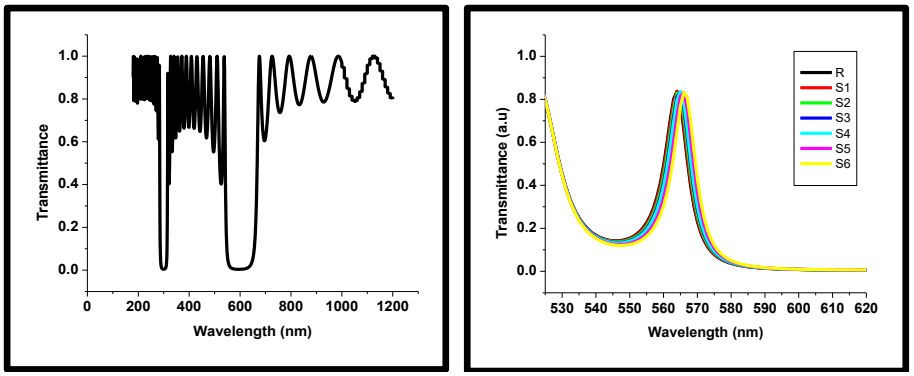

a **b**

Figure 4.6: Optical transfer properties of a) 1D ternary Silica/DNA/ZnO PC, where N=13 and b) resonance mode shift in 1D ternary Silica/DNA/ZnO in response to the defective layer BSA where R, S1, S2, S3, S4, S5 and S6 are the resonant shift modes corresponding to the RI, n= 1.3324, 1.3357, 1.3414, 1.3458, 1.3521, 1.3541, and 1.3554 respectively.

Figure 4.5.b exploits the resonance mode shift that occurs in a 1D defective Silica/ZnO PC system when the refractive index of the defective layer changes. The resonance shifts according to the refractive index values n=1.3324, 1.3357, 1.3414, 1.3458, 1.3521,

1.3541, and 1.3554 are R, S1, S2, S3, S4, S5, and S6, respectively. The biosensing responses obtained from the defective Silica/ZnO PC system are tabulated in Table 2. The tabular data reveal that the highest sensitivity, S of the PC system, is 89.3521 nm/RIU against a refractive index contrast Δn = 0.023. The average value of Q value and figure of merit F are 76.8426 and 13.03225 (1/RIU), respectively.

Figure 4.6a represents the transfer properties of 1D Silica/DNA/ZnO PC for N=13. Figure 4.6 a exemplifies precisely the formations and nature of PBGs in a 1D ternary PC system. The system has two PBGs along the optical band. Of the two PBGs, the suitable PBG to apply for biosensing purposes is the PBG that is formed at 550nm-650nm of the optical band with a bandwidth of 100 nm. This PBG region is in the visible region of the optical band and cannot interfere with the chemical and physical properties of the analyte but can make an optical mode shift due to the effective refractive index of the analyte – PC system interface. Figure 4.6 b provides information regarding the resonant mode shift as the change in the refractive index of the defective layer (analyte). The resonant modes named R, S1, S2, S3, S4, S5, and S6 correspond to the change in the analyte (BSA) refractive index, n 1.3324, 1.3357, 1.3414, 1.3458, 1.3521, 1.3541, and 1.3554, respectively. The data obtained from Figure 4.6 b is tabulated in Table 4.4. The information from Table 4 can be used to observe how be 1D ternary defective Silica/DNA/ZnO PC system would be efficient for biosensing of the BSA sample. The highest sensitivity (S) calculated from Table 4.4 is 412 nm/RIU against the refractive index, Δn contrast 0.009, and the sensitivity of the system against the highest refractive

index contrast between the reference to the BSA sample is 0.023, 340.3130 nm/RIU. The measured values of Q factor and figure of merit are displayed in Table 4.5. The average Q value and F of the PC system are 65.4313 and 42.0552 (1/RIU), respectively.

Furthermore, the observations about the theoretical studies of two systems, namely 1D binary Silica/ZnO PC system and 1D ternary Silica/DNA/ZnO PC system, reveal their efficiency in sensing the bioanalyte BSA distinctly. From the obtained data of the theoretical study, it is well clear that the 1D ternary Silica/DNA/ZnO PC system is significant for sensing BSA sample despite of the analyte concentration.

Table 4.2: Theoretical details of the biosensing of BSA samples using 1D Silica/ZnO PC system

Sl No	Weight percentage of BSA	Refractive Index (RI) n	Refractive index contrast Δn	Resonant wavelength λ_{res}(nm	$\Delta\lambda_{res}$ (nm)	Sensitivity S(nm/RIU)
1	--	1.3324	-----	395.922	----	
2	0.99	1.3357	0.0033	396.11	0.188	56.9696
3	1.47	1.3414	0.009	396.3940	0.472	52.4444
4	1.96	1.3458	0.0134	396.8659	0.9439	70.4402
5	2.43	1.3521	0.0188	397.0148	1.0928	58.127
6	2.91	1.3541	0.0217	397.6792	1.7572	80.9769
7	3.38	1.3554	0.023	397.9771	2.0551	89.3521

Table 4.3: Q value and figure of merit of the 1D Silica/ZnO PC defective system for sensing BSA

SL No.	Resonant wavelength $\lambda_{res}(nm)$	Sensitivity, S (nm/RIU)	FWHM of the resonant wavelength, λ_{FWHM}	Q factor	Figure of merit F
1	395.922	---------	4.9226	80.4294	--------
2	396.11	56.9696	5.0992	77.6808	11.1663
3	396.3940	52.4444	5.1775	76.5608	10.1292
4	396.8659	70.4402	5.0927	77.9283	13.8316
5	397.0148	58.127	5.2463	75.6751	11.0796
6	397.6792	80.9769	5.1729	76.8774	15.6540
7	397.9771	89.3521	5.4707	72.7470	16.3328

Table 4.4: Theoretical data of biosensing of BSA sample using 1D ternary Silica/DNA/ZnO PC system

Sl No.	BSA weight percentage	Refractive index(n)	Refractive index contrast Δn $n_R - n_{BSA}$)	Resonant wavelength $\lambda_{res}(nm)$	$\Delta\lambda_{res}$ (nm)	Sensitivity S(nm/RIU)
1	--	1.3324	-----	564.1472	------	------
2	0.99	1.3357	0.0033	565.4137	1.2665	383.7878
3	1.47	1.3414	0.009	567.8624	3.7152	412.80
4	1.96	1.3458	0.0134	569.1346	4.9874	372.1940
5	2.43	1.3521	0.0188	570.6382	6.491	345.2659
6	2.91	1.3541	0.0217	571.6224	7.4752	344.4792
7	3.38	1.3554	0.023	571.9754	7.8272	340.3130

Table 4.5: Figure of merit of the 1D Silica/DNA/ZnO PC defective system for sensing BSA

SL no.	Resonant wavelength $\lambda_{res}(nm)$	Sensitivity, S (nm/RIU)	FWHM of the resonant wavelength, λ_{FWHM}	Q factor	Figure of merit F
1	564.1472	------	8.5315	66.1252	-----
2	565.4137	383.7878	8.5773	65.91977	44.7565
3	567.8624	412.80	8.7886	64.61352	46.9699
4	569.1346	372.1940	8.54	66.6434	43.5824
5	570.6382	345.2659	8.5366	66.8460	40.4450
6	571.6224	344.4792	8.79	65.0309	39.1898
7	571.9754	340.3130	9.102	62.8406	37.3888

4.5 Experimental approach for sensing different concentrations of BSA sample using 1D Silica/DNA/ZnO photonic crystal system

In order to achieve the tunability, the thickness of the nanomaterials is optimized, concentration and thickness of the defective layer are based on the obtained theoretical results. The proposed structure has been realized by the sol-gel method and the dip coating Unit. The experimental methods for the fabrication of the PC system have been well explained in the Chapter.

4.5.1 Experimental Methods

The experimental methods involve the fabrication of a PC structure and analyte preparation for the performance of the proposed 1D ternary Silica/DNA/ZnO PC as a biosensor. The sol-gel method, incorporated with the dip coating method, is used to fabricate the proposed PC structure. The fabrication of the PC system was a lengthy and consuming process due to experimental lab limitations. The success of the fabrication of PC must meet several factors, include temperature and humidity of the laboratory, and absence of dust particles (need for well clean room). Apart from these concerns, the crucial parameters which would affect the film quality is the consistency of the solvents used. These parameters all together take part in the formation of a uniform stratified film structure.

a. Fabrication of 1D ternary Silica/DNA/ZnO photonic crystal

The Holmarc dip coating unit, model HO-TH-02BT, was used in the fabrication of the PC. The materials were used as silica [30], DNA and ZnO. The solvents dimethyl sulfoxide (DMSO), methanol, and water were used for making the films of silica, DNA, and ZnO, respectively. The DNA thin film was achieved by using the surfactant material CTAB to make DNA-CTAB complex film form [33-36]. The selected materials have nearly adjacent refractive index values (n_{Silica} =1.49, n_{DNA} 1.506, and n_{SILICA} 1.47 at 600 nm) [31-40]. The optical thickness of silica, DNA-CTAB complex film and silica were designed to be λ/6. The refractive index of the defect layer, BSA (analyte), was obtained by an Abbe refractometer. The solution of silica was made in DMSO

where 1.23 weight percentage (wt %) silica was added in 80 ml of DMSO, and the mixture was stirred until the mixture became homogeneous by forming a transparent color. The 2.44 wt % DNA solution was made in 80 ml of DI water. The sonication made the solution of silica of the mixture 5.88 wt % silica and 2-methoxy ethanol until a transparent homogenous solution was formed. All the experiments were carried out at room temperature and pressure.

The fabrication process of PC using dip coating is highly challenging and it needs careful attention to obtain optimized thickness of the elemental layers [58]. The height of all the solutions was maintained the same throughout the experiment to ensure uniform thickness of the film. After depositing each layer coating, the sample is annealed at 80°C for 30 minutes to remove any residual solvents and to achieve improved surface uniformity [58]. The Bragg mirror consisting of 13unit cells of 1D ternary Silica/DNA/ZnO was successfully fabricated. However, the fabrication of PC required careful attention to achieve a uniform thickness of each coating of the layers.

The concentration of BSA samples was prepared as mentioned in the Table 4.1. The measured quantity of BSA samples was readily dissolved in DI water using an ultrasound sonicator in each well of cleaned sample bottles. The time duration of sonication taken for making BSA solution was 30 minutes. Figure 4.7 represents a schematic representation of fabrication of a PC system using dip coating method.

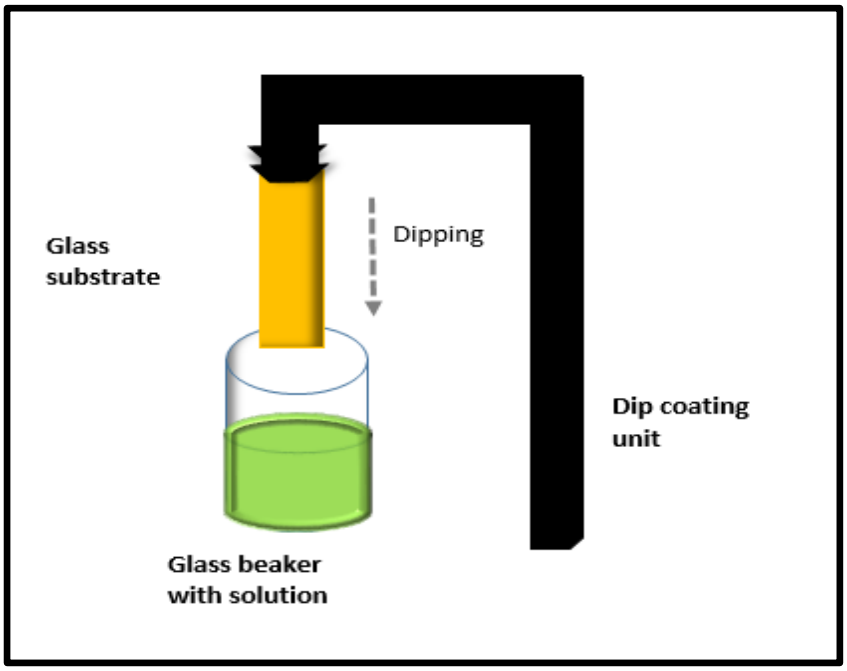

Figure 4.7: Schematic representation of the fabrication PC using the DIP coating method

4.5.2 Experimental results for sensing BSA detection

The experimental results involve the analysis of the photonic bandgap effect of a 1D ternary Silica/DNA/ZnO PC system and the defective 1D ternary Silica/DNA/ZnO PC system. The defective 1D ternary Silica/DNA/ZnO PC system is used to perform as a biosensor for the detection of BSA.

a. Optical characterization of experimentally obtained 1D ternary Silica/DNA/ZnO PC system

The HOLMARC Spectra G 300 spectrometer was used to obtain the optical characterization (reflectance and transmittance) of the fabricated PCs. Figure 4.8 represents a schematic representation of the optical characterization of a PC using a reflectometer setup. Figure 4.9 a shown the photograph of the surface of the 1D ternary Silica/DNA/ZnO PC system where 4.9b displays the photograph of reflection image of the 1D defective Silics/DNA/PC system. Figure 4.10 represents the SEM image of the unit cell of 1D ternary Silica/DNA/ZnO PC system.

However, the unit cell of the 1D PC system contains three layers, which come in a relation of $n_{Silica}<n_D>n_{ZnO}>n_{Silica}$, where n_{Silica}, n_D, and n_{ZnO} are the refractive indices of Silica, DNA, and ZnO. The relation according to the electromagnetic variational theory, the electromagnetic modes with high resonant frequency will concentrate their energy on the low dielectric material region of the PC. At the same time, the electromagnetic modes with low resonant frequency will concentrate their energy in the high dielectric material region of the PC [2]. The reflectance properties of the Silica/DNA/ZnO have been monitored for N=13 with defective PC as well. The defective system has been employed in four cases of refractive index variations due to the technical limits. The values of the refractive index of BSA samples taken are n= 1.3324, 1.3357, 1.3414, and 1.3458. The experimental observations of reflection and resonance mode shift of the defective PC systems are elaborated in Figures 4.11 and 4.12.

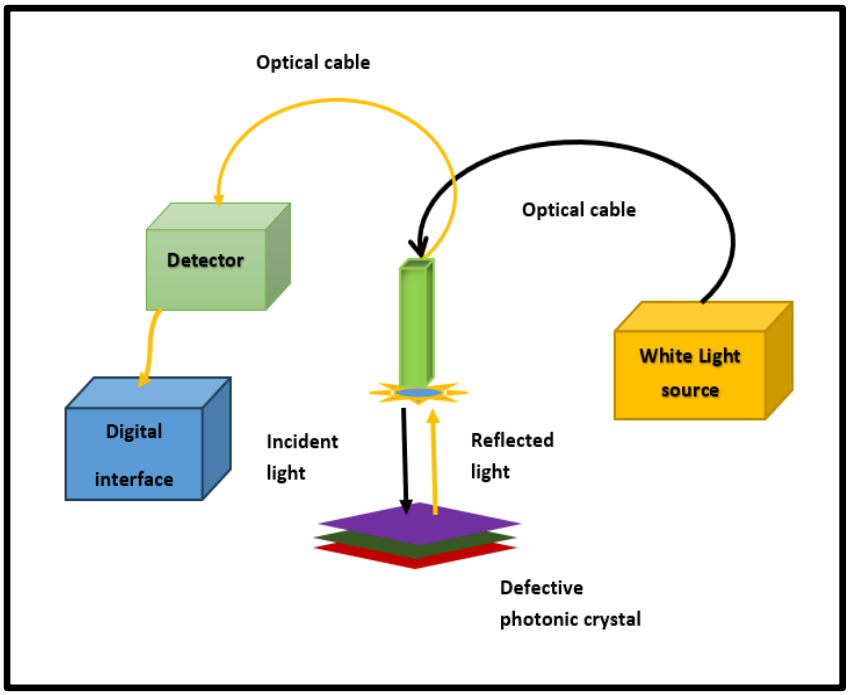

Figure 4.8: A schematic representation of the optical characterization of a 1D ternary defective PC using a reflectometer

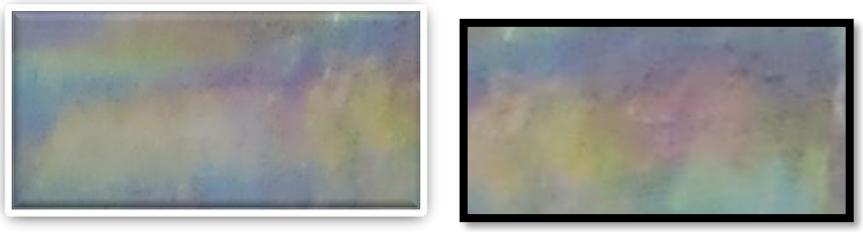

a **b**

Figure 4.9: Surface of a) 1D ternary Silica/DNA/ZnO PC, and b) defective 1-D ternary Silica/DNA/ZnO PC, where N=13.

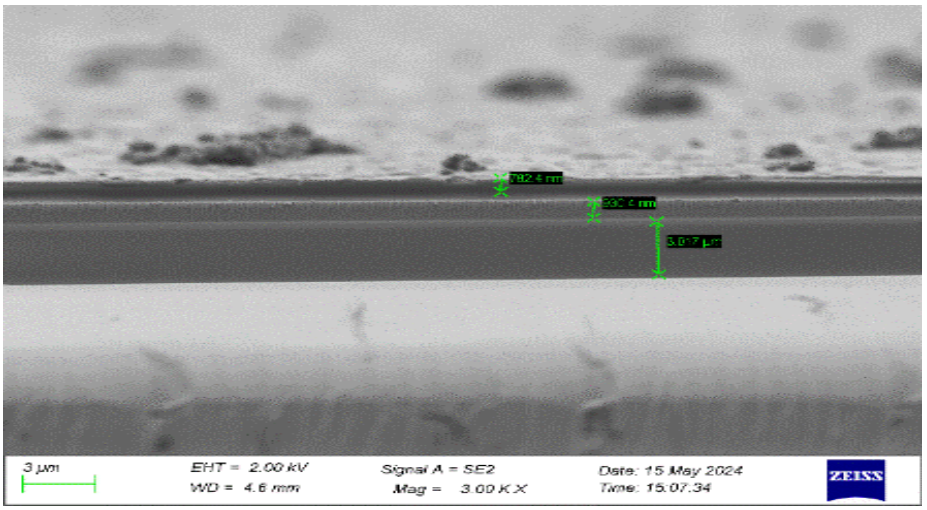

Figure 4.10: SEM image of unit cell of 1D Silica/DNA/ZnO PC system

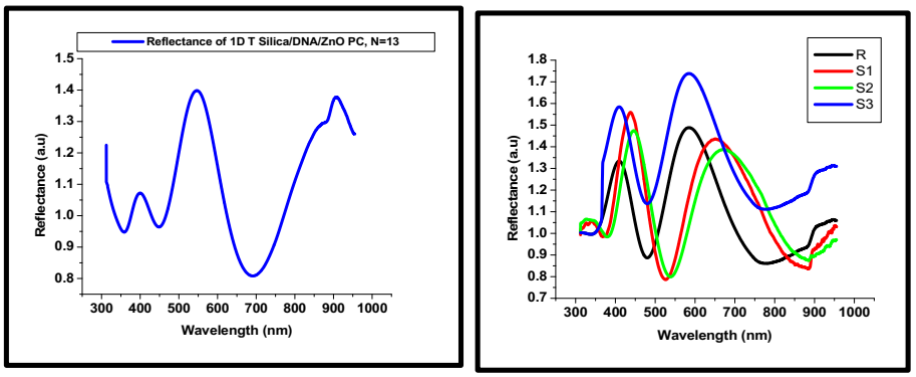

Figure 4.11: Reflectance properties of 1D ternary Silica/DNA/ZnO PC for N=13 b) defect mode of defective 1D ternary Silica/DNA/ZnO where R1 is the defect mode of refractive index n=1.3324, 1.3357, 1.3414, and 1.3458 corresponding to R, S1, S2, S3 and S4 modes respectively

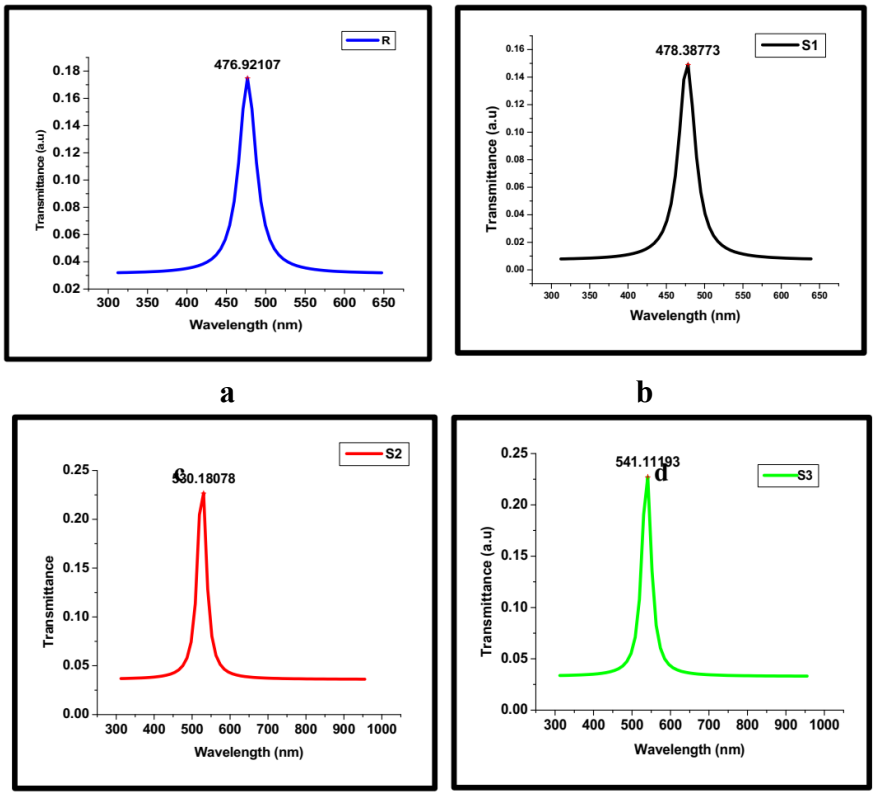

Figure 4.12: Resonant mode peaks obtained by Lorentz linear fitting for a) R, b) S1, c) S2, and d) S3 respectively.

Figure 4.11a displays the experimentally obtained results of reflection of the 1D ternary Silica/DNA/ZnO PC for N=13. The number, intensity, and position of the obtained photonic band gaps are observed from Figure 4.11a. The Silica/DNA/ZnO PC structure has formed two reflectance peaks within the optical band as observed in the theoretical results of the same structure. Figure 4.11a shows that a narrow PBG is formed at 350 nm-450 nm, and the rest band gap is formed at 600 nm-700 nm. The results of the reflectance properties meticulously agreed with the theoretical results shown in Figure 4.5a. The width and the intensity are slightly varied because the experimental conditions are

slightly different from the expected ideal condition set in the theoretical results. The precision in the thickness is the most challenging task for fabricating the thin film for the proposed PC system. The ideal condition of the laboratory was not pragmatic. Hence, the error associated with the thickness affected the shift in the position of the obtained photonic band gaps and intensity as well.

Figure 4.11b exemplifies the formation of a resonant wavelength in order to the introduction of the defect layer BSA. The BSA was placed in the 7^{th} unit cell, where DNA is replaced. The remarkable difference in the transmission properties after placing a BSA layer is well understood in Figure 4.11b. The structure shows a wide bandgap from 600nm to 800nm prior to the introduction of the defective layer. As the defective layer was introduced, the PBG position has been shifted towards the UV region, and a defect transmission mode was formed in the range of 500nm-700nm. These experimental results agree with the theoretical results obtained from TMM. The discrepancy between the theoretical and experimental results is due to the lack of ideal experimental conditions in the experimental laboratory. The experimental study was carried out using six concentrations of BSA. The normal concentration of BSA in a living human being is found to be 42mg/mL [3-5]. The reference used for the experiment is water.

The distinctive representation of the resonance mode shift of the 1D ternary defective Silica/DNA/ZnO PC for the four concentrations of BSA namely R, S1, S2, and S3 is represented in Figure 4.12a-d using Lorentzs curve fitting method. This method is adopted to obtain the parameters such as resonant mode, and FWHM essentially required for

measuring S. The shift in the defect mode (resonant wavelength) with respect to the difference in the concentration of the defect sample is tabulated in Table 4.6 to find out the sensitivity of the proposed biosensor. The shift in the resonant wavelength was found by the difference between the defect mode caused by the reference film to the defect mode caused by the increase in the concentration of the BSA in the water. The biosensing data obtained from the experimental results are tabulated in Table 4.6, and the Q value and F are expressed in Table 4.7.

However, the highest sensitivity obtained from the experimental result of the defective BSA is 5917.8444 nm/RIU against the refractive index contrast 0.009. The average Q value of the PC is 18.8572, and F for the refractive index contrast 0.009 is 220.0842 (1/RIU). Despite of the experimental limitations, these experimental results comparatively agreed with the theoretical results of the detection of BSA.

Table 4.6: Experimentally obtained BSA sensing data of defective 1D ternary Silica/DNA/ZnO PC system according to the varying concentration of defective layer BSA.

Sl. No	Wt% of BSA	Refractive index (n)	Refractive index contrast Δn (n_{DBSA}-n_{NBSA})	Resonant wavelength λ_{res} (nm)	$\Delta\lambda_{res}$ (nm)	Sensitivity S
1	0	1.3324	---	476.9201		--
2	0.99	1.3357	0.0033	478.3877	1.4676	444.7272
3	1.47	1.3414	0.009	530.1807	53.2606	5917.8444
4	1.96	1.3458	0.0134	541.1119	64.1918	4790.4328

Table 4.7: Experimental details of Q factor and figure of merit of the biosensing 1D ternary Silica/DNA/ZnO PC system

SL no.	Resonant wavelength $\lambda_{res}(nm)$	Sensitivity, S (nm/RIU)	FWHM of the resonant wavelength, λ_{FWHM}	Q factor	Figure of merit F
1	476.9201	------	26.083	18.2847	-----
2	478.3877	444.7272	26.114	18.3192	17.03022
3	530.1807	5917.8444	26.889	19.7173	220.0842
4	541.1119	4790.4328	28.319	19.10773	165.6500

4.6 Conclusions

This chapter analysed a 1D binary PC system and a 1D ternary PC system for biosensing of BSA detection. The behaviour of the PC systems on optical band of frequency range 270 THz- 750 THz (350nm- to 1100nm.) has been theoretically studied using TMM and COMSOL software. In order to carry out the investigation, a comparative analysis between a 1D binary Silica/ZnO PC system and a 1D ternary Silica/DNA/ZnO PC system is conducted. The theoretical analysis includes band structure, transmittance, electric field distribution of these two systems, and evaluated parameters of the two microstructures for biosensing. The ternary PC system provides two PBGs, which are formed at 430nm - 457 nm and 650-750 nm of the optical band.

Additionally, defect mode analysis is theoretically performed in the system by forming an asymmetric defective PC where BSA is taken as the defect layer. The sensitivity obtained by theoretical simulation for a 1D binary Silica/ZnO PC system is 89.3521 nm/RIU against a refractive index contrast $\Delta n = 0.023$. The average values of the Q factor and the figure of merit (F) are 76.8426 and 13.03225 (1/RIU), respectively. The theoretical results of the 1D Silica/DNA/ZnO system show that the 1D ternary PC (PC) has the highest sensitivity (S) of 412 nm/RIU against a refractive index contrast Δn of 0.009. The average Q value and F of the PC system are 65.4313 and 42.0552 (1/RIU), respectively. From the theoretical data, it is found that the 1D ternary Silica/DNA/ZnO PC system is more efficient for biosensing of BSA detection than the 1D binary Silica/ZnO PC system.

Based on the theoretical results, a ternary system of 1D Silica/DNA/ZnO PC is experimentally achieved. By keeping the theoretical results, the performance of the PC as a biosensor for the detection of BSA was carried out experimentally. The BSA sample is used as the defect layer placed in the place of DNA in the 7^{th} unit cell of the PC. The experimental performance of the PC was carried out for the four concentrations of the BSA sample. The results show that the sensitivity of the defective ternary PC against the concentration of the BSA is in good agreement with the theoretical result obtained for the same concentration. The obtained results of sensitivity (S) are 5917.8444 nm/RIU against the refractive index contrast of 0.009. The average Q value of the PC is 18.8572, and F for the refractive index

contrast 0.009 is 220.0842 (1/RIU). Despite the experimental limitations, these experimental results agreed with the theoretical results of the detection of BSA. Thereupon, the presented 1D ternary Silica/DNA/ZnO PC can be a promising system for bio-sensing applications.

References

[1] Meade, R. D. V., Johnson, S. G., & Winn, J. N. (2008). Photonic crystals: Molding the flow of light.

[2] Q. Gong and X. Hu (2014), "Photonic Crystals: Principles and Application", Pan Stanford Publishing Pte. Ltd

[3] Wu, K., Gu, W. X., Wu, C., Ma, J. L., & Ma, X. Y. (2014). Study on the Optical Transmission Properties of One-dimensional Photonic Crystal of MoS2. Advanced Materials Research, 1056, 42-46.

[4] Pandey, J. P. (2017). Transfer matrix method for one-dimensional photonic crystals. J. Ramanujan Soc. Math Math Sc, 6(1), 121-130.

[5] Akbar, F., Syahriar, A., & Lubis, A. H. (2014, November). Dispersion relation of 1-D photonic crystal. In 2014 International Conference on Electrical Engineering and Computer Science (ICEECS) (pp. 69-73). IEEE.

[6] Armenise, M. N., Campanella, C. E., Ciminelli, C., Dell'Olio, F., & Passaro, V. M. (2010). Phononic and photonic band gap structures: modelling and applications. Physics Procedia, 3(1), 357-364.

[8] Lv, X., Zhong, B., Huang, Y., Xing, Z., Wang, H., Guo, W., ... & Zhang, Z. (2023). Research progress in the preparation and application of photonic crystals. Chinese Journal of Mechanical Engineering, 36(1), 39.

[9] Gangwar, R. K., Pathak, A. K., & Kumar, S. (2023, October). Recent progress in photonic crystal devices and their applications: a review. In Photonics (Vol. 10, No. 11, p. 1199). MDPI.

[10] Barsukova, M., Grisé, F., Zhang, Z., Vaidya, S., Guglielmon, J., Weinstein, M. I., ... & Rechtsman, M. C. (2024). Direct observation of Landau levels in silicon photonic crystals. Nature Photonics, 1-6.

[11] Kaczmarczyk, A., van Vliet, S., Jakob, R. P., Teixeira, R. D., Scheidat, I., Reinders, A., ... & Jenal, U. (2024). A genetically encoded biosensor to monitor dynamic changes of c-di-GMP with high temporal resolution. Nature Communications, 15(1), 3920.

[12] Mehrotra, P. (2016). Biosensors and their applications–A review. Journal of oral biology and craniofacial research, 6(2), 153-159.

[13] Guo, L., Zhao, Y., Huang, Q., Huang, J., Tao, Y., Chen, J., ... & Liu, H. (2024). Electrochemical protein biosensors for disease marker detection: progress and opportunities. Microsystems & Nanoengineering, 10(1), 65.

[14] Bollella, P., & Katz, E. (2020). Biosensors—Recent advances and future challenges. Sensors, 20(22), 6645.

[15] Pitruzzello, G., & Krauss, T. F. (2018). Photonic crystal resonances for sensing and imaging. Journal of Optics, 20(7), 073004.

[16] Sandeep, S. (2012). Investigations of nonlinear optical effects and ultrafast laser Induced plasma in nanostructured media (Doctoral dissertation).

[17] Naresh, V., & Lee, N. (2021). A review on biosensors and recent development of nanostructured materials-enabled biosensors. Sensors, 21(4), 1109.

[18] Nasr, D. M., Mostafa, S. I., & El Naggar, M. A. (2024). Enhanced 1D photonic crystal biosensor for blood components and blood infection detection. The European Physical Journal D, 78(5), 1-14.

[19] Zaman, N. A., Akash, N. A., & Nayan, M. F. (2023). A high-performance biosensor design for waterborne bacteria detection based on a one-dimensional photonic crystal. Physica Scripta, 98(8), 085518.

[20] Sayed, H., Swillam, M.A. & Aly, A.H. (2023). Annular one-dimensional photonic crystals for salinity sensing. Sci Rep **13**, 20593

[21] S E-S Abd El-Ghany, Walaa M N., Z S Matar, Zaky A Z.& Arafa H A.(2020), Optimized bio-photonic sensor using 1D-photonic crystals as a blood hemoglobin sensor, 2020, *Phys. Scr.* **96** 035501, **DOI:** 10.1088/1402-4896/abd49c

[22] Banerjee, A. (2009). Enhanced refractometric optical sensing by using one-dimensional ternary photonic crystals. Progress In Electromagnetics Research, 89, 11-22.

[23] El Mouncharih, A., Takassa, R., Farkad, O., Tchenka, A., Elfatouaki, F., Ibnouelghazi, E. A., & Abouelaoualim, D. (2023). One-dimensional photonic crystal-based biosensor for the detection of glucose concentration in human urine. Journal of Nanophotonics, 17(2), 026007-026007.

[24] Shiveshwari, L. (2013). Complete photonic band gaps in one-dimensional ternary photonic crystals containing a single harmful material. Optik, 124(22), 5646-5648.

[25] Almawgani, A. H., Taya, S. A., Daher, M. G., Alhawari, A. R., Colak, I., & Patel, S. K. (2023). Design of a novel protein sensor of high sensitivity using a defective ternary photonic crystal nanostructure. Silicon, 15(2), 775-782.

[26] Zhuo, Y., & Cunningham, B. T. (2015). Label-free biosensor imaging on photonic crystal surfaces. Sensors, 15(9), 21613-21635.

[27] Konopsky, V. N., Karakouz, T., Alieva, E. V., Vicario, C., Sekatskii, S. K., & Dietler, G. (2013). Photonic crystal biosensor based on optical surface waves. Sensors, 13(2), 2566-2578.

[28] Al-Dossari, M., Awasthi, S. K., Mohamed, A. M., Abd El-Gawaad, N. S., Sabra, W., & Aly, A. H. (2022). Bio-alcohol sensor based on one-dimensional photonic crystals for detection of organic materials in wastewater. Materials, 15(11), 4012.

[29] Gryga, M., Ciprian, D., Gembalova, L., & Hlubina, P. (2023). One-dimensional photonic crystal with a defect layer utilized as an optical filter in narrow linewidth LED-based sources. Crystals, 13(1), 93.

[30] Sayed, H., Swillam, M. A., & Aly, A. H. (2023). Annular one-dimensional photonic crystals for salinity sensing. Scientific Reports, 13(1), 20593.

[31] Divya, J., Selvendran, S., & Raja, A. S. (2018). Photonic crystal-based optical biosensor: a brief investigation. Laser Physics, 28(6), 066206.

[32] Birhanu, R., Gemta, A. B., Tolessa Maremi, F., & Kumela, A. G. (2024). One-dimensional photonic crystal biosensors encompassing a defect layer for bloodstream bacteria detection. Journal of Optics, 1-12.

[33] Sharifi, H., & Eskandari, S. (2024). Sensing blood components and cancer cells with a photonic crystal resonator biosensor. Results in Optics, 14, 100593.

[34] Aly, A. H., Mohamed, B. A., Awasthi, S. K., Abdallah, S. A. O., & Amin, A. F. (2023). MATLAB simulation-based study on poliovirus sensing through a one-dimensional photonic crystal with a defect. Scientific Reports, 13(1), 9422.

[35] Bhagyasree, G. S., Reena, V. N., Abith, M., Sabari Girisun, T. C., & Nithyaja, B. (2023). Enhanced adsorption and non-linear optical properties of DNA-CTAB functionalized mesoporous silica nanoparticles and their influence on the enhancement of photoluminescence of Rhodamine 6G dye. AIP Advances, 13(5).

[36] Prajzler, V., Jung, W., Oh, K., Cajzl, J., & Nekvindova, P. (2020). Optical properties of deoxyribonucleic acid thin layers deposited on an elastomer substrate. Optical Materials Express, 10(2), 421-433.

[37] Hebda, E., Jancia, M., Kajzar, F., Niziol, J., Pielichowski, J., Rau, I., & Tane, A. (2012). Optical properties of thin films of DNA-CTMA and DNA-CTMA doped with Nile blue. Molecular Crystals and Liquid Crystals, 556(1), 309-316.

[38] Kokkiligadda, S., Dugasani, S. R., Komarala, E. P., Jeon, S., Jeong, J. H., & Park, S. H. (2021). Controlling physical characteristics of DNA and DNA-CTMA thin films by embedding with graphene oxide and riboflavin. Journal of Physics D: Applied Physics, 54(37), 375401.

[39] Malitson, I. H. (1965). Interspecimen comparison of the refractive index of fused silica. Josa, 55(10), 1205-1209.

[40] Tan, C. Z. (1998). Determination of refractive index of silica glass for infrared wavelengths by IR spectroscopy. Journal of Non-Crystalline Solids, 223(1-2), 158-163.

[41] Inagaki, T., Hamm, R. N., Arakawa, E. T., & Painter, L. R. (1974). Optical and dielectric properties of DNA in the extreme ultraviolet. The journal of chemical physics, 61(10), 4246-4250.

[42] Bond, W. L. (1965). Measurement of the refractive indices of several crystals. Journal of Applied Physics, 36(5), 1674-1677.

[43] Birer, A. M., Gözmen, B., Sönmez, Ö., & Kalderis, D. (2021). Evaluation of sewage sludge biochar and modified derivatives as novel SPE adsorbents for monitoring of bisphenol A. Chemosphere, 268, 128866.

[44] Malitson, I. H., & Dodge, M. J. (1972). Refractive index and birefringence of synthetic sapphire. J. Opt. Soc. Am, 62(11), 1405.

[45] Dodge, M. J. (1986). Refractive index in Handbook of Laser Science and Technology, Volume IV, Opt. Mater., p. 30.

[46] Bodurov, I., Vlaeva, I., Viraneva, A., Yovcheva, T., & Sainov, S. (2016). Modified design of a laser refractometer. Nanosci. Nanotechnol, 16, 31-33.

[47] Chen, L., Tuo, B., & Dong, H. (2016). Regulation of intestinal glucose absorption by ion channels and transporters. Nutrients, 8(1), 43.

[48] Burhans, M. S., Hagman, D. K., Kuzma, J. N., Schmidt, K. A., & Kratz, M. (2018). Contribution of adipose tissue inflammation to the development of type 2 diabetes mellitus. Comprehensive Physiology, 9(1), 1.

[49] Guo, L., Zhao, Y., Huang, Q., Huang, J., Tao, Y., Chen, J., ... & Liu, H. (2024). Electrochemical protein biosensors for disease marker detection: progress and opportunities. Microsystems & Nanoengineering, 10(1), 65.

[50] Bollella, P., & Katz, E. (2020). Biosensors—Recent advances and future challenges. Sensors, 20(22), 6645.

[51] Naresh, V., & Lee, N. (2021). A review on biosensors and recent development of nanostructured materials-enabled biosensors. Sensors, 21(4), 1109.

[52] Shi, Y., Yu, Z., Chen, M., & Lang, T. (2021). Bovine serum albumin detection using side-hole fiber sensors. Optical Fiber Technology, 65, 102596.

[53] Berghela, M. (2025). Investigating the Influence of Human Serum Albumin Concentration on (Z)-4-Hydroxytamoxifen Treatment of Breast Cancer (Master's thesis, Albany College of Pharmacy and Health Sciences).

[54] Caffin, J. P., Poutrel, B., & Rainard, P. (1983). Physiological and pathological factors influencing bovine immunoglobulin G1 concentration in milk. Journal of Dairy Science, 66(10), 2161-2166.

[55] Hirayama, K., Akashi, S., Furuya, M., & Fukuhara, K. I. (1990). Rapid confirmation and revision of the primary structure of bovine serum albumin by ESIMS and Frit-FAB LC/MS. Biochemical and biophysical research communications, 173(2), 639-646.

[56] Majorek, K. A., Porebski, P. J., Dayal, A., Zimmerman, M. D., Jablonska, K., Stewart, A. J., & Minor, W. (2012). Structural and

immunologic characterization of bovine, horse, and rabbit serum albumins. Molecular immunology, 52(3-4), 174-182.

[57] Alrowaili, Z. A., Gaber, H. M., Aljoufi, L. S., Elsayed, H. A., Taha, T. A., & Mehaney, A. (2022). Prediction of the resistivity of YBa2Cu3O7-δ superconductor by a highly sensitive one-dimensional phononic crystal sensor. Materials Science in Semiconductor Processing, 152, 107109.

[58] Puthiya Purayil, N., Kakekochi, V., Dalimba, U. K., & Keloth, C. (2021). All-optical diode action through enhanced nonlinear response from polymeric photonic crystal microcavity. ACS Applied Electronic Materials, 4(1), 138-148.

Chapter 5

Synthesis and Characterization of Tailored Structural and Nonlinear Optical Properties of DNA Templated Nanoparticles

This chapter outlines a brief investigation into a slightly modified biotemplate-based synthesis method for nanoparticles and their characterization. The chapter also describes how the conventional synthesize method can be modified for obtaining nanoparticles with tailored morphological and optical properties. Alongside, it covers the synthesis of two vital nanoscale materials - silica and polyoxometalate (silicotungstate), which are considered highly relevant in current materials research. The biopolymer used for the bio-template method is the well-known biomolecule, deoxyribonucleic acid (DNA). Hence, the chapter exemplifies the synthesis process, features, and role of DNA as a bio-template, and characterization of the obtained nanoparticles as well. Moreover, the study reveals that the materials obtained through a bio-template exhibit promising nonlinear optical properties, indicating their potential application in the development of nonlinear photonic crystals. The broader scope of these nanoparticles in emerging technological research is also discussed.

The results of this chapter are published as

1. Bhagyasree, G. S., Reena, V. N., Abith, M., Sabari Girisun, T. C., & Nithyaja, B. (2023). Enhanced adsorption and non-linear optical properties of DNA-CTAB functionalized mesoporous silica nanoparticles and their influence on enhancement of photoluminescence of Rhodamine 6G dye. *AIP Advances*, *13*(5).

2. GS, B., B, N., VN, R., A, D., & Sabari Girisun, T. C. (2025). Tunable nonlinear optical responses in defective DNA-capped polyoxometalate ([α-SiW12O40] 4-) one-dimensional silica/DNA/ZnO ternary photonic crystal systems. *Applied Optics*, *64*(9), 2125-2138.

5.1 Introduction

Nanomaterials are fascinating and fundamental components of nanotechnology, composed of particles in the nanoscale range. Due to their unique physical, chemical, optical, and electrical properties, nanomaterials find wide applications in material science, including catalysis, material functionalization, nonlinear optical devices, integrated photonic and electronic systems, and sensing technologies. The concept of nanotechnology gained momentum after the iconic 1959 lecture by Nobel laureate Richard Feynman titled "There's Plenty of Room at the Bottom," which sparked a revolution in material science. The development of advanced characterization tools such as FESEM, TEM, XRD, and UV-VIS spectroscopy further accelerated progress in this field by enabling detailed studies of nanostructures and their morphology [1-25].

According to the SI system, nanoparticles are defined within the size range of approximately 1–100 nm. Nanomaterials can be made from a wide range of elements and compounds, including organic molecules, carbon-based materials, metals, and metal oxides. They exhibit diverse shapes such as spherical, tubular, cylindrical, conical, spiral, hollow, or even irregular geometries. These structural variations, along with factors like synthesis method, chemical environment, temperature, and pressure, influence the physical and optical properties of the materials [1-25].

Nanomaterials can be synthesized through two general approaches: the bottom-up and top-down methods [1-5, 25]. The bottom-up approach

involves building nanoparticles from atomic or molecular units. This method promotes controlled growth of nanostructures and typically yields uniform size and morphology [1-5,25]. Standard techniques under this approach include sol-gel synthesis, chemical vapor deposition (CVD), pyrolysis, biosynthesis using biological agents, and spinning methods [1-5, 25]. In contrast, the top-down approach involves reducing bulk materials into nanoscale structures. It is generally a mechanical or physical reduction process that includes techniques such as nanolithography, sputtering, laser ablation, thermal decomposition, and mechanical milling. While this method is effective for mass production, it often leads to less control over particle uniformity and surface defects [1-5, 25].

Characterization of nanomaterials involves various techniques to determine their structure, composition, and functional properties. These include FESEM and TEM for morphology, UV-Vis spectroscopy for optical behavior, FTIR for functional group identification, Zeta potential analysis for surface charge, and XRD for crystallinity and phase analysis. Due to their versatility and tunable properties, nanomaterials are extensively used in medical, environmental, energy, chemical, and biological applications, making them an integral part of sustainable advancements in material science.

This chapter explores explicitly the synthesis and properties of silica, and silicotungstate nanoparticles using the sol-gel method. In this synthesis, deoxyribonucleic acid (DNA) is employed as a biotemplate and capping agent to stabilize the nanoparticles and influence their

growth. The role of DNA in enhancing reaction kinetics and controlling nanoparticle morphology is also analyzed in detail.

5.2 Nonlinear optical properties of a material

The realm of nonlinear optics deals with the interaction of light and matter. The nonlinear properties of materials are exploited for the realization of nonlinear optical devices. The research based on the nonlinear optical properties of materials is one of the advancing fields in the domain of photonic research. More precisely, the term, nonlinear optical phenomenon, is linked to the response of matter to the interaction with high intensity coherent light field. The light source, which is used for the nonlinear optical studies, must have coherence, a high degree of purity in spectral lines, and directionality.

The nonlinear optical property of a material can be understood with the material dipole moment orientation (polarization P(t)) under the influence of an external electric field E (t). According to this the relation between polarization and can be mathematically expressed as [75-79]

$$\mathbf{P}(t) = \chi^{1}\mathbf{E}(t) \qquad 5.1$$

where the constant of proportionality χ1 is called the linear optical susceptibility. The nonlinear optical behaviour of the material can be observed when the applied external electric field is high and intense. Thus, the time dependent polarization, **P**(t) of the material can be expressed as a power series of the applied electric field **E**(t) as [74-80];

$$\mathbf{P}(t)= \chi^{1}\mathbf{E}(t)+ \chi^{2}\mathbf{E}^{2}(t)+ \chi^{3}\mathbf{E}^{3}(t)+\chi^{4}\mathbf{E}^{4}(t)+\ldots\ldots\ldots \qquad 5.2$$

where $\chi 2$, $\chi 3$ are the second and third order nonlinear susceptibilities, respectively [74-85].

The second and third order polarizations can be expressed as [75-85];

$$\mathbf{P}^2(t) = \chi^2 \mathbf{E}^2(t) \quad 5.3$$

$$\mathbf{P}^3(t) = \chi^3 \mathbf{E}^3(t) \quad 5.4$$

The physical phenomenon that causes second and third-order nonlinear polarizations is different from each other. The second-order nonlinear property will occur only in non-centrosymmetric crystal. Whereas, third-order nonlinear property is regarded as a special case, as it is the lowest order nonlinearity exhibited by most of the materials. In recent scenarios, the third-order optical susceptibility is treated as a complex quantity having both real and imaginary components [74-85].

Such that;

$$\chi^3 = \chi^3_R + \chi^3_I \quad 5.5$$

where the real and imaginary parts are related to the nonlinear refractive index and nonlinear absorption coefficient (β) respectively [74-78].

5.2.1 Nonlinear optical absorption (NLA)

The intensity of the electromagnetic field has a pivotal role in the light-matter interaction. At the low intensity of light, the absorption rate of light by any absorbing medium is in a linear relation with the increase of intensity, called linear absorption of light. In such a case, the

absorbing material would absorb a single photon of energy. At an intense optical field, the absorbing material would absorb more than a single photon before it attains its ground state. At this point, complicated energy transitions will take place in complex molecular systems. This absorption process can be defined as saturable or reverse saturable absorption.

In a reverse saturable absorption process (RSA), two absorptive mechanisms are involved—the two or mutiphoton absorption and the excited state absorption (ESA). The two-photon absorption (TPA) or multiphoton absorption describes a transition from the ground state of a system to a higher energy state by the simultaneous absorption of two or more photons from the incident radiation. This process requires different selection rules than those of single photon absorption. Figure 5.1 displays a schematic representation of TPA. The interstate between the excited state and the ground state is a virtual state, allowing the system to absorb two photons simultaneously [86, 111].

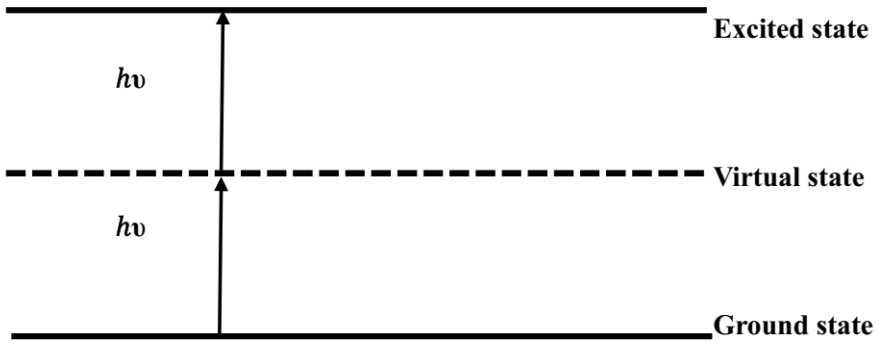

Figure 5.1: Schematic diagram of two-photon absorption [86, 111]

In such a case, the absorption of the light is nonlinear and is proportional to the square of the simultaneous intensity (I), and the relation is described as [74-86]

$$\frac{dI}{dz} = -\alpha I - \beta I^2 \quad 5.6$$

Where α is the linear absorption coefficient and β is the two-photon absorption coefficient.

The multiphoton (2n+1) absorption due to a single optical beam traces a relation as

$$\frac{dI}{dz} = -(\alpha + \gamma^{n+1} I^n) I = \alpha I \quad 5.7$$

The intensity-dependent absorption coefficient can be deduced from equation 5.7 such that

$$\alpha(I) = \frac{\alpha_0}{1+\frac{I}{I_{SAT}}} \quad 5.8$$

Where α_0 is the linear (unsaturated) absorption coefficient, I is the incoming optical intensity, and I_{SAT} is the saturation intensity at which absorptions are reduced to half of their original value.

Looking at equations 5.7 and 5.8, when I goes to infinity, which says that the material becomes transparent to the incoming light. At low intensity, the relation caused by the absorption of light is linear. In principle, as light increases, a material's ability to absorb light can reach a particular point, called the saturation point, at which no further absorption of photons will occur in proportional to the increase of intensity of light. It occurs so as the material's ability to absorb light is limited by

the number of available states (usually the valence band and ground electronic state) that can absorb the light. It is called the NSA mechanism.

Generally, there are specific facts which are crucial for exhibiting a material its NSA property. They are: low intensity, increasing intensity, ground state depletion, and saturation. At low intensity, the rate of absorption of photons would be low, though the material absorbs photons, and electrons reach higher energy states. This effect can be obtained by controlling the intensity of the applied Gaussian light source. At high intensity, the rate of absorption increases, while the ground-level electron number will be low. The delay in decay to the ground level can significantly reduce the nonlinear optical absorption. It will be another cause of NSA occurrence. Another factor that also contributes to bringing NSA property in materials is the saturation of the excited state population.

At a specific point, due to the increase of intensity, the absorption of photons by the ground state electrons increases which resulting in a sufficiently high population of electrons at the excited state. It will prohibit proportional absorption of photons, resulting in the material exhibiting NSA. At this time, the material will be highly transparent to the incoming laser source. Such a situation is highly demanded in ultrafast optics, especially in mode-locking lasers and optical switching.If the incident intensity is sufficiently high, as that of saturation intensity, the excited state can become remarkably populated. In such a situation, the excited electrons can rapidly make a transition to higher excited states before returning to their ground state.

However, this work involves the biotemplate based synthesis of nanoparticles, it is mandatory to discuss the nonlinear optical behaviour of organic compounds such that DNA belongs to the organic compound family. In the case of organic materials, the transitions are possible to higher energy singlet (Sn) and triplet state (Tn) manifolds. The transitions of the excited electrons to the higher excited singlet state Sn and the triplet state Tn depend on the pulse duration, pump intensity, and the wavelength. This mechanism is known as the excited state absorption (ESA). When the cross section for ESA or TPA exceeds linear absorption, the RSA occurs. In other words, if the RSA occurs, the incident intensity of light is sufficiently high to increase the transition of electrons from the ground state to the excited state. In the case of ESA, the excited state absorption cross section is higher than the absorption cross section from the ground state to the first excited state.

The nonlinear optical phenomenon can be extended to diverse opportunities based on the tuned material properties. The most commonly accepted nonlinear optical property of a material is its nonlinear optical absorption mechanism. Apart from the nonlinear optical absorption (NLA) mechanism, there lies another property that has equally importance in the nonlinear optical domain. It is nothing but nonlinear optical saturation absorption (NSA). This mechanism has been widely occupied in various nonlinear optical applications including passive Q-switching, mode-locking, optical limiting, optical switching, optical data storage, nonlinear filtering, and nonlinear absorption microscopy. These kinds of applications are crucial in areas such as laser technology, communication, and imaging. In essence, the invention of engi-

neered materials that are capable of exhibiting NAS mechanics would have a great place in the nonlinear optical domain [74].

The Z-scan technique is used to elucidate the third-order nonlinear effect, and the details of which are provided in the following section [76].

5.2.2 Open Aperture Z-scan to study NLA of a material

Since, the work is interested only in intensity dependent optical absorption, therefore, the experiments were restricted to open aperture technique only. The Z-scan technique is a subtle and robust single-beam method developed by Sheik Bahae [76] to measure the sign and magnitude of both the real and imaginary parts of third-order nonlinear susceptibility, $\chi 3$. In this experimental setup, a monochromatic high-intensity laser beam is allowed to fall on a nonlinear material (medium). After the intense beam passing through the material, the medium itself acts like a lens which results self -focusing of the beam due to the photo-induced varying refractive index of the nonlinear material [74]. The Z-scan technique can exploit both the dynamics of the laser beam inside the nonlinear material and the self-refraction of the material.

The schematic representation of the experimental setup for the Z-scan technique is provided in Figure 5.2. In this experimental setup, the Gaussian laser beam is primarily focused by a concave lens and the focused intense beam is allowed to fall on the nonlinear material. The sample is moved along the direction of propagation direction of the focused laser beam while measuring the transmittance of the focused Gaussian beam.

The sample should be thin and the length of the sample should be kept less than the Reyleigh's range Z_0. In order to determine the nonlinear absorption coefficient βeff, the intensity-dependent absorption coefficient (α (I)) for ESA-assisted TPA open-aperture Z-scan recordings was fitted theoretically using the equation given by [97, 111-113]

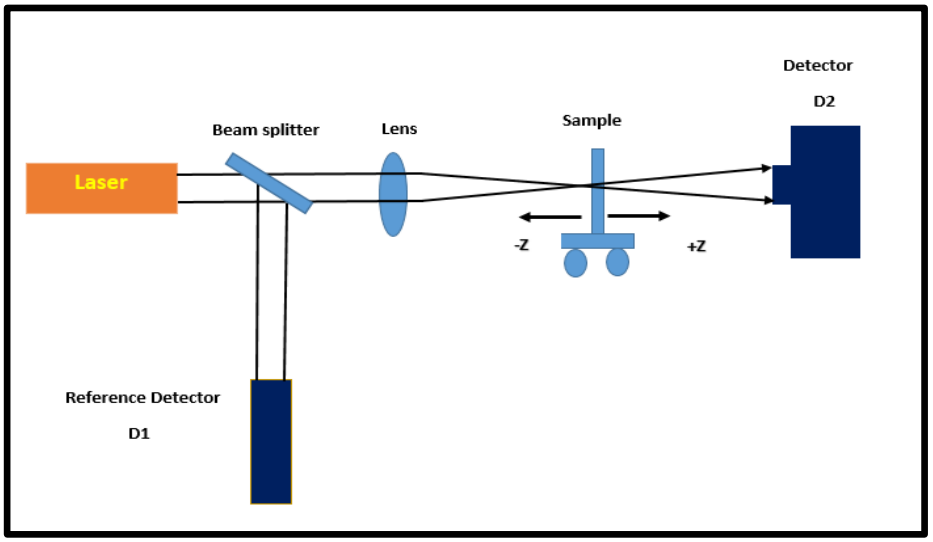

Figure 5.2: Schematic diagram of open aperture Z-scan experimental setup [51-52]

$$\alpha(I) = \frac{\alpha_0}{1+I/I_s} + \beta_{eff} I \qquad 5.9$$

Where $\alpha(I)$ is the linear absorption coefficient, I is the incident laser intensity, Is is the saturation intensity at which the intensity of the incoming light becomes half, βeff is the nonlinear absorption coefficient associated with the reverse saturation absorption (RSA)[102-105]

The nonlinear absorption in this case is proportional to the square of the simultaneous intensity (I), given by

$$\frac{dI}{dz} = -\left[\frac{\alpha_0}{1+I/I_0}\right] I - \beta_{eff} I^2 \qquad 5.10$$

Where, z is the propagation distance within the sample. The first term in equation (5.11) expresses the SA and the second term indicates effective TPA part.

Normalized transmittance is given by,

$$T(z) = \frac{1}{q_0(z)\sqrt{\pi}} \int_{-\infty}^{\infty} ln\left[1 + q_0(z) e^{-z^2}\right] dz \qquad 5.11$$

Where $q_0(z) = \frac{\beta_{eff} I_0 L_{eff}}{1+\frac{z^2}{z_0^2}}$ 5.12

And $L_{eff} = \frac{1-e^{-\alpha L}}{\alpha_0}$ 5.13

L_{eff} is the effective sample length, L is the sample length, α_0 is the unsaturated linear absorption coefficient, and z is the position of the sample

$$Z_0 = \frac{\pi \omega_0^2}{\lambda} \qquad 5.14$$

is the Raleigh range, ω_0 is the beam waist radius at the focal point, and λ is the wavelength of the laser beam. The imaginary part of the third-order nonlinear susceptibility (χ^3) is given by,

$$\chi^{(3)} = \frac{n_0^2 \varepsilon_0 c \lambda \beta_{eff}}{2\pi} \qquad 5.15$$

Where n_0 is the linear refractive index, c is the speed of light, and ε_0 is the permittivity of free space. Using equations 5.12 and 5.15, the

experimental data were fitted to the theoretical model to obtain nonlinear parameters.

5.3 Biotemplate method and its role in the synthesis of nanoparticles with tuned morphological and optical properties

The invention of a variety of novel synthesis methods and fabrication techniques facilitates the growth of nanoscience. Despite of outburst of fabrication techniques, the novelty of synthesizing methods away from the conventional way bags the attention of the material research field that uses template materials or known as stabilizing agents (capping agents) for tailored properties of nanoparticles at desired requirements. In principle, a template material (catalyst) can alter the performance of a chemical reaction by controlling the duration and structure of precipitation. The controlling nature of template materials is due to their structural and chemical peculiarities, which meet the conditions of a chemical reaction in which they take part. The common factors that all template materials have are that they are pH independent, morphologically adaptive, and good adsorbent materials. When they take part in a chemical reaction, they will not interfere with the direction of the reaction. Instead, their presence accelerates the reaction rate to form precipitation quickly without wasting time. Gradually, the scope of template materials has been widened. So, the morphological appearance of the synthesized particles is found to be changed due to the presence of capping agents. This novelty helped to enhance the modifications of synthesizing nanoparticles and accelerate the growth of nanoscience. There are different types of template materials being exploited for synthesize methods, including inorganic and organic materials. Among

these, organic template materials are of two kinds they are polymer and non-polymer. It is found that biomaterials can influence the transformation of unique morphological texture and properties of the nanoparticles [1-68].

Decades after the emergence of nanotechnology, various types of materials have been explored as template materials for bringing up unique properties and geometry in nanomaterials. However, the demand for economically favorable and ecologically non-toxic materials has recently been sounded affects the emergence of green synthesis. Thus, the role of template utilization was also switched from inorganic to biotemplate materials. Hence, they are widely accepted for synthesizing nanoparticles in different shapes and properties in the nano size range. Naturally occurring biomaterials, including tissues derived from plants, and animals (like DNA, protein polymers (BSA), plant cellulose, etc.), and microorganisms (DNA and RNA from bacteria and viruses), are found to be applicable as biotemplate materials. Due to their abundant source in nature (economically cheap), diverse structure, non-toxicity, and easy handling nature make them attractive for using as biotemplate materials [69-99].

5.4 Synthesis of DNA-capped silica nanoparticles incorporating with DNA-template and their tailored structural and nonlinear optical properties.

The emergence of silica nanoparticles drew attention in material chemistry since the 1970s, soon after the development of nanotechnology. In general, silica has diverse features including transparency, odourless,

vitreous lustre, non-conductive to electricity, diamagnetic, and amorphous. In fact, these properties of silica limit their roles in certain applications like substrate for thin film making, fibre optics, ceramics, semiconductors, etc. Since the invention of the Stober process in 1968, it has been proven that nano-level, controllable spherical silica particles can be achieved. Subsequently, various synthesis methods were reported to obtain tunable and uniform-sized silica nanoparticles in material science for different industrial and chemical aspects. Moreover, the material research field realized that silica nanoparticles underwent surface modification under different experimental conditions and acquired adsorptive and nonlinear optical properties. The size of the morphologically modified silica particles is specified as mesoporous silica nanoparticles, in which the pore size falls to 1-10 nm. They offer a number of additional features, including porous structure, tunable size, large surface area, biocompatibility, and ordered uniform structure [1-59]. That awakened the material chemistry in a way that silica can be subject to various usages due to its enhanced morphological adaptations and nonlinear optical features. Over the last decades, various chemical and physical methods have been introduced to enhance the properties of silica nanoparticles at different morphological and functional levels. Based on the ease of production and physico-chemical features, nowadays silica nanoparticles have become one of the classes of materials which are known for their different roles in the chemical industry, such as nanomedicine, catalysis, plasmonic colour thin films, surface enhanced spectroscopy, DNA extraction, magnetic separation, and photonic devices and instrumentation development. Nowadays, porous nanomaterials are widely used for tuning laser systems and cell

imaging purposes. Among the porous nanomaterials, silica nanoparticles are treated as a favourable subject in material science, so that silica-incorporated research works have become a focus in tuning dye laser systems [20-29]. These applications of silica are merely based on its unique mesoporous surface properties. The surface properties of silica nanoparticles can be modified for different purposes. These features of the mesoporous silica nanoparticles help to attach the functional chemical groups to them in comparison with amorphous colloidal silica. The reported research papers revealed that mesoporous silica nanoparticles can influence structural, microstructural, and biological properties of polymer nanocomposites. Functionalized mesoporous silica nanoparticles are widely recognized for their stable chemical properties, controlled bioactive compound release, adsorbent-adsorbate stability, thermal stability, control on hydrophilicity, and pH resistant. The surface properties of silica nanoparticles can be enhanced by altering various parameters like temperature, pressure, molar ratio of reagents, pH, and chemical additives as well. The presence of chemical additives during the precipitation of silica nanoparticles can control the growth of nanoparticles within the mesoporous limit, along with the surface modification, and other parameters. Since the features of silica nanoparticles in terms of porosity, size of the pores, pore volume, surface area, and biocompatibility, etc., are found to be enhanced by the presence of chemical additives, different methods and chemical additives have been reported [1-33, 35]. In 2009, Qiao. et al [36] reported the synthesis of mesoporous silica nanoparticles through a controlled hydrolysis process using cetyl trimethyl ammonium chloride (CTAC). In which they claimed that they could control the size of the silica na-

noparticles to a range of 25 nm to 200nm. In 2012, Lodha et al. [37] stated that they had synthesized mesoporous silica nanoparticles for the drug loading of a purely water-soluble drug. They used cetyl trimethyl ammonium bromide (CTAB) and concentrated HCl for the synthesis of mesoporous silica nanoparticles. In 2017, Niara et. al [38] claimed that they could achieve to form silica particles having a pore volume size of 2.5 nm to 2.8nm. They have used CTAB as the pore-generating agent. In 2020, Presentato et. al. [39] stated that they have prepared biodegradable, high pore volume mesoporous silica nanoparticles using CTAB and concentrated HCl. These reported silica particle synthesis methods were carried out using the Stober process method. Such mesoporous silica nanoparticles are applicable to the biomedical field for target drug delivery, bio-sensing, cellular uptake, etc. Since their role in the bio-medical field is found to increase, the recent works mainly focus on making mesoporous silica functionalised and biocompatible using different surfactants like cetyl trimethyl ammonium chloride (CTAC) [1-69].

This work introduces a bio-template to prepare mesoporous silica nanoparticles by incorporating the Stober synthesis method and also seeks the morphological and nonlinear properties of the obtained silica particles. Among the available reported synthesis methods of silica nanoparticles, the bio-template to obtain a tailored morphology of silica particles is considered. The bio-template was synthesized by forming a complex of deoxyribonucleic acid and the cationic surfactant cetyltrimethylammonium bromide (CTAB). A key role of surfactants is played in nanoparticle synthesis by adsorbing to the nanoparticles sur-

face and lowering the surface energy of the nanoparticles soon after they are formed. It is the way in which the aggregation of particles has been prevented and the formation of size-controlled and surface-controlled nanoparticles. So far, the stabilizing mechanism of DNA in nanoparticle formation has been recognized, as its usage is being increased in material science as a bio-template, and conjugate polymer as well. Studies show that the nanoparticles that are formed in the presence of a DNA template exhibit excellent physicochemical properties [69-99]. Figure 5.3 illustrates a schematic representation of the polynucleotide structure of DNA. Since DNA is considered a fascinating biophotonic material, as it is verified in many research papers that it can improve the functional properties of photonic device materials. Moreover, the seductive factor that makes DNA a vital material in material science is the double helical, lengthy polymer structure of the molecule. Due to the unique double helical structure, DNA possesses high transparency, thermal stability, nonlinear optical activity, amplified emission, and its applications are widely found in electron blocking, hole transport, hosting of laser dyes, modification capability, electrical interconnectors, thin films, lasing, and sensing purposes. The strands of the double helical structure are made of alternating sugar (deoxyribose) and phosphate groups. The sugar group is attached to one of the four bases: adenine (A), cytosine(C), guanine (G), or thymine (T). The stability of the dsDNA molecule depends on GC base pairs and length. It is found that longer molecules are more stable. Long DNA helices with a high GC content have more strongly interacting strands, while short helices with high AT content have more weakly interacting strands. The structural features that define a DNA

polymer to engage in a reaction are length, base sequence, temperature, and buffer conditions [69-100].

As far as the diverse properties of DNA are concerned, it is found that they can be incorporated with nanoparticles that have a positive charge. Mainly, DNA is used for functionalizing with metal nanoparticles to form functionalized or conjugated polymer under a buffer condition. It confirmed the negative charge of the DNA that resembles the chemical behaviour of a ligand. The studies dealt with its conjugating effect as they are taking part in a chemical reaction with other polymers (surfactants, metal nanoparticles, etc.), and they got functionalized. So that they can form organic-inorganic complexes and salt with the polymers. In turn, the functionalized DNA has diverse properties that it can tune nanomaterials about their size, shape, and surface compatibility with adsorbents, electrical, magnetic, optical, and biological properties [69-99].

In the Stober process, the solvent used to synthesis silica nanoparticles is an alcohol medium (either ethanol or methanol). So, DNA alone cannot dissolve in alcoholic solvents. So this problem can be avoided by transforming DNA into its complex with a cationic surfactant. Considering the properties of functionalized DNA polymer, the surfactant cetyl trimethyl ammonium bromide (CTAB) is selected. They are also used for synthesizing mesoporous silica nanoparticles. It is a known cationic surfactant that belongs to the compounds of the cetrimonium cation family. The fascinating feature of CTAB is that it is widely used as the main component of the buffer solution for the extraction of

DNA, so that it reacts with the polysaccharide chains of the DNA [85, 96-99].

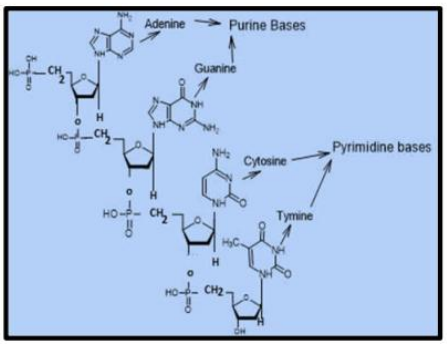

Figure 5. 3: Portion of polynucleotide chain of DNA [100-103]

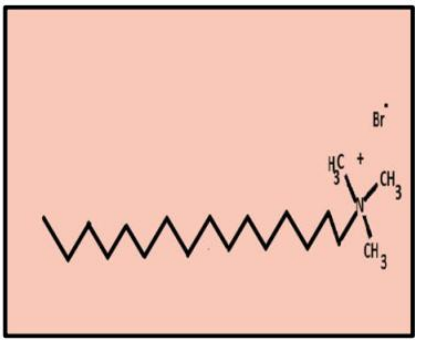

Figure. 5.4: Chemical structure of CTAB [104-105]

Its chemical formula is hexadecyltrimethyl ammonium bromide ($[C_{16}H_{33}]\ N(CH_3)_3]Br$) and is highly biocompatible. Figure. 5.4 is a schematic representation of the CTAB structure. It is a familiar compound to be used for nanoparticle synthesis. It has 16 carbon atoms as a long tail and an ammonium head group with three methyl groups attached. In some cases, functionalized biomolecules such as DNA cannot sufficiently penetrate a dense layer of capping agents or replace them. Therefore, surfactant surfactant-assisted methods aim to modify the surface ligands by adding an excess of small molecules with higher affinity towards dielectric nanoparticles. In the case of the DNA molecule, the deoxyribose-phosphate groups contribute to the backbone of the DNA strand. Among these groups, the phosphate group comprises one negatively charged oxygen atom, is responsible for the negative charge of the entire DNA strand. It is the result of the bond between the phosphorous and oxygen. Hence, the cationic surfactant becomes

attached to the phosphate group of the DNA and forms a DNA-surfactant complex [31-33, 36-38,69-99].

Combining the properties of CTAB and DNA, CTAB was selected as the cationic surfactant. Without using any additional buffer chemicals, a reaction between CTAB solution and DNA solution was carried out to form the CTAB-DNA (CD) complex. It is found that the CD complex can dissolve in the alcohol group. The obtained mesoporous silica nanoparticles have shown an enhanced tailored morphology along with controllable adhesive properties. It is also proven that the CD biocomplex template was an effective template to incorporate with the Stober process to enhance the particle size, pore size, volume, and area of the silica particles. The nonlinear optical properties of dielectric materials with metal composites have been investigated for two decades for fabricating nonlinear optical devices. In those studies, the nonlinear optical properties of metal nanoparticles doped with silica glass substrate were only considered [100]. It pointed out that the nonlinear optical property of mesoporous silica nanoparticles alone seems ignorant in nonlinear optical physics. However, silica glass inclusion with semiconducting materials and metal nanoparticles in order to enhance the nonlinear optical properties of the doping materials is still a research interest. In this context, the nonlinear optical properties of CD-templated silica nanoparticles were investigated using the Z-scan technique

5.4.1 Experimental methods

Chemicals used were CTAB, DNA, tetraethyl orthosilicate (TEOS), ammonium hydroxide (NH_4OH), methanol, hydrochloric acid (HCL), acetone, and deionized (DI) water. All chemicals except DNA were purchased from Merck Life Science Private Limited. DNA powder was purchased from Sisco Research Private Limited. All the glassware used for the experiment was cleansed by acetone, followed by DI water and dried in a hot air oven at 100 0C, and was again subject to Piranha cleaning, followed by DI water cleansing and dried at 100 °C using a hot air oven.

a. Synthesis of DNA-CTAB complex

The complex of DNA and the cationic surfactant CTAB in different concentrations of DNA solution. The DNA solution with 0.1, 0.5, 0.15, and 0.1525 of weight-percentage (wt %) was prepared by dissolving DNA in DI water, followed by sonication at room temperature for 30 minutes to achieve a homogenous DNA solution. In another beaker, 0.4 g of CTAB was taken, and 30 ml of DI water was poured into the beaker, and the mixture was sonicated until the CTAB was dissolved entirely at room temperature. The solution was a colorless and viscous solution. This solution was added slowly into the DNA solution under constant stirring using sonication at room temperature. This process allowed to precipitate of a white colloidal form of the CD complex where the surfactant CTAB is attached to the DNA molecule. The precipitation was filtered and washed with DI water many times to re-

move unreacted CTAB. The CD complex precipitate was kept in a hot air oven at 60°C for 24 hours to obtain CD complex powder [85-86].

b. Synthesis of silica nanoparticles using the Stober process

The silica nanoparticles were synthesized by the Stober process, a known sol-gel process to synthesize spherical nanoparticles of silica. A precursor solution of Siica is made by adding 5 ml of TEOS solution into a solution of 150 ml of methanol and 40 ml of DI water under constant stirring using sonication at room temperature in a 500ml boro-silicate glass beaker. The stabilizing agent NH4OH was taken in an amount of 14 ml in a Burette and added slowly into the solution under constant stirring. The solution was kept stirring for 35 minutes at room temperature. A white colloidal precipitation was formed. The precipitation is filtered by waterman filter paper and washed 5 times with DI water, followed by methanol. The filtered precipitation was kept in a hot air oven at 70°C for 1 hour for drying. Then the obtained silica powder was calcined at 10°C/minute [1-28].

c. Formation of silica nanoparticles using CTAB

The silica nanoparticles were synthesized by the Stober process, where CTAB was used as the stabilizing agent. Typically, 0.4g of CTAB was dissolved in 40 mL of DI water by sonication at room temperature. Under constant stirring, 150 mL of methanol is added to the solution. After 5 minutes of stirring, 5 mL of TEOS was added and followed by the addition of 14 mL of NH_4OH dropwise into the solution under constant stirring at room temperature. The constant stirring was maintained until a white colloidal precipitate was formed. The precipitation

is filtered by waterman filter paper and washed 5 times with DI water, followed by methanol. The filtered precipitation was kept in a hot air oven at 70°C for 1 hour for drying. Then the obtained silica powder was calcined at 10 °C/ minute [1-28].

d. Formation of silica nanoparticles using CD complex

The silica nanoparticles were synthesized in the presence of the CD complex under the conditions of the Stober process. The samples of 0.01, 05, 0.15, and 0.1525 wt% of CD complex powder are assigned as CD1, CD2, CD3, and CD4. Each CD complex samples were dissolved in 150 mL of methanol under constant stirring. After obtaining a complete transparent solution, 35 ml of DI water was added to each four CD complex-methanol (CDM) solutions under constant stirring for 10 minutes at room temperature. 5 ml of tetraethyl orthosilicate solution was added to each solution of CDM under constant stirring using sonication at room temperature in a 500 ml borosilicate glass beaker, and 14 ml of ammonium hydroxide as a catalyst was added slowly into the solution under constant stirring. The solution was kept stirring for 35 minutes at room temperature. A white colloidal precipitation was formed. The precipitation is filtered by waterman filter paper and washed 5 times with DI water, followed by methanol. The filtered precipitation was kept in a hot air oven at 70°C for 1 hour for drying. Then the obtained silica powder was calcined at 10°C/minute.

e. Formation of silica nanoparticles using the CD complex in the peptization method

The peptization method has evolved from the Stober process [102-104]. In which the synthesis process is carried out slightly in an acidic medium. The CD solution of CD4 was dissolved in 150 mL of methanol under constant stirring using an ultrasound sonicator. After getting a transparent solution, 35 ml of DI water was added under constant stirring for 10 minutes. 5 ml of TEOS was added to the stirring solution and kept stirring for 10 minutes and followed by adding 5 ml of HCL slowly into the stirring solution. A white precipitation was seen. The precipitation was filtered, and the silica gel was washed with DI water and followed by methanol. The silica gel was dried at 70°C for two hours to form silica powder. The obtained silica powder was calcined at 10^0 C/minute.

5.4.2 Results and Discussions

The obtained silica nanoparticles were subject to different characterization processes to analysis the features and changes in the existing properties. The characterization tools used for the sample analysis are XRD, UV-Vis spectroscopy, SEM, surface area analysis, and nonlinear optical analysis. The detailed discussion on the characterization is provided in the following sections.

a. XRD Analysis

The two differently prepared powder samples of silica were subject to XRD analysis. One of the samples was synthesized in the presence of

0.1525 wt % of CD complex (S1), and the remaining sample was prepared in the absence of CD complex template to examine the effects of CD complex in making nanoparticles. The XRD patterns of S1 and S2 are provided in Fig. 3. From the XRD pattern, the peak intensity, position, and full width at half maximum (FWHM) data using the Gaussian fitting method were determined. The diffraction angles 2θ range was taken between 200–800. The XRD patterns for both samples show an amorphous nature by the single broad peak and which ratifies that the sample is silica by forming the broad peak at 22.61° for S1 and 23.53° for S2, which come in the range of amorphous silica found generally in the XRD pattern for silica particles [105-106]. The diffraction peak obtained for S1 is broader than that of S2, the mean size of the silica nanoparticles. The mean size of the two samples is estimated using the Debye-Sherrer formula, and they are 1.65nm and 2.63 nm for S1 and S2, respectively [107-110].

$$D = \frac{0.89\lambda}{b\cos\theta} \qquad 5.15$$

Where 0.89 is the shape factor, λ is the X-ray wavelength = 1.54056 Å for Copper Kα X-ray, b is the line broadening at FWHM in radians, and θ is the Bragg angle.

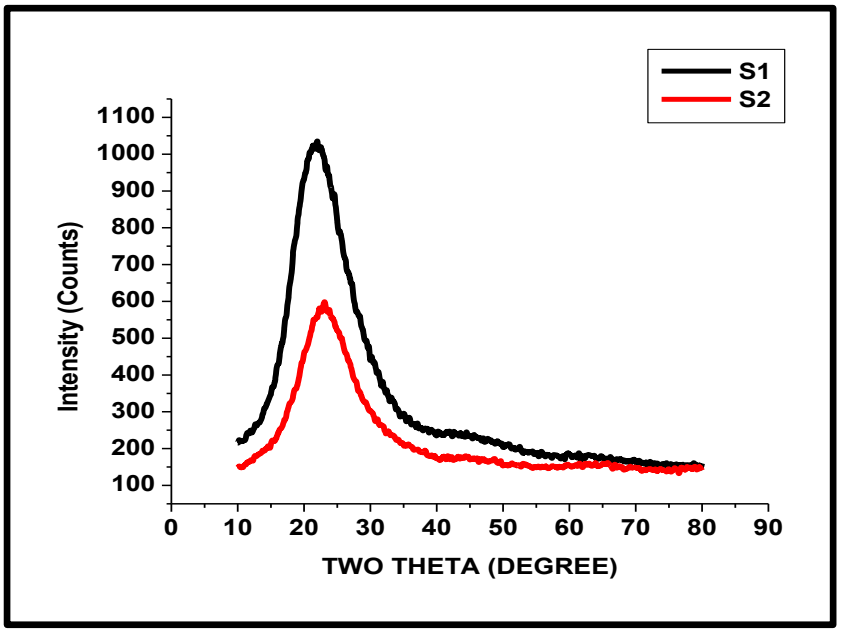

Figure 5. 5: XRD of silica nanoparticles formed in the presence of CD complex in peptization method (S1) and silica particles formed in the absence of CD complex (S2) in Stober process.

Figure 5.5 shows that the difference between the FWHM of S1 and S2 is due to the presence of the CD complex template. When comparing the XRD patterns of S1 and S2, the diffraction peak of S1 tends to move lower angle and gets narrower than the peak of S2. These features of S1 indicate that the silica particles may have a crystalline structure or better orientation [72]. From the difference observed between the measurements of FWHM, it is understood that the size of the particles of S1 is smaller than that of S2, since the XRD results validate that the presence of the CD complex template influences the size of the silica particles to reduce them to the nanoscale range.

b. UV-VIS Analysis

Optical absorption spectra of the samples were carried out using UV-Vis spectrophotometry in the scan range of 230-800 nm. The silica samples subjected to UV spectrophotometry were S1, S2, S3, S4, S5, S6, S7, and S8 corresponding to silica prepared by the Stober process, the Stober process using CTAB as a stabilizing agent, 0.01 wt% %, 0.05 wt% %, 0.15 wt% %, and 0.1525 wt % of DNA concentrations of CD complex in Stober process, and peptization process with 0.1525 wt % of CD complex template respectively. The amount of CTAB used for synthesizing sample S2 is approximately the same as the amount of CTAB used for preparing samples S7 and S8. This experimental condition is maintained for differentiating the background role of CTAB in CTAB incorporated Stober process, CD complex template involving Stober and peptization processes for forming the nanoparticles. The solvent used for UV analysis was dimethyl sulphoxide (DMSO). Figure 5.6 represents the UV absorption spectra of silica samples. It illustrates that the absorption peaks for silica prepared in the CD complex show a blue shift (samples S2-S8). The peak blue shift for S8 is approximately 10 nm. It indicated that as the concentration of the CD complex template increases, the particle size goes on decreasing. This result exemplifies that the presence of the CD complex reduces the size of the silica nanoparticles.

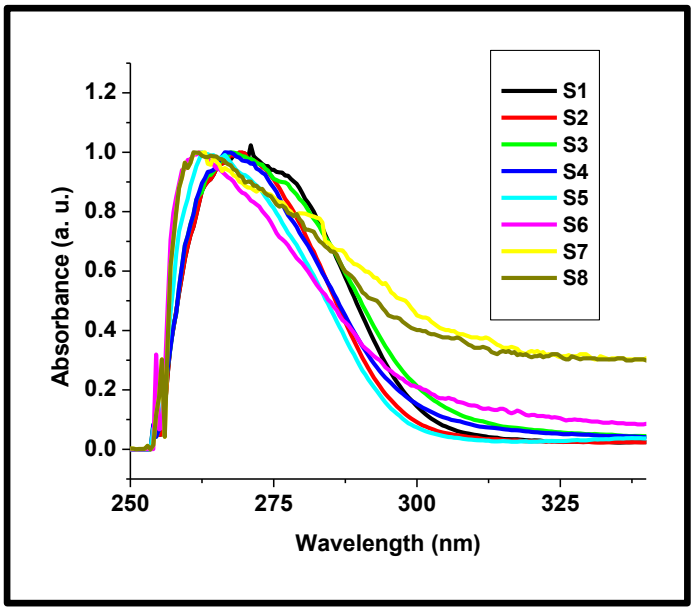

Figure. 5.6: UV absorption of silica nanoparticles prepared via S1) Stober process S2) Stober process incorporated with CTAB, S3) peptization method S4) Stober process with 0.01 wt % of CD complex S5) Stober process 0.05 wt % of CD complex, S6) Stober process with 0.15 wt % of CD complex, and S7) Stober process with 0.1525 wt % of CD complex, and S8) peptization process with 0.1525 wt % of CD complex.

The peak shift difference between S3 and S8 indicates that the CD complex can also make an impact in acidic conditions, so that S3 and S8 are prepared under acidic conditions.

c. Surface Area Analysis

Surface area is one of the quantities to explain the particle size, particle morphology, surface texturing, and porosity of any particle. It is considered one of the vital factors that explain the potential of physical properties of particles in taking part in biological and inorganic catalytic activities. To endorse the surface area of the silica

nanoparticles derived from the CD complex templated method, Brunauer- Emmet- Teller (BET) analysis was conducted. Based on the BET analysis results, N2 adsorption/desorption isotherms were employed to identify surface parameters. The BET analysis was conducted against the six samples of silica particles. The samples were named as S1, S2, S3, S4, S5, and S6 corresponding to the silica particles prepared by the Stober process, prepared by using 0.01 wt% , 0.05 wt %, 0.15 wt %, 0.1525 wt % of DNA in Stober process, peptization method, 0.1525 wt % of DNA template in peptization method. The BET results discussed the size of the pores, the type of pores, whether it is open or closed, and the pore diameter distribution. The N2 adsorption/desorption isotherm curves of the six samples of SNP exhibit a type IV hysteresis loop with two branches, adsorption (capillary condensation) and desorption (evaporation). These hysteresis loops indicate the presence of open pores between the particles and the mesoporous surface. Since, Stober process gives mesoporous silica nanoparticles, this general feature is supported by the hysteresis loops of all six samples [111].

The adsorption branch of type IV is a composite of types I and II. At low relative pressure (p/p_0), the uptake of gas molecules is associated with the filling of micropores (forms monolayer adsorption). These type IV loops are often found with aggregated crystals of zeolites, some mesoporous zeolites, and micro-mesoporous carbon. The isotherm curves of samples shown in Figure 5.7 illustrate that the adsorption pore volume of the samples increased as going from sample S1 to S6 in accordance with the pore diameter, which shows a gradual

increase on increasing the concentration of CD complex template increases.

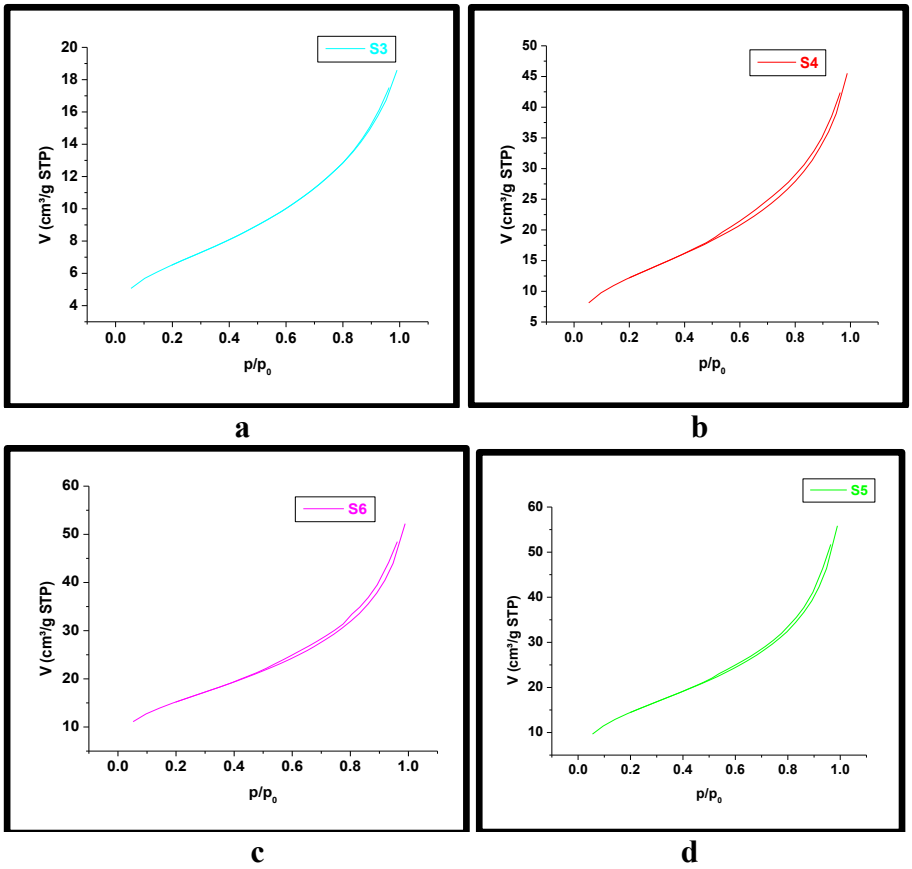

Figure 5. 7: BET isotherm results of a) silica nanoparticles synthesized in Stober process, silica nanoparticles synthesized in b) 0.01 wt % of CD complex template, c) 0.05 wt % of CD complex template, d) 0.15 wt % of CD complex template, e) peptization method in 0.1525 wt % of CD complex template, and f) 0.1525 wt % of CD complex template

The highest value of BET surface area is for sample S6. It is evident from the isotherm data shown in Table 1 of the samples that, for large pore size, the BET surface area is comparably found to be low, which implicates that for low mesoporous properties and such a surface

cannot adsorb particles to its surface than particles having small pores on their surface. For small pores, the BET surface area and pore volume are large. This feature implies that their adsorption stability is high. It is evident from the isotherm curves of the samples S1-S6 shown in Figure 5.7 that at higher relative pressure (p/p_0), the hysteresis loop width is relatively wider for samples S5 and S6 compared with other samples. The fact that connects the loop width and adsorption property is that the wider the loop is, the adsorption stability is also higher.

Table 5.1 Experimental data obtained from N2 adsorption–desorption isotherms

Sample	Mean pore diameter (nm)	Pore Volume (cm^3/g)	BET surface area (m^2/g)
S1 (Silica WoD)	7.942	0.019	9.543
S2(0.05 wt % DNA	6.532	0.029	21.496
S3 (0.15 wt % DNA)	6.379	0.035	22.686
S4(0.1525 wt %DNA)	6.188	0.070	45.516
S5(Peptization)	5.063	0.086	54.172
S6 (Peptization in 0.1525)	5.946	0.081	54.335

Moreover, the hysteresis loop width is found to increase as one goes from S1 to S6. The only factor that varies as going from S1 to S6 is the concentration of the CD complex template. The samples S5 and S6 were made in the presence of a high concentration of CD complex template (0.1525 wt% %) among other samples. Another fact obtained

from the BET results is that the pore size of all the samples comes within the mesoporous range (2nm <pore diameter< 50 nm). Among the six samples, S6 exhibited a small value of mesoporous size by analyzing the size distribution of the pores. In fact, this pointed out that the presence of the CD complex induces to make the porous surface of the silica nanoparticles to become a more adsorbent surface, in which the adsorbents cannot escape easily. It is generally accepted that DNA is a double-stranded stranded lengthy biopolymer, and CTAB is also a lengthy polymer. These together form a complex structure that is spanned between the silica particles. Due to the lengthy network of the CD complex, the silica particles cannot be aggregated beyond a particular range, and thus, nanoparticles are formed since the nanoparticles are confined in the CD complex surface, after the removal of the CD complex, which leads to voids in the surface of the silica nanoparticles, which in turn causes the silica particles to become mesoporous. This feature makes them a good adsorbent, and that can be efficiently used for drug delivery agents, doping agents, and gas sensing applications.

d. SEM analysis

The SEM images of the silica particles are shown in Figure 5.8. The silica particles prepared without the CD complex template are seen in Figure 5. 8a. The particles are showing a spherical geometry with a smooth surface. Figure 5.8b represents the silica particles prepared in the presence of the CD complex. In which the particles are seen in an aggregated spherical and flat surface, but irregular in size.

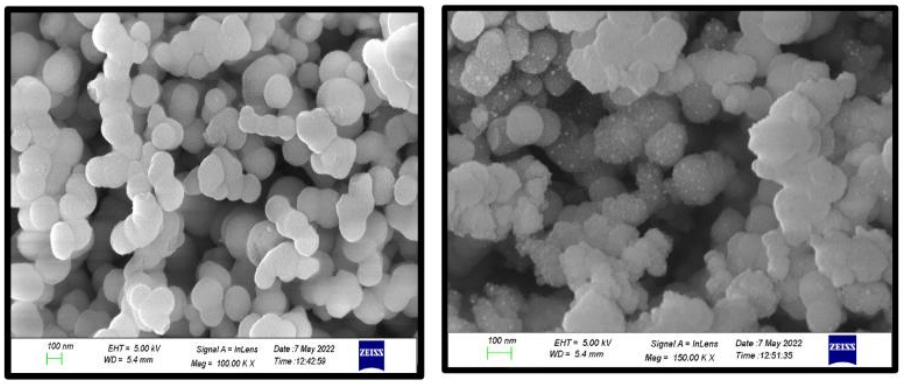

a b

Figure 5. 8: SEM images of silica particles formed a)without the presence of CD complex, b) with the presence of CD complex

The surfaces of the particles seemed to be irregular spherical structures that were seen as projecting from the surface. These projected like spherical nanoparticles can enhance the surface area. Hence, the SEM results show that the presence of CD complex influences the morphology of the silica particles to a favorable feature of mesoporous surface, and this synthesis method could preserve the spherical shape of the silica particles, which is seen as a general feature of the Stober process.

e. Third-order nonlinear optical studies of DNA-CTAB complex-templated silica nanoparticles

The nonlinear optical property of a material is the result of the interaction of the material with a high-intensity Gaussian pulse. However, the nonlinear optical properties of silica under different conditions have been well studied previously. In 2011, A. N. Golubev et.al. [117] experimented with open open-aperture Zscan experiment to examine the nonlinear optical properties of silica glass with copper nanoparticles deposited by ion implantation. They reported that the

system exhibited reverse saturable absorption (RSA) at 450-540 nm and saturation absorption (SA) at 550-585nm. They suggested that the RSA is due to the two-photon absorption from the bound d states, and the SA is due to the saturation of plasma excitation. In 2015, Dehghani, Z. et al. [118] reported their third-order nonlinear optical studies of the matrix of porous polyurethane composite to which silica and alumina nanoparticles were infiltrated. Their experiment reported that the presence of nanoparticles in the polymer matrix increased the third-order nonlinear optical absorption. The same year saw another nonlinear optical research work by A Le Rouge et al [119]. They studied second-order nonlinear optical characteristics of porous silica matrix embedded with zirconia-coated gold nanoparticles. They reported that the system exhibited saturable absorption behavior. In the following year, 2016, Gharaati et al [120] reported a theoretical method to enhance third-order nonlinear optical properties of silica glass by using metallo nanoparticles. The Maxwell-Gernett theory was exploited for their study. They used silver, copper, and gold nanoparticles where they examined their different structures for the study, and the report suggested that the spherical structure of the nanoparticle can improve the nonlinear optical behavior of the silica matrix than other geometrical structures. In the year 2020, Sattar AL-Ibraheemi et al. [121] reported their investigation of nonlinear optical phenomena in gold-silica nanoparticle matrix prepared by the laser ablation method. They suggested that the nonlinear absorption value was improved while replacing water with polyvinyl pyrrolidone (PVP) as the surrounding liquid.

However, these previously reported research works conveyed the nonlinear optical phenomenon in silica/porous silica glass matrix,

incorporating the presence of another metal nanoparticle. The third-order nonlinear optical behavior of porous silica nanoparticles is less considered for research purposes. This may be due to their dielectric nature that hinders them from showing an impressive nonlinear behavior. Hence, it is relevant to investigate nonlinear optical phenomena in the surface-modified spherical silica nanoparticles.

1. Nonlinear absorption studies of DNA templated silica nanoparticles

DNA, the major component of the biotemplate CD complex, is a well-known nonlinear optical material [70-73, 78, 91, 96-99]. It is proven that nonlinear materials can influence nonlinear optical properties of another material when they functionalize each other [78, 94-99]. In order to understand whether any change has been formed in the nonlinear optical property of the silica particles, the open-aperture Z-scan experiment was conducted. The open-aperture Z-scan analysis was carried out under 100 μJ laser excitation (532 nm, nine ns pulse rate) with an on-axis intensity of 2.46 GW cm^{-2}. The transmitted beam was measured without an aperture in front of the detector to determine the nonlinear absorption of the molecules. The linear transmittance was set at 71%. Figure 5.7. a, c, e, g, and i show the open aperture Z-scan signatures of silica particles prepared at different concentrations of CD complex template in different methods. The silica particles were uniformly dispersed in DMSO for carrying out open-aperture Z-scan analysis. The interaction of the laser beam with the molecules produces a valley pattern, i.e., the transmittance of the molecules decreases gradually towards the focal point and reaches a minimum with the deep transmittance trough at the focus, where the curves are symmetric at Z=0, which signifies the RSA behavior of the molecules with the

positive NLA of the incident light. On the nanosecond time scale, the RSA is combined with TPA and ESA, which is collectively as the effective TPA process [97, 111-113]. The experimental data match well with the theoretical model for ESA ESA-assisted TPA process in all six samples of silica nanoparticles.

The numerically fitted OA Z-scan results brought to light the enhanced NLO responses of the mesoporous silica nanoparticles synthesized at different concentration of CD complex template in Stober process method and peptization method. The obtained β_{eff} were tabulated in the Table 5.2.

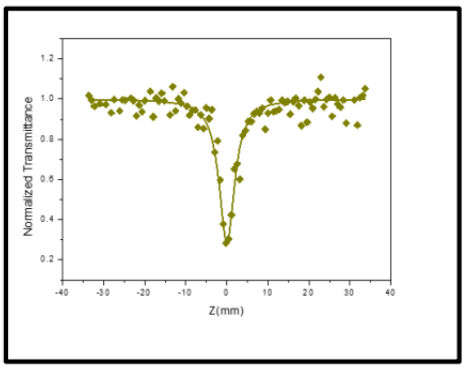

a

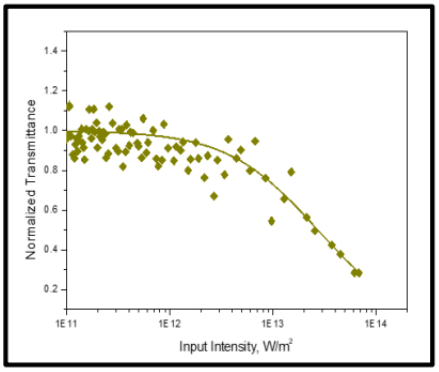

b

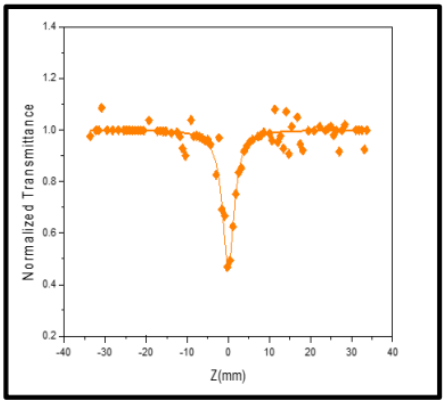

c

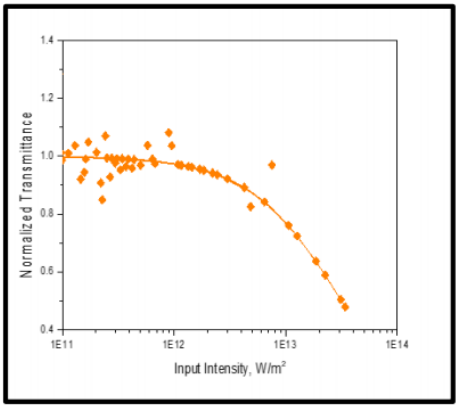

d

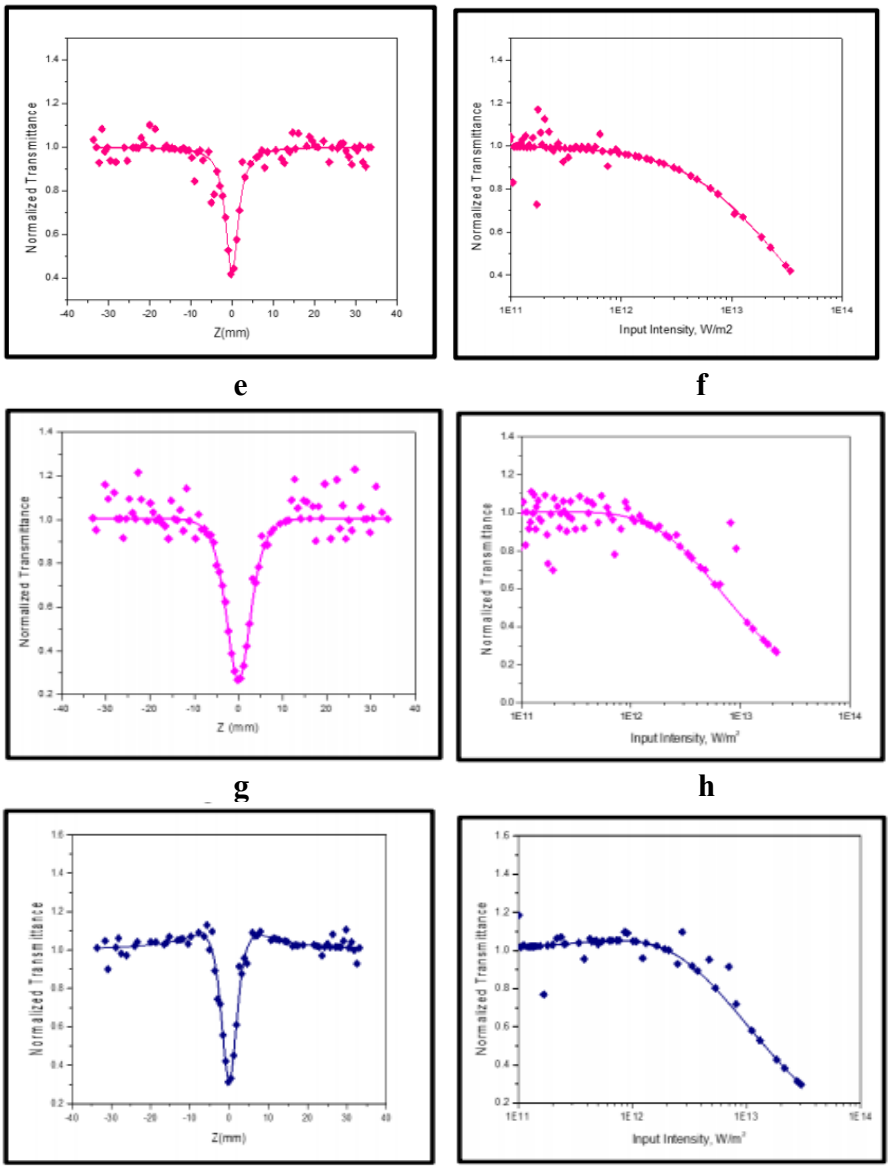

Figure. 5.9: Z Scan curves of silica particles synthesized at a) 0.05 wt%, and c) 0.15 wt%, e)0.1525 wt% of DNA in CD complex template, g) peptization method, and i) 0.1525 wt% of DNA in CD complex template peptization method along with OL characteristics of silica particles synthesized at b) 0.05 wt%, d) 0.15 wt%, f) 0.1525 wt% of DNA in CD complex template, h) peptization method, and j) 0.1525 wt% of DNA in CD complex template in peptization method

2. Nonlinear optical limiting studies

The optical limiting data of silica samples for different concentrations of DNA of CD complex template were extracted from the graphs of normalized transmittance obtained from open aperture Z–scan analysis against input fluence (Figure 5.9b, d, f, h, and j). From the graph, the onsets of limiting action (the value of input fluence at which the intensity of output transmittance starts decreasing) are observed at 3.29, 4.74, 5.23, 8.97, 1.46 and 2.16 W/m^2 for silica particles obtained corresponding to 0.05 wt %, 0.15 wt %, and 0.1525 wt % of DNA in CD complex template, peptization method and 0.1525 wt % of DNA in CD complex template in peptization method respectively and the limiting threshold (LT) values (the value of input fluence at which the intensity of output pulse becomes 50% of the initial value) for the corresponding samples are 2.43, 2.35, 2.21, 1.24, and 0.75 of the order of 10^{13} W/m^2 respectively. The values of the optical limiting threshold corresponding to each sample were tabulated in Table 5.2. From the results, it is evident that the particles in the present study exhibit exceptional optical limiting action with low onset and limiting threshold values. The open-aperture Z-scan report shows that the sample S5 shows a significant nonlinear absorption coefficient and has a low optical limiting threshold value. It is noticed that the enhancement of nonlinearity may be due to the influence of the CD complex template during the formation of silica particles. However, the materials in the present study have shown remarkable nonlinear response with a substantial increment in the β_{eff} of the order 10^{-10} m W^{-1} and exceptionally well optical limiting behaviour with very high

limiting threshold, making them capable materials for optical power limiting devices in photonics.

In principle, both the surface and optical properties of silica can be influenced under an optimum concentration of DNA in CD complex template.

Table 5.2 The nonlinear optical data of silica nanoparticles

Sample	**Nonlinear Absorption Coefficient, β x10^{-10} m/W**	**Onsets of limiting action 10^{12} W/m^2**	**Optical Limiting Threshold x 10^{13} W/m^2**
S1 (0.05 wt% of DNA)	0.45	1.35	2.43
S2 (0.15 wt % DNA)	0.49	1.05	2.35
S3(0.1525 wt % DNA)	0.58	0.88	2.21
S4 (Peptization method)	1.24	0.75	1.24
S5(0.1525 wt% DNA in peptization)	2	0.65	0.75

5.5 Synthesis of DNA capped polyoxometalate (silicotungstate ($\alpha[SiW_{12}O_{40}]^{-4}$)) and its nonlinear optical properties

The class of Polyoxometalates (POMs) is known for their unique and versatile features in material science that have been studied for several decades. Their intricate structure and tunable properties open diverse possibilities in various fields that making them applicable in a wide range of fields, including catalysis, material science, and medicine. POMs are generally anion metal clusters having a negative charge. They have a high valent metal atom often symbolically represented as M, which is from transition metals from the periodic table like Mo, W, or V. Their class widens from small oxometalates to bulk solid-state metal oxides. Their properties, such as acidity, redox activity, and photoactivity, make them an ideal candidate to exploit metal oxide features at the molecular level. While considering the metal-oxide cluster, the structure of POM is incorporated with another semiconducting metal, usually represented as hetero atom X, so-called Hetero POMs. Due to their structural vulnerability, as they possess hetero metal POMs, they are amenable to chemical tuning, as their structure and properties can be tailored by varying the hetero atom X (X=B, Si, P, etc.). Since the POMs are termed as anion metal clusters, the vital material properties can be tuned by varying the corresponding counter cation to make polar materials. Thus, POM has been a good candidate for the tunable nonlinear optical experiments since the beginning of the 21st century [122-126].

Numerous nonlinear optical studies were conducted on polyoxometalates based on their diversification of polarizability,

shape, composition, and size. In 2009, Jean-Dnaiel Compain et al. reported that they had synthesized nonlinear optically active salts with stibazolium derivatives and polyoxometalate counterions to explore the reactivity between the various POM and the centrosymmetric salt. The diffuse reflectance experiments illustrate that a charge transferring between organic and inorganic components in salts is seen, and they exhibit second-order nonlinear optical properties [127]. In 2012, Zhang T et. al. investigated redox and second-order nonlinear optical properties of POM, where they chose the hybrid structures that involve organic-inorganic (Keggin polyoxoanion) combinations to study. The effects of element substitution in POM (heteroatoms), charge transferring from organic groups to the Keggin polyanion, were evaluated. They observed that the hybrid compound possesses a large molecular second-order polarisability and is a potential NLO material [128]. In 2015, Zhang et al. reported their theoretical observations on second-order nonlinear optical properties of Strandberg-type polyoxometalates with alkali metal cations by density functional theory. They observed that the cations have an important impact on the second-order NLO polarizabilities [129]. In 2022, Wang L.S. et.al studied the third-order nonlinear optical and super broadband optical limiting properties of polyoxometalates by substituting addenda atoms. They chose polyoxomolybdovanadates, $[TBA]^3[VMo_5O_{19}]$ (V_1Mo_5), $[TBA]^4[V_8Mo_2O_{28}].2CH_3CN$($V_8Mo_2$), $[TBA]^3[VMo_5O_{19}]$ (V_1Mo_5), where TBA is called tetrabutylammonium. They reported that by substituting addenda atoms to the POM, the systems possess tunable third-order nonlinear optical properties [130]. In 2023, Saleem U et al remarked that their study on switchable third-order nonlinear optical response of hybrid structures of Anderson polyoxometalate with porphyrine incorporated with inpyridyl using Z-scan measurements

[131]. The effect of linker length and substituent on nonlinear optical responses has been studied. They concluded that alpha-Anderson POM-porphyrin hybrid structures have a lower bandgap, shorter length, and proximity than that of other polyoxometalate structures.

However, the existing research reports on POM highlight that they are one of the interested candidates among other nonlinear optical materials. For over one decade, their peculiar features have been observed meticulously through employing nonlinear optical studies. The reviews revealed that contributions over their different structures, compositions with hetero atoms and addenda atoms, and linkage with other organic polymers have been studied. This work is rationally concentrated on the formation of POM in the presence of a bio-template, which should be a nonlinear optical material. That is how DNA would come as a first choice, as it has already been proven that DNA can enhance the nonlinear optical properties of nanoparticles [96-97]. This work involved the method where the kegging structure of silicotungstate $[\alpha\text{-}SiW_{12}O_{40}]^{4-}$ POM would be obtained and observe how their nonlinear optical properties have been changed due to the involvement of biotemplate during their formation [80-99, 132-136].

5.5.1 Synthesis of DNA templated polyoxometalite (silicotungstate: $[\alpha\text{-}SiW_{12}O_{40}]$) compound

All chemicals used were purchased from Sigma-Aldrich. DNA sodium salt, extracted from salmon sperm, was used as the capping agent. Laboratory glassware was thoroughly cleaned using the piranha solution method and subsequently dried in a hot air oven at 100°C. Deionized (DI) water was used throughout for both cleaning and synthesis. To prepare the DNA solution, 0.1523 g of DNA was dissolved in

18.75 mL of DI water with continuous stirring. The solution was heated to boiling to ensure complete dissolution. Once the DNA was fully dissolved, 11.35 g of sodium tungstate was added under vigorous stirring. Subsequently, 10.3125 mL of 4 M hydrochloric acid was added dropwise to this mixture while maintaining vigorous stirring, assisted by an ultrasonic sonicator. In a separate preparation, 0.6875 g of sodium silicate was dissolved in 6.25 mL of DI water under constant stirring to obtain a clear, homogeneous solution. This sodium silicate solution was then combined with the previously prepared sodium tungstate–DNA mixture. Simultaneously, an additional 3.12 mL of 4 M hydrochloric acid was added dropwise under stirring. The resulting mixture was stirred continuously at 100 °C for 1 hour using a magnetic stirrer. Throughout the process, the pH of the solution was maintained between 5 and 6. Upon completion, a white precipitate of DNA-capped POM was formed [131-132].

5.5.2. Results and discussion

The obtained particles were subject to different characterizations to confirm the presence of POM. Additionally, the nonlinear optical studies of the particles were also conducted.

a. Material characterization of D-POM

The obtained POM particles were subjected to UV-Vis spectroscopy, SEM, and XRD characterization to observe their optical and geometrical properties. Figure 5.10 demonstrates the UV-Vis absorption property of the D-POM. Generally, the UV absorption peaks of silicotungstate fall in the range of 250-300nm. Figure 5.3a shows two peaks at 255nm and 295 nm, respectively. These peaks

correspond to the electronic transitions involving the tungsten centers and oxygen ligands. Along with this, in slicotungstates, the charge transfer also takes place between the tungsten centres within the structure. It also results in the UV-Visible region of the spectrum.

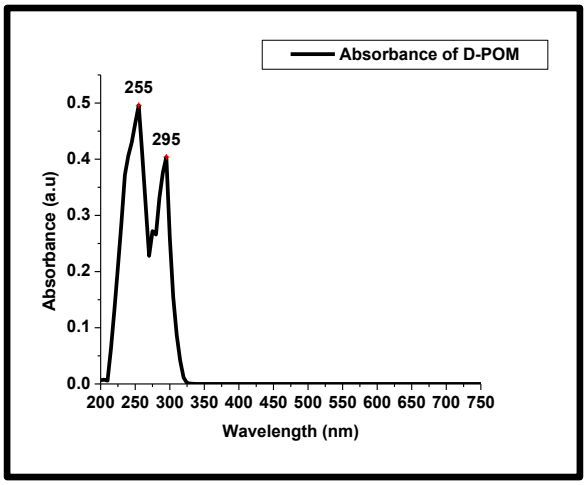

Figure. 5.10: UV-VIS absorption spectra of D-POM

In silicotungstate, energy transfer primarily occurs between the metal–oxide clusters, contributing to its UV-visible absorption characteristics. Additionally, the overall structure of the polyoxometalate, which includes a cluster of tungsten atoms surrounded by oxygen atoms and a silicon atom, can significantly impact the energy levels and transitions. The connectivity and the environment around the tungsten centres can influence the exact nature and energy of these transitions. The schematic representation of DNA-encapsulated POM is illustrated in Figure 5.10. Generally, POMs are negatively charged ligands. Hence, double helical DNA is also considered a negatively charged ligand. The deoxyphosphate group takes part in the contribution of negative charge to the DNA.

In the same way, the tungsten-oxygen framework is responsible for providing the negative charge to the POM. Hence, these two conditions may be involved in suitably locating the POM around the corners of the backbone of the double-stranded DNA. In this way, the DNA helps to reduce the interaction between the metal-oxygen clusters by keeping them apart. This way, POM can be subject to structural modification at will [130].

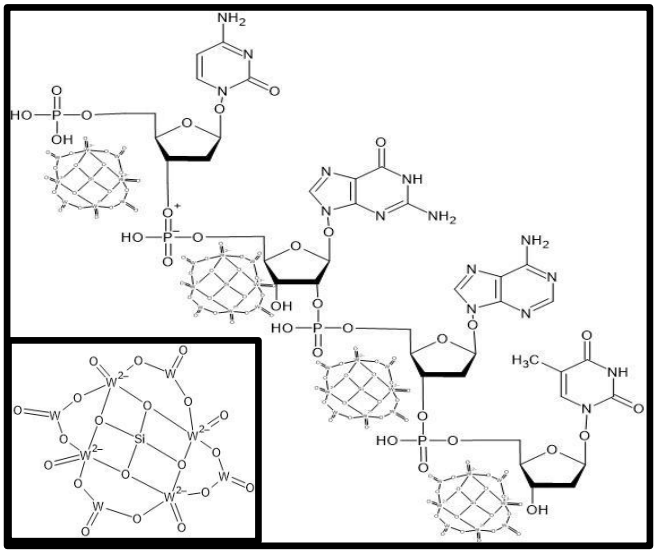

Figure 5.11: The schematic representation of DNA-encapsulated POM. The inset shows the molecular structure of POM.

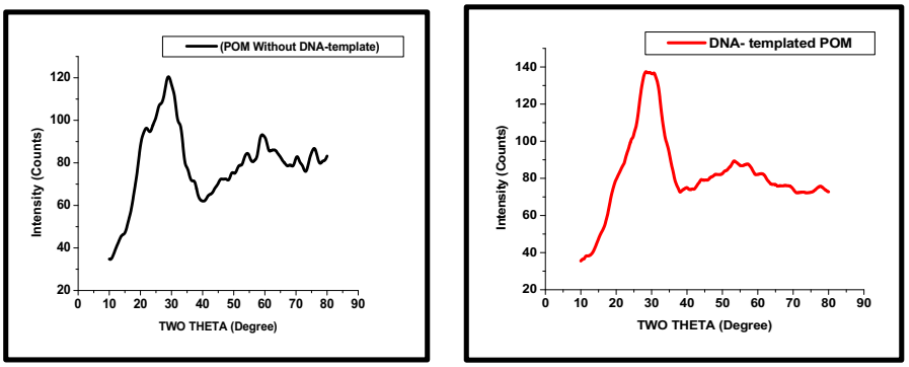

Figure 5.12: Powder XRD pattern of a) silicotungstate (POM) without DNA capping and b) silicotungstate (D-POM) prepared using DNA as a capping agent.

Figure 5.12. shows the powder XRD of the obtained POM. In the absence of the exact reported XRD profile of the proposed silicotungstate (POM), a comparison study between the XRD of the obtained POM samples and the literature records confirms the presence of silicotungstate. The XRD pattern of the POM varied on the basis of the type of metal-oxide group [132-134].

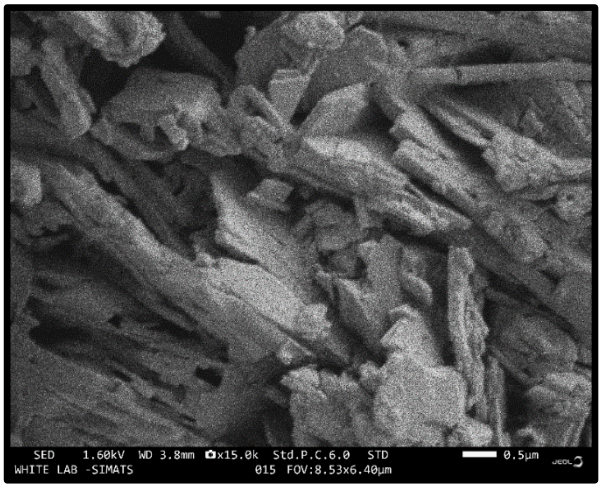

Figure 5.13: SEM image of DNA-capped POM

Figure 5.13 illustrates the SEM image of the DNA-capped POM. The picture resembles the shape of a POM, which comes in the silicotungstate category. Depending on the type of transition metal present in the POM, the geometrical shape of the particles varied. Although from the literature records, the structures seen in the SEM result are rectangular in dimension at the nanoscale range and provide a large surface area, which confirms that the obtained particles are POM. [132-134]. Hence, the characterization and the literature assure the presence of POM in the obtained sample.

b. Nonlinear optical properties of D-POM

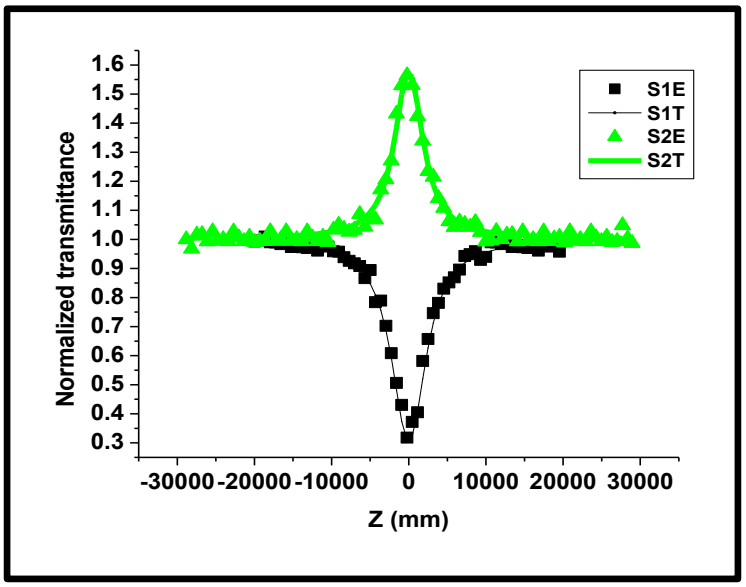

Figure 5.14: Open aperture Z-scan results of samples S1 (POM prepared without DNA template) and S2 (POM prepared with the presence of DNA), where E represents experimental results and T represents theoretical fitting, respectively.

The nonlinear optical properties of the POM family bagged the attention of functional material research a few years ago. The main

attractive factor that takes part in the nonlinear optical properties may be their large enclosed three-dimensional metal-oxygen framework. Their structure is mainly composed of transition metal atoms (V, Ta, Mo, and W) with oxygen atoms known as polymetal oxyanions. They can be seen in a number of structures, including Keggin, Anderson, lacunar, sandwich, and heteropolyacid structures. Basically, all these structures has one or more addenda atoms to which oxygen atoms are attached by making a covalent bond between the atoms. Many of them contain a central hetero atom (Ar, P, Si, and B) to which oxygen atoms are attached by sharing electrons with each other. Due to these abundant electron possession and high oxidation states of metal atoms, the metal-oxygen clusters experience negative charge and act as ligands. The factors which are crucial for making a material to be nonlinear optically active are electronic configuration, band gap, charge distribution (delocalized pi electrons), charge transfer transitions (where electrons move between different molecular sites), and symmetry. While considering the features of polyoxometalate, the metal-oxygen framework provides a vast opportunity for charge transfer transitions between the adjacent metal-metal centers within the same molecule, metal-metal centres between neighboring molecules, and metal-oxygen atoms. Hence, these may be the reason for showing nonlinear optical properties among the polyoxometalate family.

When looking at silicotungstate particles, it is crucial to observe how the above-mentioned factors will affect on nonlinear optical properties of both silicotungstate prepared in the absence of DNA template and D-POM. The nonlinear optical properties of the Figure display the

open aperture Z-scan results, where the data S1 indicates the Z-scan result of POM (silicotungstate) prepared without the presence of DNA template the results show that the sample S1 shows significant nonlinear optical absorption. The nonlinear optical property of a material is highly influenced by several factors, such that the presence of pi electrons, as they have a delocalized nature, so that they can easily get polarized under an external electric field. Compounds with rich pi electrons are more likely to exhibit more potent nonlinear optical properties. Thus, silicotungstates are compounds rich with metal atoms (addenda atoms) which are at their highest oxidation state. They form a bond with oxygen atoms by sharing electrons via a covalent bond.

Meanwhile, the hetero atoms (silicon atoms) also pair with oxygen atoms through a covalent bond. The d- d-electrons and pi- pi-electrons in the metal atoms mainly contribute to the delocalization of electrons. Hence, the charge transferring occurs between the adjacent metal atoms within the compound, and also between adjacent metal centres. Figure 5.14. displays the Z-scan results of samples S1 and S2where S1 has a nonlinear optical absorption coefficient; the result supports the structural and composition advantages of silicotungstate.

In order to consider the nonlinear optical properties of the sample S2, made by using the DNA template, several factors should be considered. One of the influencing factors is the structural modification of the silicotugnstate acquired by the presence of the DNA template during its synthesis. Despite the advantage in the structure of silicotungstate, the presence of DNA may cause an alteration among

the metal-oxygen clusters due to the dynamic, lengthy polymer chain and negative polarity of the DNA. Hence, the metal-oxygen clusters in the silicotungstate may get separated significantly. It may create a chance of hindering the delocalization of charge transferring between the metal clusters. The nonlinear optical property mainly depends on the delocalization of charge (delocalization of pi electrons). Hence, the assumption is evident in the Z-scan result of sample S2 (D-POM). Figure 5.14. shows nonlinear optical saturation behaviour of the sample S2. Thus, the Z-scan result supports the structural modifications acquired by the silicotungstate particles during their biotemplate-based synthesis.

In general, polyoxometalates (POMs) can exist in their nanoparticle form. These are anionic clusters composed of transition metal oxides, and they can be synthesized to form nanoparticles through various methods, such as sol-gel processes, hydrothermal synthesis, or self-assembly techniques. When POMs are formed into nanoparticles, they can exhibit unique properties, such as enhanced catalytic activity, increased surface area, and improved solubility in different media. These nanoparticles can be utilized in various applications, including catalysis, drug delivery, and as sensors. The ability to manipulate their size and morphology allows for tailoring their properties for specific uses.

Moreover, the Z-scan results highlight the tuning feature of silicotungstate under DNA template-based synthesis. Hence, the Z-scan results suggest that the D-POM can be helpful in switching applications in photonic devices. Under suitable conditions, DNA

templated silicotungstate can be applicable in tunable nonlinear optical purposes. The surface properties of the POM can be moulded as it can exist in either nanoparticle powder form or in aqueous solution. Therefore, they can be made into thin films. Hence, their nonlinear optical properties can be incorporated into the realm of photonic crystals.

5.6 Conclusions

Mesoporous silica nanoparticles were synthesized using the Stober process and the peptization method, in which surface-modified DNA with CTAB was used as the capping agent. The characterization results show that the CD complex provides twin benefits of both DNA and CTAB during the synthesis procedure. The CD complex acted as a stabilizer that enhanced the morphological and the non-linear optical properties of the obtained silica nanoparticles without altering the spherical geometry of the silica nanoparticles. The XRD and UV results confirmed the formation of silica nanoparticles. XRD analysis revealed that the FWHM was higher for silica nanoparticles synthesized in the presence of the CD complex, indicating a smaller crystallite size. UV-Vis spectroscopy further confirmed that DNA concentration influences the size and porosity of the silica particles. The effect of DNA on particle size was evident, as increasing the DNA concentration resulted in a blue shift in the absorption peak, suggesting a reduction in particle size. This indicates that the presence of DNA during the synthesis process significantly influences the morphology of the silica particles. Additionally, BET surface area analysis, along with BJH pore size distribution, was employed to study the surface

properties and porosity of the obtained silica nanoparticles. BET results show that on increasing the CD complex concentration, the pore diameter was found to decrease within the mesoporous range. The silica nanoparticles obtained from the CD complex template have a remarkable hysteresis loop. This property of theirs helped to stick the adsorbent tightly to the adsorbate. The SEM characterization revealed that the surface modification occurred in the silica nanoparticles formed in the presence of the CD complex template. In addition to this, the SEM results showed that the presence of the CD complex did not alter the specificity of the Stober process. Z-scan techniques also performed non-linear optical characterization. This shows that the novel silica nanoparticles show a significant improvement in non-linear optical absorption property, and their nonlinear absorption coefficient is found to increase as on increasing the concentration of CD complex template and the optical limiting threshold value of the CD complex templated silica nanoparticles was also reduced on increasing the concentration of DNA increases.

All the characterization results pointed out that the CD complex works effectively as a stabilizing agent by being encompassed with the conventional Stober process for synthesizing mesoporous nano-sized non-linear optical silica nanoparticles. This method can be performed both in acidic (peptization method (HCL)) and basic medium (Stober process in which ammonia is used as the catalyst). Hence, the CD complex incorporating the Stober process is a novel, non-toxic, and cost-effective method for synthesizing surface-modified, tunable, structured, biocompatible, and enhanced nonlinear optical silica

nanoparticles. These features of the silica nanoparticles make them to be used for drug delivery, catalysts, surface-modified thin films using doped surfaces, lasing, bio-sensing, gas sensing, bio-imaging, and semiconducting-photonic devices.

The nanoparticles of silicotungstate were prepared by using the DNA template synthesis method. The obtained particles show deviations in the nonlinear optical absorption properties. The sample, which was prepared by the conventional way, shows high nonlinear optical absorption property, while the particles made by the DNA template method exhibit high nonlinear saturation of absorption. From the observations, it is considered that the structural deviation occurred due to the presence of the DNA template is responsible for the drastic change in the nonlinear optical saturation of absorption. Hence, from the experimental results, it is confirmed that DNA is a perfect template to modify the structural-nonlinear optical properties of polyoxometalate (silicotungstate). Therefore, the obtained tunable nonlinear optical DPOM particles can be suitably applied for optical switching applications in photonic devices.

References

[1] Rane, A. V., Kanny, K., Abitha, V. K., & Thomas, S. (2018). Methods for synthesis of nanoparticles and fabrication of nanocomposites. In Synthesis of inorganic nanomaterials (pp. 121-139). Woodhead publishing.

[2] Ealia, S. A. M., & Saravanakumar, M. P. (2017, November). A review on the classification, characterisation, synthesis of nanoparticles and their application. In IOP conference series: materials science and engineering (Vol. 263, No. 3, p. 032019). IOP Publishing.

[3] Mekuye, B., & Abera, B. (2023). Nanomaterials: An overview of synthesis, classification, characterization, and applications. Nano select, 4(8), 486-501.

[4] Stöber, W., Fink, A., & Bohn, E. (1968). Controlled growth of monodisperse silica spheres in the micron size range. Journal of colloid and interface science, 26(1), 62-69.

[5] Niculescu, V. C. (2020). Mesoporous silica nanoparticles for bio-applications. Frontiers in Materials, 7, 36.

[3] Niculescu, V. C. (2020). Mesoporous silica nanoparticles for bio-applications. Frontiers in Materials, 7, 36.

[4] Niculescu, V. C. (2020). Mesoporous silica nanoparticles for bio-applications. Frontiers in Materials, 7, 36.

[5] Iturrioz-Rodríguez, N., Correa-Duarte, M. A., & Fanarraga, M. L. (2019). Controlled drug delivery systems for cancer based on mesoporous silica nanoparticles. International journal of nanomedicine, 3389-3401.

[6] Iturrioz-Rodríguez, N., Correa-Duarte, M. A., & Fanarraga, M. L. (2019). Controlled drug delivery systems for cancer based on mesoporous silica nanoparticles. International journal of nanomedicine, 3389-3401.

[7] Kuang, Y., Zhai, J., Xiao, Q., Zhao, S., & Li, C. (2021). Polysaccharide/mesoporous silica nanoparticle-based drug delivery systems: A review. International journal of biological macromolecules, 193, 457-473.

[8] Wang, Y., Zhao, Q., Han, N., Bai, L., Li, J., Liu, J., ... & Wang, S. (2015). Mesoporous silica nanoparticles in drug delivery and biomedical applications. Nanomedicine: Nanotechnology, Biology and Medicine, 11(2), 313-327.

[9] Wang, Y., Zhao, Q., Han, N., Bai, L., Li, J., Liu, J., ... & Wang, S. (2015). Mesoporous silica nanoparticles in drug delivery and biomedical applications. Nanomedicine: Nanotechnology, Biology and Medicine, 11(2), 313-327.

[10] Siddiqui, B., Haq, I. U., Al-Dossary, A. A., Elaissari, A., & Ahmed, N. (2022). Exploiting recent trends for the synthesis and surface functionalization of mesoporous silica nanoparticles towards biomedical applications. International journal of pharmaceutics: X, 4, 100116.

[11] Xiao, D., Jia, H. Z., Zhang, J., Liu, C. W., Zhuo, R. X., & Zhang, X. Z. (2014). A dual-responsive mesoporous silica nanoparticle for tumor-triggered targeting drug delivery. Small, 10(3), 591-598.

[12] Vallet-Regí, M., Colilla, M., Izquierdo-Barba, I., & Manzano, M. (2017). Mesoporous silica nanoparticles for drug delivery: Current insights. Molecules, 23(1), 47.

[13] Mamaeva, V., Sahlgren, C., & Lindén, M. (2013). Mesoporous silica nanoparticles in medicine—Recent advances. Advanced drug delivery reviews, 65(5), 689-702.

[14] Knežević, N. Ž., & Durand, J. O. (2015). Targeted treatment of cancer with nanotherapeutics based on mesoporous silica nanoparticles. ChemPlusChem, 80(1), 26-36.

[15] Taleghani, A. S., Nakhjiri, A. T., Khakzad, M. J., Rezayat, S. M., Ebrahimnejad, P., Heydarinasab, A., ... & Marjani, A. (2021). Mesoporous silica nanoparticles as a versatile nanocarrier for cancer treatment: A review. Journal of Molecular Liquids, 328, 115417.

[16] Taleghani, A. S., Nakhjiri, A. T., Khakzad, M. J., Rezayat, S. M., Ebrahimnejad, P., Heydarinasab, A., ... & Marjani, A. (2021). Mesoporous silica nanoparticles as a versatile nanocarrier for cancer treatment: A review. Journal of Molecular Liquids, 328, 115417.

[17] Castillo, R. R., Lozano, D., González, B., Manzano, M., Izquierdo-Barba, I., & Vallet-Regí, M. (2019). Advances in mesoporous silica

nanoparticles for targeted stimuli-responsive drug delivery: an update. Expert opinion on drug delivery, 16(4), 415-439.

[18] Lohiya, G., & Katti, D. S. (2022). Carboxylated chitosan-mediated improved efficacy of mesoporous silica nanoparticle-based targeted drug delivery system for breast cancer therapy. Carbohydrate Polymers, 277, 118822.

[19] Li, Z., Zhang, Y., & Feng, N. (2019). Mesoporous silica nanoparticles: synthesis, classification, drug loading, pharmacokinetics, biocompatibility, and application in drug delivery. Expert opinion on drug delivery, 16(3), 219-237.

[20] Natarajan, S. K., & Selvaraj, S. (2014). Mesoporous silica nanoparticles: importance of surface modifications and its role in drug delivery. RSC advances, 4(28), 14328-14334.

[21] Farjadian, F., Roointan, A., Mohammadi-Samani, S., & Hosseini, M. (2019). Mesoporous silica nanoparticles: synthesis, pharmaceutical applications, biodistribution, and biosafety assessment. Chemical Engineering Journal, 359, 684-705.

[22] Z. Li, J. C. Barnes, A. Bosoy, J. F. Stoddart, J. I. Zink, Mesoporous silica nanoparticles in biomedical applications, Chem Soc Rev. 2012;41(7):2590-605.

[23] S. Wuttke, M. Lismont, A. Escudero, B. Rungtaweevoranit, W. J. Parak. Positioning metal-organic framework nanoparticles within the context of drug delivery–a comparison with mesoporous silica nanoparticles and dendrimers, Biomaterials. 123(2017)172-83.

[24] M. T. Anderson, J. E. Martin, J. G. Odinek, P. Newcomer, Synthesis of Periodic Mesoporous Silica Thin Films. MRS Proceedings, 431(1996), https://doi.org/:10.1557/proc-431-217

[25] https://kindle-tech.com

[26] Z. Li, Y. Zhang, N. Feng, Mesoporous silica nanoparticles: synthesis, classification, drug loading, pharmacokinetics, biocompatibility, and application in drug delivery. Expert Opin. Drug Deliv., 2019, https://doi.org/:10.1080/17425247.2019.1575

[27] S. Nasreen, U. Rafique, S. Ehrman, M. A Ashraf – Ekoloji, Synthesis and Characterization of Mesoporous Silica Nanoparticles for Environmental Remediation of Metals, PAHs and Phenols,

Foundation Environmental Protection and Research, Ekoloji 27(106): 1625-1637 (2018)

[28] D. Das, Y. Yang, J. S. O. Brien, D. Breznan, S. Nimesh, S. Bernatchez, M. Hill, A. Sayari, R. Vincent, P. Kumarathasan, Synthesis and Physicochemical Characterization of Mesoporous SiO2 Nanoparticles, J. Nanomater. (2014), http://doi.org/:10.1155/2014/176015

[29] L. Usgodaarachchi, C. Thambiliyagodage, R. Wijesekera, M. G. Bakker, Synthesis of mesoporous silica nanoparticles derived from rice husk and surface-controlled amine functionalization for efficient adsorption of methylene blue from aqueous solution. Current Research in Green and Sustainable Chemistry, 4(2021)100116, https://doi.org/:10.1016/j.crgsc.2021.100116.

[30] D. F. Mohamad, N. S. Osman, M. K. H. M. Nazri, A. A. Mazlan, M. F. Hanafi, Y. A. M. Esa M. I. I. M. Rafi, M. N. Zailani, N. N. Rahman, A. H. Abd Rahman, N. Sapawe, Synthesis of Mesoporous Silica Nanoparticle from Banana Peel Ash for Removal of Phenol and Methyl Orange in Aqueous Solution, Mater. Today: Proc., 19(2019)1119–1125, https://doi.org/:10.1016/j.matpr.2019.11.004

[31] M. Ghaferi, M. K. M. Esfahani, A. Raza, S. Al Harthi, H. E. Shahmabadi, S. E. Alavi (2020). Mesoporous silica nanoparticles: synthesis methods and their therapeutic use-recent advances, J. Drug Target, (2020)1–67, https://doi.org/:10.1080/1061186x.2020.1812614.

[32] M. Khoeini, A. Najafi, H. Rastegar, M. Amani, M Improvement of hollow mesoporous silica nanoparticles synthesis by hard-templating method via CTAB surfactant. Ceram. Int., 45(2019)12820-12824, https://doi.org/:10.1016/j.ceramint.2019.03

[33] H. Zhou, J. Sun, B. Ren, F. Wang, X. Wu, S. Bai, S. (2014). Effects of alkaline media on the controlled large mesopore size distribution of bimodal porous silicas via sol-gel methods. Powder Technol., 259(2014)46–51. https://doi.org/:10.1016/j.powtec.2014.03.06.

[34] V. N. Reena, H. Misha, G. S. Bhagyasree, B. Nithyaja, Enhanced photoluminescence and color tuning from Rhodamine 6G-doped sol–gel glass matrix via DNA templated CdS nanoparticles, AIP Adv., 12(2022)105217, https://doi.org/10.1063/5.0123529.

[35] G. Correa Carvalho, G. D. Marena, J. C. F. Karnopp, J. Jorge, R. Miguel Sábio, M. A. U. Martines, T. M. Bauab, M. Chorilli, Cetyltrimethylammonium bromide in the synthesis of mesoporous silica nanoparticles: General aspects and in vitro toxicity, Adv. Colloid Interface Sci., 307(2022)102746, https://doi.org/10.1016/j.cis.2022.102746.

[36] Z. A. Qiao, L. Zhang, M. Guo, Y. Liu, Q. Huo, Synthesis of Mesoporous Silica Nanoparticles via Controlled Hydrolysis and Condensation of Silicon Alkoxide, Chem. Mater., 21(2009)3823–3829. https://doi.org/:10.1021/cm901335k.

[37] A. Lodha, M. Lodha, A. Patel, J. Chaudhuri, J. Dalal, M. Edwards, D. Douroumis, Synthesis of mesoporous silica nanoparticles and drug loading of poorly water soluble drug cyclosporin A, J. Pharm. Bioallied Sci., 4(2012)92. https://doi.org/:10.4103/0975- 7406.94153.

[38] N. I. Vazquez, Z. Gonzalez, B. Ferrari, Y. Castro, Synthesis of mesoporous silica nanoparticles by sol–gel as nanocontainer for future drug delivery applications, Bol. Soc. Esp. Ceram. Vidr., 56(2017)139–145, https://doi.org/:10.1016/j.bsecv .2017.03.002.

[39] A. Presentato, F. Armetta, A. Spinella, D. F. C. Martino, R. Alduina, M. L. Saladino, Formulation of Mesoporous Silica Nanoparticles for Controlled Release of Antimicrobials for Stone Preventive Conservation, Front. Chem., 8(2020)699. https://doi.org/:10.3389 /fchem.2020.00699

[40] R. K. Satvekar, M. R. Phadatare, V. A. Karande, R. N. Patil, B. M. Tiwale, S. H. Pawar, Influence of silane content on the optical properties of sol-gel derived spin-coated silica thin films, Int. j. basic appl. sci., 1(2012)468-476. https://doi.org/10.14419/ ijbas.v1i4.292

[41] J. Kobler, Thin films from porous nanoparticles (Doctoral dissertation, LMU). 2008

[42] A. Escobar, L. Yate, M. Grzelczak, H. Amenitsch, S. E. Moya, A. V. Bordoni, P. C. Angelomé, One-Step Synthesis of Mesoporous Silica Thin Films Containing Available COOH Groups, ACS Omega, 2(2017)4548–4555. https://doi.org/:10.1021/acsomega .7b00560

[43] J. Adira Jaafar, N. K. H. N. Kamarudin, N. D. H. Setiabudi, S. N. Timmiati, T. L. Peng Mesoporous Silica Nanoparticles and Waste Derived-Siliceous Materials for Doxorubicin Adsorption and Release, Mater. Today: Proc., 19(2019) 1420–1425. https://doi.org/:10.1016/j.matpr.2019.11.163.

[44] J. Verma, A. Bhattacharya, Analysis on synthesis of silica nanoparticles and its effect on growth of T. Harzianum & Rhizoctonia species, Biomed. j. sci. Technol. res., 10(2018), 7890-7897. https://doi.org/: 10.26717/BJSTR.2018.10.001972.

[45] S. Chandra, G. Beaune, N. Shirahata, F. M. Winnik, A one-pot synthesis of water soluble highly fluorescent silica nanoparticles, J Mater Chem B., 5(2017), 1363– 1370, https://doi.org/:10.1039/c6tb02813f.

[46] A. Mehdi, S. Dourdain, J. F. Bardeau, C. Reyé, R. J. Corriu, A. Gibaud, A., First direct synthesis of highly ordered bifunctionalized mesoporous silica thin films, J. Nanosci. Nanotechnol., 6(2006)377-381. https://doi.org/::10.1166/jnn.2006.913.

[47] V. Selvarajan, S. Obuobi, P. L. R. Ee, Silica Nanoparticles- A Versatile Tool for the Treatment of Bacterial Infections, Front. Chem., 8(2020)602. https://doi.org/:10.3389/fchem.2020.00602.

[48] A. M. Ali, A. A. Ismail, R. Najmy, A. Al-Hajry, Preparation and characterization of ZnO– SiO2 thin films as highly efficient photocatalyst, *J. Photochem. Photobiol*. A, 275(2014)37-46. https://doi.org/:10.1016/j.jphotochem.2013.11.002.

[49] X. Li, O. Niitsoo, A. Couzis, Electrostatically driven adsorption of silica nanoparticles on functionalized surfaces, J. Colloid Interface Sci, 394(2013)26–35. https://doi.org/:10.1016/j.jcis.2012.11.042.

[50] S. H. Wu, C. Y. Mou, H. P. Lin, Synthesis of mesoporous silica nanoparticles, Chem. Soc. Rev. 42(2013)3862-3875. https://doi.org/:10.1039/c3cs35405a.

[51] X. D. Wang, Z. X. Shen, T. Sang, X. B. Cheng, M. F. Li, L. Y. Chen, Z. S. Wang, Preparation of spherical silica particles by Stober process with high concentration of tetra-ethyl- orthosilicate, J. Colloid Interface Sci, 341(2010)23-29. https://doi.org/:10.1016 /j.jcis.2009.09.01

[52] S. García-Revilla, J. Fernández, M. A. Illarramendi, B. García-Ramiro, R. Balda, H. Cui, D. Levy, Ultrafast random laser emission in a dye-doped silica gel powder, Opt. Express, 16(2008) 12251- 12263. https://doi.org/:10.1364/oe.16.012251

[53] Y. Shin, D. Lee, K. Lee, K. H. Ahn, B. Kim, Surface properties of silica nanoparticles modified with polymers for polymer nanocomposite applications, J. Ind. Eng. Chem., 14(2008)515–519. https://doi.org/:10.1016/j.jiec.2008.02.002

[54] X. Li, O. Niitsoo, A. Couzis, Electrostatically driven adsorption of silica nanoparticles on functionalized surfaces, J. Colloid Interface Sci, 394(2013)26–35. https://doi.org/:10.1016/j.jcis.2012.11.042

[55] L. Zych, A. M. Osyczka, A. Łacz, A. Różycka, W. Niemiec, A. Rapacz-Kmita, E. Stodolak- Zych, How surface properties of silica nanoparticles influence structural, microstructural and biological properties of polymer nanocomposites. Materials, 14(2021)843. https://doi.org/:10.3390/ma14040843.

[56] I. Ojea-Jiménez, P. Urbán, F. Barahona, M. Pedroni, R. Capomaccio, G. Ceccone, D. Gilliland, Highly flexible platform for tuning surface properties of silica nanoparticles and monitoring their biological interaction, ACS Appl. Mater. Interfaces, 8(2016)4838–4850. https://doi.org/:10.1021/acsami.5b11216.

[57] S. Gupta, P. Kumar, Drug Delivery Using nanocarriers: indian perspective, Proc Natl Acad. Sci. India Sect. B. Biol. Sci ., 82(2012)167–206. https://doi.org/:10.1007/s40011-012- 0080/7

[58] M. Qasim, J. Ananthaiah, S. Dhara, P. Paik, D. Das, Synthesis and characterization of ultra- fine colloidal silica nanoparticles, Adv Sci Eng Med.., 2014, 6(9), 965-973.

[59] H. Guleryuz, I. Kaus, C. Filiàtre, T. Grande, M. A. Einarsrud, Deposition of silica thin films formed by sol–gel method. Journal of Sol-Gel Science and Technology, 54(2010)249–257. https://doi.org/:10.1007/s10971-010-2190-0.

[60] I. A. Rahman, V. Padavettan, Synthesis of silica nanoparticles by sol-gel: size-dependent properties, surface modification, and applications in silica-polymer nanocomposites review. J. Nanomater., 2012(2012)8-8. https://doi.org/:10.1155/2012/132424.

[61] D. Djouadi, A. Chelouche, A. Aksas, M. Sebais, Optical properties of ZnO/silica nanocomposites prepared by sol-gel method and deposited by dip-coating technique. Phys. Procedia, 2(2009)701–705. https://doi.org/:10.1016/j.phpro.2009.11.01.

[62] A. Mukherjee, T. Darlington, R. Baldwin, C. Holz, S. Olson, P. Kulkarni, S. E. Lupold, Development and screening of a series of antibody-conjugated and silica-coated iron oxidenanoparticles for targeting the prostate-specific membrane antigen, Chem. Med. Chem., 9(2014)1356–1360. https://doi.org/:10.1002/cmdc.201300549

[63] B. Díaz de Greñu, R. de los Reyes, A. M. Costero, P. Amorós, J. V. Ros-Lis, Recent progress of microwave-assisted synthesis of silica materials, Nanomaterials, 10(2020)1092. https://doi.org/:10.3390/nano10061092.

[64] C. O. Metin, J. R. Baran, Q. P. Nguyen, Adsorption of surface functionalized silica nanoparticles onto mineral surfaces and decane/water interface. J. Nanopart. Res., 14(2012) https://doi.org/:10.1007/s11051-012-1246-1.

[65] L. Zych, A. M. Osyczka, A. M., Łacz, A., Różycka, A., Niemiec, W., Rapacz-Kmita, A.E. Stodolak-Zych, How Surface Properties of Silica Nanoparticles Influence Structural, Microstructural and Biological Properties of Polymer Nanocomposites. Materials, 14(2021)843. https://doi.org/:10.3390/ma14040843.

[66] A. M. Ali, A. A. Ismail, R. Najmy, A. Al-Hajry, Preparation and characterization of ZnO–SiO2 thin films as highly efficient photocatalyst. J. Photochem. Photobiol. A., 275(2014)37-46. https://doi.org/:10.1016/j.jphotochem.2013.11.002

[67] Y. Gao, D. Gao, J. Shen, Q. Wang, A review of mesoporous silica nanoparticle delivery systems in chemo-based combination cancer therapies, Front. Chem., 8(2020)598722.https://doi.org/:10.3389/fchem.2020.598722

[68] S. Kwon, R. K. Singh, R. A. Perez, E. A. A. Neel, H. W. Kim, W. Chrzanowski, Silica-based mesoporous nanoparticles for controlled drug delivery. J. Tissue Eng., 4(2013) 204173141350335. https://doi.org/:10.1177/2041731413503357.

[69] M. Waseem, S. Mustafa, A. Naeem, K. H. Shah, I. Shah, Ihsan-ul-Haque, Synthesis and Characterization of silica by sol-gel method, J. Pak. Mater. Soc. 3(2009)19-21

[70] B. Shi, Y. K. Shin, A. A. Hassanali, S. J. Singer, DNA binding to the silica surface. J. Phys. Chem. B, 119(2015)11030-11040. https://doi.org/10.1021/acs.jpcb.5b01983.

[71] S. R. Dugasani, B. Gnapareddy, M. R. Kesama, S. Jeon, J. H. Jeong, S. H. Park, Optoelectronic properties of DNA thin films implanted with titania nanoparticle-coated multiwalled carbon nanotubes, AIP Adv., 9(2019)015011 https://doi.org/:10.1063/1.5063446.

[72] M. Samoc, A. Samoc, J. G. Grote, Complex nonlinear refractive index of DNA, Chem. Phys. Lett., 431 (2006)132–134. https://doi.org/:10.1016/j.cplett.2006.09.0.

[73] M. R. Kesama, S. R. Dugasani, Y. J. Cha, J. Son, B. Gnappareddy, S. Yoo, S. H. Park, Optoelectrical and mechanical properties of multiwall carbon nanotube-integrated DNA thin films. Nanotechnology, 30(2019)245704. https://doi.org/:10.1088/1361-6528/ab0b0f.

[74] Laud, B. B. (1986). Lasers and nonlinear optics.

[75] Antoine, R., & Bonačić-Koutecký, V. (2017). Liganded silver and gold quantum clusters. Towards a new class of nonlinear optical nanomaterials. Springer.

[76] Sheik-Bahae, M., Said, A. A., Wei, T. H., Hagan, D. J., & Van Stryland, E. W. (2002). Sensitive measurement of optical nonlinearities using a single beam. IEEE journal of quantum electronics, 26(4), 760-769.

[76] Hora, H. (1986). YR Shen, The Principles of Nonlinear Optics, John Wiley & Sons, New York, 1984, 576 pages. Laser and Particle Beams, 4(2), 318-319.

[77] Van Stryland, E. W., & Sheik-Bahae, M. (2018). Z-scan. In Characterization techniques and tabulations for organic nonlinear optical materials (pp. 671-708). Routledge.

[78] B. Nithyaja, H. Misha, V. P. N. Nampoori, Synthesis of silver nanoparticles in DNA template and its influence on nonlinear optical

properties, J. Nanosci. Nanotechnol., p-ISSN:22163-257X e-ISSN: 2163 2588, (2012); 2(4): 99-103, doi: 10.5923/j.nn.20120204.02.

[79] Sandeep, S. (2012). Investigations of nonlinear optical effects and ultrafast laser Induced plasma in nanostructured media (Doctoral dissertation).

[80] Durairaj, M., & TC, S. G. (2023). Nanobelt and nanoplatelet structured molybdenum disulfide thin film as a saturable absorber under nanopulsed green laser excitation. Journal of Solid State Chemistry, 320, 123865.

[81] Pratkasem, V. (2005). 330nm UV Generation from combined cavity's DVD laser diode and nonlinear crystal (Doctoral dissertation, The Kochi University of Technology).

[82] Shettigar, S., Chandrasekharan, K., Umesh, G., Sarojini, B. K., & Narayana, B. (2006). Studies on nonlinear optical parameters of bis-chalcone derivatives doped polymer. Polymer, 47(10), 3565-3567.

[83] Hutchings, D. C., Sheik-Bahae, M., Hagan, D. J., & Van Stryland, E. W. (1992). Kramers-Krönig relations in nonlinear optics. Optical and Quantum Electronics, 24(1), 1-30.

[84] Shettigar, S., Umesh, G., Chandrasekharan, K., & Kalluraya, B. (2007). Third order nonlinear optical properties and two photon absorption in newly synthesized phenyl sydnone doped polymer. Synthetic metals, 157(2-3), 142-146.

[85] Udayakumar, D., Kiran, A. J., Adhikari, A. V., Chandrasekharan, K., Umesh, G., & Shashikala, H. D. (2006). Third-order nonlinear optical studies of newly synthesized polyoxadiazoles containing 3, 4-dialkoxythiophenes. Chemical physics, 331(1), 125-130.

[86] Eshun, A. (2021). Investigations of Organic Molecules Using Entangled Photons as a Novel Spectroscopic Tool (Doctoral dissertation).

[86] V. Arasu, S. R. Dugasani, J. Son, B. Gnapareddy, S. Jeon, J. H. Jeong, S. Ha Park, Thickness, morphology, and optoelectronic characteristics of pristine and surfactant- modified DNA thin films. J. Phys. D, 50(2017)415602. https://doi.org/:10.1088/1361- 6463/aa8795.

[82] K. Liu, L. Zheng, C. Ma, R. Göstl, A. Herrmann, A. (2017). DNA–surfactant complexes: self- assembly properties and

applications, Chem. Soc. Rev., 46(2017)5147–5172. https://doi.org/:10.1039/c7cs00165g.

[83] A. Cuervo, P. D. Dans, J. L. Carrascosa, M. Orozco, G. Gomila, L. Fumagalli, Direct measurement of the dielectric polarization properties of DNA, Proc. Natl. Acad. Sci., 111(2014)E3624–E3630. https://doi.org/:10.1073/pnas.1405702111.

[84] D.M. Joyce, The development of DNA – based bio- polymer hybrid thin films for capacitor applications, The School of Engineering of the University of Dayton, 2013.

[85] B. Singh, N. S. Sariciftci, J. G. Grote, F. K. Hopkins, Bio-organic-semiconductor-field-effect-transistor based on deoxyribonucleic acid gate dielectric, J. Appl. Phys., 100(2006)024514, https://doi.org/:10.1063/1.2220488.

[86] S. Husaini, R. G. Bedford, E. M. Heckman, A. C. Lesko, Nonlinear optical properties of a graphene-based DNA composite, CLEO, (2014)1-2. https://doi.org/:10.1364/cleo_si.2014.sm3h.

[87] A. Tane, F. Kajzar, R. Zgarian, I. Rau, D. Grabarek, P. Karpinski, A. Miniewicz, Refractive index and surface relief grating formation in DNA based dye-doped films, Macromol. Res.,21(2013)331–337. https://doi.org/:10.1007/s13233-013-1131-5.

[88] M. Yoshikawa, M. Maruhashi, Y. Iwamoto, N. Ogata, Optical resolution of racemic amino acids through DNA-Poly(4-vinylbenzyl)trimethylammonium Polyion Complex Membranes, Polym. J., 39(2007)193–1198. https://doi.org/:10.1295/polymj.pj2007080.

[89] O. Ikkala, Functional materials based on self-assembly of polymeric supramolecules, Sci., 295(2002)2407–2409. https://doi.org/:10.1126/science.1067794.

[90] E. Alizadeh, L. Sanche, Role of humidity and oxygen level on damage to DNA induced by soft X-rays and low-energy electrons, J. Phys. Chem. C., 117(2013)22445–22453. https://doi.org/:10.1021/jp403350j.

[91] H. You, H. Spaeth, V. N. L. Linhard, A. J. Steckl, Role of surfactants in the interaction of dye molecules in natural DNA polymers, Langmuir, 25(2009)11698–11702. https://doi.org/:10.1021/la901646d.

[92] L. Wang, J. Yoshida, N. Ogata, S. Sasaki, T. Kajiyama, Self-Assembled Supramolecular Films Derived from Marine Deoxyribonucleic Acid (DNA)−Cationic Surfactant Complexes: Large-Scale Preparation and Optical and Thermal Properties, Chem. Mater., 13(4) (2001)1273–1281. https://doi.org/:10.1021/cm000869g.

[93] A.J. Steckl, H. Spaeth, H. You, E. Gomez, J. Grote, DNA as an optical material, OPN Optics and Photonics News, University of Cincinnati, 35(2011).

[94] C. Cheng, S. Y. Ran, Interaction between DNA and Trimethyl-Ammonium Bromides with Different Alkyl Chain Lengths, Sci. World J.,2014(2014)1–9. https://doi.org/:10.1155/2014/863049.

[95] T. B. Singh, N. S. Sariciftci, J. G. Grote, Bio-Organic Optoelectronic Devices Using DNA, Adv Polym Sci .,223(2010)73–112. https://doi.org/:10.1007/12_2009_6.

[96] C. Yang, D. Moses, A. J. Heeger, Base-Pair Stacking in Oriented Films of DNA– Surfactant Complex, Adv. Mater., 15(2003)1364–1367. https://doi.org/:10.1002/adma.200305171.

[97] J. S. Hwang, S. W. Hwang, D. Ahn, Formation of electrical interconnects by self-trapping of deoxyribonucleic acid molecules, Jpn. J. Appl. Phys., 43(2004), 3803–3805. https://doi.org/:10.1143/jjap.43.3803.

[98] Y. W. Kwon, C. H. Lee, D. H. Choi, J.-I. Jin, 2008, Materials science of DNA, J. Mater. Chem., 19(2009)1353-1380. https://doi.org/: 10.1039/b808030e.

[99] N. Slesiona, S. Thamm, H. Lisa K. S. Stolle, V. Weißenborn, P. Müller, A. Csáki, W. Fritzsche, DNA-Biofunctionalization of CTAC-capped gold nanocubes, Nanomaterials10(2020)1119. https://doi.org/:10.3390/nano10061119.

[100] Z. Yu, W. Li, J. A. Hagen, Y. Zhou, D. Klotzkin, J. G. Grote, A. J. Steckl, Photoluminescence and lasing from deoxyribonucleic acid (DNA) thin films doped with sulforhodamine, Appl. Opt., 46(2007)1507. https://doi.org/:10.1364/ao.46.001507.

[101] Travers, A., & Muskhelishvili, G. (2015). DNA structure and function. The FEBS journal, 282(12), 2279-2295.

[102] Dickerson, R. E., & Ng, H. L. (2001). DNA structure from A to B. Proceedings of the National Academy of Sciences, 98(13), 6986-6988.

[103] Schenk, J. J., Becklund, L. E., Carey, S. J., & Fabre, P. P. (2023). What is the "modified" CTAB protocol? Characterizing modifications to the CTAB DNA extraction protocol. Applications in Plant Sciences, 11(3), e11517.

[104] Li, Y., Liu, T., Li, T., & Peng, X. (2015). Hydrothermal fabrication of controlled morphologies of MoO3 with CTAB: Structure and growth. Materials Letters, 140, 48-50.

[105] Llombart, P., Palafox, M. A., MacDowell, L. G., & Noya, E. G. (2019). Structural transitions and bilayer formation of CTAB aggregates. Colloids and Surfaces A: Physicochemical and Engineering Aspects, 580, 123730.

[101] S. R. Dugasani, B. Gnapareddy, M. R. Kesama, S. Jeon, J. H. Jeong, S. H. Park, Optoelectronic properties of DNA thin films implanted with titania nanoparticle- coated multiwalled carbon nanotubes, AIP Adv., 9, 1(2019)015011 https://doi.org/:10.1063/1.5063446.

[102] N. Balan, M. Hari, V. P. N. Nampoori, Selective mode excitation in dye-doped DNA polyvinyl alcohol thin film, Appl. Opt., 48(2009) 3521-3525. https://doi.org/:10.1364/ao.48.003521

[103] B. Nithyaja, H. Misha, V. P. N. Nampoori, Fluorescence enhancement of silver nanoparticles using DNA as a stabilizing agent, Proc. of SPIE,8173 (2011)383-388.

[104] B. Nithyaja, H. Misha, V. P. N. Nampoori, Synthesis of silver nanoparticles in DNA template and its influence on nonlinear optical properties, Nanosci. Nanotechnol., 2(2012)99- 103, https://doi.org/: 10.5923/j.nn.20120204.02.

[105] N. A. F. Aboul-Maaty, H. A. S. Oraby, Extraction of high-quality genomic DNA from different plant orders applying a modified CTAB-based method, Bull Natl Res Cent., 43(2019)1-10. https://doi.org/:10.1186/s42269-019-0066-1.

[106] Clarke, J. D. (2009). Cetyltrimethyl ammonium bromide (CTAB) DNA miniprep for plant DNA isolation. Cold Spring Harbor Protocols, 2009(3), pdb-prot5177.

[107] Liberman, A., Mendez, N., Trogler, W. C., & Kummel, A. C. (2014). Synthesis and surface functionalization of silica nanoparticles for nanomedicine. Surface science reports, 69(2-3), 132-158.

[108] Verma, J., & Bhattacharya, A. (2018). Analysis on synthesis of silica nanoparticles and its effect on growth of T. Harzianum & Rhizoctonia species. Biomedical Journal of Scientific & Technical Research, 10(4), 7890-7897.

[109] Lee, Y. K., Yoon, Y. R., & Rhee, H. K. (2000). Preparation of colloidal silica using peptization method. Colloids and surfaces A: Physicochemical and engineering aspects, 173(1-3), 109-116.

[110] Darabi, H., Adelifard, M., & Rajabi, Y. (2019). Characterization of nonlinear optical refractive index for graphene oxide–silicon oxide nanohybrid composite. Journal of Nonlinear Optical Physics & Materials, 28(01), 1950005.

[111] Joni, I. M., Nulhakim, L., Vanitha, M., & Panatarani, C. (2018, August). Characteristics of crystalline silica (SiO2) particles prepared by a simple solution method using sodium silicate (Na2SiO3) precursor. In Journal of Physics: Conference Series (Vol. 1080, p. 012006). IOP Publishing.

[112] Bokuniaeva, A. O., & Vorokh, A. S. (2019, December). Estimation of particle size using the Debye equation and the Scherrer formula for polyphasic TiO2 powder. In journal of physics: Conference series (Vol. 1410, No. 1, p. 012057). IOP Publishing.

[113] Monshi, A., Foroughi, M. R., & Monshi, M. R. (2012). Modified Scherrer equation to estimate more accurately nano-crystallite size using XRD. World journal of nano science and engineering, 2(3), 154-160.

[114] Hossain, M. S., Mahmud, M., Mobarak, M. B., Sultana, S., Shaikh, M. A. A., & Ahmed, S. (2022). New analytical models for precise calculation of crystallite size: application to synthetic hydroxyapatite and natural eggshell crystalline materials. Chemical Papers, 76(11), 7245-7251.

[115] Rabiei, M., Palevicius, A., Monshi, A., Nasiri, S., Vilkauskas, A., & Janusas, G. (2020). Comparing methods for calculating nano crystal size of natural hydroxyapatite using X-ray diffraction. Nanomaterials, 10(9), 1627.

[116] R. Matshitse, Brunauer-Emmett-Teller (BET) surface area analysis, Rhodes Univ. Natl. Res. Found, 384(2010).

[117] Golubev, A. N., Nikitin, S. I., Smirnov, M. A., & Stepanov, A. L. (2011, October). Spectral dependence of nonlinear optical absorption of silica glass with copper nanoparticles. In Journal of Physics: Conference Series (Vol. 324, No. 1, p. 012038). IOP Publishing.

[118] Dehghani, Z., Nadafan, M., Malekfar, R., & Ara, M. M. (2017). Measurement of third-order nonlinear optical susceptibility of polyurethane-containing silica nanocomposites by Z-scan method. Inorganic and Nano-Metal Chemistry, 47(9), 1342-1347.

[119] Le Rouge, A., El Hamzaoui, H., Capoen, B., Bernard, R., Cristini-Robbe, O., Martinelli, G., ... & Bigot, L. (2015). Synthesis and nonlinear optical properties of zirconia-protected gold nanoparticles embedded in sol–gel derived silica glass. Materials Research Express, 2(5), 055009.

[120] Gharaati, A., & Kamaldar, A. (2016). Enhancement of nonlinear optical properties of compounds of silica glass and metallic nanoparticle. Pramana, 86(6), 1329-1342.

[121] Sattar, A. I., Al-Ibraheemi, F. A., & Gatea, M. A. (2019, August). Nonlinear Optical Properties of Gold-silica Nanoparticles. In 2019 2nd International Conference on Engineering Technology and its Applications (IICETA) (pp. 25-30). IEEE.

[122] Xu, L., Tong, Q., & Hu, B. (2024). Silicotungstate@ ZIF-67 as an effective catalyst for an extraction and oxidative desulfurization system. RSC advances, 14(49), 36622-36632.

[123] Sarr, B., Mbaye, A., Diop, C. A., Sidibe, M., Melin, F., Hellwig, P., ... & Dessapt, R. (2021). Two new inorganic–organic hybrid materials based on β-and γ-octamolybdate clusters: Synthesis, structure determination, and solid-state photochromic properties. Polyhedron, 194, 114919.

[124] Patel, A., & Sadasivan, R. (2021). Modified Mn substituted POMs: Synthetic strategies, structural diversity to applications. Progress in Materials Science, 118, 100759.

[125] Khan, M. I., & Swenson, L. S. (2013). Open-framework hybrid materials and composites from polyoxometalates. New and Future

Developments in Catalysis: Hybrid Materials, Composites, and Organocatalysts, 27-54.

[126] B. R. Hood, Y. de Coene, C. F. Jones, I. Lopez Poves, N. Deveaux, N. R. Halcovitch, and J. Fielden, "Synthesis and Optical and Nonlinear Optical Properties of Linear and Two-Dimensional Charge Transfer Chromophores Based on Polyoxometalates", Inorg. Chem. 63(51), 24250-24261(2024).

[127] Compain, J. D., Mialane, P., Dolbecq, A., Marrot, J., Proust, A., Nakatani, K., ... & Sécheresse, F. (2009). Second-order nonlinear optical properties of polyoxometalate salts of a chiral stilbazolium derivative. Inorganic chemistry, 48(13), 6222-6228.

[128] T. Zhang, L. Yan, S. Wen, S. Cong, J. Wang, and Z. Su, "A DFT study on the second-order nonlinear optical properties of the plenary mixed-metal polyoxometalate", Mol. Simul., 38(6), 518-524(2012).

[128] T. Zhang, W. Guan, S. Wen, T. Ma, L. Yan, and Z. Su, "Theoretical exploration to the cation effect on the second-order nonlinear optical properties of Strandberg-type polyoxometalates", JTCC, 14(01), 1550007 (2015).

[128] L. S. Wang, Y.Wang, C.L. Lv, C. Guo, F. Y. Xing, Y. J. Dong, and Y. G.Wei, "Polyoxometalates with tunable third-order nonlinear optical and superbroadband optical limiting properties", Inorg. Chem. Front., 9(17), 4413-4424(2022).

[129] U. Saleem, M. Tariq, F. K. Shehzad, K. Ahmad, J. Khan, H.M. Asif, and Z. M. El-Bahy, "Investigations of switchable non-linear optical response inpyridyl containing porphyrin@ Anderson polyoxometalate hybrid by Z-scan measurements", Inorg. Chem. Commun., 156, 111270 (2023).

[130] Uji, S., Nakamura, K., & Kobayashi, N. (2024). The effect of a polymer capping agent on electrodeposited silver nanoparticles in a silver deposition-based electrochromic device. Physical Chemistry Chemical Physics, 26(23), 16466-16476.

[131] A. Lesbani, R. D. Tarmizi, T. Taher, N. R. Palapa, and R. Mohadi, "Preparation of Ni-Al LDH: Influence of intercalated polyoxometalate anion (α-SiW12O40)4- on the interlayer gallery distance", The 2nd international conference on science, Mathematics, environment, and education., AIP Conf. Proc., 2194, 020054 (2019), https://doi.org/10.1063/1.5139786

[132] M. Ammam, "Polyoxometalates: formation, structures, principal properties, main deposition methods and application in sensing", J. Mater. Chem. A, 1(21), 6291(2013). doi:10.1039/c3ta01663c

[133] D.C. Batalha, S. O. Ferreira, R. C. Silva, and M. J. Silva, "Cesium-Exchanged Lacunar Keggin Heteropolyacid Salts: Efficient Solid Catalysts for the Green Oxidation of Terpenic Alcohols with Hydrogen Peroxide", ChemistrySelect, 5(6), 1976–1986 (2020). doi:10.1002/slct.201903437

[134] T. Takashima, R. Nakamura, K. Hashimoto, "Visible Light Sensitive Metal Oxide Nanocluster Photocatalysts: Photo-Induced Charge Transfer from Ce(III) to Keggin-Type Polyoxotungstates." J. Phys. Chem. C, 113, 17247–17253(2009)

[135] L. Yang, J. Lei, J. Fan, R. Yuan, M. Zheng, J. Chen, and Q. Dong, "The intrinsic charge carrier behaviors and applications of polyoxometalate clusters based materials", Adv. Mater., 2005019(2021), DOI: 10.1002/adma.202005019

[136] García-Ramírez, E. V., Almaguer-Valenzuela, S., Sánchez-Dena, O., Baldovino-Pantaleón, O., & Reyes-Esqueda, J. A. (2016). Third-order nonlinear optical properties of colloidal Au nanorods systems: saturable and reverse-saturable absorption. Optics Express, 24(2), A154-A167.

[137] Neupane, T., Yu, S., Rice, Q., Tabibi, B., & Seo, F. J. (2019). Third-order optical nonlinearity of tungsten disulfide atomic layer with resonant excitation. Optical materials, 96, 109271.

Chapter 6

Tunable nonlinear optical responses in 1D ternary asymmetric Silica/DNA/ZnO photonic crystal with defect DNA capped POM for photonic applications

This chapter is an insight of nonlinear optical studies of a 1D ternary photonic crystal (PC) system. The discussion of this chapter includes theoretical analysis of electromagnetic waves through a 1D ternary PC system and its experimental realization, characterization and nonlinear optical studies. The experimentally fabricated 1D ternary PC consists of Silica, cetyltrimethylammonium bromide-deoxyribonucleic acid complex film, and zinc oxide. The defective PC is obtained by incorporating DNA-capped polyoxometalate (silicotungstate) (D-POM) thin film. The proposed PC system has been fabricated using the dip coating method. The linear optical properties are studied using the transfer matrix method and COMSOL software. A reflectometer experimentally observes the optical transfer properties. The open Z-scan aperture experiment has been conducted to observe nonlinear optical behavior. As on increasing the number of periods increases, the nonlinear absorption has been found to decrease. Simultaneously, the system shows an increase in saturable absorption at low threshold energy. The defective PC shows a drastic rise in saturable absorption. Hence, based on the nonlinear studies, the system can be applicable for tuning nonlinear optical properties. For a small number of periods, the PC provided high reverse saturable absorption (RSA) at a low threshold limiting value. The PC begins to behave as a saturable absorber as the number of unit cells increases. For this reason, 1D ternary silica/DNA/ZnO PC system, incorporated with D-POM embedded defective PC system, can be tuned for photonic device applications.

The results of this chapter are published as

GS, B., B, N., VN, R., A, D., & Sabari Girisun, T. C. (2025). Tunable nonlinear optical responses in defective DNA-capped polyoxometalate ([α-SiW12O40] 4-) one-dimensional silica/ DNA/ZnO ternary photonic crystal systems. *Applied Optics*, *64*(9), 2125-2138.

6.1 Introduction

The diverse applications of photonic crystals determine the nature of defects introduced during their design. Generally, a defect can be introduced by a significantly different material from that of the elemental materials [1-14]. While considering a defect, the properties such as optical nonlinearity, thickness and dielectric constant, and conductivity will be taken into account in the formation of the resonance mode in the PBG range [15-23]. In 2024, Y. Liu et al. suggested a polyvinylidene fluoride/graphene oxide layer embedded 1D nonlinear PC. The paper discussed the propagation and localization of light through the nonlinear PC [15]. They reported that PVDF/GO embedded NLO PC can enhance the localization capability of the electric field of light. In 2009, S. Kim et al. proposed theoretical observations on 1D nonlinear PC for efficient second harmonic generation [16]. They proposed a four-layer elemental structure for designing PC. Doubly resonant second harmonic generation with high conversion efficiency is achieved by choosing the geometrical parameters of the elementary cell optimally and controlling the band structure.

In the light of these observations, the optical nonlinear properties of PCs remain a prominent area of interest for potential applications in lasing devices. In this study, third-order optical nonlinearity in 1D ternary PCs has been explored through both theoretical and experimental approaches. The elemental unit of the PC is made of three distinctive materials, namely, silica, deoxyribonucleic acid (DNA)- CTAB complex, and ZnO. The supremacy of 1D ternary PC

among other classes of PC is that they show high transparency in the visible range, along with multiple PBGs in the UV region and near-IR region of light. That increases their demand for optical limiting devices, as they meet the criteria for lasing application, such that the materials have to transmit the waves that come in the visible range of frequencies. Hence, 1D ternary PC can be put in a dominion role in lasing devices. The other crucial side of the objective of the work is that the materials chosen for the proposed ternary PC have met the criteria for achieving the goals of the work.

The upper surface layer at which the light will interact is fabricated from silica, which has low electrical conductivity and significant internal and external resistance. Besides, it can be applied to thin films under low temperature treatment [24-25]. The silica can be molded to obtain tailored properties such as surface and nonlinear optical properties by using appropriate surface capping materials. The surface-modified silica exhibits improved film quality, so that it can be subject to low low-temperature film treatment process. Over and above, it exhibits improved nonlinear optical properties [26]

The middle layer of the unit cell is designed with DNA-CTAB complex, a biopolymer that exhibits vivid properties, exhibiting a high dielectric constant among other organic polymers. Moreover, it can act as an insulator in the visible range of light and exhibits optical nonlinear behavior with laser light as well [27-36]. The third layer, ZnO, is a metal oxide, highly transparent in visible light, and exhibits good dielectric properties [37-39]. The refractive index contrast

between the adjacent layers is found to be very small, but it would be favorable for achieving the criteria for lasing application.

The defective 1D ternary PC is achieved by embedding DNA-templated silicotungstate (POM), which belongs to the polyoxometalate (POM) group. Generally, they possess a negative charge as they are metal-oxygen anion clusters in form. They are rich in transition metal atoms, which possess a high oxidation state that can make them provide large active sites to be exposed with other functional materials. POMs are formed in two general types, Keggin structure and Dawson structure. In Keggin structure, it contains one hetero atom, 12 metal atoms, which are surrounded by four oxygen atoms to form a tetrahedron, and each metal atom is linked to six oxygen atoms to form an octahedron. The assembly of three octahedra yields a trimetallic group M_3O_{13}. The trimetallic groups are connected to others, and a common site of M_3O_{13} is linked to the central heteroatom. Though they are categorized as ligands, due to the presence of hetero atom like Si, they have a semiconductor-like electronic structure which contains an electron-occupied valence band (VB) and an unoccupied conduction band. Hence, the band structure can be adjusted by changing the heteroatoms (Si) or adjusting the valence states of metal atoms in order to make them suitable for required uses such as semi-conducting devices and photocatalytic activities. Generally, POMs are prepared by the condensation process at optimum pH and temperature. As they are flexible to change their physico-chemical properties by undergoing preparation with suitable organic or inorganic capping materials, they can be functionalized to

achieve a desired active POM structure. The self-assembly properties of the DNA double helix can be exploited to make a variety of structures. It has played a crucial role in achieving tailored geometrical and optical properties of nanoparticles [40-49].

Additionally, DNA is regarded as another organic ligand; therefore, this can have an impact on POM particle formation widely. The versatile inorganic class materials exhibit better film properties and can be made into a stable film at low temperature film treatment. Thereby, POM is chosen as the defective layer for the proposed system [26, 35,50].

General features of the PCs are mainly utilized for integrated photonic devices, optical lasing devices, biosensing, and environmental monitoring. Among these, the nonlinear optical features have been found to play a vital role, so that the availability and performance of material at the nonlinear optical regime is still a pragmatic issue. Hence, the proposed system is subjected to a linear optical characterization using TMM and COMSOL software theoretically and experimentally as well. The nonlinear optical behavior of these 1D nonlinear ternary Silica/DNA/ZnO PC system along with defective 1D ternary PCs incorporated with DNA-templated silicotungstate, has been studied by the open Z Scan method apart from their linear optical characterization.

6.2 Theoretical approach for the linear optical property of 1D ternary photonic crystal

So far, the nonlinear optical property of PC has been treated as an interesting matter in photonics research. Though it has been two decades since the theory and structure of PC were invented, its vivid properties are still treated as a pivotal focus for the applications of photonic devices. The linear optical transfer properties of the proposed system have been carried out using the theoretical method TMM. The behavior of the systems has been shown in Figure. 6.1. A comparative study on the optical transfer properties of both systems, such as standard ternary PC and defective ternary PC, with respect to their corresponding binary PC systems has been approached. All the systems have been studied under same number of periods. The central wavelength is fixed on λ=532 nm, around which no transmission of photons takes place; moreover, the PBG is designed at that particular wavelength. The Bragg reflection condition determines the thickness of the elementary layers. The optical thickness for the constructive interference of a multilayer thin film stack is

$$m\lambda = 2\sum n_i d_i \qquad 6.1$$

Where $n_i d_i$ is the optical thickness. For a system having three layers, equation 6.6 becomes,

$$m\lambda = 2(n_1 d_1 + n_2 d_2 + n_3 d_3) \qquad 6.2$$

where n_1, n_2, and n_3 are the refractive indices of the three distinct dielectric layers and d_1, d_2, and d_3 are their thicknesses, respectively.

When $n_1d_1 = n_2d_2 = n_3d_3$, 6.3

$M\lambda = 6n_1d_1$ 6.4

$$t = \frac{\lambda}{6n} \quad 6.5$$

Where λ, is the central wavelength about which PBG is designed to occupy, and n and t are the refractive index and thickness of the respective elementary layer. From the theoretical design, we have optimized the thickness of the layers for the binary PC system to be 89.26 nm and 66.5 nm, corresponding to the layers of silica and ZnO, respectively. The designed thicknesses of the elemental layers of the ternary PC are 59.50 nm, 59.10 nm, and 44.33 nm against silica, DNA, and ZnO, respectively.

The linear optical behavior of the two systems, ternary PC and bilayer PC, shows remarkable observations. The properties to be concerned about are PBG formation, the oscillation density, photon density, the defect mode peak formation, and the photon density at the defect mode. Figure 6.1a represents the linear optical transfer properties of the bilayer PC of the Silica/ZnO system. The transfer properties of the bilayer PC describe that the system has a photonic band gap around 532 nm, having a width of 525 nm-630 nm of light. Figure 6.1b represents the linear transfer properties of the defective bilayer PC system. The thickness of the defective layer is designed to be 100 nm. When the defect is introduced to the system, the transmission property shows significant variation in transmission modes and PBG. The differences are found in the oscillation density and band positions.

From Figure 6.1a, the oscillation density is found to be very intense around photonic band edges. While considering the defective system shown in Figure 6. 1b, the photon density is reduced around the band edges. Furthermore, the PBG shows a slight shift from the central wavelength. On that account, the defect mode peak is located at 536 nm of light with a percentage of photon density is 85.69.

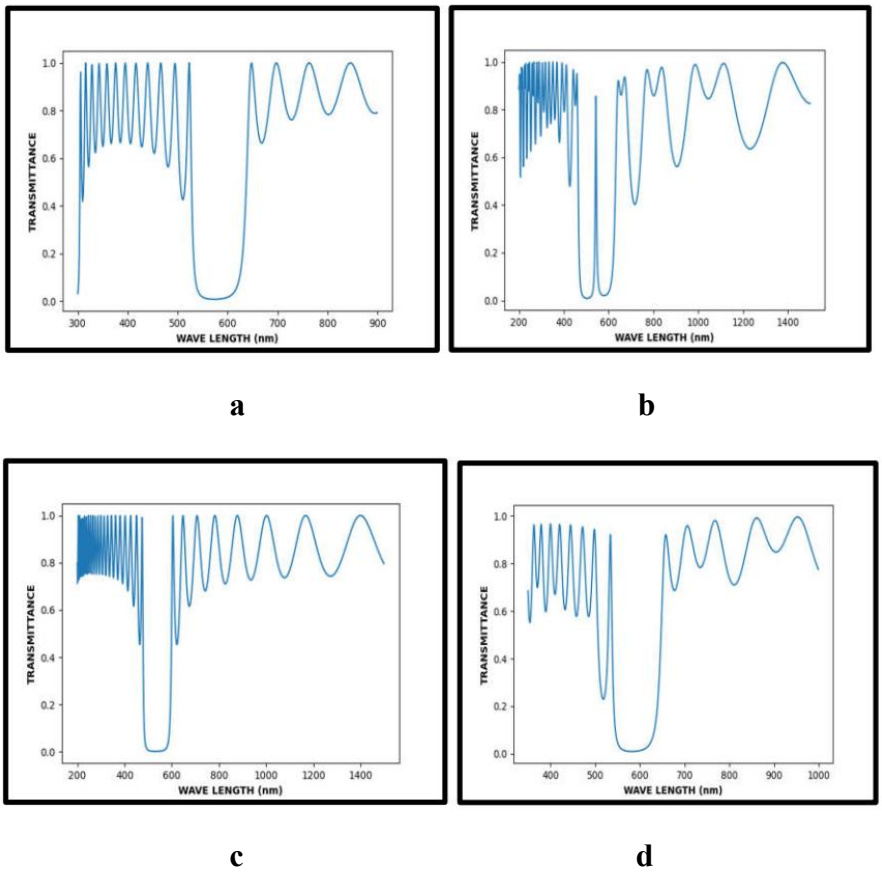

Figure 6.1: The optical transfer properties of a) 1D binary Silica/ZnO PC where N=13, b)1D defective binary Silica/ZnO PC where N=13, c) 1D ternary Silica/DNA/ZnO PC where N=13, and d) 1D defective Silica/DNA/ZnO PC where N=13.

Figure 6. 1c shows the transfer properties of the ternary PC, where the oscillation density of the photon about photonic band edges is comparatively lesser than that of the binary PC system. The PBG is formed between the light wavelengths that range from 520nm- 610nm. The defective layer thickness is optimized as 110 nm. The transfer properties are illustrated in Figure 6.1d. A significant change is seen in the defective transfer properties of the system as compared with the standard ternary PC system. The transmission mode bandwidth is reduced, and the PBG is shifted along the higher frequency region. The defect mode peak is seen at 535 nm. The density of defect mode is 94.59 % which is a relatively larger value than the value obtained in the defective binary PC.

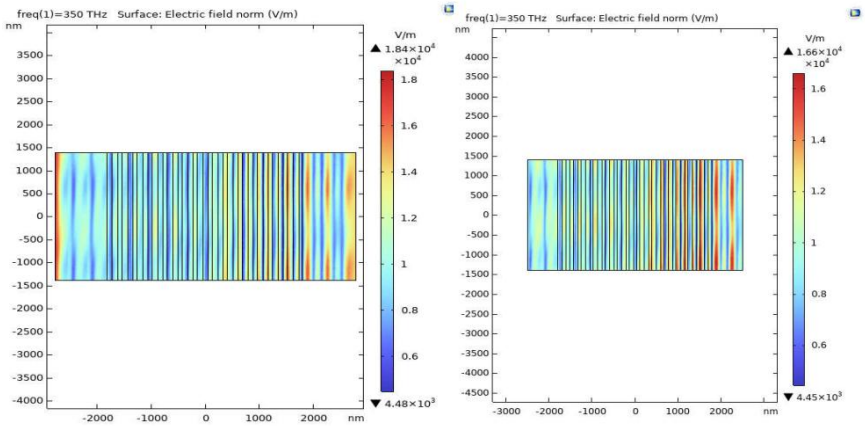

a **b**

Figure 6.2: Electric field distribution in a) 1D ternary Silica/DNA/ZnO PC system for N=13 and b) POM embedded defective 1D ternary Silica/DNA/ZnO system for N=13

Figure 6.2 interprets the electric field distribution of a 1D ternary Silica/DNA/ZnO system using COMSOL 6.1 version software, and the

results elaborated on how the electric field intensity changes as it passes away from the source. Figure 6.2a represents the electric field distribution along the 1D ternary Silica/CD/ZnO PC system for N=13. The field strength is concentrated chiefly as the waves propagate away from the source. The intensity strength scales fall around 1.3- 1.4 $x10^4$ V/m range. On the other hand, the electric field distribution of the defective POM embedded Silica/DNA/ZnO PC for N=13 is shown in Figure 6.2b. The electric field intensity around the defective layer domain is found to increase. The field strength as the waves propagate away from the source is found to increase than the standard Silica/DNA/ZnO PC system with having same period. The field strength of the defective PC is obtained as 1.4-1.6 $x10^4$ V/m.

6.3 Experimental procedure

The experimental section of this work involved two parts. The first part is the synthesis of DNA- capped silicotungstate. The synthesis of the preparation DNA-capped silicotungstate was briefly mentioned in Chapter 5. The second part involved the fabrication of 1D ternary PC of composition of silica, DNA and ZnO and its defective structure incorporating with DNA-capped silicotungstate.

6.3.1 Fabrication of 1D ternary Silica/DNA/ ZnO photonic crystal system

The fabrication of 1D ternary PC is executed by the dip coating method. The schematic representation of experimental setup is provided in chapter 4. All the solutions were taken in equal quantities to ensure an even height for the films. The optimization of the

thickness of the films is established by strictly controlling the dip coating parameters such as dipping height, dipping duration, dipping speed, film heating duration, film heating temperature, and concentration of the solution samples. **Table 6.1** illustrates the dipping parameters for each elemental layer.

Table 6.1: Dipping parameters of the elemental layers

Sl No.	Sample	Dipping height (cm)	Dipping duration (s)	Dipping speed (m/s)	Heating temperature (°C)	Heating duration	Solvent
1.	Silica	100	3s	7000	100	30 min	DMSO
2.	CD Complex	100	3s	7000	100	20 min	Methanol
3.	ZnO	100	3s	7000	100	1.5 hour	Methanol
4.	POM	100	30	7000	80	1.5 houtr	Water

The solvents for silica, CD complex, ZnO, and POM were DMSO, methanol, and water respectively. The amounts to make solutions for CD complex, silica, and POM are 1g, 0.5 g, and 0.5g, respectively. The ultra-cleaned glass substrate is used for depositing the multilayer stack system. The defect layer is placed at the 7^{th} position of the total 13 period lengthy PC.

6.4 Experimental Results and Discussion

The characterization of the obtained 1D ternary PC and its defective structure were obtained by taking its linear optical response and nonlinear optical response. The linear optical response was exploited by using reflectometer. The nonlinear optical response was carried out using open aperture Z-scan method. The characterization results have been described in the following section.

6.4.1 Linear optical response of the PC system

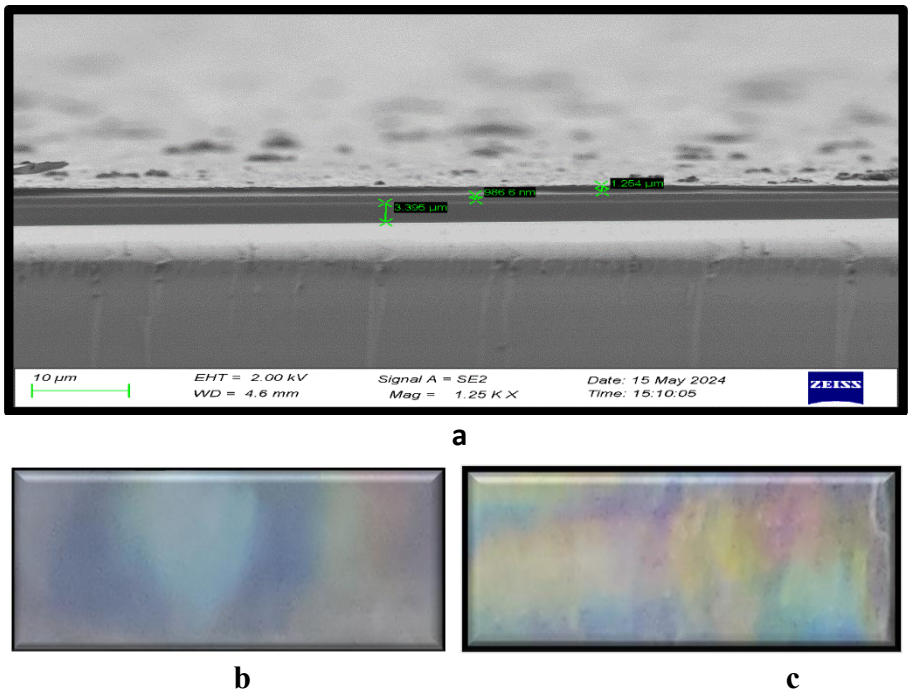

Figure 6.3: a) SEM image of unit cell of 1D ternary Silica/DNA/ZnO PC, Reflection surface of b)1D ternary Silica/DNA/ZnO PC, and c)1D ternary defective Silica/DNA/ZnO PC where N=13.

Experimentally obtained 1D ternary Silica/DNA/ZnO was subjected to SEM analysis. Figure 6.3a represents the SEM image of unit cell of the structure. The result says that the obtained structure belongs to micro size, however, the experimental limitations prevented the structure from attaining theoretically expected size of the elemental layer.

Figure 6.3b shows the reflection of the surface of the 1D ternary Silica/DNA/ZnO PC structure where N=13. Apart from the structural imperfections, the surface reflects high intense yellow lines of light. Figure 6.3c exemplifies the reflection of 1D ternary defective Silica/DNA/ZnO PC system where N=13. From Figure 6.3c the surface of the defective structure seems it reflects blue lines of the optical band. Apart from the experimental strains, the reflection spectrum and SEM analysis pointed out that the obtained structure shows the same features of theoretically expected 1D ternary Silcia/DNA/ZnO PC system.

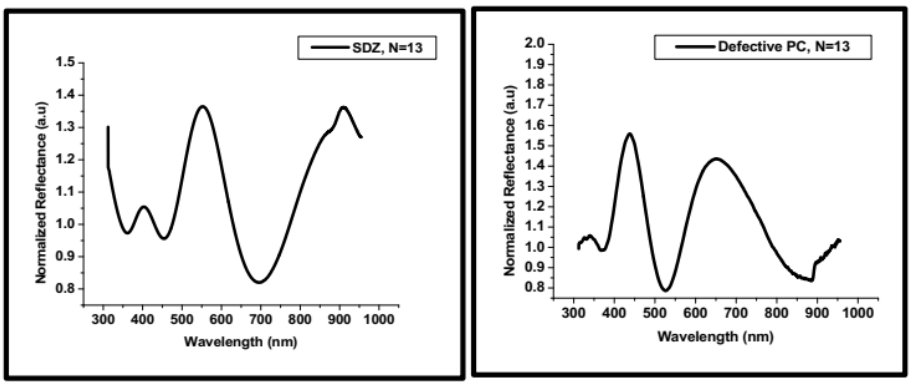

a **b**

Figure 6. 4: Experimentally obtained optical response of a) 1D Ternary Silica/DNA/ZnO, where N=13, and b) D-POM embedded defective 1D Ternary Silica/DNA/ZnO, where the defective layer is placed at the 7th unit cell, in which D-POM replaces the DNA layer.

Figure 6.4 elaborates the experimental results of linear optical properties of the 1D ternary Silia/DNA/ZnO. Figure 6.4a. Shows that the optical transfer properties of the 1D ternary Silia/DNA/ZnO where a wide PBG is seen around the region 450nm-700nm of light. On the other hand, the Figure 6.4b shows the transfer properties of the D-POM embedded defective 1D ternary Silica/DNA/ZnO. The defective layer D-POM is placed at the 7^{th} unit cell, where the D-POM replaces the DNA layer. After placing the defective layer, the changes in the optical response of the PC are observed. A narrow transmission mode is seen around 500 nm-550nm, which is situated in between the PBG range. The photonic band edges are also shifted accordingly. This experimental result exemplifies that the system is a promising candidate for subjecting to nonlinear optical characterization. The prominent factor that is to be considered for lasing application is whether the system shows linear optical transmission around 532nm of visible light. Hence, the system shows its defective transmission mode at 532nm; there is fine hope that it has to be experienced with NLO properties.

6.4.2 Nonlinear optical analysis of 1D ternary defective Silica/DNA/ZnO photonic crystal system

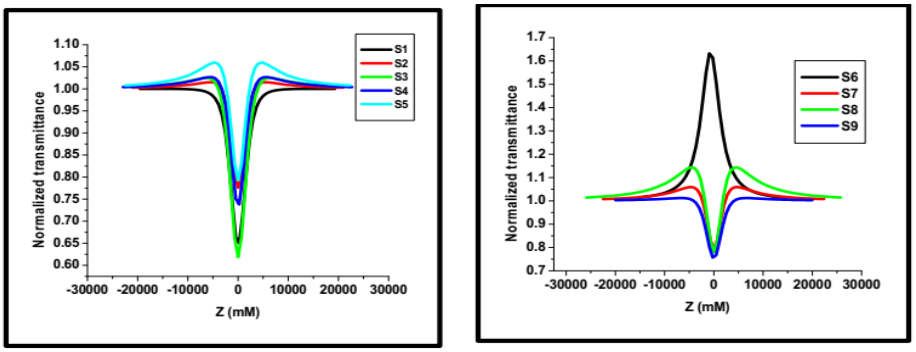

Figure 6. 5: Open aperture Z scan NLO results of samples a) S1, S2, S3, S4, S5, and b) S6, S7, S8, and S9.

The optical nonlinearity is a property that is associated with two-photon absorption. When a material is placed along the path of high-intense monochromatic Gaussian field (Laser) of wavelength in the visible range, the material will absorb two photons of the same energy simultaneously, and the resultant frequency is the sum of the frequencies absorbed. On the other hand, this implies that at sufficiently high-intensity fields, the material can absorb more than two or more photons simultaneously [35, 51].

The nonlinear absorption process can be explained by using equations 5.1-5.16 provided in chapter 5. Equation 6.6 summarizes the relation that connects the nonlinear absorption coefficient and the intensity of the incident laser beam [51].

$$\frac{dI}{dz} = -\left[\frac{\alpha_0}{1+I/I_0}\right] I - \beta_{eff} I^2 \qquad 6.6$$

Where I is the intensity of the transmitted pulse beam, I_0 is the intensity of the initial pulse beam, α_0 is the linear absorption coefficient, z is the distance moved by the sample away from the source, and β_{eff} is the nonlinear absorption coefficient. While considering the PC as the material to be placed in such a monochromatic, high intense Gaussian field, the optical behavior of PC is found to have quite interesting features. Figure 6.1, Figure 6.2 and 6.3 b and c and 6.4 show the linear optical behavior of the PC at low intensity fields. While the system is subjected to high high-intensity laser beam, the behavior is shown in Figure 6.5.

The nonlinear optical properties of the 1D ternary silica/DNA/ZnO have been measured by an open-aperture Z-scan experiment along with defective D-POM embedded PC. The excitation was carried out with a 532 nm laser beam with a pulse rate of 9 ns. The laser beam has been directed towards the sample through a convex lens of focal length 12 cm. The open Z-scan aperture results of samples exemplify the significant effect of structural periodic variation from PC to the defective PC on account of the nonlinear optical absorption parameter. The Z scan study has been subjected for eight different samples namely; S1, S2, S3, S4, S5, S6, S8 and S9 corresponding to 1 D ternary Silica/DNA/ZnO of period N=1, 4,8, 10, and 13, and 1 D defective Silica/DNA/ZnO with defective layer D-POM, D-POM, and POM without DNA capping respectively. The samples S5 and S7 are the same.

The NLO studies have been conducted on the basis of two parameters. The role of period and the defective layer on the NLO property of the 1D ternary silica/CD/ZnO PC system. Figure 6.4a exemplifies that the NLO property of 1D ternary silica/CD/ZnO PC has been improved as on increasing the number of periods increases. The nonlinear optical absorption has been found to be high for a small number of periods. However, as the period increases, the nonlinear optical absorption is found to decrease; simultaneously, the saturable absorption is found to increase. Figure 6.4b shows the effect of a defective layer D-capped POM on the NLO property of the PC Figure 6.4b illustrates the NLO behavior of defective PC (S6), PC (5=7), D-capped POM (S8), and POM without DNA capping to distinguish the contribution of each component to the NLO property of the PC. The NLO absorption

property is found to decrease as it goes from S9 to S6. The nonlinear optical absorption of POM without DNA capping is higher than that of DNA-capped POM.

On the other hand, DNA DNA-capped POM shows higher saturable absorption property than POM without DNA capping. Hence, the effect of DNA-capped POM (D-POM) on the PC is shown in Figure 6.4b. By adding the D-POM as the defective layer at the 7th unit cell of the PC by replacing the CD layer, the NLO property of S6 shows that the saturable absorption process has been found to increase drastically.

The sample S6 (D-POM embedded ternary PC) shows the highest saturation absorption (SA) property among other samples. The samples S1 and S4 are the PCs fabricated at the same number of periods but having a difference in the number of elemental layers in the unit cell structure. The prominent change observed is the rapid rise in the SA property of ternary PC structures.

Moreover, from these observations, the anomaly in the nonlinear absorption process observed in the samples S1-S5 and S6-S9 is due to the results of specific facts. It may be associated with both structural peculiarities of S1 and the defective layer D-POM. The sample S6 is defective ternary PC, and S5 is the ternary PC without a defect for the same number of periods. Between these two samples, S5 has the SA property, which is higher than that of S1-S4 but less than that of S6. Therefore, the rise in SA property of sample S5 among S1-S4 may be associated with structural peculiarity, such that the NLO property is associated with the number of periods. Recollecting the theoretical results of linear transfer properties of the PC systems, the unit cell of the PC makes significant changes in the optical behavior of the PC

systems. The unit cell of the ternary PC contains three elementary layers having nearly adjacent values of refractive indices. Relative to the binary system, this fact affects the ternary system to have low oscillation density in photonic band edges. Similarly, this condition also exists in the defective PC as compared with its binary counter systems. That leads to the formation of PBG that is not much wider than the PBG formed in the binary PC system. In this case, the PBG is formed around 532 nm, so the NLO field is designed for a 532 nm laser. Hence, at the photonic band edge, the transmission modes are not very available. Aside from, as the number of periods is increased, the PBG is also able to shift slightly, and the corresponding band edge modes are also shifting away from 532 nm. That will create a situation that prohibits the laser from interacting with the material. Thus, the system has reduced the efficiency of the nonlinear absorption process. Another fact that adversely affects the NLO absorption process is reduced field enhancement. PCs can enhance local electromagnetic fields through resonant effects. If the period increases, shifting these resonances away from 532 nm, the local field enhancement will decrease, leading to a reduced nonlinear absorption.

Along with the introduction of a defective layer, D-POM, which has shown SA property, can affect or modify the defect states within the PC structure. By its presence, the defect mode has been formed exactly around 510-540 nm. However, the defective mode states are found to low. Thereby, this will adversely affect to nonlinear absorption process. Another crucial factor related to the nonlinear absorption process is the photon lifetime and escape probability. The rise in SA property in regards with the increase in the number of periods points that the photon escape probability in a narrow bandwidth is greater

than that of a wider bandwidth. Another fact reveals that, the adequate photon lifetime within the structure is reduced. That is also possible to reduce the interaction between light and matter, which results in reduced nonlinear absorption. Hence, they pointed out that the effective nonlinear optical coefficient of the PC can be changed with the period and defective layer.

So far, the way the structural parameters, such as elemental layers and number of periods, contribute to the nonlinear absorption property of the system has been discussed. In summary, the decrease in nonlinear absorption and low threshold limiting value with an increase in the period, and number of elemental unit cell of the PC, substitution of suitable material that has NLO property embedded in the elementary cell as defective layer can be attributed to changes in the photonic band structure, reduced field enhancement, modification of defect states, the life time of photon in the excited electronic states and escape probability can tune the effective nonlinear coefficient of the system.

Table 6.2: Nonlinear optical results of samples

Samples	Saturation Intensity, Is x 10^{11} W/m^2	Nonlinear Absorption Coefficient, β x 10^{-11} m/W	Optical Limiting Threshold x 10^{12} W/m^2
S1	40	4.88	4.36
S2	90	4.39	4.49
S3	60	2.36	6.39
S4	40	2.83	5.55
S5	30	2.44	6.12
S6	150	-0.32	-
S8	20	3.52	4.62
S9	70	3.05	5.10

The Table 6.2 summarizes the open aperture Z scan results of the samples. From which the sample S1 has got large nonlinear absorption coefficient and also has the least optical limiting threshold. The sample S8 which is D-POM has more nonlinear absorption coeffiecient than the POM (S9) that is prepared without DNA capping. Among these 8 samples, the highest saturation intensity belongs to the sample S6, defective 1D ternary PC system.

Hence, the nonlinear optical details of the samples clearly stated that the defective D-POM embedded 1D ternary PC has a low NLO absorption coefficient, but high SA property. That remark suggests that the system can be suitably tuned for a saturable absorber for lasing applications. A saturable absorber is an optical component having a definite absorption loss against light, but the absorption loss can be reduced at high optical intensities. For achieving a lossless saturable absorber, a dopant has been added to the materials. In these experimental results, the system itself behaves as a saturable absorber and enhances the condition in a defective cavity mode. Thus, it is evident from Figure 6.4, such that, on increasing the number of periods, the nonlinear absorption process gradually decreases and the corresponding saturable absorption increases. Therefore, in a small number of periods, the ternary PC behaves as a good nonlinear optical absorption material. In defective mode, it can be suitably applied for a nonlinear saturable absorber. As the system shows SA property as on increasing the number of periods increases, practically the size of the system is getting large. That will affect the configuration of the PC system and optical devices, though an infinitely large scale cannot be

applicable for the miniature-sized integrated photonic device technology. Therefore, such a situation can be avoided by choosing a suitable material that can have twin benefits, such that it should have nonlinear optical behavior and film properties. When considering all these facts together, D-POM meets both criteria. That turns to consider it is a good choice for a defective layer for tuning the nonlinear optical response of a ternary PC system.

Additionally, the NLO response can be carried out at a low optical limiting threshold value. The main applications of saturable absorbers are found in passive mode locking and Q switching of lasers for the generation of short optical pulses, and laser resonators for optical signal processing and cleaning up pulse shapes. Hence, the experimental results agree that our system can be a promise for tuning lasing devices and integrated photonic devices.

6.5 Conclusions

Concisely, a 1D ternary PC system containing 13 elementary cells has been designed and fabricated with the dip coating method. The optical properties of the system have been studied theoretically using TMM in the Python platform and the COMSOL software tool. The optical properties have been experimentally realized by taking reflection spectroscopy. A surface-modified D-POM has been used as a defective layer to realize a defective ternary PC system. The defective system is subject to open open-aperture Z scan experiment to study the optical nonlinear response of the system. The Z-scan results revealed that the system shows a tuned nonlinear optical property. For lowering the

period number, high nonlinear optical absorption has been observed. As the period rises, the saturation absorption starts to rise. The SA property has been rapidly increased as the D-POM embedded defective PC with a saturation intensity of 150 10^{11} W/m^2. Hence, the nonlinear property of 1D ternary Silica/CD/ZnO PC and D-POM embedded defective Silica/CD/ZnO can be tailored for lasing applications such as optical limiting devices, saturable absorbers in photonic devices.

References

[1] Joannopoulos, J. D., Johnson, S. G., Winn, J. N., & Meade, R. D. (2008). Molding the flow of light. Princet. Univ. Press. Princeton, NJ [ua], 12.

[2] Q. Gong, and X. Hu, "Photonic Crystals: Principles and Applications", Pan Stanford Publishing Pte. Ltd, (2014)

[3] K. Wu, W. X. Gu., C. Wu, J. L. Ma., and X. Y. Ma, (2014). "Study on the optical transmission properties of one-dimensional photonic crystal of MoS_2", Adv. Mater. Res., 1056,42-46(2014), doi:10.4028/www.scientific.net/AMR.1056.42.

[4] J. Pandey, "Transfer matrix method for one-dimensional photonic crystals", *J.Ramanujan Math Soc.* 6,1, 121-130 (2017), ISSN: 2319-1023.

[5] F. Akbar, A. Syahriar, and A. H. Lubis, "Dispersion Relation of 1D Photonic Crystal", IEEE International Conference on Electrical Engineering and Computer Science, Bali, Indonesia, 24-25,(2014).

[6] M. N. Armenise, C. E. Campanella, and C. Ciminelli, "Phononic and photonic band gap structures: modelling applications", Phys. Procedia, 357–364(2010), doi:10.1016/j.phpro.2010.01.047.

[7] Y. Liu, H. Wang, J.Ho, and R. C. Ng, "Structural color three-dimensional printing by shrinking photonic crystals", Nat. Commun., 10:4340(2019), doi.org/10.1038/s41467-019-12360-w.

[8] X. Lv, B. Zhong, Y. Huang, et al., "Research Progress in Preparation and Application of Photonic Crystals", Chin. J. Mech. Eng., 36(1), 39,(2023).

[9] R. K. Gangwar, A. K. Pathak, and S. Kumar,2023, "Recent Progress in Photonic Crystal Devices and Their Applications: A Review", *Photonics 10*(11), 1199; https://doi.org/10.3390/photonics10111199.

[10] L. Shiveshwari, "Complete photonic band gaps in one-dimensional ternary photonic crystals containing single negative materials", Optik - Int. J. Light Electron Opt. (2013), http://dx.doi.org/10.1016/j.ijleo.2013.04.037

[11] Rahul Kumar Gangwar, Akhilesh Kumar Pathak, and Santosh Kumar, "Recent Progress in Photonic Crystal Devices and Their

Applications: A Review", Photonics (2023), 10, 1199. https://doi.org/10.3390/photonics10111199

[12] Sharma, G., Kumar, S., Prasad, S., and Singh, V., "Theoretical modelling of one-dimensional photonic crystal-based optical demultiplexer", J. Mod. Opt. 63(10),995–999(2015). doi:10.1080/09500340.2015.10880

[13] G. Von Freymann, Kitaev, V., Lotsch, B. V., G. A. Ozin, "Bottom-up assembly of photonic crystals", Chem. Soc. Rev.,42(7), 2528–2554(2013). doi:10.1039/c2cs35309a.

[14] B. Suthar, and G. N. Pandey, "Optical Properties of One Dimensional Ternary Metamaterial Photonic Crystal", Macromolecular Symposia, 397(1), 2000340(2021). doi:10.1002/masy.202000340

[15] L. Yong, L. Wei-Guo L., Z. Ye-Chuan, Z. Shun, D. Zhong-Hua, S. Xue-ping, G. Shao-Bo, G. Wen-Hao, and W. Zhi-Heng, "Propagation and localization of light in one-dimensional nonlinear photonic crystals embedded polyvinylidene fluoride /graphene oxide layers", Opt. Mater., 151, 115255(2024), https://doi.org/10.1016/j.optmat.2024.115255.

[16] S. Kim, K. Kim, F. Rotermund, and H. Lim, "Computational design of one-dimensional nonlinear photonic crystals with material dispersion for efficient second-harmonic generation". Opt. Express, 17(21), 19075(2009). doi:10.1364/oe. 17.019075.

[17] N. P. Purayil, A. K. Satheesan, S. Edappadikkunnummal, and C. Keloth. "Photonic band-edge assisted enhanced nonlinear absorption of carbon encapsulated gold nanostructures in polymeric multilayers", *Opt. laser technol* 159, 109009(2023).

[18] N. P. Purayil, C. Keloth**, "**Hybrid Plasmonic Coupled Nanophotonic Cavity-Mediated Tunable Nonlinear Absorption in Cobalt Phthalocyanine", J. Phys. Chem. C, 127, 28, 13846-13853 (2023), DOI: 10.1021/acs.jpcc.3c02182

[19] Samad Roshan E., "Reshaping of Gaussian light pulses via defective nonlinear one-dimensional photonic crystals", Opt. laser technol. 164, 109508(2023)

[20] A. K. Satheesan, L. V. Nair, J. S. Gopinath, P. Parameswaran, C. Keloth, "Nonlinear optical studies of [Pt17(CO)12(PPh3)8] n+ Metal

Nanoclusters and Their Enhancement via All-Plastic Photonic Crystal Cavity", Phys. Chem. C, 127, 568−576(2023), https://doi.org/10.1021/acs.jpcc.2c06026.

[21] N. P. Purayil, V. Kakekochi, U. K. Dalimba, and C. Keloth, “All-Optical Diode Action through Enhanced Nonlinear Response from Polymeric Photonic Crystal Microcavity”, ACS Appl. Electron. Mater. 4, 138−148(2022).

[22] V. Kakekochi, U. Kumar, P. P. Nikhil, and K. Chandrasekharan, “Effects of substituents on the enrichment of the optical limiting action of novel imidazo [2, 1-b][1, 3, 4] thiadiazole fused thiophene-based small molecules”. NJC, 43(23), 9232-9242 (2019).

[23] M. Scalora, J. P. Dowling, C. M. Bowden, and M. J. Bloemer, “The photonic band edge optical diode”, J. Appl. Phys., 76(4), 2023–2026 (1994). doi:10.1063/1.358512.

[24] G. Giménez, G.Ybarra, and G.J.A.A. Soler-Illia, “Preparation of mesoporous silica thin films at low temperature: a comparison of mild structure consolidation and template extraction procedures”, J. Solgel Sci. Technol, 96(2), 287–296(2020). doi:10.1007/s10971-020-05410-z

[25] T. Seo, H. Park, G. Jeon, J.Yun, S. Park, S. Seong, and Y. Chung, “Low-Temperature Fabrication (≤ 150 °C) of High-Quality Sputtered Silicon Oxide Thin Film with Hydrogen Plasma Treatment”, ACS Appl. Electron. Mater. (2020) doi:10.1021/acsaelm 0c00631

[26] G. S. Bhagyasree, V. N. Reena, M. Abith, T. C. Sabari Girisun, B. Nithyaja, "Enhanced adsorption and nonlinear optical properties of DNA-CTAB functionalized mesoporous silica nanoparticles and their influence on enhancement of photoluminescence of Rhodamine 6G dye", AIP Adv., 13, 055017 (2023); doi: 10.1063/5.0149009

[27] A. J. Steckl, “DNA–a new material for photonics?”, Nat. Photonics, 1(1), 3-5(2007)

[28] A.J. Steckl, H. Spaeth, H. You, E. Gomez, and J. Grote, “DNA as an Optical Material”, OPN, Vol 22, Issue 7, pp. 34-39(2011), https://doi.org/10.1364/OPN.22.7.000034

[29] R. Khazaeinezhad, S. Hosseinzadeh Kassani, B. Paulson, H. Jeong, J. Gwak, F. Rotermund, and K. Oh, “Ultrafast nonlinear optical properties of thin-solid DNA film and their application as a saturable

absorber in femtosecond mode-locked fiber laser", Sci. Rep.., 7(1), 41480 (2017).

[30] P. Gheorghe, A. Petris, and A.M. Anton, "Optical limiting properties of DNA biopolymer doped with natural dyes", Polymers, 16(1), 96 (2023).

[31] L. Wang, J. Yoshida, N. Ogata, S. Sasaki, and T. Kajiyama, "Self-Assembled Supramolecular Films Derived from Marine Deoxyribonucleic Acid (DNA)−Cationic Surfactant Complexes: Large-Scale Preparation and Optical and Thermal Properties", Chem. Mater., 13, 1273-1281(2001).

[32] C. Cheng, and S.Y. Ran, "Interaction between DNA and Trimethyl-Ammonium Bromides with Different Alkyl Chain Lengths", TSWJ., 1–9. (2014), doi:10.1155/2014/863049.

[33] A. Samoc, M. Samoc, J.G. Grote, A. Miniewicz, A., and B. Luther-Davies, "Optical properties of deoxyribonucleic acid (DNA) polymer host", Optical Materials in Defence Systems Technology III.(2006) doi:10.1117/12.691239

[34] M. Yoshikawa, M. Maruhashi, Y. Iwamoto, and N. Ogata, "Optical resolution of racemic amino acids through DNA-Poly(4-vinylbenzyl)trimethylammonium polyion complex membranes", Polym. J., 39(11),(2007) 1193–1198. doi:10.1295/polymj.pj2007080

[35] B. Nithyaja, H. Misha, V. P. N. Nampoori, Synthesis of silver nanoparticles in DNA template and its influence on nonlinear optical properties, J. Nanosci. Nanotechnol., p-ISSN:22163-257X e-ISSN: 2163 2588, (2012); 2(4): 99-103, doi: 10.5923/j.nn.20120204.02.

[36] V. N. Reena, H. Misha, G.S. Bhagyasree, G.S., and B. Nithyaja, "Enhanced photoluminescence and color tuning from Rhodamine 6G-doped sol–gel glass matrix via DNA templated CdS nanoparticles". AIP Adv., 12(10)(2022).

[37] D. Guo, K. Sato, S. Hibino, T. Takeuchi, H. Bessho, and K. Kato, "Low-temperature preparation of (002)-oriented ZnO thin films by sol–gel method", Thin Solid Films, 550, 250–258(2014). doi:10.1016/j.tsf.2013.11.004

[38] M. J. Zhao, Z.T. Sun, C.H. Hsu, P.H. Huang, X.Y. Zhang, W.Y. Wu, W.Z. Zhu, Zinc Oxide Films with High Transparency and Crystallinity Prepared by a Low Temperature Spatial Atomic Layer

Deposition Process. Nanomater., 10(3), 459(2020). doi:10.3390/nano10030459.

[39] N. Hasuike, T. Harada, T. Kiyohara, K. Nishio, K. Kisoda, and H. Harima, "Low temperature synthesis of ZnO thin films by spin-coating technique", Physica Status Solidi (c), 8(2), 506–508(2010). doi:10.1002/pssc.201000497

[40] T. Zhang, W. Guan, S. Wen, T. Ma, L. Yan, and Z. Su, "Theoretical exploration to the cation effect on the second-order nonlinear optical properties of Strandberg-type polyoxometalates", JTCC, 14(01), 1550007 (2015).

[41] B. R. Hood, Y. de Coene, C. F. Jones, I. Lopez Poves, N. Deveaux, N. R. Halcovitch, and J. Fielden, "Synthesis and Optical and Nonlinear Optical Properties of Linear and Two-Dimensional Charge Transfer Chromophores Based on Polyoxometalates", Inorg. Chem. 63(51), 24250-24261(2024).

[42] U. Saleem, M. Tariq, F. K. Shehzad, K. Ahmad, J. Khan, H.M. Asif, and Z. M. El-Bahy, "Investigations of switchable nonlinear optical response inpyridyl containing porphyrin@ Anderson polyoxometalate hybrid by Z-scan measurements", Inorg. Chem. Commun., 156, 111270 (2023).

[43] T. Zhang, L. Yan, S. Wen, S. Cong, J. Wang, and Z. Su, "A DFT study on the second-order nonlinear optical properties of the plenary mixed-metal polyoxometalate", Mol. Simul., 38(6), 518-524(2012).

[44] L. S. Wang, Y.Wang, C.L. Lv, C. Guo, F. Y. Xing, Y. J. Dong, and Y. G.Wei, "Polyoxometalates with tunable third-order nonlinear optical and superbroadband optical limiting properties", Inorg. Chem. Front., 9(17), 4413-4424(2022).

[45] A. Lesbani, R. D. Tarmizi, T. Taher, N. R. Palapa, and R. Mohadi, "Preparation of Ni-Al LDH: Influence of intercalated polyoxometalate anion (α-SiW12O40)4- on the interlayer gallery distance", The 2nd international conference on science, Mathematics, environment, and education., AIP Conf. Proc., 2194, 020054 (2019), https://doi.org/10.1063/1.5139786

[46] M. Ammam, "Polyoxometalates: formation, structures, principal properties, main deposition methods and application in sensing", J. Mater. Chem. A, 1(21), 6291(2013). doi:10.1039/c3ta01663c

[47] D.C. Batalha, S. O. Ferreira, R. C. Silva, and M. J. Silva, "Cesium-Exchanged Lacunar Keggin Heteropolyacid Salts: Efficient Solid Catalysts for the Green Oxidation of Terpenic Alcohols with Hydrogen Peroxide", ChemistrySelect, 5(6), 1976–1986 (2020). doi:10.1002/slct.201903437

[48] T. Takashima, R. Nakamura, K. Hashimoto, "Visible Light Sensitive Metal Oxide Nanocluster Photocatalysts: Photo-Induced Charge Transfer from Ce(III) to Keggin-Type Polyoxotungstates." J. Phys. Chem. C, 113, 17247–17253(2009)

[49] L. Yang, J. Lei, J. Fan, R. Yuan, M. Zheng, J. Chen, and Q. Dong, "The intrinsic charge carrier behaviors and applications of polyoxometalate clustersbased materials", Adv. Mater., 2005019(2021), DOI: 10.1002/adma 202005019

[50] V. N. Reena, G. S. Bhagyasree, T. Shilpa, R. Aswati Nair, H. Misha, and B. Nithyaja, "Photocatalytic, Antibacterial, Cytotoxic and Bioimaging Applications of Fluorescent CdS Nanoparticles Prepared in DNA Biotemplate". J. Fluoresc., 34(1), 437-448(2024).

[51] M. Sheik-Bahae, A. A. Said, T. H. Wei, D. J. Hagan, and E. W. Van Stryland, "Sensitive measurement of optical nonlinearities using a single beam", IEEE J. Quantum Electron., 26, no. 4, 760-769(1990).

Chapter 7

Transfer properties of DNA templated 1D Silica/DNA/PVA photonic crystal system for 3D inkjet printing using TMM method.

This chapter briefly highlights the scope of the temperature-treated 1D ternary photonic crystal to be employed for the fabrication of 3D shapes using the inkjet printing method. The work enquires how features of photonic band can be incorporated with the 3D inkjet printing process. The study involves the theoretical analysis of photonic bandgap structures and materials for designing 1-D ternary photonic crystals. The optical range considered for this analysis spans from 350 nm to 750 nm. The proposed structure of 1D ternary systems consists of polymers, including DNA and polyvinyl alcohol (PVA), along with silica. The work also highlights the unique optical features exhibited by these polymer-based 1D ternary photonic crystals.

The results of this chapter are published as

Bhagyasree, G. S., Sreenilayam, S., Brabazon, D., Reena, V. N., & Nithyaja, B. (2022). Transmission characteristics of DNA templated 1D photonic crystal system for 3D printing applications: simulation. Results in Engineering, 16, 100750.

7.1 Introduction

Additive manufacturing (AM), also known as three-dimensional (3D) printing, has been a focus of technological interest since 1980. AM is a process by which digitized 3D design data is used to build up components or complex structures and devices in a layer-by-layer manner, hence the name [1-4]. Based on the materials and applications of 3D printing, AM is classified into different types. They are fused deposition modeling, stereolithography, DLP 3D printing, photopolymer phase change inkjet (polyJet), powder bed and inkjet 3D printing, thermal phase change inkjets, and laminated object manufacturing (LOM). 3D material extrusion is now an inevitable part of the technological world. The revolution in 3D printing technology meets different commercial needs in designing instruments to a great extent. The demand for AM printing extends to various industrial fields and improves technological standards [1-15]. The applications of AM printing are found mainly in aerospace, automotive, biomedical, and tooling, in particular for plastics processing and consumer goods [1-15]. The advantage of AM or 3D printing over other existing traditional manufacturing technologies is that it increases the degree of design freedom. The 3D fabrication process can also provide a high level of dimension precision. It can be used to fabricate lightweight structures with complex internal channels if required in the design. This technology requires no additional tools for modeling structures and promotes material waste reduction and shorter production times. These features encourage the use of AM to replace conventional prototype production technologies. Besides these advantages, AM has

faced certain limitations also. For powder-based techniques, the dimensional accuracy of the produced product is dependent on the powder particle size distribution. Large-scale production of specific parts is achievable for some products versus conventional production in a single-step process. There is usually some level of porosity present after additive manufacturing. Apart from these, the material physical properties such as temperature, humidity, and anisotropic behavior also hinder to achieve high high-quality part production—these drawbacks of AM point towards some areas where more research is needed. The modifications are mainly wanted in the development of advanced 3D printer systems and the development of new materials for these systems [1-22].

Keeping these views in mind, the role of the 3D inkjet printing process deserves special attention among different 3D printing processes due to its adaptive technological opportunities. Over the years, 3D inkjet printing technology has been widely recognized for its incredible adaptability with a wide range of liquid materials or solid suspensions, as it provides high printing resolutions to both insulating and conductive structures. Additionally, it does not require any further post-processing steps. This layer-by-layer deposition process requires low temperature and ambient low-pressure conditions. The range of materials that can be extruded through this printing process includes polymers, dielectric nanoparticles, and conductive nanoparticles. A 3D inkjet printer has a small nozzle within a print head that raster scans over a substrate to extrude materials as multilayer structures in a layer-by-layer manner. Curing processes of each layer are carried out in

between successive depositions, and they may vary depending on the materials that are being extruded. In 3D inkjet printing, the curing process takes a short time. The deposited layers are fragile, and the curing parameters (temperature, pressure, and nozzle size) can be easily tuned with different viscosities and curing requirements [23-24].

In 3D printing, the scope of photonic crystal is recognized as its optical and geometrical features meet the requirements of 3D inkjet printing processes. In general, photonic crystals are periodic dielectric microstructures that restrict a specific range of the electromagnetic spectrum from passing through them [25]. The presence of a bandgap effect in them helps them to tune the propagation of light. This peculiarity of the photonic crystals is achieved and modified by the structural parameters (thickness and number of dielectric layers) and refractive index contrast (Δn) between the periodically aligned dielectric layers of the photonic crystal system [25]. Due to their ability to modulate electromagnetic waves, they have been recognized in different technological applications such as fiber optics, Bragg reflectors, solar cell back reflectors, and sensing devices [1-10]. The advantage of photonic crystals in 3D printing is that they are a layer-by-layer system, so that they can be applied to form a well-closed pack order with negligible porosity. Typically, the photonic crystals are dielectric, so that they are non-conductive and water resistant as well. In addition to these, they can produce a tunable multicolor spectrum of visible light. The structural color of the photonic crystals is based on the geometrical parameters and Δn of the system. Thus, the multicolor appearance is a non-fading and lasting property. The materials that can

be built as photonic crystals are available in both liquid form and polymer as well. These adaptations help to use them for the 3D inkjet printing process. The other benefits of using photonic crystals are that the materials which are used for photonic crystal fabrication reduce the risk of toxicity, as they can be used instead of dyes for making exquisite cultural and creative articles. Using these possibilities of photonic crystals, nowadays, research works are focused on extending their applications for 3D printing. In 2022, J. Liao et al. [53] reported that they were able to develop colloidal photonic crystals (c-photonic crystal) and fabricate digitally defined macroscale geometries and structural colors on the sub-micron level by combining c-photonic crystal ink with a digital 3D printing system. In 2019, Y. Liu et al. [39] reported that photonic crystals can be applied for multicolor 3D printing by the thermally shrinking method. In 2013, J. Wang et al. [40] and H. Nam et al. in 2016 [41] reported that c-photonic crystal can be effectively used for inkjet printing.

The main objectives of the work are to provide non-toxic and cost-effective materials for 3D printing. One of the challenging criteria of these requirements is that the chemicals that are used for extruding 3D objects should be safe for health. Studies have shown that the emission of chemicals during the extrusion of materials can contribute to air pollution and may include carcinogenic substances. In this perspective, recent trends in DNA thin films have gained attention. DNA thin films are now recognized as effective photonic materials, and biopolymers—particularly those based on salmon DNA—have shown significant potential in optoelectronic device applications. Their structural

tunability enables them to form bulk films, lyotropic as well as thermotropic liquid crystals, and hydrogels. The significant features of DNA, such as low weight, cost-effective, and amenable to a variety of low-temperature film fabrication processes, including inkjet printing, helped to bring them to polymer applications. DNA films have been reported to have a dielectric constant in the range of 7.0-8.0(1KHz), and the DNA-CTMA dielectric constant is higher than 5, which is higher than most synthetic polymers. So, this can be adaptable for photonic crystal features specifically due to its high dielectric constant as compared with other organic polymers and comparable dielectric strength [42-43]. In 2021, S. Kokkiligadda et al. [44] reported that the refractive index of the DNA thin film can be tuned by varying the thickness of the film. This property of DNA is effective for designing DNA-incorporated photonic crystals. The structural color of photonic crystals is mainly based on Δn between the adjacent constituent layers and layer thickness. Besides, in 2020, V. Prajzler et al. [45] reported that DNA exhibits good surface compatibility with objects and is transparent in visible light. They were able to fabricate DNA thin films as well.

Apart from this, DNA is basically a readily biodegradable organic polymer. Based on these reported facts, DNA is assigned as the key layer of the proposed 1D ternary PC system [46-47]. The other materials selected for designing a three-layered unit cell of the proposed photonic crystal, along with DNA, are silica and PVA. Silica is a cosmopolitan chemical in the world. It is readily available and cost-effective. It has good dielectric properties and film quality as well.

Silica is a famous material for PC applications. Silica has been treated as the primary constituent dielectric material in most of the early reported PCs, where they are suggested for different applications such as biosensors, waveguides, and optical reflectors [68-70]. The third component, PVA, is a synthetic polymer that is also non-toxic, biodegradable, readily available, and cost-effective [48-59].

The transmission properties, including the photonic bandgap effect, of the proposed 1D ternary Silica/DNA/PV PC system are carried out using TMM. The transfer properties of the design are evaluated, and it is found that the proposed system exhibits good optical features in the visible region of light. The standard deviation of the transmission coefficients is also found. Based on the theoretical results, a 1D ternary Silica/DNA/PVA system can be exploited for PC applications. Moreover, the toxic and health-hazardous dyes can be replaced by DNA thin films along with PVA and silica in 3D inkjet printing processes [38-59].

7.2 Transfer matrix method for 1D ternary photonic crystal

The theoretical study of the proposed 1D ternary PC structures was conducted by using the TMM method. The theoretical explanation of designing a 1D ternary PC is provided in detail in equations 2.1-2.53, chapter 2. The optical response (transmission spectrum) of the proposed structure was obtained using equations 2.52-2.53 provided in chapter 2. The dispersion relation of the structure is obtained using equations 2.57-2.58 provided in chapter 2.

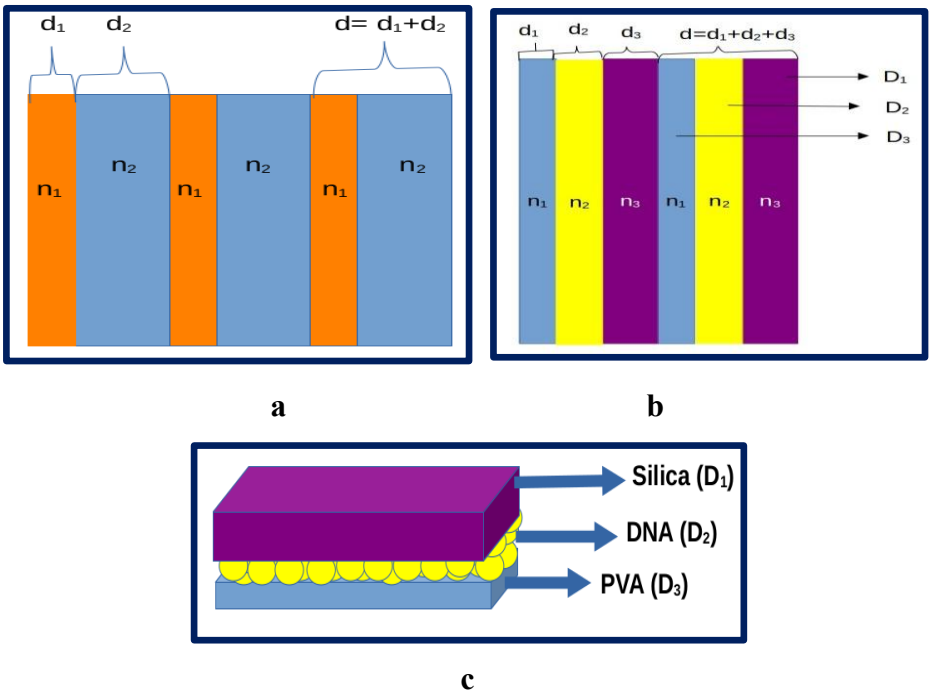

Figure 7. 1 Schematic demonstration of (a) 1D binary PC, (b) 1D ternary PC, (c) cross-sectional view of the unit cell of DNA-templated Silica/PVA PC.

Figure 7.1a is a schematic representation of a 1D binary Silica/PVA PC system, and Figure 7.1b represents a 1D ternary Silica/DNA/PVA PC system, where Figure 7.1c is a schematic representation of the unit cell of the 1D ternary Silica/DNA/PVA PC system.

7.3 Results and Discussions

This section involves results and analysis of the photonic bandgap of the proposed system under different criteria of parameters. The propagation of light through the PC is studied on account of varying its period number. The nature of photonic bandgap on varying period, dispersion relation and the effect of period length are also covered in this section.

7.3.1 Transmission properties of 1D ternary photonic crystal system using TMM

To study the PBG formation of the proposed 1D PC system, the following parameters were considered: the refractive index, thickness, and number of layers of the PC. The DNA template (bio-polymer) in the periodic arrangement of the dielectric layer alters the periodicity (basic step length) of the microstructures in a way that introduces additional interfaces between the bilayer periodic arrangement. When introducing a layer (interface) as a template for every layer of the unit cell, the thickness of the entire unit cell (basic step length) has been changed. That will alter the periodicity of the PC, so the band gap. The changes can be analysed using TMM. The materials selected for the theoretical simulation are silica (SiO2) and polyvinyl alcohol (PVA), and DNA. The refractive index of the silica, PVA, and DNA are 1.4585, 1.4839, and 1.5826, respectively [65-70]. The thickness of layers, *d* of the PC system, is taken as 200 nm, 100 nm, and 150 nm for silica, DNA, and PVA, respectively. The number of period (N) of the PCs are taken as 1, 50, and 100, respectively.

a. Transmission properties of the unit cell of photonic crystal with and without the presence of DNA template

As a periodic system, the periodic boundary conditions of PC restrict the eigenvalues of the propagation of light in a unit cell. It can be effectively used for tuning band structures in the visible region for structural coloration of PCs. The number and thickness of the dielectric layers in a unit cell of the PC are repeated periodically for the entire system to form the PC.

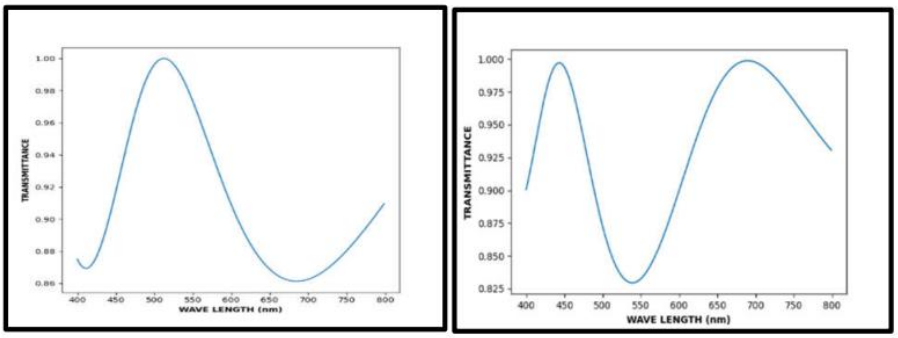

(a) **(b)**

Figure 7.2: Transmittance properties of Silica/PVA ID PC (a) without DNA template; (b) with DNA template for N=1, d_{Silica}=200 nm, d_{DNA}=100, and d_{PVA}=150.

Here, the transmission behaviour of the PC of the unit cell, both in the absence and the presence of the DNA template, is observed. Figure 7.2 illustrates the effects of transmission properties of a unit cell PC system. In the absence of DNA template (refer to Figure 7. 2a), the transmission property is maximum within the range of 400-700 nm region. A dip in transmittance is present as the wavelength goes into higher values. Figure 7.2 (b) shows the plot of transmission properties of 1D DNA templated Silica/PVA PC for a unit cell. In this case, the presence of DNA template alters the basic step length (lattice parameter) of the multilayer structure, hence the band gap, a band gap around 550 nm. The Δn between the Silica and PVA is approximately equal to 0.0254. From Figure 7. 2a, it is clear that small values of Δn could create a significant pass band in the visible region in a unit cell, irrespective of the step length (thickness of the constituent layers). Thus, by the introduction of the DNA template, the Δn between silica and DNA has been improved slightly by a few units, which equals Δn = 0.1241. It reveals that for small change in Δn between the interfaces of the dielectric layer leads to the formation of PBGs, even though the

width of the band gap is significantly small. The only thing done to create a band gap is the introduction of the DNA template as an additional interface into the PC. That creates a discrete continuity in the step length of the unit cell of the PC system. The changes due to the additional interface could be realised by using a nearly adjacent refractive index medium with respect to the other constituent layers of the PC. The refractive index of the DNA lies between Silica and PVA. This feature of DNA helps to understand the difference in transmission properties between the bilayer and three-layered PC systems.

In general, the band gap width can be increased by several methods, that as by introducing large Δn, by increasing individual dielectric thickness (t), and increasing the number of periods (N). The length of the lattice parameter (step length) is increased by increasing the number of dielectric layers having small values of refractive index in the unit cell, which results in the formation of band gaps controlled to obtain in the visible region, and the number of band gaps is increased with reduced width. That agrees that PCs can be tuned for multi-colour appearance by increasing the number of layers having relatively adjacent values of refractive indices in the unit cell system.

b. Transmission properties of photonic rystal for N=10, 50, and 100 layers with and without the presence of DNA Template

Figure 7.3a, c, e demonstrates the transmission properties of the 1D binary Silica/PVA PC for N = 10, 50, and 100, respectively. The results reveal that the density of the transmitted waves and the number of photonic band gaps are increased by increasing the period. In the

case of 1D Silica/PVA PC, a narrow band gap is visible around 500 nm-550 nm.

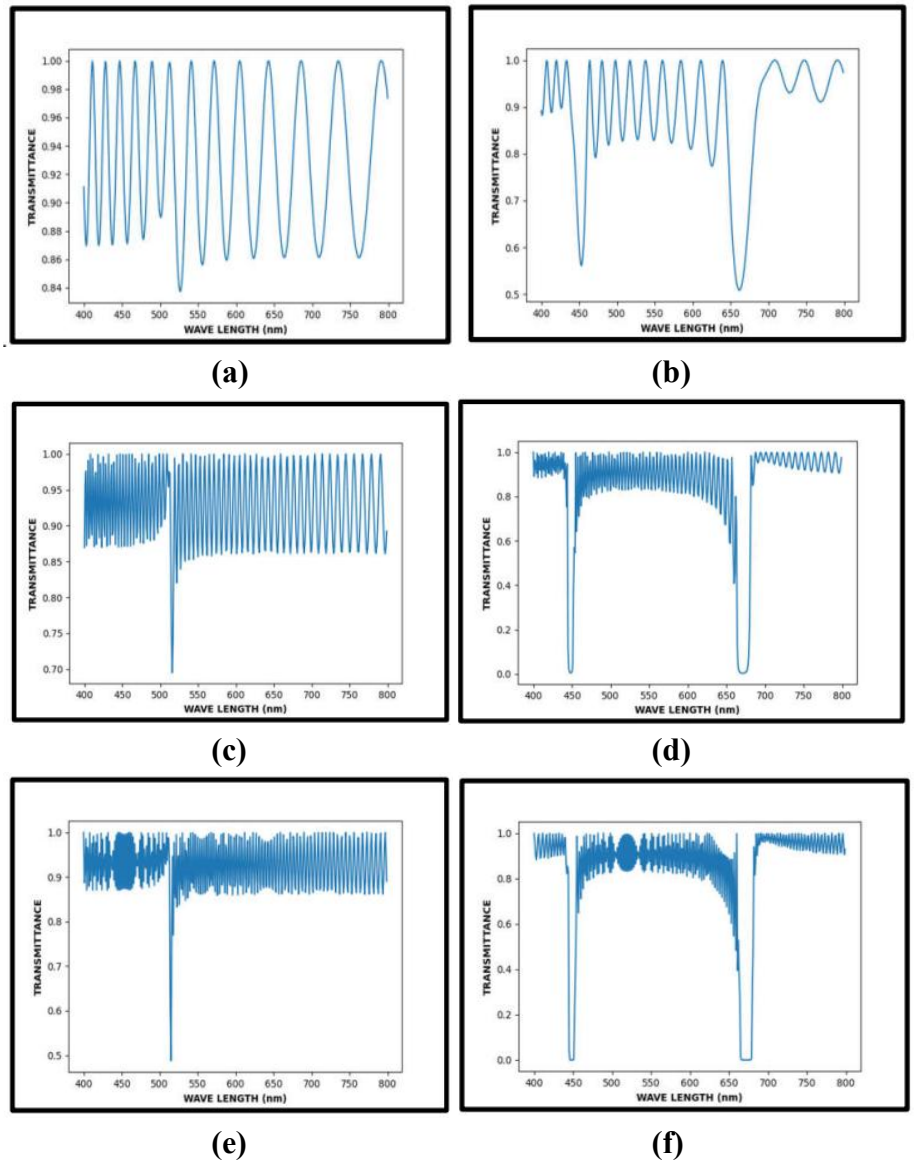

Figure 7.3. Transmission properties of (a) Silica/PVA PC, (b) Silica/DNA/PVA PC for N=10, and (c) Silica/PVA PC, (d) Silica/DNA/PVA PC for N=50 and (e) Silica/PVA PC, (f) Silica/DNA/PVA PC for N=100, where d_{Silica}=200 nm, d_{DNA}=100 nm, and d_{PVA}=150 nm respectively

Similarly, Figures 7.3(b, d, and f) represent the transmittance properties of DNA templated ID Silica/PVA PC, respectively, for N =10, 50, and 100. Here, the changes occurred in the transmission property due to the presence of the DNA template. The width and the number of band gaps, as well as the density of the transmittance, are increased proportional to the increase in the period. In the presence of a DNA template, the position of the band gap is shifted to the longer wavelength region. The band gaps are seen around 450 nm and 675 nm. An additional feature visible in Figure 7. 3 is that the density of oscillations is not uniform as the order of N increases. In general, the oscillation density has to follow a gradual periodic increase and decrease up to the bandgap [8, 23]. In this case, both non-DNA templated Silica/PVA and DNA templated Silica/PVA systems exhibit the anomalous feature of density of oscillation (Figure 7.4). This behaviour is due to the small Δn between the interfaces. By comparing Figure 7. 3 e and f, this anomalous behavior of transmission property is vivid in Figure 7. 3f, and it is shifted to higher wavelengths along with the bandgap shift. In DNA templated 1D PC, the factor that affects the density of the transmission apart from the Δn is the increase in the interfaces of the step length (lattice parameter of the unit cell). Hence, the results ensure that the increase in the interface of the unit cell in a PC system significantly affects the transmission property and bandgap formation as well.

The optimization of the bandgap is achieved by selecting a continuous sequence of periods (N). From Figure 7.3, it is clear that the fluctuations in the oscillation density are more evident in the DNA

templated 1D PC than the silica/PVA 1D PC system. In order to understand the discrepancy, of oscillation density standard deviation of the transmission coefficients has been found.

Figure 7.4 represents the behavior of oscillation density for the two systems by taking the standard deviation of the transmission coefficient against the order of the period in the range of 450 nm -650 nm of the visible region of light. In the case of 1D Silica/PVA PC system, the fluctuations of oscillation density are negligible. On the other hand, the DNA templated Silica/PVA 1D PC system exhibits a wave-like fluctuation. At a specific range of orders, the oscillation density decreases.

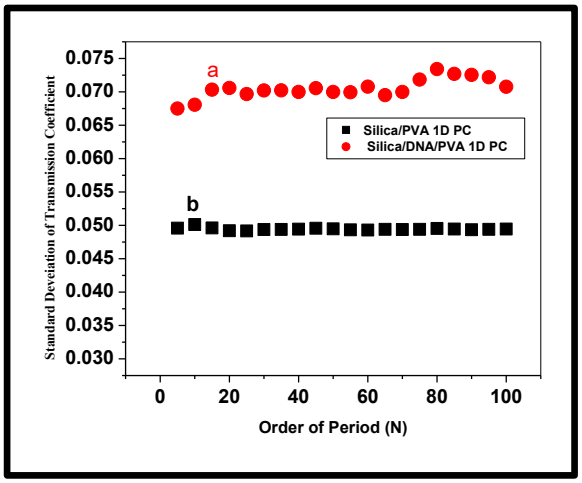

Figure 7.4. Graph of the Standard deviation of transmission coefficients of a) Silica PVA 1D PC and b) Silica DNA/PVA 1D PC with respect to the number of order (N)

The presence of an additional interface (DNA template) between the silica and PVA layers causes a decrease in the photon density in this region. It increased the step length of the unit cell (period) of the PC

system. When considering the additional two interfaces formed by the presence of the DNA template, the refractive index contrast is also increased. The refractive index of silica is smaller than that of DNA. For the left, the refractive index of PVA is smaller than that of DNA but greater than the refractive index of silica. Hence, there is a chance of confinement of electric fields between these interfaces. These factors lead to multiple scattering through the stratified medium, which in turn increases the number of bandgap formations. Due to this, the transmission spectrum exhibits wave-like fluctuations in the DNA templated 1D silica/PVA PC system.

c. Dispersion relation of 1D ternary photonic crystal system

The dispersion relation of 1D bilayer PC and 1D three-layered PC systems is illustrated in Figure 7.5. The band gap structures of the 1D PC system are obtained from the equation. For plotting the dispersion relation, frequency and wave vector are normalised to d/π and d/λ. The dispersion relation actually shows how the frequency relates to both the lattice parameter and the wave number.

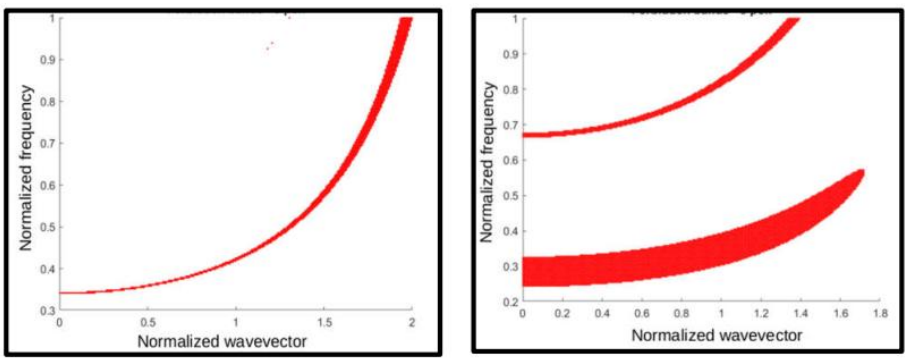

a **b**

Figure 7. 5 The photonic band structure of (a) a bilayer 1D Silica/PVA PC system and (b) three three-layered 1D Silica/DNA/PVA PC system

Figure 7.5a exhibits the dispersion relation or propagation of the electric field through the stratified 1D Silica/PVA PC system. A narrow-structured band gap is shown and which is found to be increasing and goes out of the plane. Narrow band structure is formed due to the small Δn between the interfaces. The out-of-plane feature indicates that for low Δn, the frequency is real and the energy states show degeneracy. Hence, the electric field will transmit through the medium without any loss. For longer wave numbers (visible band), the low Δn interfaces exhibit no band gap formation (transmission). It is necessary to occur multiple scattering from the regions of different dielectric constants for bandgap formation. It shows (Figure 7.5 a) that there is not enough scattering along the kz propagation direction. The out-of-plane feature is one of the general features of 2D PCs [25]. This feature of the 2D PC is utilized for optical waveguide applications. Considering this fact, it implies that low-index 1D PCs also exhibit off-axis propagation (out-of-plane band gap structure). The dispersion diagram of bilayer 1D Silica/PVA PC shows that the PBG is presented for small values of wave vector, that is, the PBG is limited to the longer wavelength. This feature of low index 1D dielectric PC emphasis that this proposed multilayer system can be subjected to modifications to replace materials for 3D printing.

Figure 7.5b displays the photonic band structure for the DNA-templated 1D Silica/PVA system. Compared with Figure 7.5a, the band gaps present in Figure 7.5 b tend to go out of the plane. The width of the band structure is also larger. The DNA templated 1D PC system has a fine structure of a three-layered periodic system with

small Δn between the interfaces. Due to the increase in the number of layers in the unit cell, the periodicity has been altered and formed more interfaces of small Δn. It provides off-axis propagation for small k values, and a multi-colour appearance can be obtained within the visible wavelength region. Such an event suggests that the proposed system is compatible with PC applications, especially for incorporating sustainable structural colors within 3D printed parts. Thus, a multi-colour structure with uniform PBG width for fine dielectric microstructures can be obtained.

7.4 Conclusions

In this work, a coalition between the working principle of 3D inkjet printing technology and the property of the PC system to extrude 3D articles has been made. Technically, it is found that the limiting parameters (temperature and pressure) of the precursors (materials to be extruded) used for inkjet printing agree with the materials of PC systems. Therefore, it is important to evaluate PC systems for applying their specific features to 3D inkjet printing applications. For this, a 1D PC of a three-layer unit cell is configured with silica and biodegradable polymers. The constituent layers selected for such a unit cell were silica, DNA, and PVA, and the three layers in the unit cell were in the exact order they were mentioned. The refractive indices of these three materials have nearly adjacent values. Thereby, the step length (period or lattice parameter, d) of the unit cell of the PC system was increased. In general, in the case of a PC system, the step length is increased without altering the number of interfaces. However, in this work, the way in which the number of interfaces affects the bandgap formation is

observed. Then, theoretically investigated the light transmission properties of DNA templated 1D Silica/PVA PC system along with a 1D PC of Silica\PVA system without DNA template. This comparison study was carried out to understand the role of the DNA template in making the bandgap formation in a three-layer unit cell containing 1D PC. The TMM method was used as the theoretical method, as it is better for studying 1D PC having more than two kinds of materials. The transmission properties were studied in the optical band of the wavelength range 400 nm-800 nm.

The reason for considering DNA as the template layer between silica and PVA is that, even for a low Δn, the bandgap formation can be controlled to obtain in the visible region for a three-layered PC. Theoretical results show that the DNA-templated three-layer 1D PC could form band gaps within the visible region. In addition to this, the bandgap obtained in the case of the Silica/PVA system is around 450nm. When introducing a DNA template, between the unit cells, the bandgap was shifted to longer wavelengths with high resolution. That points out that this design can be helpful to optimize the bandgap at the desired wavelength.

Additionally, the variation in the parameters to change the region of the bandgap accordingly to our requirement can also be performed. The dispersion relation also confirmed that such a design can provide the features of a 2D PC. From these observations, a DNA templated Silica/PVA system can be executed for extruding cost-effective, non-toxic, multicolored 3D objectives by incorporating the 3D inkjet printing technology.

References

[1] Mpofu, T. P., Mawere, C., & Mukosera, M. (2014). The impact and application of 3D printing technology.

[2] Ngo, T. D., Kashani, A., Imbalzano, G., Nguyen, K. T., & Hui, D. (2018). Additive manufacturing (3D printing): A review of materials, methods, applications, and challenges. Composites Part B: Engineering, 143, 172-196.

[3] K. Reddy, & Dufera. (2019), Additive manufacturing technologies, Solomon.

[4] Hsueh, M. H., Lai, C. J., Wang, S. H., Zeng, Y. S., Hsieh, C. H., Pan, C. Y., & Huang, W. C. (2021). Effect of printing parameters on the thermal and mechanical properties of 3D-printed PLA and PETG, using fused deposition modeling. Polymers, 13(11), 1758.

[5] Khan, S., Joshi, K., & Deshmukh, S. (2022). A comprehensive review of the effect of printing parameters on the mechanical properties of FDM printed parts. Materials Today: Proceedings, 50, 2119-2127.

[6] J. Wu, Study on optimization of 3D printing parameters. In IOP conference series: materials science and engineering, IOP Publishing, Vol. 392, No. 6, p. 062050.2018.

[7] Y.W.D. Tay, M.Y. Li, M.J.Tan, Effect of printing parameters in 3D concrete printing: printing region and support structures, Journal of Materials Processing Technology, 271, 261-270.2019.

[8] M. Pivar, D. Gregor-Svetec, D. Muck, Effect of printing process parameters on the shape transformation capability of 3D printed structures. Polymers, 14(1), 117.2021.

[9] N. Shahrubudin, T.C. Lee, R. Ramlan, An overview on 3D printing technology: technological, materials, and applications, Procedia Manufacturing, 35, 1286-1296.2019.

[10] P. Wang, B. Zou, H. Xiao, S. Ding, C. Huang, Effects of printing parameters of fused deposition modeling on mechanical properties, surface quality, and microstructure of PEEK. Journal of Materials Processing Technology, 271, 62-74.2019.

[11] M. Ouhsti, B. El Haddadi, S. Belhouideg, Effect of printing parameters on the mechanical properties of parts fabricated with open-source 3D printers in PLA by fused deposition modeling, Mechanics and Mechanical Engineering, 22(4), 895-908.2018

[12] Kianian, Babak. Wohlers report: 3d printing and additive manufacturing state of the industry, annual worldwide progress report: Chapters titles: The middle east, and other countries." (2017).

[13] Frazier, E. William, Metal additive manufacturing: a review, Journal of Materials Engineering and performance 23.6 (2014): 1917-1928.2014.

[14] Piazza, Merissa, A. Serena, Additive manufacturing: a summary of the literature, 2015.

[15] Bourell, David, Materials for additive manufacturing. CIRP annals 66.2 (2017): 659- 681.2017

[16] T. Colton, C. Inkley, A. Berry, A., N.B. Crane, Impact of inkjet printing parameters and environmental conditions on formation of 2D and 3D binder jetting geometries, Journal of Manufacturing Processes, 71, 187-196.2021.

[17] A. Elkaseer, S. Schneider, Y. Deng, S.G. Scholz, Effect of process parameters on the performance of drop-on-demand 3D inkjet printing: Geometrical-based modeling and experimental validation. Polymers, 14(13), 2557.2022.

[18] Jun, H. Y., Kim, S. J., & Choi, C. H. (2021). Ink formulation and printing parameters for inkjet printing of two-dimensional materials: a mini review. Nanomaterials, 11(12), 3441.

[19] Zawadzki, M., Zawada, K., Kowalczyk, S., Plichta, A., Jaczewski, J., & Zabielski, T. (2022). 3D reactive inkjet printing of aliphatic polyureas using the in-air coalescence technique. RSC advances, 12(6), 3406-3415.

[20] Sieber, I., Thelen, R., & Gengenbach, U. (2020). Enhancement of high-resolution 3D inkjet-printing of optical freeform surfaces using digital twins. Micromachines, 12(1), 35.

[21] Chen, G., Chen, C., Yu, Z., Yin, H., He, L., & Yuan, J. (2016). Color 3D Printing: Theory, method, and application. New Trends in 3D Printing, 25-51.

[22] Aliakbari, M. (2012). Additive manufacturing: state-of-the-art, capabilities, and sample applications with cost analysis.

[23] Žitňan, M., Müller, L., Zub, K., Schubert, U. S., Galusek, D., & Wondraczek, L. (2022). Low-cost inkjet printing of thin-film mullite structures. International Journal of Applied Glass Science, 13(1), 135-142.

[24] Glinsek, S., Song, L., Kovacova, V., Mahjoub, M. A., Godard, N., Girod, S., ... & Defay, E. (2022). Inkjet-printed piezoelectric thin films for transparent haptics. Advanced Materials Technologies, 7(8), 2200147.

[25] Joannopoulos, J. D., Johnson, S. G., Winn, J. N., & Meade, R. D. (2008). Molding the flow of light. Princet. Univ. Press. Princeton, NJ [ua], 12.

[26] Divya, J., Selvendran, S., & Raja, A. S. (2018). Photonic crystal-based optical biosensor: a brief investigation. Laser Physics, 28(6), 066206.

[27] Prajzler, V., Jung, W., Oh, K., Cajzl, J., & Nekvindova, P. (2020). Optical properties of deoxyribonucleic acid thin layers deposited on an elastomer substrate. Optical Materials Express, 10(2), 421-433.

[28] Nithyaja, B., Misha, H., & Nampoori, V. P. N. (2012). Synthesis of silver nanoparticles in DNA template and its influence on nonlinear optical properties. Nanosci Nanotechnol, 2(4), 99-103.

[29] Akbar, F., Syahriar, A., & Lubis, A. H. (2014, November). Dispersion relation of 1-D photonic crystal. In 2014 International Conference on Electrical Engineering and Computer Science (ICEECS) (pp. 69-73). IEEE.

[30] Wu, K., Gu, W. X., Wu, C., Ma, J. L., & Ma, X. Y. (2014). Study on the Optical Transmission Properties of One-dimensional Photonic crystal of MoS2. Advanced Materials Research, 1056, 42-46.

[31] Gong, Q., & Hu, X. (2013). Photonic crystals. In Principles and Applications. Pan stanford publishing.

[32] Inan, H., Poyraz, M., Inci, F., Lifson, M. A., Baday, M., Cunningham, B. T., & Demirci, U. (2017). Photonic crystals: emerging biosensors and their promise for point-of-care applications. Chemical society reviews, 46(2), 366-388.

[33] Arunkumar, R., Suaganya, T., & Robinson, S. (2019). Design and analysis of 2D photonic crystal based biosensor to detect different blood components. Photonic Sensors, 9, 69-77.

[34] Armenise, M. N., Campanella, C. E., Ciminelli, C., Dell'Olio, F., & Passaro, V. M. (2010). Phononic and photonic band gap structures: modelling and applications. Physics Procedia, 3(1), 357-364.

[35] Cunningham, B. T., Zhang, M., Zhuo, Y., Kwon, L., & Race, C. (2015). Recent advances in biosensing with photonic crystal surfaces: a review. IEEE Sensors Journal, 16(10), 3349-3366.

[36] Malitson, I. H. (1965). Interspecimen comparison of the refractive index of fused silica. Josa, 55(10), 1205-1209.

[37] Tan, C. Z. (1998). Determination of refractive index of silica glass for infrared wavelengths by IR spectroscopy. Journal of Non-Crystalline Solids, 223(1-2), 158-163.

[38] Inagaki, T., Hamm, R. N., Arakawa, E. T., & Painter, L. R. (1974). Optical and dielectric properties of DNA in the extreme ultraviolet. The journal of chemical physics, 61(10), 4246-4250.W.L.Bond, Measurement of the refractive indices of several crystals, J.Appl.Phys.. 36, 1674-1677(1965)

[39] Malitson, I. H., & Dodge, M. J. (1972). Refractive index and birefringence of synthetic sapphire. J. Opt. Soc. Am, 62(11), 1405. M. J. Dodge, "Refractive Index" in Handbook of Laser Science and Technology, Volume IV, Optical Materials: Part 2, CRC Press, Boca Raton, 1986, p. 30

[40] Aly, A. H., Ameen, A. A., Mahmoud, M. A., Matar, Z. S., Al-Dossari, M., & Elsayed, H. A. (2021, September). Photonic crystal enhanced by metamaterial for measuring electric permittivity in the GHz range. In Photonics (Vol. 8, No. 10, p. 416). MDPI.

[41] Aly, A. H., Mohamed, D., & Mohaseb, M. A. (2020). Metamaterial control of hybrid multifunctional high-Tc superconducting photonic crystals for 1D Quasi-periodic structure potential applications. Materials Research, 23(3), e20190695.

[42] Watan, A. W., Mohammed, I. A., Hameed, H. K., Jasim, K. A., & Shaba, A. H. (2022). Thermal and Mechanical Behaviour of Heat-resistant Clay-silica Composites. NeuroQuantology, 20(3), 43.

[43] Aly, A. H., Sabra, W., & Elsayed, H. A. (2017). Cutoff frequency in metamaterials photonic crystals within the Terahertz frequencies. International Journal of Modern Physics B, 31(15), 1750123.

[44] Al-Dossari, M., Awasthi, S. K., Mohamed, A. M., Abd El-Gawaad, N. S., Sabra, W., & Aly, A. H. (2022). Bio-alcohol sensor based on one-dimensional photonic crystals for detection of organic materials in wastewater. Materials, 15(11), 4012.

[45] Zhang, X., Jiao, Y. C., Weng, Z. B., Zhang, Y. X., & Feng, S. (2019). Wideband magneto-electric dipole antenna with a claw-shaped reflector for 5G communication systems. Microwave and Optical Technology Letters, 61(9), 2098-2104.

[46] Natesan, A., Govindasamy, K. P., Gopal, T. R., Dhasarathan, V., & Aly, A. H. (2019). Tricore photonic crystal fibre-based refractive index sensor for glucose detection. IET Optoelectronics, 13(3), 118-123.

[47] A.H. Aly, S.S.A. Ghany, B.M. Kamal, D. Vigneswaran, Theoretical studies of hybrid multifunctional YaBa2Cu3O7 photonic crystals within visible and infra-red regions. Ceramics International, 46(1), 365-369.2020.

[48] Hossain, M. S., & Sen, S. (2021). Design and performance improvement of optical chemical sensor based photonic crystal fiber (PHOTONIC CRYSTAL) in the terahertz (THz) wave propagation. Silicon, 13(11), 3879-3887.

[49] Aly, A. H., & Mohamed, D. (2015). BSCCO/SrTiO 3 one dimensional superconducting photonic crystal for many applications. Journal of Superconductivity and Novel Magnetism, 28, 1699-1703.

[50] Zaky, Z. A., Alamri, S., Zhaketov, V. D., & Aly, A. H. (2022). Refractive index sensor with magnified resonant signal. Scientific Reports, 12(1), 13777.

[51] Aly, A. H., Awasthi, S. K., Mohamed, A. M., Al-Dossari, M., Matar, Z. S., Mohaseb, M. A., ... & Amin, A. F. (2021). 1D reconfigurable bistable photonic device composed of phase change material for detection of reproductive female hormones. Physica Scripta, 96(12), 125533.

[52] Liao, J., Ye, C., Guo, J., Garciamendez-Mijares, C. E., Agrawal, P., Kuang, X., ... & Zhang, Y. S. (2022). 3D-printable colloidal photonic crystals. Materials Today, 56, 29-41.

[53] Liu, Y., Wang, H., Ho, J., Ng, R. C., Ng, R. J., Hall-Chen, V. H., ... & Yang, J. K. (2019). Structural color three-dimensional printing by shrinking photonic crystals. Nature communications, 10(1), 4340.

[54] Wang, J., Wang, L., Song, Y., & Jiang, L. (2013). Patterned photonic crystals fabricated by inkjet printing. Journal of Materials Chemistry C, 1(38), 6048-6058.

[55] Nam, H., Song, K., Ha, D., & Kim, T. (2016). Inkjet printing-based mono-layered photonic crystal patterning for anti-counterfeiting structural colors. Scientific reports, 6(1), 30885.

[56] Joyce, D. M. (2013). The development of DNA-based bio-polymer hybrid thin films for capacitor applications (Doctoral dissertation, University of Dayton).

[57] Dugasani, S. R., Gnapareddy, B., Kesama, M. R., Jeon, S., Jeong, J. H., & Park, S. H. (2019). Optoelectronic properties of DNA thin films implanted with titania nanoparticle-coated multiwalled carbon nanotubes. AIP Advances, 9(1).

[58] Kokkiligadda, S., Dugasani, S. R., Komarala, E. P., Jeon, S., Jeong, J. H., & Park, S. H. (2021). Controlling physical characteristics of DNA and DNA-CTMA thin films by embedding with graphene oxide and riboflavin. Journal of Physics D: Applied Physics, 54(37), 375401.

[59] Prajzler, V., Jung, W., Oh, K., Cajzl, J., & Nekvindova, P. (2020). Optical properties of deoxyribonucleic acid thin layers deposited on an elastomer substrate. Optical Materials Express, 10(2), 421-433.

[60] Hebda, E., Jancia, M., Kajzar, F., Niziol, J., Pielichowski, J., Rau, I., & Tane, A. (2012). Optical properties of thin films of DNA-CTMA and DNA-CTMA doped with Nile blue. Molecular Crystals and Liquid Crystals, 556(1), 309-316.

[61] Nithyaja, B., Misha, H., & Nampoori, V. P. N. (2012). Synthesis of silver nanoparticles in DNA template and its influence on nonlinear optical properties. Nanosci Nanotechnol, 2(4), 99-103.

[62] Martin, J. E., Anderson, M. T., Odinek, J., & Newcomer, P. (1997). Synthesis of periodic mesoporous silica thin films. Langmuir, 13(15), 4133-4141.

[63] Rahman, I. A., & Padavettan, V. (2012). Synthesis of silica nanoparticles by sol-gel: size-dependent properties, surface modification, and applications in silica-polymer nanocomposites—a review. Journal of nanomaterials, 2012(1), 132424.

[64] Satvekar, R. K., Phadatare, M. R., Karande, V. A., Patil, R. N., Tiwale, B. M., & Pawar, S. H. (2012). Influence of silane content on the optical properties of sol gel derived spin coated silica thin films. Int. J. Basic Appl. Sci, 1(9).

[65] Ankita, Suthar, B., & Bhargava, A. (2021). Biosensor application of one-dimensional photonic crystal for malaria diagnosis. Plasmonics, 16(1), 59-63.

[66] Aly, A. H., Zaky, Z. A., Shalaby, A. S., Ahmed, A. M., & Vigneswaran, D. (2020). Theoretical study of hybrid multifunctional one-dimensional photonic crystal as a flexible blood sugar sensor. Physica Scripta, 95(3), 035510.

[67] Koo, J., Kim, J. W., Kim, M., Yoon, S., & Shim, J. H. (2021). Inkjet printing of silica aerogel for fabrication of 2-D patterned thermal insulation layers. International Journal of Precision Engineering and Manufacturing-Green Technology, 8, 445-451.

[68] ar, M., Doll, T., kovi, J., & Scherer, A. (2000). Design and fabrication of silicon photonic crystal optical waveguides. Journal of lightwave technology, 18(10), 1402.

[69] Inoue, K., & Ohtaka, K. (Eds.). (2004). Photonic crystals: physics, fabrication and applications (Vol. 94). Springer Science & Business Media.

[70] Soukoulis, C. M. (2002). The history and a review of the modelling and fabrication of photonic crystals. Nanotechnology, 13(3), 420.

[71] Cheng, C. C., & Scherer, A. (1995). Fabrication of photonic bandgap crystals. Journal of Vacuum Science & Technology B: Microelectronics and Nanometer Structures Processing, Measurement, and Phenomena, 13(6), 2696-2700.

[72] Busch, K., Lölkes, S., Wehrspohn, R. B., & Föll, H. (Eds.). (2006). Photonic crystals: advances in design, fabrication, and characterization. John Wiley & Sons.

[73] Cuervo, A., Dans, P. D., Carrascosa, J. L., Orozco, M., Gomila, G., & Fumagalli, L. (2014). Direct measurement of the dielectric polarization properties of DNA. Proceedings of the National Academy of Sciences, 111(35), E3624-E3630.

[74] Bond, W. L. (1965). Measurement of the refractive indices of several crystals. Journal of Applied Physics, 36(5), 1674-1677.

[75] M. J. Dodge. (1986) "Refractive Index" in Handbook of Laser Science and Technology, Volume IV, Optical Materials: Part 2, CRC Press, Boca Raton, p. 30.

[76] Bodurov, I., Vlaeva, I., Viraneva, A., Yovcheva, T., & Sainov, S. (2016). Modified design of a laser refractometer. Nanosci. Nanotechnol, 16, 31-33.

[77] Gong, Q., & Hu, X. (2013). Photonic crystals. In Principles and Applications. Pan stanford publishing.

[78] Divya, J., Selvendran, S., & Raja, A. S. (2018). Photonic crystal-based optical biosensor: a brief investigation. Laser Physics, 28(6), 066206.

[79] Hudak, Y. I. (2017). On the mathematics problem of multilayered dielectric systems in the classical electrodynamic. Russian Technological Journal, 5(3), 160-188.

[80] Pandey, J. P. (2017). Transfer matrix method for one-dimensional photonic crystals. J. Ramanujan Soc. Math Math Sc, 6(1), 121-130.

[81] Villa-Villa, F., & Gaspar-Armenta, J. A. (2006). Brewster angle and optical tunneling in one-dimensional photonic crystals composed of left-and right-handed materials. JOSA B, 23(2), 375-380.

[82] Lekner, J. (2013). Theory of reflection of electromagnetic and particle waves (Vol. 3). Springer Science & Business Media. [67] Pedrotti, F. L., Pedrotti, L. M., & Pedrotti, L. S. (2018). Introduction to optics. Cambridge University Press.

[83] Abbas, S., Salman, S. R., & Abbas, A. S. (2021). Studying of the polarization modes TE and TM for oblique incidence of light on thin films. Digest Journal of Nanomaterials and Biostructures, 16(2), 647-657.

[84] Pendry, J. B. (1994). Photonic band structures. Journal of modern optics, 41(2), 209-229.

Chapter 8

Conclusions and Future Prospects

8.1 General Conclusions

The present work investigates the modulation of a 1D ternary PC under various conditions, including modifications involving DNA-incorporated elemental structures, engineered defects, and nonlinear optical properties. The studies traced the features of 1D ternary PC over its bilayer 1D PC, and its potential applications including sensors, optical filters and nonlinear optical devices. The work employs five different analyses of 1D PC for exploiting its significant properties.

Among the five different studies, both theoretical and experimental analyses were conducted. The theoretical investigation of the 1D ternary PC systems was carried out using the Transfer Matrix Method (TMM) and COMSOL Multiphysics software. The theoretical analysis is based on the master equations using fundamental Maxwell's differential equations for electromagnetic wave dynamics in dielectric media. The properties of 1D ternary PCs are theoretically examined with dielectrics (silica, ZnO, alumina, and graphite oxide), biopolymers (DNA), and polymer (PVA). The theoretical analysis is based on the dependency of period, thickness, and defect on the photonic bandgap effects of 1D ternary PCs. From the theoretical analysis, Silica/DNA/ZnO gives significant results such as a wide photonic bandgap, defective mode with a wide FWHM, and high defect mode intensity. These features can be exploited for sensing, optical filters, and nonlinear optical applications. The photonic bandgap effects are tunable according to the desired requirements. More precisely, the frequency range where it is wanted to bring the photonic bandgap can be tuned. Most of the time, the precision of the

photonic bandgap, oscillation density in the transmission range cannot be obtained due to the limitation of the bilayer PC structure. These issues can be addressed by using a one-dimensional (1D) ternary PC, as our studies reveal that it provides more than one photonic bandgap within a short frequency range. The bandwidth can be tuned by appropriately adjusting the number of periods, layer thicknesses, and material choices. The materials chosen for theoretical analysis exhibit a low refractive index contrast, allowing control over the formation of photonic bandgaps within the terahertz range, where many optical filters, sensors, and nonlinear optical devices operate.

The objectives of the work cover to the fabrication of PC at low-cost expenses. Keeping this view, the materials selected for designing the PC structures are abundant in nature such as silica, ZnO, DNA and PVA (synthetic but cost-effective polymer). Based on the significant results obtained from the theoretical analysis, these materials are seeming to be the best materials to be used for the fabrication of PC.

The fabrication of PCs aims to enable applications in biosensing, optical filtering, and nonlinear optics. Therefore, the PCs must exhibit features suitable for these purposes. The materials selected for fabrication include metal oxides (silica and ZnO), a polymer (DNA), and a ligand (polyoxometalate). These materials need to be deposited as thin films on glass substrates. With this in mind, silica nanoparticles were prepared using a novel bio-templated method. This method utilizes a DNA–CTAB complex as the biotemplate, resulting in mesoporous silica nanoparticles with enhanced surface area and improved nonlinear optical properties. These are referred to as DNA-

templated silica nanoparticles. This approach offers dual advantages: the resulting silica nanoparticles are soluble in DMSO, which is the solvent used for coating silica onto glass surfaces, and their nonlinear optical properties can be exploited to enhance the nonlinear optical functionality of the PCs.

In addition, silicotungstate, which belongs to the inorganic polyoxometalate group and exhibits thin film forming properties, was prepared using a DNA template. The silicotungstate is a metal-oxygen cluster mainly used for catalytic purposes due to its structural benefits. However, its nonlinear optical properties using nonlinear optical studies of a 1D ternary PC have been analysed. Hence, the obtained DNA-capped silicotungstate shows excellent nonlinear optical saturation properties. The nonlinear optical saturation of property can be applicable in many vital functions in nonlinear optical applications, including optical switching.

The fabrication of 1D ternary PC using silica, DNA, and ZnO is found successful, and the obtained 1D ternary Silica/DNA/ZnO PC system is experimented as a biosensor for the detection of BSA. The performance of the proposed 1D ternary Silica/DNA/ZnO for the detection of BSA shows a significant result of sensitivity as 5917.8444 nm/RIU against the refractive index contrast of 0.009. The result shows a remarkable resolution of the system.

The nonlinear optical domain of a 1D ternary PC is yet to be disclosed. In this study, the nonlinear optical properties of the proposed 1D ternary Silica/DNA/ZnO PC are examined, including its defective

structure in which DNA-templated silicotungstate is used as the defect layer. The nonlinear optical studies are done by using the open-aperture Z-scan method. The study is carried out in two different conditions. The nonlinear optical response of the 1D ternary Silica/DNA/ZnO PC was observed to vary with an increasing number of periods. The structure exhibited a gradual transition from nonlinear absorption to nonlinear saturation up to a period number of 13. Subsequently, a defective Silica/DNA/ZnO PC was introduced, in which the DNA layer was replaced with a defect layer in the 7th unit cell. This modification led to a significant shift from nonlinear absorption to nonlinear saturation. Thus, the system demonstrates tunable nonlinear optical properties. This tunable nonlinear optical feature of 1D ternary Silica/DNA/ZnO can be exploited for various nonlinear optical applications, including optical limiters, Q- switching in lasers for creating high-power, short pulses, optical bistable devices, and optical logic gates.

The features of 1D ternary PCs are not limited to the metal oxide/DNA composition; it is extended to metal oxides/polymers as well. The structure is designed for liquid-based inkjet droplets. Therefore, all the materials proposed for the work are available in stable solutions. The features of the composition Silica/DNA/PVA are considered for the theoretical analysis to be employed for 3D inkjet printing applications to configure 3-D multi coloured shapes. The study is suitable for obtaining cost-effective and easily fabricable structures. Also, the structure shows multiple tunable photonic band gaps for low refractive

index contrast as well. Hence, the 3D inkjet printing can be used as an alternative method for fabricating 1D ternary PCs at a low temperature.

In summary, the features of 1D ternary PCs make them an interested candidate in both science and technology. The proposed 1D ternary PC involves a novel biopolymer (DNA) based microstructure. Their tunable photonic bandgap effects can be exploited in a variety of potential applications in biosensing, optical filters, nonlinear optical devices, and 3D modelling.

8.2. Future prospects

The future scope of this work offers various opportunities in both science and technology. The results of the study on the modulation of photonic bandgap effects in 1D ternary PCs extend the potential applications of PCs in various fields such as solar cells, biosensors, laser devices, and 3D modeling. The tunability of photonic bandgap effects depends on various configurations of PCs, including 1D ternary defective PCs and 1D ternary nonlinear optical PCs. These different configurations provide various features that make PCs suitable for different applications.

The theoretical investigation of photonic bandgap features involves six configurations of 1D ternary PCs, where DNA is used as one of the elemental layers. The introduction of DNA represents a novel step in demonstrating that DNA-incorporated thin film structures can have many potential applications in photonic devices. The study highlights the ability to fabricate DNA-based periodic microstructures for multifaceted applications, including solar cells, sensors, and laser

systems. The core of the theoretical results from the six configurations of DNA-based 1D ternary PCs reveals that these structures exhibit tunable photonic bandgap effects. These bandgaps can be achieved within the visible region of the optical spectrum. In addition, they provide a larger number of photonic band gaps, and the photon density between these gaps is high. These features are advantageous for optical filters, especially in solar cells, where light trapping is crucial within the 450 nm to 750 nm range of the optical spectrum. The transmission of light beyond the upper and lower limits of these band edges leads to decreased solar cell efficiency, as such light can cause damage to the chemical composition of the solar cell due to photon-induced chemical reactions.

Moreover, the composition of the proposed 1D ternary PCs consists mainly of isotropic transparent thin films of Silica/DNA/ZnO. This composition helps to preserve the structure from damage caused by chemical oxidation. Thus, DNA-incorporated 1D ternary structures hold promises for solar cell applications. Future work will focus on designing and fabricating 1D ternary PC-based solar cells and optical filters.

The theoretical results of the 1D Silica/DNA/ZnO PC also highlight its potential for sensing applications. The defective 1D ternary PC provides a tunable defect mode with high full width at half maximum (FWHM), making it suitable for high-resolution sensor applications. The experimental analysis of the proposed structure validated the theoretical results. The structure also offers advantages such as ease of fabrication and low material cost. Therefore, the 1D ternary

Silica/DNA/ZnO configuration is promising for sensing applications. Future work will extend to cost-effective fabrication techniques that meet the criteria of high precision and sensitivity. The study will also explore additional configurations of DNA-based microstructures for sensor development.

The 1D ternary Silica/DNA/ZnO configuration also exhibits nonlinear optical tunability, including tunable defect modes with high FWHM. It indicates that the structure can be employed in nonlinear optical applications. Furthermore, the nonlinear optical signatures of the 1D ternary Silica/DNA/ZnO structure show tunable nonlinear optical properties, particularly in its defective configuration, where the DNA-capped silicotungstate serves as the defect layer. As a result, these structures can be applied in various nonlinear optical domains, including optical limiters, optical switching, logic gates, and optical bistable devices.

Additionally, this work extends the application of DNA as both a biotemplate and a micro-thin film material. Silica and silicotungstate nanoparticles exhibit tunable and enhanced morphological and nonlinear optical properties when prepared in the presence of DNA. It highlights DNA as a promising biotemplate for synthesizing nanoparticles with improved morphological and optical characteristics. Such nanoparticles hold potential in nonlinear optical devices, bioimaging, and catalytic applications. Future research will focus on the experimental realization of DNA-templated nanoparticles for use in a variety of material science applications.

This research work highlights the scope of cost effective, durable, ecofriendly and simple fabrication technique to realize the fabrication of 1D ternary PC structures using low temperature thin film treatment.

The theoretical analysis done in this entire work strengthens the objective. The theoretical work on polymer based 1D ternary PC structures is an insight of the objective of this entire work. From that the research work handled the fabrication and significant roles of DNA based ternary biotemplated PCs in the photonic applications where apart from DNA, PVA and solgel form of metal oxides such as silica, ZnO, alumina, and graphite oxide are suggested to fabricate into thin films using inkjet printing and dip coating methods.

In summary, this work motives to fabricate DNA-templated 1D ternary PCs in a simple and cost-effective way to accelerate its significant roles in integrated photonic and laser devices.